

Optical phase conjugation in fiber-optic transmission systems

Citation for published version (APA):

Jansen, S. L. (2006). *Optical phase conjugation in fiber-optic transmission systems*. [Phd Thesis 1 (Research TU/e / Graduation TU/e), Electrical Engineering]. Technische Universiteit Eindhoven.
<https://doi.org/10.6100/IR610247>

DOI:

[10.6100/IR610247](https://doi.org/10.6100/IR610247)

Document status and date:

Published: 01/01/2006

Document Version:

Publisher's PDF, also known as Version of Record (includes final page, issue and volume numbers)

Please check the document version of this publication:

- A submitted manuscript is the version of the article upon submission and before peer-review. There can be important differences between the submitted version and the official published version of record. People interested in the research are advised to contact the author for the final version of the publication, or visit the DOI to the publisher's website.
- The final author version and the galley proof are versions of the publication after peer review.
- The final published version features the final layout of the paper including the volume, issue and page numbers.

[Link to publication](#)

General rights

Copyright and moral rights for the publications made accessible in the public portal are retained by the authors and/or other copyright owners and it is a condition of accessing publications that users recognise and abide by the legal requirements associated with these rights.

- Users may download and print one copy of any publication from the public portal for the purpose of private study or research.
- You may not further distribute the material or use it for any profit-making activity or commercial gain
- You may freely distribute the URL identifying the publication in the public portal.

If the publication is distributed under the terms of Article 25fa of the Dutch Copyright Act, indicated by the "Taverne" license above, please follow below link for the End User Agreement:

www.tue.nl/taverne

Take down policy

If you believe that this document breaches copyright please contact us at:

openaccess@tue.nl

providing details and we will investigate your claim.

Optical phase conjugation in fiber-optic transmission systems

PROEFSCHRIFT

ter verkrijging van de graad van doctor
aan de Technische Universiteit Eindhoven,
op gezag van de Rector Magnificus, prof.dr.ir. C.J. van Duijn,
voor een commissie aangewezen door het College voor Promoties
in het openbaar te verdedigen
op maandag 26 juni 2006 om 16.00 uur

door

Sander Lars Jansen

geboren te Maartensdijk

Dit proefschrift is goedgekeurd door de promotoren:

prof.ir. G.D. Khoe
en
prof.ir. A.M.J. Koonen

Copromotor:
dr.ir. H. de Waardt

CIP-DATA LIBRARY TECHNISCHE UNIVERSITEIT EINDHOVEN

Jansen, Sander L.

Optical phase conjugation in fiber-optic transmission systems / by Sander Lars Jansen. -
Eindhoven : Technische Universiteit Eindhoven, 2006.

Proefschrift. - ISBN-10: 90-386-1803-4

ISBN-13: 978-90-386-1803-6

NUR 959

Trefw.: optische telecommunicatie / nietlineaire optica / optische signaalverwerking /
vezeloptica.

Subject headings: optical fibre communication / optical phase conjugation / optical fibre
dispersion / optical fibres.

Copyright ©2006 by Sander Lars Jansen

All rights reserved. No part of this publication may be reproduced, stored in a retrieval system,
or transmitted in any form or by any means without the prior written consent of the author

Typeset using L^AT_EX, printed in the Netherlands

Abstract

As the data rate of long-haul transmission links is increased, the design and realization of the transmission link becomes more difficult. As a result, more sophisticated methods are required to improve the transmission quality. The robustness of a transmission link can be increased and its structure greatly simplified by the use of mid-link optical phase conjugation (OPC). OPC is a promising technology to compensate for deterministic, phase related impairments (i.e. the Kerr effect and chromatic dispersion) in long-haul transmission systems.

This thesis assesses the regenerative capabilities of OPC for the compensation of distortions that occur in modern transmission systems. The focus of the research is on transmission systems where OPC is employed to compensate for both chromatic dispersion and nonlinear impairments. The dispersion map (i.e. the dispersion as a function of the transmission distance) of such a transmission system is completely different from that of a conventional transmission system. The accumulated dispersion along the link of an OPC-based transmission system is significantly higher than that of a conventional transmission system.

We investigated the influence of the dispersion map of OPC on nonlinear impairments using the non return-to-zero amplitude-shift-keying (NRZ-ASK) modulation format. As a result, it is shown that the peak powers that occur in the OPC transmission system are at a 10-Gbit/s/channel data rate significantly higher than the peak powers that occur in a conventional transmission system. The higher peak powers in the OPC based transmission system lead to an increased self-phase modulation (SPM) penalty. Through phase conjugation most of the SPM impairments are compensated for. However, when multiple wavelength division multiplexed (WDM) channels at narrow channel spacing are used for transmission, cross-phase modulation (XPM) is the dominating transmission impairment. Although XPM is principally a deterministic distortion, it must be treated as non-deterministic due to the dispersion of the transmission link. With simulations and experiments we show that because of this, the XPM compensation through OPC is marginal.

At a 40 Gbit/s data rate, the peak powers that occur in the OPC-based transmission system are similar to those that occur in the conventional transmission system. In 40 Gbit/s WDM transmission systems the influence of XPM is relatively low. These transmission systems are rather limited by intra-channel nonlinear impairments such as SPM, intra-channel XPM (IXPM) and intrachannel FWM (IFWM). We show experimentally that in this case, the performance of the OPC transmission system is better than that of the conventional transmission system.

When OPC is used to compensate for the chromatic dispersion, the OPC must be placed in the middle of the transmission link. This technique is often referred to as “mid-link OPC”. However, in some transmission links it is not possible to place the OPC exactly in the middle. Therefore, several configurations with a transmission length of 700 km to 900 km were assessed where the OPC was placed 100 km from the middle of the transmission

link. In this experiment practically no bit-error ratio (BER) degradation was observed in the off-center configuration.

Recently, strong interest has been shown in phase-shift keying modulation (PSK) formats such as differential phase-shift-keying (DPSK). DPSK's main advantages over ASK are that it is more robust to narrowband optical filtering and has a 3 dB higher sensitivity in combination with balanced detection. However, unlike ASK signals PSK signals can be distorted by nonlinear phase noise (NPN). For long-haul transmission systems, the impact of NPN is so severe that the performance of DPSK is in some cases even worse than that of ASK. The impact of nonlinear phase noise is studied for 10.7-Gbit/s DPSK in an 800-km transmission link. In this experiment it is shown that impairments due to nonlinear phase noise can be significantly reduced using optical phase conjugation. The dependence of the location of the OPC within the transmission link is assessed as well. Allowing a penalty of 1 decade in BER from the optimum, the OPC-unit can be varied over a wide range, from nearly 1/3 to 2/3 of the transmission link.

The combination of mid-link OPC is assessed with 21.4-Gbit/s return-to-zero differential quadrature phase-shift keying (RZ-DQPSK) in an ultra long-haul transmission experiment. Error-free transmission after FEC is realized over 10,200 km for all 22 WDM channels. In this experiment, a single OPC-unit is used in the middle of the link to compensate for an accumulated chromatic dispersion of over 160,000 ps/nm. Along the transmission line, the dispersion accumulates in this experiment to more than 80,000 ps/nm. This is significantly higher than the maximum accumulated dispersion in the conventional transmission system (approximately 3,000 ps/nm). The high accumulated dispersion results in an extreme overlap of the pulses along the transmission line. With this experiment we show that despite the high dispersion, the feasible transmission distance of the OPC based transmission system is 44% greater than that obtained in the conventional transmission system.

By doubling the data rate and keeping the 50-GHz channel spacing, a 0.8-bit/s/Hz spectral efficient WDM transmission system is realized. At 42.8-Gbit/s RZ-DQPSK, transmission over 5,000 km was realized with mid-link OPC. Compared to the feasible transmission distance obtained at 21.4-Gbit/s, the feasible transmission distance is reduced by about 50%. This reduction of transmission distance with 50% corresponds to the 3-dB OSNR penalty that is present between 21.4-Gbit/s and 42.8-Gbit/s RZ-DQPSK in the back-to-back configuration. For the conventional transmission system, a greater reduction in the feasible transmission distance (factor of 2.4) is measured due to increased penalties that result from a combination of self phase modulation and nonlinear phase noise. Comparing the feasible transmission distance of the OPC to the conventional transmission system an improvement of 60% is observed in this experiment.

Contents

1	Introduction	1
1.1	Motivation	2
1.2	Structure of this thesis	4
2	Transmission impairments	5
2.1	Fiber loss	6
2.2	Chromatic dispersion	8
2.3	Polarization mode dispersion	10
2.4	Kerr effect	11
2.4.1	Self-phase modulation	13
2.4.2	Cross-phase modulation	14
2.4.3	Four-wave mixing	15
2.4.4	Intra-channel XPM and intra-channel FWM	15
2.5	Non-elastic scattering effects	17
2.5.1	Stimulated Raman scattering	17
2.5.2	Stimulated Brillouin scattering	18
2.6	Summary	18
3	Fiber-optic transmission systems	21
3.1	Transmitter and receiver	21
3.2	Loss compensation	23
3.3	Dispersion compensation	27
3.4	Modulation formats	30
3.4.1	Amplitude-shift keying	32
3.4.2	Duobinary	33
3.4.3	Differential phase-shift keying	36
3.4.4	Differential quadrature-phase-shift keying	38
3.5	Summary	41
4	Optical phase conjugation	43
4.1	Processes	43
4.1.1	Four-wave mixing	44
4.1.2	Difference-frequency generation	44

CONTENTS

4.1.3	Cascaded second-harmonic generation and difference-frequency generation	45
4.2	Media	46
4.2.1	Silica	47
4.2.2	Indium gallium arsenide phosphide	47
4.2.3	Lithium niobate	49
4.2.4	Aluminum gallium arsenide	51
4.3	Subsystems	52
4.3.1	Parallel polarization diversity	52
4.3.2	Counter-directional polarization diversity	53
4.4	Transmission systems	54
4.4.1	OPC concept	54
4.4.2	Inline optical phase conjugation	59
4.4.3	Mid-link optical phase conjugation	60
4.5	Summary	62
5	ASK based transmission	65
5.1	XPM-limited 10-Gbit/s ASK transmission	65
5.1.1	Simulation	66
5.1.2	Experiment	73
5.2	WDM 40-Gbit/s ASK transmission	75
5.3	Asymmetric OPC-placement	79
5.4	Mixed data rate, mixed modulation format transmission	81
5.5	Summary	84
6	Nonlinear phase noise compensation	85
6.1	Nonlinear phase noise in long-haul transmission systems	85
6.2	Theory of nonlinear phase noise	86
6.3	Experiment	91
6.3.1	Nonlinear phase noise impairment on DPSK transmission	92
6.3.2	OPC for nonlinear phase noise compensation	93
6.3.3	Verification through simulations	96
6.3.4	OPC placement	97
6.4	Summary	98
7	DQPSK based transmission	101
7.1	21.4-Gbit/s DQPSK transmission	101
7.1.1	DCF-based DQPSK transmission	102
7.1.2	OPC-based DQPSK transmission	105
7.2	42.8-Gbit/s DQPSK transmission	109
7.2.1	DCF-based DQPSK transmission	111
7.2.2	OPC-based DQPSK transmission	113
7.2.3	OPC-based transmission without Raman amplification	117

7.3 Summary	118
8 Conclusions	121
9 Outlook	125
A List of symbols and abbreviations	127
A.1 List of symbols	127
A.2 List of Abbreviations	129
B Performance evaluation of a transmission link	133
B.1 Eye opening penalty	133
B.2 Q-factor	134
C Periodically-poled lithium-niobate component	137
Bibliography	139
List of publications	153
Samenvatting	159
Acknowledgments	161
Curriculum Vitae	163

CONTENTS

Chapter 1

Introduction

Fiber-optic transmission systems revolutionized the communication technology, but despite the fact that these systems play an important role in today's society, most people will not have a notion of it. Since the development of the internet and the introduction of the World Wide Web (WWW) in the late 80s [1], the demand for data transmission capacity has increased exponentially. In order to meet this growing demand of both home users and large enterprise customers, telecommunication providers employ fiber-optic transmission systems for most transmission links. Figure 1.1 illustrates the architecture of today's telecommunication network. The network is divided into the core, the metropolitan and the access network [2].

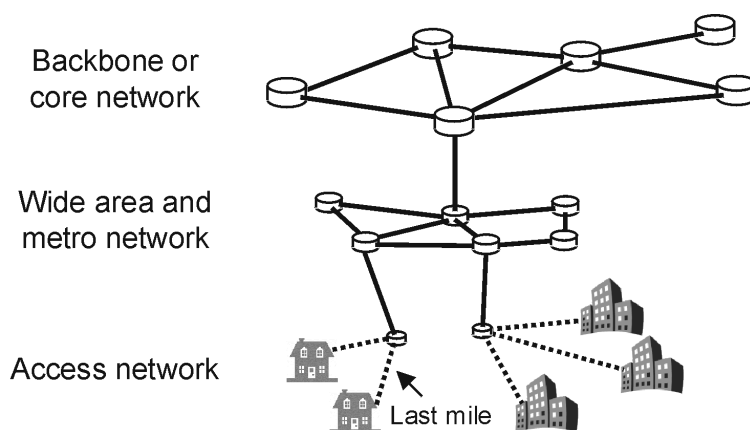


Figure 1.1: *Simplified illustration of today's telecommunication network.*

To date, fiber-optics is the method of choice for most transmission links. The part of the communication system that is mostly non-optic is the access network. The main part of the access network is the connection to the end user, usually referred to as the "last mile". In many households this connection is a co-axial or twisted pair copper wire. The bandwidth of these connections is limited, especially when the distance from the local exchange node to the end user is long. "Fiber-to-the-X" can be used to overcome these

limitations, with X as Building, Curb, Home, Street, etc. [3, 4]. Different access networks are connected through the metropolitan network. The transmission lines of such a network have a length up to 500 km.

Large cities around the world are connected by the core or backbone network. The core network can be considered as the “photonic highway” of communication systems where large amounts of traffic are transmitted over long distances. Typically, the transmission distances in the backbone network are long-haul (> 500 km) and can be up to several thousands of kilometers long. At the nodes of this network, data streams of the metropolitan networks are aggregated and multiplexed together into high data rate channels. Vice versa, the high data rate streams are demultiplexed to be routed into the metropolitan network.

In the backbone of today’s transmission networks, solely single-mode optical fibers are used, made from silica glass. The attenuation of these fibers is the lowest around the wavelength of 1550 nm (≈ 0.2 dB/km) thus allowing transmission over more than 100 km fiber before amplification is required. Furthermore, the optical bandwidth of a fiber is extremely high. In the low-loss window (from 1460 nm to 1625 nm), the total usable bandwidth is larger than 20 THz.

Commercial transmission systems in the backbone employ data rates of 10 Gbit/s and 40 Gbit/s with many wavelength division multiplexed (WDM) channels. In WDM systems, lightwaves emitted by multiple sources with different optical frequencies are multiplexed and transmitted over the same fiber link. Thereby, the link capacity is significantly increased. The total transmission capacity of a commercial fiber-optic transmission system employing 80x40-Gbit/s channels is 3.2 Tbit/s. Note that this can be achieved on a single optical fiber which has a core diameter in the order of 8-9 micrometer. Not surprisingly, the fiber-optic systems are considered to have virtually unlimited bandwidth as many fibers occupy a small space.

1.1 Motivation

Due to the wavelength dependence of the propagation velocity of light in an optical fiber, a signal is dispersed during transmission. For data rates higher than 2.5 Gbit/s, this dispersion has to be compensated for. In conventional transmission systems inline dispersion compensating fiber (DCF) modules are employed for chromatic dispersion compensation after each span. When the chromatic dispersion is compensated for, a trade-off exists between noise from optical repeaters and nonlinear impairments. The influence of amplifier noise is reduced by increasing the launch power at the input of the fiber spans. When however the input power is too high, nonlinear impairments limit the performance of the transmission link.

The dispersion compensation scheme strongly influences the nonlinear impairments that occur in the system, and is therefore a critical design parameter for high data-rate transmission links. By optimizing the dispersion as a function of the transmission distance, usually referred to as dispersion map, the transmission performance can significantly be

improved. However, the optimal dispersion map is dependent on many system parameters such as the total transmission length, the span length, the number of channels, the channel spacing and the channel data rate. In order to further extend the transmission reach optical-electric-optical (OEO) repeaters or optical regenerators must be employed.

OPC is a method to simplify the transmission system and improve its robustness towards nonlinear impairments. In Figure 1.2 the concept of OPC is illustrated. Suppose

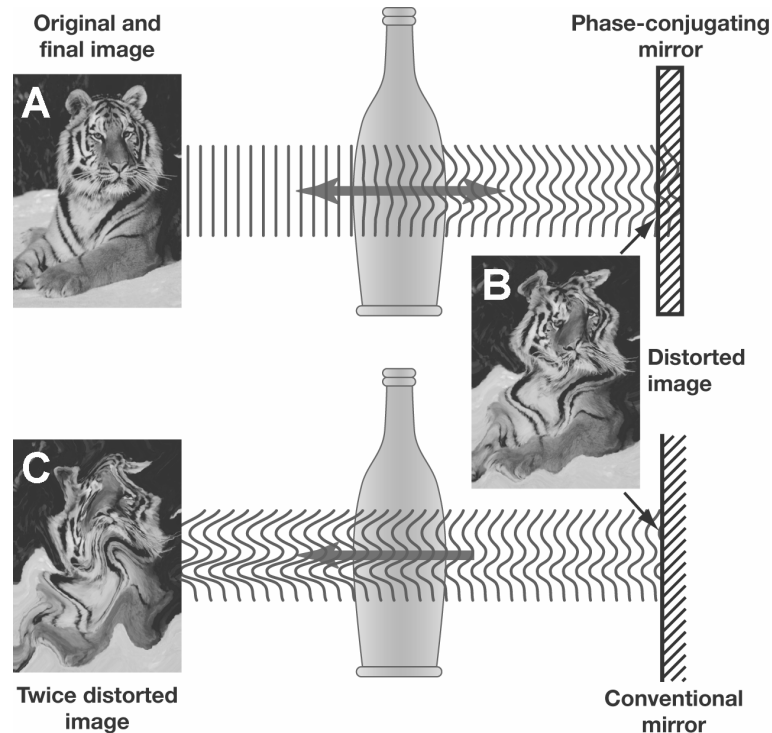


Figure 1.2: *The concept of optical phase conjugation. source: www.wikipedia.com*

that we look at the image of a tiger “Image A”. If we place a bottle between us and the image, the image of the tiger is deformed due to the irregular shape of the bottle (Image B). If we now insert a conventional mirror opposite to the image and let the light travel through the bottle twice, the image will be distorted twice (Image C). However, when the conventional mirror is replaced with a phase-conjugating mirror, the original image (Image A) will be seen after passing through the bottle twice. The reason for this is that the distortions of the bottle are exactly the same the first and the second time the light travels through the bottle. Therefore, through phase conjugation, the distortions that occur the second time the image travels through the bottle cancel the distortions that occur the first time.

In fiber-optic transmission systems this concept is exactly the same. In a mid-link OPC transmission link, the phase of the signals is conjugated mid-link. At that point, the signal is severely distorted by chromatic dispersion and nonlinear impairments. As a result, the distortions that occur in the second part of the link after the OPC, revert

the impairments that were accumulated in the first part. Full compensation for nonlinear impairments occurs when the nonlinear effects before and after OPC are identical.

The use of mid-link OPC is twofold. Firstly, mid-link OPC can compensate for impairments caused by the Kerr-effect. The Kerr effect causes a change in the refractive index of the transmission fiber in response to an electric field. In fiber-optic transmission systems, the Kerr effect leads to distortions in the phase of the signals and can significantly reduce the system performance. Through the compensation for Kerr-effect, the feasible transmission distance is significantly extended and the amount of required OEO repeaters reduced. Secondly, OPC can be used to compensate for chromatic dispersion. In such a link, no inline DCF modules are required. The omission of DCFs translates into reduced losses per span, which enables the use of single stage amplifiers instead of two stage amplifiers required in DCF-based transmission systems. As a result, mid-link OPC enables a simplified and cost efficient amplifier design.

In this thesis, the feasibility to use mid-link OPC for the compensation of chromatic dispersion as well as the compensation of nonlinear effects is assessed. An emphasis is placed on long-haul transmission systems as well as on the combination of mid-link OPC with advanced modulation formats.

1.2 Structure of this thesis

The structure of the thesis is as follows. In Chapter 2, the linear and nonlinear characteristics of a single-mode fiber are discussed that are relevant for long haul transmission systems. Chapter 3 provides an description of a conventional fiber-optic transmission system. Chapter 4 then covers several aspects of OPC-based transmission. Processes are described to realize OPC as well as the media with which these processes can be realized. Subsystems are discussed to create a polarization independent OPC. Finally OPC is described from a transmission perspective.

Several OPC-based transmission experiments are discussed in Chapter 5 using the amplitude-shift-keying (ASK) modulation format. Simulations and experiments are reported on the transmission performance of 10-Gbit/s transmission. Several 40-Gbit/s experiments are discussed. The compensation of nonlinear phase noise through OPC is assessed in Chapter 6. Through theory, simulation and experiment it is shown that nonlinear phase noise can be compensated for in an OPC-based transmission system.

Long-haul transmission experiments using 21.4-Gbit/s and 42.8-Gbit/s DQPSK are discussed in Chapter 7. In this chapter, the performance of an optimized conventional transmission system is compared to the performance of mid-link OPC. Chapter 8 summarizes the obtained results and conclusions are given. Finally, an outlook on OPC-based transmission systems is given in Chapter 9.

Chapter 2

Transmission impairments

In 1966, Kao *et al.* proposed to use glass fibers as a waveguide for long distance communication at optical frequencies [5]. Since its introduction, many different fiber types have been developed. Figure 2.1 shows a typical cross section of an optical fiber and the refractive index-profile. In this figure, the three main regions are depicted: the core, the cladding and the coating. The core is the center of the fiber, which is surrounded by a cladding with a slightly lower refractive index. For silica fibers, the core of the fiber typically has a refractive index of $n \approx 1.48$ and depending on the fiber type, the refractive index of the cladding is 0.2 to 3 percent lower [6]. The cladding confines the light into the core through total internal reflection and reduces the scattering loss at the core-cladding boundary. The coating or jacket of the fiber provides strength and protection. The refractive index-profile depicted in Figure 2.1 is that of a step-index fiber. Graded index fibers exist as well, where

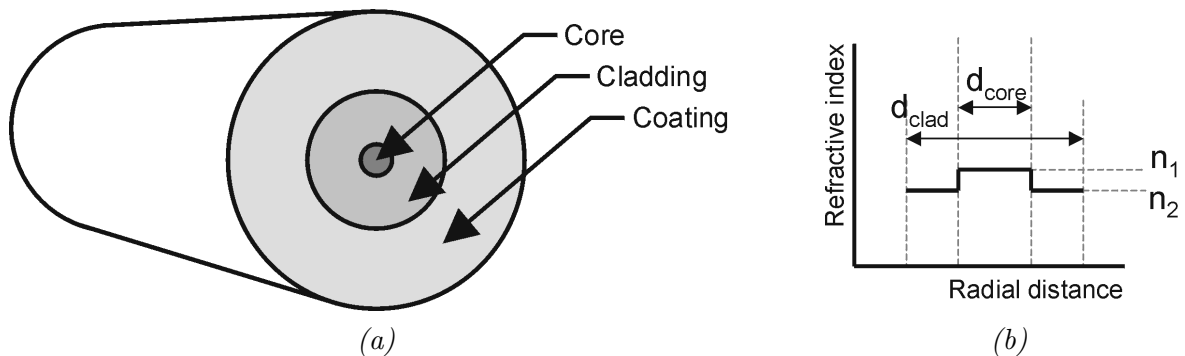


Figure 2.1: *Optical fiber, a) Cross section b) refractive index-profile.*

the refractive index within the core of the fiber is a function of the radius. Fibers are either designed for single-mode or multi-mode operation. In single-mode operation only one mode of propagation exists whereas in multi-mode operation many different modes (> 100) can be present. Whether single-mode or multi-mode propagation occurs in a fiber depends on the wavelength of the signal and the diameter of the core of the fiber. For the wavelengths used in long-haul transmission system, a typical core diameter is $d_{core} = 9 \mu\text{m}$ for single-mode and $d_{core} \geq 50 \mu\text{m}$ for multi-mode propagation [7]. The advantage of a

thick core is that it simplifies coupling light into the fiber and between fibers. However, the main disadvantage is that the different modes within the fiber have slightly propagation constants due to refractive index differences and thereby cause intermodal dispersion. Due to the intermodal dispersion, pulse spreading occurs when a signal travels along the fiber. In other words, intermodal dispersion limits the feasible transmission distance. For this reason, solely single-mode propagation is used in long-haul applications [8].

In this chapter impairments that are relevant for long-haul fiber-optic communication systems are discussed. An in-depth study of single-mode fibers can be found in [9]. The impairments discussed in this chapter can be divided into linear impairments such as fiber loss, chromatic dispersion and polarization mode dispersion and nonlinear impairments such as the Kerr-effect and non-elastic scattering effects.

2.1 Fiber loss

When an optical signal propagates through a fiber, its optical power is attenuated due to scattering loss and absorption. If P_{in} in $[W]$ is the optical power that is coupled into a fiber, the optical power $P(z)$ in $[W]$ at point z is given by [8]

$$P(z) = P_{in} \cdot \exp(-\alpha z) \quad (2.1)$$

where α is the attenuation coefficient in Neper per kilometer $[Np/km]$ and z represents the transmission distance in $[km]$. Equation 2.1 shows that due to fiber loss, the signal power decreases exponentially along the transmission line. Conventionally, the attenuation coefficient is expressed in $[dB/km]$, which is related to Neper by

$$\alpha_{dB} = \frac{10}{\ln(10)}\alpha \approx 4.343\alpha \quad (2.2)$$

Figure 2.2 shows the typical loss of a single-mode fiber as a function of the wavelength and the frequency. The wavelength (λ) and the frequency (f) of an optical signal are related according to $\lambda = c/f$, where $c = 2.998 \cdot 10^8$ m/s represents the speed of light in vacuum. The minimum loss for most silica fibers is obtained near a wavelength of 1550 nm. The transmission fiber with the lowest loss to date has an attenuation coefficient of $\alpha_{dB} = 0.1484$ dB/km, obtained at 1570 nm [10]. A typical attenuation coefficient for single-mode fibers is $\alpha_{dB} = 0.20$ dB/km [7].

Two fundamental loss mechanisms govern the loss profile of an optical fiber: Rayleigh scattering and intrinsic absorption [9]. Rayleigh scattering results from local microscopic fluctuations in the material density that are created during the manufacturing process. The density fluctuations lead to small variations within the refractive index of the glass, that cause scattering. The distances of these refractive index variations are significantly smaller than the optical wavelength. For large wavelengths (> 1660 nm), intrinsic absorption becomes the dominating loss mechanism that strongly increases the fiber attenuation. Intrinsic absorption is caused by vibrational resonances of the optical signal with the silica molecules of the fiber.

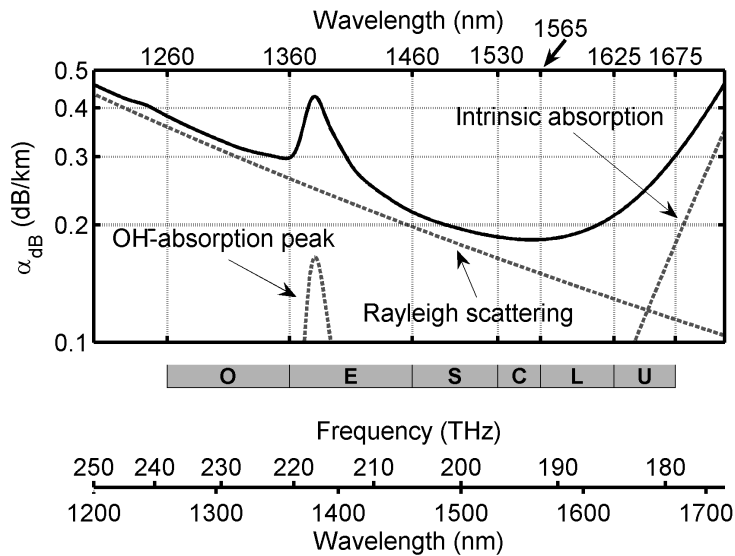


Figure 2.2: *Fiber attenuation as a function of the optical wavelength and frequency.*

Apart from Rayleigh scattering and intrinsic absorption, an absorption peak is present near 1400 nm caused by OH^- absorption in the fiber [6]. The OH^- absorption peak separates two low loss transmission regions at 1330 nm and at 1550 nm. However, the absorption peak is not a fundamental loss and can be eliminated by taking special precautions in the production of the fiber [11, 12].

Additional losses are caused by small defects, created during the manufacturing of the fiber, for instance: waveguide roughness at the core/cladding interface, crystallized regions in the glass, variation of the core radius along the fiber length, etc. Significant improvements in the manufacturing methods of optical fibers in the last decades have realized that the impact of these additional losses is small in practice [6].

In order to create a general framework for fiber-optic transmission, many different standards have been introduced. The telecommunication section of the standardization organization International Telecommunication Union (ITU-T) defined six bands for transmission using single-mode fiber [13]: the O, E, S, C, L and U-band. Figure 2.2 shows in addition to the fiber attenuation the wavelength ranges of these transmission bands. Most commercial transmission systems employ the conventional band (C-band), from 1530 nm to 1565 nm, where the fiber loss is the lowest. When more bandwidth is required, the transmission capacity can be increased by using the long-wavelength band (L-band), from 1565 nm to 1625 nm. Alternatively, the short-wavelength band (S-band) from 1460 nm to 1530 nm can be used. Due to the relatively high attenuation, the extended band (E-band) and the ultra long-wavelength band (U-band) are less interesting for most fiber-optic applications. As the name implies, the original band (O-band) was used in early long-haul transmission systems. Nowadays, practically no long-haul system employs the O-band. However, the O-band is used almost exclusively for the client interface in the access network [3, 14, 15, 16]. This thesis focuses on transmission in the C-band, since this band is

the most relevant for long-haul fiber-optic transmission systems [8].

2.2 Chromatic dispersion

The speed of light in a dielectric medium such as an optical fiber is lower than c . When v_p represents the phase velocity of an optical signal in a fiber, c is related to v_p as [17]

$$c = n \cdot v_p \quad (2.3)$$

where n is the refractive index of the dielectric medium. Since the refractive index of a fiber is dependent on the optical frequency, different spectral components of a pulse travel at different velocities. This phenomenon is called material dispersion. The effect of dispersion on a modulated signal can be described by considering the mode-propagation constant β , which is related to the refractive index according to [8, 6]

$$\beta(\omega) = n(\omega) \frac{\omega}{c} \quad (2.4)$$

where $\omega = 2\pi f$, in $[rad/s]$, represents the angular frequency of the optical signal. Expanding equation 2.4 in a Taylor series with respect to the center or reference frequency ω_0 gives [8, 2]

$$\beta(\omega) = n(\omega) \frac{\omega}{c} \approx \beta_0 + \beta_1(\omega - \omega_0) + \frac{1}{2}\beta_2(\omega - \omega_0)^2 + \frac{1}{6}\beta_3(\omega - \omega_0)^3 + \dots \quad (2.5)$$

where

$$\beta_m = \left. \frac{d^m \beta}{d\omega^m} \right|_{\omega=\omega_0} \quad (\text{for } m = 0, 1, 2, \dots) \quad (2.6)$$

In equation 2.5, β_0 in $[km^{-1}]$ represents a constant phase shift and β_1 in $[ps/km]$ corresponds to the group-velocity as $\beta_1 = 1/v_g$. β_2 in $[ps^2/km]$ and β_3 in $[ps^3/km]$ represent the group velocity dispersion (GVD) and dispersion slope, respectively. Instead of the propagation constant β_2 , it is more common to use the dispersion parameter D , related to β_2 as

$$D = -\frac{2\pi c}{\lambda^2} \beta_2 \quad (2.7)$$

The dispersion parameter D is expressed in $[ps/nm/km]$. The dispersion slope β_3 represents the change in dispersion as a function of the reference frequency ω_0 . Often, the dispersion slope parameter S is used instead of β_3 .

$$S = \frac{4\pi c}{\lambda^3} \beta_2 + \left(\frac{2\pi c}{\lambda^2} \right)^2 \beta_3 \quad (2.8)$$

where S is expressed in $[ps/nm^2/km]$ [8]. Apart from material dispersion, another important dispersion effect that occurs in single-mode fibers is waveguide dispersion. Waveguide

2.2. CHROMATIC DISPERSION

dispersion is caused by the fact that the optical field is not totally confined to the core of a fiber and thus partly propagates through the cladding [6]. And as the refractive index of the core and the cladding is different, waveguide dispersion arises. The contribution of the waveguide dispersion is dependent on fiber parameters such as the radius of the core and the difference in refractive index between the core and the cladding. Therefore, the fiber design determines the dispersion profile of the fiber.

In standard single-mode fiber (SSMF), the dispersion profile is mainly determined by the material dispersion. Only near so called zero dispersion wavelength λ_0 , where $D = 0$, both waveguide and material dispersion have a similar contribution. The zero dispersion wavelength of SSMF is present near 1320 nm [9]. In the C-band the dispersion parameter for SSMF varies between $D = 15\text{-}18$ ps/nm/km. The dispersion slope is typically $S = 0.06$ ps/nm²/km. By increasing the waveguide dispersion, the zero dispersion wavelength is shifted to longer wavelength. As a result, fiber types have been introduced where the zero dispersion wavelength is in or near the C-band, such as dispersion-shifted fiber (DSF) and non-zero dispersion-shifted fiber (NZDSF) [8]. Figure 2.3 depicts the dispersion as a function of the wavelength for these three fiber types. The thesis focuses on transmission

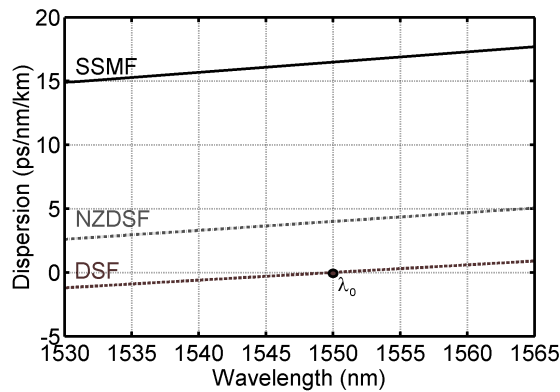


Figure 2.3: *The chromatic dispersion for different fiber types.*

through SSMF, since this is the most used fiber type in commercial transmission systems today.

By using waveguide dispersion in combination with a complex refractive index profile it is possible as well to create a fiber with the a negative dispersion parameter in the C-band, usually referred to as dispersion compensating fiber (DCF) [18]. DCF is widely used in fiber-optic transmission systems to compensate for chromatic dispersion and will be further discussed in Section 3.3

The propagation of a signal along the transmission fiber including fiber loss and chromatic dispersion is described by the linear Schrödinger equation (LSE) [8]

$$\frac{\partial A}{\partial z} = -\frac{\alpha}{2}A - \frac{j}{2}\beta_2\frac{\partial^2 A}{\partial T^2} + \frac{1}{6}\beta_3\frac{\partial^3 A}{\partial T^3} \quad (2.9)$$

where A represents the complex envelope of the optical field, z the propagation distance in km , α the attenuation coefficient in Neper and

$$T = t - \beta_1 z = t - z/v_g \quad (2.10)$$

the time measured in a retarded frame. The LSE describes the signal evolution with GVD and dispersion slope. Note that in equation 2.9 higher order dispersion terms are not considered and furthermore that polarization dependent effects are neglected.

In fiber-optic transmission systems, dispersion may lead to pulse spreading and thereby to inter-symbol interference (ISI). For an impulse with initial pulse width T_0 , the broadening through dispersion is characterized by the dispersion length, defined as [2]

$$L_D = \frac{T_0^2}{|\beta_2|} \quad (2.11)$$

The dispersion length L_D indicates when the pulse is broadened by a factor of $\sqrt{2}$ due to first β_2 order dispersion. The pulse width T_0 is inversely proportional to the data rate as $T_0 \propto 1/f_{data}$. As a result it can easily be seen from equations 2.11 that the impact of dispersion is dependent on the square of the data rate.

2.3 Polarization mode dispersion

Polarization mode dispersion (PMD) is caused by the fact that single-mode transmission fibers support two orthogonal polarization modes with different transmission characteristics [19, 20]. In an ideal fiber with isotropic material and circular symmetry, the properties of both modes are identical. However, in practice the core of the fiber is not fully circular in geometry and the material is not fully isotropic, which leads to birefringence Δn . If x and y denote the two orthogonal polarization states, Δn can be expressed as [20]

$$\Delta n = \frac{|\beta_{1,x} - \beta_{1,y}|}{k_0} = |n_x - n_y| \quad (2.12)$$

where $k_0 = 2\pi/\lambda$. For a fiber with $n_x < n_y$, the orthogonal polarization mode with the smaller mode index (n_x) is referred to as “fast axis” and the orthogonal polarization mode with the larger mode index (n_y) “slow axis”. The first order PMD is commonly referred to as the differential group delay (DGD). The principle of DGD is shown in Figure 2.4 for a fiber with a constant birefringence. When two pulses travel a distance L , one pulse along the fast and one pulse along the slow axis of the transmission fiber, the arrival time difference $\Delta\tau$ of the two pulses at the output of the fiber is the DGD

$$\Delta\tau = |\beta_{1,y} - \beta_{1,x}| L = \frac{\omega\Delta n}{c} \quad (2.13)$$

However, for real transmission fiber, the birefringence changes randomly over time, frequency and fiber length due to environmental changes such as stress induced fluctuations

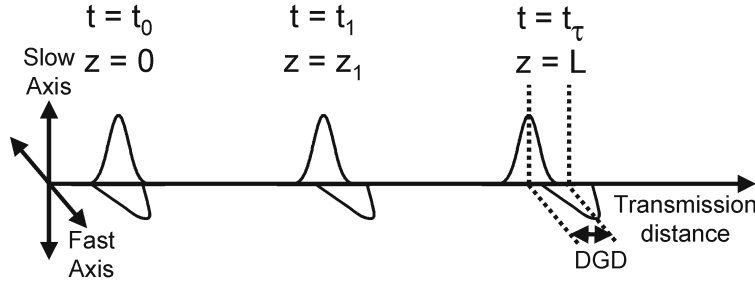


Figure 2.4: DGD due to birefringence of an optical fiber.

of the shape of the core, temperature changes, etc. [2]. As a result, PMD is a stochastic process with a non-constant DGD value. The expected DGD value, $E\{\Delta\tau\}$, is referred to as the PMD value and is related to the DGD as $E\{\Delta\tau\} = \overline{\Delta\tau}$, where $\overline{\Delta\tau}$ represents the mean DGD value. The probability density function for the DGD, $p(\Delta\tau)$, can be characterized by a Maxwellian distribution [19]

$$p(\Delta\tau) = \sqrt{\frac{2}{\pi}} \frac{(\Delta\tau)^2}{q^3} \exp\left(-\frac{(\Delta\tau)^2}{2q^2}\right) \quad (2.14)$$

where $q = \sqrt{\frac{\pi}{8}} E\{\Delta\tau\}$. The frequency dependence of the DGD, $\Delta\tau$, causes higher order PMD effects. As illustrated in Figure 2.4, PMD impairs the performance of a transmission system through ISI. The impact of DGD scales with the data rate. Higher data rates go along with smaller bit-slots and therefore more ISI occurs with the same DGD. For long-haul transmission systems, the PMD increases due to its random birefringence behavior with the square root of the transmission distance. The PMD-coefficient k_{PMD} can in this case be expressed by [19]

$$k_{PMD} = E\{\Delta\tau\} / \sqrt{L} \quad (2.15)$$

where k_{PMD} is expressed in $[ps/\sqrt{km}]$. The PMD-coefficient of a fiber is a measure for the quality of the fiber. PMD is especially problematic when old fibers with a high PMD coefficient ($k_{PMD} \approx 0.5 ps/\sqrt{km}$) are used for transmission. In this case, PMD compensation schemes can be employed to enable high-bitrate transmission [21]. In the transmission experiments conducted in this thesis, high quality transmission fibers were used with a low PMD value ($k_{PMD} < 0.1 ps/\sqrt{km}$), therefore no PMD compensation is required.

2.4 Kerr effect

The Kerr effect causes a change in the refractive index of a material in response to an electric field. As a result, the Kerr effect distorts the phase of an optical signal. As an optical fiber is a nonlinear medium, the relation between the total polarization \mathbf{P} induced

by electric dipoles and the electric field \mathbf{E} can be described by [20]

$$\mathbf{P} = \epsilon_0 \left(\chi^{(1)} \cdot \mathbf{E} + \chi^{(2)} : \mathbf{E}\mathbf{E} + \chi^{(3)} : \mathbf{E}\mathbf{E}\mathbf{E} + \dots \right) \quad (2.16)$$

where ϵ_0 is the permittivity of vacuum and $\chi^{(n)}$ is the n^{th} order susceptibility ($n = 1, 2, 3, \dots$). The contributions of susceptibilities higher than the 3rd order are in general small in transmission systems and can be neglected. $\chi^{(1)}$, the linear susceptibility, is responsible for the linear behavior of the fiber and includes effects like fiber loss and material dispersion. This is the main contribution to \mathbf{P} . For low optical signal powers, all higher order susceptibilities can be neglected. The second order susceptibility $\chi^{(2)}$ causes for instance difference frequency generation (DFG). This nonlinear effect can be employed in a periodically-poled lithium-niobate (PPLN) waveguide to phase conjugate an optical signal, as further discussed in Section 4.1. The silica glasses used for optical fibers have a symmetric molecule structure (SiO_2), therefore nonlinear effects due to the second order susceptibility are negligible [20]. The third order susceptibility $\chi^{(3)}$ is responsible for the Kerr effect. Due to the third order susceptibility, the refractive index n of an optical fiber is dependent on the optical power $|A|^2$ of the transmitted signal and can be expressed as [6]

$$n(\omega, |A|^2) = n_0(\omega) + n_2 \frac{|A|^2}{A_{eff}} \quad (2.17)$$

where A_{eff} is the effective mode area of the fiber and $n_0(\omega)$ and n_2 are the linear and nonlinear refractive index, respectively. By adding a term for the Kerr effect to equation 2.9, the propagation of a signal along the transmission fiber is described by the nonlinear Schrödinger equation (NLSE) [2]

$$\frac{\partial A}{\partial z} = -\frac{\alpha}{2}A - \frac{j}{2}\beta_2 \frac{\partial^2 A}{\partial T^2} + \frac{1}{6}\beta_3 \frac{\partial^3 A}{\partial T^3} + j\gamma |A|^2 A \quad (2.18)$$

where the nonlinear coefficient γ is expressed in [$W^{-1}km^{-1}$] and defined as

$$\gamma = \frac{n_2\omega_0}{c A_{eff}} \quad (2.19)$$

Similar to equation 2.9, higher order dispersion terms and polarization dependent effects are not considered. From equation 2.18 it can be concluded that the impact of the Kerr effect is proportional to the optical signal power $|A|^2$. As the signal power exponentially reduces along a transmission line due to the fiber attenuation, the influence of the Kerr effect is the strongest in the first part of the fiber. This first part of the fiber is usually referred to as the high power region. For a fiber with length L , the high power region is defined by the effective length L_{eff} [2]

$$L_{eff} = \frac{1 - \exp(-\alpha L)}{\alpha} \quad (2.20)$$

The effective length of a 100-km SSMF with an attenuation coefficient of $\alpha = 0.2$ dB/km is $L_{eff} = 21.5$ km. In these first 21.5 km, practically all chirp through the Kerr effect is introduced. Figure 2.5 illustrates the envelope of the signal power as a function of the transmission distance. In this figure, the effective length is depicted as well as the high power region.

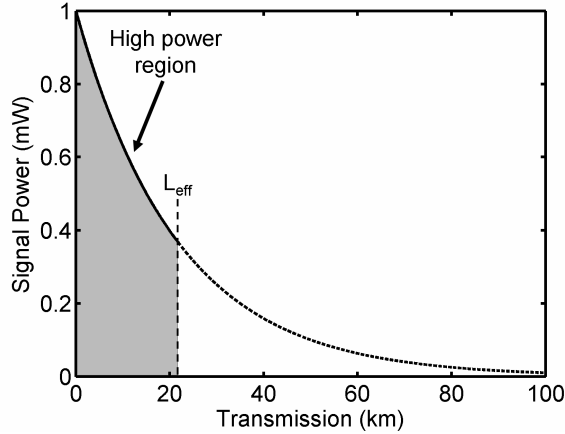


Figure 2.5: *Signal power as a function of the transmission distance.*

The impact of the Kerr-effect on a transmission system with length L is given by the nonlinear length L_{NL} , which is defined as

$$L_{NL} = \frac{1}{\gamma \cdot P_{in}} \quad (2.21)$$

where P_{in} is the optical power launched into the fiber and γ the fiber's nonlinear coefficient. In general it can be said that the Kerr-effect does not introduce significant system impairments when the nonlinear length is well below the system length $L_{NL} \ll L$ [20].

2.4.1 Self-phase modulation

The dependence of the refractive index on the intensity, causes an intensity dependent phase shift to the signal, referred to as self-phase modulation (SPM). The impact of SPM can be studied by neglecting the effects of chromatic dispersion ($\beta_2 = \beta_3 = 0$) in the NLSE equation (equation 2.18) [20]

$$\frac{\partial A}{\partial z} = -\frac{\alpha}{2}A + j\gamma|A|^2 A \quad (2.22)$$

The solution of this equation is given by

$$A(z, T) = A(0, T) \cdot \exp(-\alpha z/2) \cdot \exp\left(j\Phi_{SPM}(z, T)\right) \quad (2.23)$$

where $A(0, T)$ represents the field amplitude at $z = 0$ and the SPM induced phase modulation Φ_{SPM} is defined as

$$\Phi_{SPM}(z, T) = \gamma |A(0, T)|^2 L_{eff} \quad (2.24)$$

where L_{eff} is the effective length as defined in equation 2.20. An amplitude modulated signal is phase modulated by SPM, which at its turn causes broadening of the signal's spectrum. It can be concluded from equation 2.23 that SPM only affects the phase of the signal, not its shape. As stated before, the effect of chromatic dispersion is neglected. Through the interplay of chromatic dispersion with SPM, phase distortions are converted to amplitude distortion. Equation 2.24 shows that the phase shift introduced by SPM is proportional to the nonlinear coefficient γ , the signal power $|A(0, t)|^2$ and the effective length L_{eff} [6].

The GVD of SSMF is negative in the anomalous regime ($\beta_2 < 0$) where GVD induced chirp is the inverse of the SPM induced chirp. As a result, GVD can (partly) compensate for the effect of SPM. A total compensation of SPM is obtained for soliton transmission where distortion free transmission can be realized [22, 23]. However, soliton transmission requires a small amplifier spacing (≈ 50 km) [23]. Furthermore, the use of solitons in WDM transmission systems is not straightforward [24]. In WDM systems dispersion management can be used to minimize impairments through SPM as further discussed in Chapter 3.

2.4.2 Cross-phase modulation

Cross-phase modulation (XPM) occurs in WDM transmission systems. The mechanism behind XPM is similar to SPM: due to the intensity dependent refractive index, power fluctuations in a WDM channel are converted into phase fluctuations in other (co-)propagating WDM channels [2]. The XPM induced phase fluctuations are subsequently converted to intensity fluctuations through chromatic dispersion. Additionally, XPM scales with the walk-off length which is defined as the propagation length for which a faster moving pulse is shifted by one bit with respect to a slower moving pulse of a co-propagating channel. The walk-off length, L_W , for two channels located at λ_1 and λ_2 is [6]

$$L_W = \frac{T_B}{|d_{12}|} \quad (2.25)$$

where T_B is the bit period and d_{12} is the walk-off parameter, defined as:

$$d_{12} = 1/v_{g1} - 1/v_{g2} = D\Delta\lambda \quad (2.26)$$

where $1/v_{g1}$ and $1/v_{g2}$ are the group velocities of the two channels and $\Delta\lambda = |\lambda_1 - \lambda_2|$. XPM is most severe when the difference in GVD of the channels is small so that the neighboring WDM channels propagate almost completely synchronous along the transmission line. In practice this occurs when the channel spacing between the WDM channels is small or when the dispersion coefficient of the fiber is low. When the difference in GVD is large (high walk-off parameter), the induced phase fluctuation of a certain bit is spread

over several bits of the neighboring channels and hence the XPM-induced impairments are small. From equation 2.25 it can be concluded as well that XPM scales with the pulse width and thereby with the data rate. The higher the data rate, the smaller the pulse width and hence the smaller the walk-off length. At data rates of 40 Gbit/s and higher the influence of XPM can be neglected in most cases [25]. Finally, XPM is dependent on the polarization of the WDM channels. The XPM effect is the strongest for co-polarized and the weakest for orthogonal polarized (interleaved) WDM channels [20].

2.4.3 Four-wave mixing

Four-wave mixing (FWM) is a mixing process where three waves, co-propagating along a fiber, generate an optical wave at a fourth frequency. In the quantum mechanical picture, photons from one or more wavelengths are annihilated to be replaced by photons at different frequencies. As the name implies, four photons take part in the FWM process. Since the net energy is conserved, the FWM frequency ω_{FWM} that is generated by three frequencies at ω_1 , ω_2 and ω_3 , can be expressed by [6]

$$\omega_{FWM} = \omega_1 \pm \omega_2 \pm \omega_3 \quad (2.27)$$

The most efficient and thereby most observed variant of FWM is [20, 6]

$$\omega_{FWM} = \omega_1 + \omega_2 - \omega_3 \quad (2.28)$$

FWM only occurs when the phases between the interacting signals are matched. However, due to chromatic dispersion, the phase-velocity is not the same for all interacting signals. The smaller the difference in phase-velocity, the better the phase matching between different WDM channels is and hence the stronger the FWM generation. Therefore, FWM is mostly a problem for transmission systems with low dispersive fibers (e.g. DSF, NZDSF, etc.) and at narrow channel spacings. For fibers with a high dispersion in the C-band such as SSMF, FWM does in general not limit the transmission performance and can be neglected [20].

Similar to XPM, FWM is a multi-channel effect and dependent on the optical power, polarization and channel spacing of the WDM channels. FWM especially becomes problematic with even frequency-spaced WDM channels. In this case the FWM products are generated within the neighboring channels.

2.4.4 Intra-channel XPM and intra-channel FWM

Intra-channel cross-phase mixing (IXPM) and intra-channel four-wave mixing (IFWM) are in general the dominating impairments for transmission systems in the pseudo linear regime [26, 25]. The pseudo linear regime is the regime where due to the high data rate, large pulse spreading occurs through dispersion. At data-rates of ≥ 40 Gbit/s the transmission for SSMF is mostly in the pseudo linear regime. In this regime, the dispersion length is significantly smaller than the nonlinear length ($L_D \ll L_{NL}$) [27]. Therefore, the pulses

are spread before SPM, FWM or XPM can take place. The regime is called pseudo linear since, similar to linear transmission, the optimum residual dispersion for single channel transmission is near 0 ps/nm. Similar to SPM, as discussed in Section 2.4.1, IXPM and IFWM are intra-channel impairments originating from the Kerr effect. With SPM (or sometimes referred to as ISPM) the amplitude change of a bit induces phase fluctuations mostly within its own bitslot whereas with IXPM and IFWM through the large bit-spread, bit to bit interactions occurs.

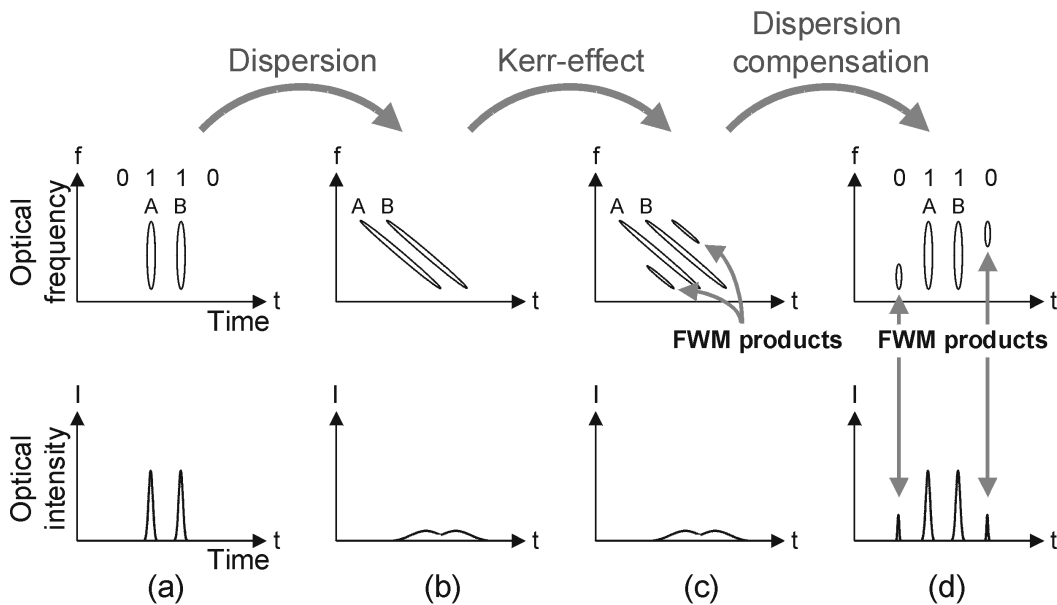


Figure 2.6: *Principle of intra-channel FWM (after [26]).*

The principle of intra-channel FWM is depicted in Figure 2.6. The upper row of plots illustrates the optical spectrum as a function of time. The lower row of plots depicts the optical signal power of the waveform as a function of time. Consider a return-to-zero (RZ) signal modulated with the sequence '0, 1, 1, 0' (Figure 2.6a). Because of the dispersion of the fiber, a large pulse spreading occurs and thereby the two pulses 'A' and 'B' overlap (Figure 2.6b). Due to the pulse overlap, pulses 'A' and 'B' interact through the Kerr effect and produce two four-wave mixing products (Figure 2.6c). After transmission, when the dispersion is compensated for, two 'ghost pulses' will be present in the neighboring bitslots due to IFWM (Figure 2.6d) [27].

The principle of IXPM is similar to that of IFWM. However, IXPM generates a frequency shift due to the intensity change of the overlapping bits. Through dispersion, the IXPM induced frequency shift is then converted into timing jitter [27].

2.5 Non-elastic scattering effects

Apart from the Kerr effect based nonlinear impairments, two non-elastic scattering effects can impair fiber-optic transmission systems, namely stimulated Raman scattering (SRS) and stimulated Brillouin scattering (SBS). These nonlinear impairments are caused by an interaction of light with the Silica molecules of the transmission fiber.

2.5.1 Stimulated Raman scattering

Stimulated Raman scattering (SRS) is an interaction of the photons of an optical signal with the molecular vibrations (optical phonons) of the transmission medium [28]. When a photon is incident on a molecule of the transmission fiber's silica, in most cases it is scattered elastically through Rayleigh scattering. The scattered photon then has the same energy as the incident photon. However, for a small fraction of the photons ($\approx 10^{-6}$), Raman scattering occurs and as a result these photons are scattered at optical frequencies that differ from the incident photon [20]. What happens in this case is that the molecule absorbs some energy of the incident photon. As a result, the scattered photon has a lower energy and thus a lower frequency than the incident photon. The scattered photon is referred to as the Stokes photon [28].

When co-propagating channels are present within the Raman bandwidth, amplification through stimulated emission can occur. In this case SRS causes a power transfer from shorter to longer wavelengths channels. The principle of stimulated emission is the same as used in other optical amplifiers such as EDFAs and SOAs. The efficiency of the power transfer through SRS is dependent on the wavelength and can take place for channels placed up to 125 nm apart [28]. Stimulated emission through SRS is strongly polarization dependent and only occurs when the optical power of the shorter wavelength is above a certain threshold (SRS threshold). Above this threshold, the amplification through stimulated emission scales exponentially with the power of the shorter wavelength. This effect can be used to create Raman amplifiers [2]. Raman amplification is further discussed in Section 3.2.

In a WDM transmission system SRS results in unwanted crosstalk. This crosstalk can be distinguished into a bit pattern dependent and a time averaged SRS crosstalk. Bit pattern dependent SRS is similar to XPM dependent on the walk-off between the different WDM channels. In general it can be said that for highly dispersive fibers, the influence of bit pattern dependent SRS is relatively small [29]. The principle of time averaged SRS in a WDM transmission system is depicted in Figure 2.7 for four co-propagating channels. Before transmission, all four channels have the same optical power. Due to SRS, optical power is transferred from λ_1, λ_2 (shorter wavelengths) to λ_3, λ_4 (longer wavelengths). As a result, the gain of the WDM spectrum is tilted [30, 31]. In fiber-optic transmission systems, this gain tilt can be compensated for by a gain-tilt filter or a dynamic gain equalizer (DGE).

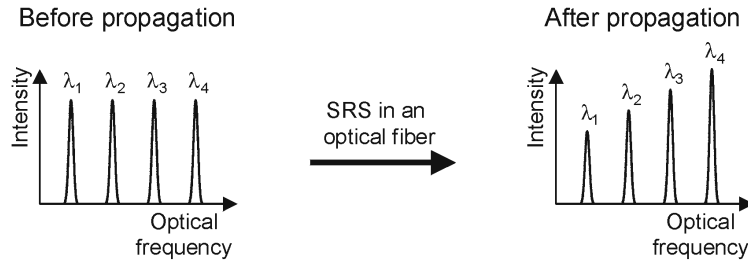


Figure 2.7: *Principle of SRS.*

2.5.2 Stimulated Brillouin scattering

Stimulated Brillouin scattering (SBS) originates from an interaction of an optical signal with acoustic waves (acoustical phonons). Similar to SRS, a Stokes wave at longer wavelength is generated. However, SBS creates effectively a reflection grating. As a result, the Stokes wave generated through SBS propagates in the backward direction, counter propagating to the optical signal. The wavelength shift of the Stokes wave compared with the transmitted lightwave is ≈ 0.1 nm, significantly smaller than the wavelength shift due to SRS [6].

In communication systems employing modulation formats with a strong optical carrier (e.g. on-off keying) SBS limits the maximum power that can be launched into a transmission fiber. The gain of SBS has a narrow bandwidth of around 20 Mhz. Therefore, the generation of SBS is significantly reduced by spreading the carrier signal's energy over a wider bandwidth through modulation of the laser source. This can be either realized by directly modulating the phase of the laser source or by an external optical phase modulator. For modulation formats without a strong carrier (e.g. DPSK) SBS can be neglected.

2.6 Summary

In this chapter, relevant impairments for single-mode fibers in fiber-optic transmission systems were discussed. The attenuation, mainly caused by Rayleigh scattering and intrinsic absorption, is a fundamental property of the transmission fiber. As a result, the signal power decreases exponentially along the transmission line in the linear regime. This thesis focuses on transmission in the C-band, where the minimum loss of a single-mode fiber is obtained.

Chromatic dispersion is caused by material and wavelength dispersion. The wavelength dependence of the refractive index causes material dispersion. Wavelength dispersion originates from the difference in refractive index between the core and the cladding of a fiber. The chromatic dispersion at a certain wavelength can be characterized by the dispersion parameter and the dispersion slope. The chromatic dispersion varies per fiber type. SSMF with $\lambda_0 = 1320$ nm is the most used fiber type installed today and used in all transmission experiments described in this thesis.

PMD is caused by birefringence of the transmission fiber. The amount of PMD is not static for a fiber, but changes depending on temperature, mechanical stress, etc. The impact of first order PMD scales linearly with the bitrate and is dependent on the quality of the transmission fiber. PMD is especially problematic for high bitrate transmission over old fibers. In the transmission experiments described in this thesis, high quality fibers are used, therefore PMD does not limit the transmission performance.

The Kerr effect originates from the dependence of the refractive index on the signal power of the optical signal. The impairments, caused by the Kerr effect, can be divided into intra-channel and inter-channel nonlinear impairments. Intra-channel nonlinear impairments (SPM and IXPM/IFWM) are mostly dominating in single channel links and WDM systems with wide channel spacing or high data rate (≥ 40 Gbit/s). Inter-channel nonlinear impairments (XPM and FWM) are in general dominating for WDM systems (< 40 Gbit/s) with narrow channel spacing.

Apart from the Kerr effect two non-elastic scattering effects occur in optical fibers: SRS and SBS. In high bitrate transmission systems SRS results mainly in a time averaged crosstalk. This crosstalk can be compensated by using a gain-tilt filter or dynamic gain equalizer. SBS limits the maximum optical power for signals with a strong optical carrier. A common method to significantly reduce the influence of SBS is by modulating the phase of the signal's carrier with a sine wave of ≈ 20 MHz.

The next chapter will discuss the configuration of a fiber-optic transmission system. In long-haul transmission systems, fiber loss and chromatic dispersion need to be compensated for. Furthermore, the dispersion compensation along the transmission link can be optimized to reduce the impact of nonlinear impairments.

Chapter 3

Fiber-optic transmission systems

Many different types of fiber-optic transmission systems exist and in general it can be said that the configuration of access, metro and long-haul networks are all totally different. In this section a WDM long-haul transmission system is discussed. Figure 3.1 depicts such a transmission system for the NRZ-ASK modulation format. In this chapter, several relevant aspects of the transmission link are discussed. The transmitter and receiver structure are assessed in Section 3.1. The compensation of fiber loss and chromatic dispersion are treated in Section 3.2 and Section 3.3, respectively. Subsequently, in Section 3.4 different modulation formats that are used in this thesis are discussed.

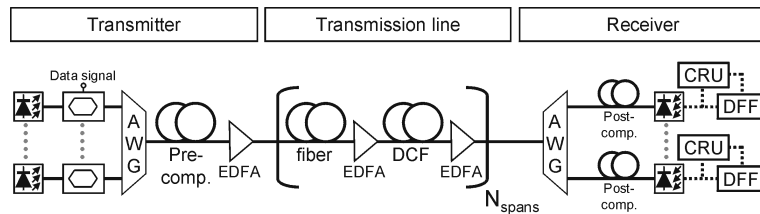


Figure 3.1: Configuration of a fiber-optic transmission system.

3.1 Transmitter and receiver

At the transmitter, the electric signal is converted into the optical domain. For this conversion either a direct modulated laser (DML) or an external modulator can be used. The main advantages of DMLs are that they are cost effective and produce a high output power. Transmission with DMLs has been reported up to 40 Gbit/s [32]. However, DMLs introduce chirp in the optical signal and have a relatively low extinction ratio at high data rates. Thus in practice, DMLs are mostly used in metro and access networks. External modulators can be manufactured to be almost chirp-free. Additionally, external modulators offer significantly higher extinction ratios than DMLs and are therefore the modulator of choice for long-haul transmission systems. In most transmission systems, external modulation is

realized by cascading a distributed feedback (DFB) laser and a Mach-Zehnder modulator (MZM).

The capacity of the transmission link can be increased by employing WDM, where multiple channels at different wavelengths are multiplexed and transmitted over the same fiber. An example of a WDM transmitter using external modulation is depicted in Figure 3.1. Optical signals of different wavelengths are combined by a multiplexer. The most frequently used techniques to optically multiplex multiple WDM channels are arrayed waveguide gratings (AWG) and thin-film filters [33, 8]. As these filters are passive, they are also used for demultiplexing at the receiver. The separation of the WDM channels varies per transmission system. Common channel spacings are 100 GHz and 50 GHz. The spacing of the WDM channels and the bit rate per channel define the transmission capacity. Often, the spectral efficiency is a figure of merit to the maximum transmission capacity obtainable for a certain optical bandwidth. The spectral efficiency is expressed in $[bit/s/Hz]$ and defined as the channel bit rate (B) divided by the channel separation (Δf).

Several standards have been introduced for fiber-optic transmission systems. The standard signal format for this system in North America is called synchronous optical network (SONET) where the data rate is expressed in optical carrier levels (OC). In Europe the synchronous digital hierarchy (SDH) is used, which expresses the data rate using synchronous transport module levels (STM). Table 3.1 provides an overview of the various SONET/SDH data rates. Commercial long-haul transmission systems employ data rates of 2.5 Gbit/s (STM-16), 10 Gbit/s (STM-64) and 40 Gbit/s (STM-256).

SONET level	SDH equivalent	Line rate (Mb/s)
OC-1	—	51.84
OC-3	STM-1	155.52
OC-12	STM-4	622.08
OC-48	STM-16	2,488.32
OC-192	STM-64	9,953.28
OC-768	STM-256	39,813.12

Table 3.1: Overview of SONET and SDH bit rates

In modern transmission systems, forward error correction (FEC) is employed to increase the robustness of the transmission link. FEC is a technique where redundant information is added to the data signal, which is used at the receiver to detect and correct bit-errors. A transmission link can be considered “error-free” when the BER is smaller than $1 \cdot 10^{-13}$ after transmission. Using a concatenated FEC code (RS(255,247) + RS(247,239)) with a 7% redundancy, an uncorrected bit error ratio (BER) of $2.3 \cdot 10^{-3}$ or lower results in a BER of smaller than $1 \cdot 10^{-13}$ after FEC [34]. Hence, the threshold for error-free transmission can be increased from $1 \cdot 10^{-13}$ to $2.3 \cdot 10^{-3}$ through FEC. Throughout this thesis the RS(255,247) + RS(247,239) FEC threshold of $2.3 \cdot 10^{-3}$ will be used as the maximum BER for error-free transmission.

In the transmission system shown in Figure 3.1 an AWG is used at the receiver to demultiplex the WDM channels. In laboratory experiments, often a channel-selection filter (CSF) is used instead of the AWG. A CSF is a band-pass filter (BPF) with a high roll-off factor, with which apart from the selected channel, all other WDM channels are suppressed. The advantage of a CSF is that the center frequency of the filter can be optimized to obtain the maximum BER performance. Furthermore, in some CSF filters the width of the filter can be adjusted as well.

The residual dispersion has a considerable influence on the BER performance. As will be discussed in Section 3.3, post compensation is applied to optimize the residual dispersion for the best BER performance. For transmission systems where the difference in residual dispersion is small after transmission, dispersion compensation can be performed for all channels at the same time, before the demultiplexer. Alternatively, per channel dispersion compensation has to be used.

The signal is converted from the optical to the electric domain via a photodiode. The current generated by the photodiode is proportional to the optical signal power. An important parameter that characterizes the performance of the photodiode is the responsivity R in units of $[A/W]$. Given an incident optical signal with intensity $I(t)$ and optical power $P(t)$, the generated current by the photodiode $i_p(t)$ is

$$i_p(t) = R \cdot P(t) \tag{3.1}$$

After the signal is converted to the electrical domain, it is split and one branch is fed to a clock recovery unit (CRU). The other branch is fed to a D-flip-flop (DFF), which is used as comparator.

3.2 Loss compensation

In long-haul transmission systems, optical amplifiers are employed to compensate for the fiber loss. In most fiber-optic transmission systems, erbium-doped fiber amplifiers (EDFA) are used every 80 km to 100 km to regenerate the power of the optical signals. When P_{in} is the optical power launched into the amplifier, the optical power at the output P_{out} is given by

$$P_{out} = G \cdot P_{in} \tag{3.2}$$

where G represents the gain of the amplifier. The amplification principle of EDFAs is based on stimulated emission, which is further discussed in [35, 36]. A side effect of the amplification process is that amplified spontaneous emission (ASE) is added to the signal. The amount of ASE noise that is present in a signal is given by the optical signal-to-noise ratio (OSNR). The OSNR is defined as the power ratio between the signal (relevant information) and the noise. For a given bandwidth, the OSNR of a signal can be described with

$$OSNR = \frac{P_{signal}}{P_{noise}} \tag{3.3}$$

where P_{signal} in $[W]$ is the total signal power and P_{noise} in $[W]$ is the power of the noise within a reference bandwidth. A common value for the reference bandwidth, usually referred to as resolution bandwidth, is 0.1 nm. Similar to equation 3.3, when a signal without ASE noise is amplified by an EDFA, the OSNR at the output of the EDFA is defined by [8]

$$OSNR = \frac{P_{out}}{P_{ASE}} \quad (3.4)$$

where P_{ASE} is the power of the ASE noise that is generated by the EDFA. As the amplification spectrum of the EDFA is smooth within the reference bandwidth, the amplification spectrum can be assumed constant. Per polarization mode, the power spectral density N_{ASE} of the EDFA can then be expressed by [35]

$$N_{ASE} = n_{sp}hf_0(G - 1) \quad (3.5)$$

where h is Planck's constant ($6.6256 \cdot 10^{-34}$ Js), n_{sp} is the spontaneous emission factor of the amplifier and f_0 the reference frequency in $[GHz]$. Within the reference bandwidth B_0 , the optical power of the noise for both polarizations can be expressed by [35]

$$P_{ASE} = 2N_{ASE}B_0 \quad (3.6)$$

where the reference bandwidth B_0 is expressed in $[GHz]$. The OSNR after amplification can then be expressed by

$$OSNR = \frac{P_{out}}{2n_{sp}hf_0B_0(G - 1)} \quad (3.7)$$

An indication of the degradation of the OSNR by the amplifier is given by the noise figure F . Considering a signal with only shot noise (no ASE) at the input and neglecting shot noise and ASE-to-ASE beat noise at the output of the amplifier, the noise figure can be expressed as [2, 27]

$$F = \frac{SNR_{in}}{SNR_{out}} = \frac{2n_{sp}(G - 1) + 1}{G} \quad (3.8)$$

where both SNR_{in} and SNR_{out} are electrical signal-to-noise ratios, determined after converting the optical signal to the electrical domain with a photodiode. In the high-gain region (generally speaking a gain of $G > 5$ dB), the noise figure of an EDFA is higher than 3 dB. Typical values for the noise figure are $F = 5-8$ dB [35].

By substituting equation 3.8 in 3.7, the OSNR after amplification can be expressed as

$$OSNR = \frac{P_{out}}{(FG - 1)hf_0B_0} = \frac{GP_{in}}{(FG - 1)hf_0B_0} \quad (3.9)$$

For a constant output power (P_{out}), equation 3.9 shows that the OSNR decreases with the amplifier gain. Signals with a low optical power require a higher amplifier gain. The

higher amplifier gain is required, the more ASE is added during the amplification process and thus the smaller the OSNR after amplification will be. It can therefore be concluded that the lower the input power is, the higher the OSNR degradation of the amplifier is.

Equation 3.9 is a valid consideration for amplification using one EDFA. However, in a long-haul transmission system, many EDFAs are cascaded to compensate for the fiber loss. In such a transmission link, the ASE noise accumulates. Under the assumption that all spans have the same span loss, the ASE noise after transmission with a chain of N_{spans} identical amplifiers is expressed by

$$P_{ASE} = N_{spans} \cdot P_{ASE}^0 \quad (3.10)$$

where P_{ASE}^0 represents the amount of ASE noise added by one amplifier. By combining equation 3.9 and equation 3.10, the OSNR in [dB] after transmission can be written as

$$\begin{aligned} OSNR[dB] &= 10\log\left(\frac{P_{out}}{N_{spans}(FG-1)hf_0B_0}\right) \\ &= P_{out}[dB] - 10\log(N_{spans}) - 10\log(hf_0B_0) - 10\log(FG-1) \end{aligned} \quad (3.11)$$

In most transmission systems, the OSNR is given with a 0.1-nm resolution bandwidth, which results at a reference frequency of $f_0 = 193.4$ THz (1550 nm) in $B_0 = 12.5$ GHz. In this case, the term $-10\log(hf_0B_0)$ equals 58 dBm. Assuming transmission spans of 80 km or more, with a span loss of more than 16 dB (80 km · 0.2 dB/km), the term $10\log(FG-1)$ approximately equals $10\log(FG)$ and equation 3.11 is then written as

$$OSNR[dB] = 58 \text{ dBm} + P_{in}[dB] - 10\log(N_{spans}) - F[dB] \quad (3.12)$$

From equation 3.12 it can be concluded that the OSNR in dB declines logarithmically with the number of amplifiers in the transmission line. Furthermore, the OSNR increases with the output power of the amplifier (P_{out}), which is proportional to the signal power launched into the transmission fiber. However, a higher launch power into the fiber will result in an increased influence of nonlinear effects. Hence, a trade-off exists between the OSNR after transmission and the amount of nonlinear effects generated along the transmission line.

Apart from EDFAs, Raman amplifiers can be used to compensate for fiber loss [28]. The gain medium for a Raman amplifier is the transmission fiber. Amplification is realized by inserting a strong CW pump signal into the transmission fiber that amplifies the optical signal through the Raman effect (see Section 2.5.1). Two types of Raman amplifiers exist, namely a forward (co-propagating) and a backward (counter-propagating) pumped Raman amplifier. Figure 3.2 depicts the power envelope along a transmission fiber with and without Raman amplification for both Raman configurations.

The optical power of the forward pumped Raman scheme $P_p^+(z)$ as a function of the transmission distance z is given by [2]

$$P_p^+(z) = P_p(0)\exp[-\alpha_p z] \quad (3.13)$$

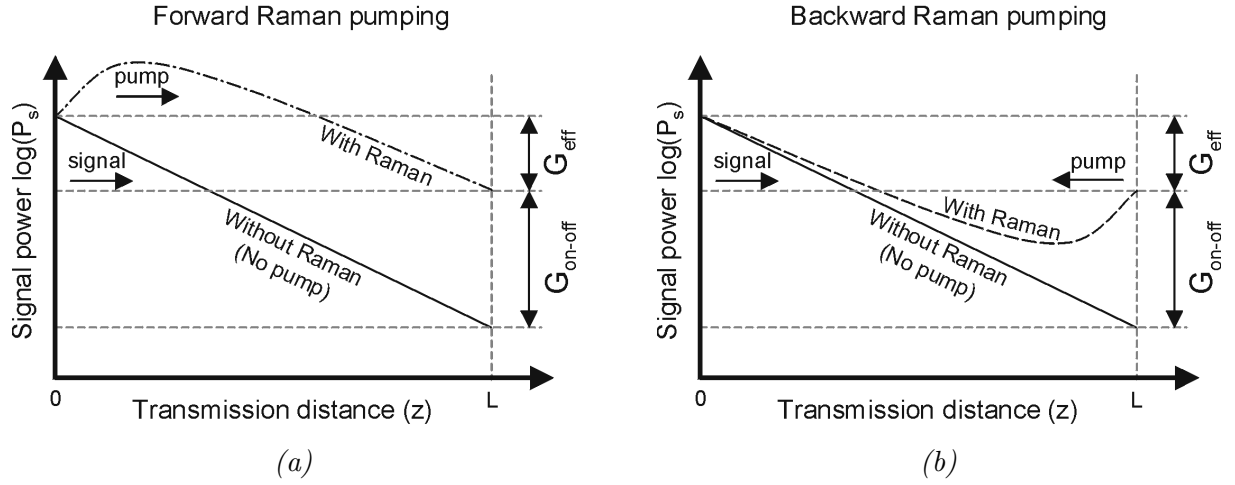


Figure 3.2: Optical signal power as a function of the transmission distance for Raman amplification. a) forward pumping, b) backward pumping

where α_p is the attenuation coefficient at the pump wavelength and $P_p(0)$ represents the optical power in [W] of the Raman pump at the input of the transmission fiber ($z=0$). The envelope of the signal power $P_s(z)$ is then given by [28]

$$P_s(z) = P_s(0) \exp \left\{ \frac{g_R}{A_{eff}} P_p(0) \frac{1}{\alpha_p} [1 - \exp(-\alpha_p z)] - \alpha_s z \right\} \quad (3.14)$$

where g_R is the Raman-coefficient as defined in [2], A_{eff} the effective mode area, α_s is the attenuation coefficient at the signal wavelength and $P_s(0)$ represents the optical power in [W] of the optical signal at the input of the transmission fiber ($z=0$).

For the backward pumped Raman amplification scheme, the optical pump power $P_p^-(z)$ as a function of the transmission distance z is given by [2]

$$P_p^-(z) = P_p(L) \exp[-\alpha_p(L - z)] \quad (3.15)$$

where $P_p(L)$ is the power in [W] of the Raman pump inserted counter propagating to the optical signal at the end of the transmission fiber ($z=L$). The envelope of an optical signal with power $P_s(z)$ can then be described with [28]

$$P_s(z) = P_s(0) \exp \left[\frac{g_R}{A_{eff}} P_p(L) \frac{1}{\alpha_p} \{ \exp[-\alpha_p(L - z)] - \exp(-\alpha_p L) \} - \alpha_s z \right] \quad (3.16)$$

The gain of a Raman amplifier is usually defined as the on-off gain $G_{on.off}$, which is the difference in optical power at the output of the transmission fiber with and without Raman amplification. For both forward and backward Raman amplification, the on-off gain is given by [28]

$$G_{on.off} = \exp \left\{ \frac{g_R}{A_{eff}} P_p \frac{1}{\alpha_p} [1 - \exp(-\alpha_p L)] \right\} \quad (3.17)$$

where $P_p = P_p(0)$ and $P_p = P_p(L)$ for forward and backward pumping, respectively. Another measure for Raman amplification is the effective gain G_{eff} , which is defined analogue to the EDFA gain (equation 3.2) as the difference between the input and output power

$$G_{eff} = \frac{P_s(0)}{P_s(L)} \quad (3.18)$$

where $P_s(0)$ and $P_s(L)$ in [W] are the input and output power of the transmission fiber.

Similar to the EDFA, the noise figure of a discrete Raman amplifier is higher than 3 dB. However, the key advantage of Raman amplification is that instead of using a discrete amplifier, the transmission fiber can be used as the amplification medium. As a result, the lowest optical power to be amplified is significantly increased resulting in an improvement of the OSNR and thus a reduction of the effective noise figure. The effective noise figure of these Raman amplifiers, is significantly lower (Typically around -3 dB) compared to that of an EDFA [28]. Another advantage of Raman amplifiers is that they are more broadband than EDFAs [28]. However, Raman amplifiers are significantly more expensive since they require high optical pump powers of typically 1 Watt and more. At these high optical powers, connectors easily burn due to dirt or dust. Furthermore, as 1 Watt optical power can cause serious injuries to the human skin and eyes, special safety precautions must be taken when using these pump lasers.

3.3 Dispersion compensation

In long-haul transmission systems with a data rate of higher than 2.5 Gbit/s, the chromatic dispersion must be compensated for. Figure 3.3 shows the eye opening penalty (EOP) as a function of the dispersion for 10-Gbit/s and 40-Gbit/s NRZ-ASK signals. The EOP, defined in appendix B, is a practical method to assess the performance of a transmission system. Allowing for instance a 1-dB EOP, the dispersion tolerance at 10-Gbit/s (2000 ps/nm) is 16 times greater than the dispersion tolerance at 40-Gbit/s (125 ps/nm): doubling the data rate results in four times less dispersion tolerance. In a fiber-optic transmission system it means that for increasing data rate, more precise matching of the residual dispersion is required.

Many different methods have been proposed to compensate for chromatic dispersion in high bit-rate transmission systems, such as DCF [37, 18], Fiber-Bragg gratings (FBG) [38], pre-distortion [39] and optical phase conjugation [40]. Most commercial transmission links to date are realized using DCF modules for dispersion compensation. Figure 3.1 depicts a transmission system where DCF modules are placed after each span of transmission fiber for dispersion compensation. Such a DCF-based transmission system can be referred to as a 'conventional' fiber-optic system. The main advantage of the DCF modules is that it is a passive device which allows simultaneous dispersion compensation of multiple WDM channels. DCF is fiber with the inverse sign of the GVD. Typical values for the dispersion and slope of a DCF are $D = -100$ ps/nm/km and $S = -0.34$ ps/nm²/km. The high negative dispersion coefficient of DCF enables to compensate for the dispersion of

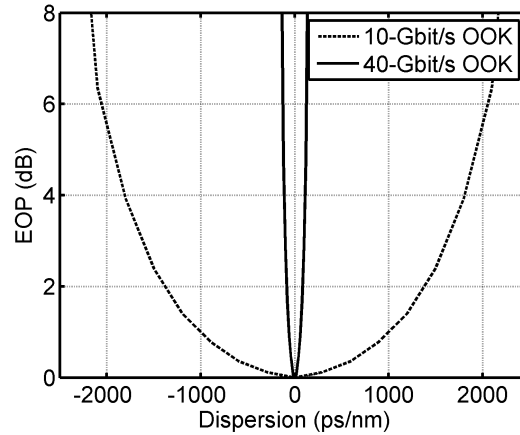


Figure 3.3: *Simulation: EOP as a function of the dispersion for 10-Gbit/s and 40-Gbit/s NRZ-ASK.*

long 100 km transmission spans with only a couple kilometers of DCF. A disadvantage of DCFs is that its nonlinear coefficient ($\gamma \approx 3 \text{ W}^{-1}\text{km}^{-1}$) is significantly higher than that of SSMF ($\gamma \approx 1.3 \text{ W}^{-1}\text{km}^{-1}$). Therefore, in order to reduce nonlinear effects in the DCF, typical launch powers into the DCF have to be chosen about 5 dB lower than the launch power used for the transmission fiber.

The course of the dispersion along a transmission line can be visualized using a dispersion map. Figure 3.4a gives an example of a dispersion map for a transmission line with twelve spans. In this figure, the dispersion parameters of the transmission line can be seen: pre-compensation D_{pre} , inline-compensation D_{inline} and post-compensation D_{post} .

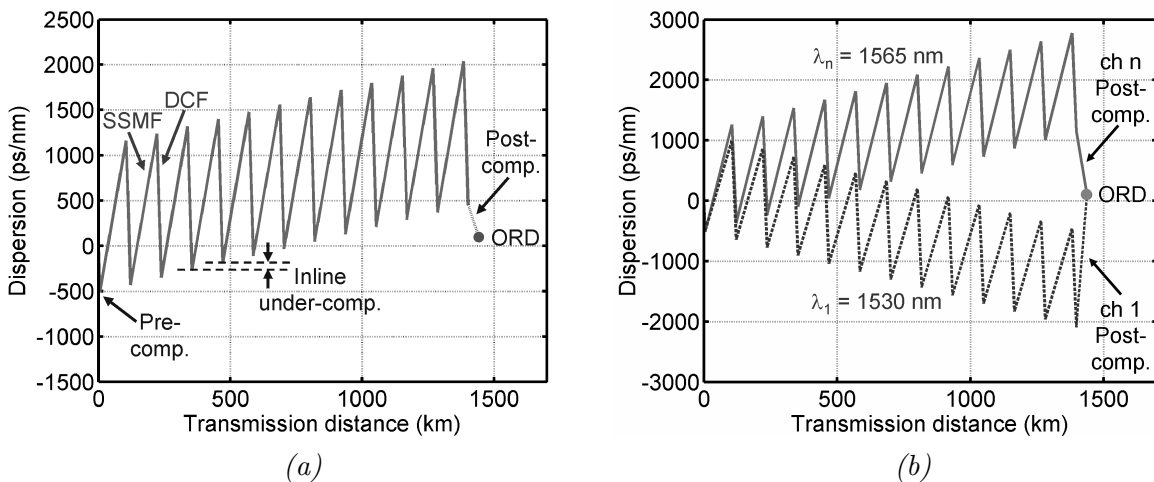


Figure 3.4: *Dispersion map: the dispersion as a function of the transmission distance, a) with slope matching, b) without slope matching*

In Figure 3.4a, a DCF module with -510 ps/nm is used as pre-compensation and the

inline-compensation equals 80 ps/nm/span. After transmission, post-compensation is applied to optimize the BER performance. The post compensation where the best BER is obtained is referred to as the optimal residual dispersion (ORD).

Due to the dispersion slope of the transmission fiber, the GVD is dependent on the wavelength. As a result, the dispersion map in a WDM transmission system is different for each channel and different amounts of post compensation are required in order to obtain the same residual dispersion for all WDM channels. This principle is illustrated in Figure 3.4b for WDM channels, present at $\lambda_1 = 1530$ nm and $\lambda_n = 1565$ nm. Modern DCF modules can be designed to be “slope-matched”. The slope of these modules is inverse and proportional to the slope of the transmission fiber. When slope-matched DCF modules are used, a similar dispersion map is obtained for all WDM channels.

The dispersion map can be used to reduce the nonlinear impairments in a long-haul transmission system. The influence of dispersion on the signal envelope of a 10-Gbit/s NRZ-ASK signal is shown in Figure 3.5. In this simulation, only the envelope change through dispersion is assessed, therefore fiber-loss and nonlinear impairments are neglected. Even

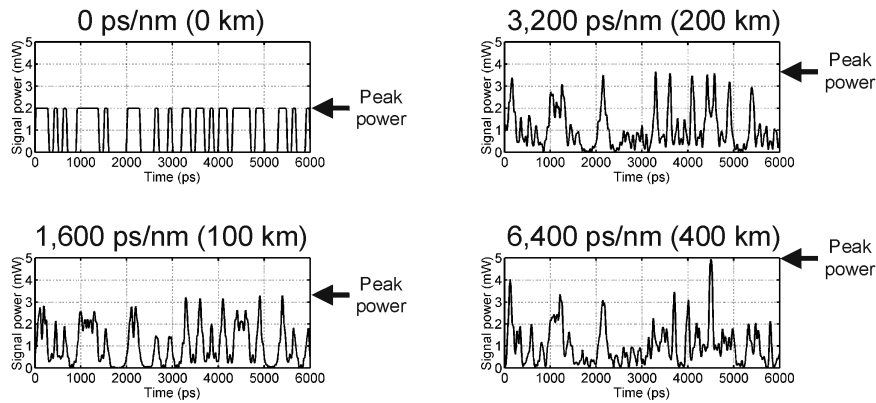


Figure 3.5: *Simulation: Envelope of a 10-Gbit/s NRZ-ASK signal after 0-km, 100-km, 200-km and 400-km transmission through SSF.*

though the average signal power is the same in the four plots (1 mW) depicted in Figure 3.5, it can clearly be seen that the signal’s peak power is strongly dependent on the dispersion. The peak power of the signal with a residual dispersion of 6,400 ps/nm is about 2.5 times as high as the peak power of the signal without dispersion. As described in Section 2.4, practically all chirp caused by the Kerr-effect is induced in the high power region of the fiber. The dispersion map can therefore be used to minimize the peak powers in the high power regime and thereby reduce the nonlinear chirp caused by the Kerr-effect.

In a multi-span transmission link using EDFAs for amplification, the high power regions are present directly after each EDFA. In the dispersion map depicted in Figure 3.6 the high power regions are marked. The pre-compensation and inline-compensation can be used to minimize the peak powers of the optical signal in these higher power regions. Additionally, inline-compensation can be employed to reduce the phase matching of inter-channel nonlinear impairments.

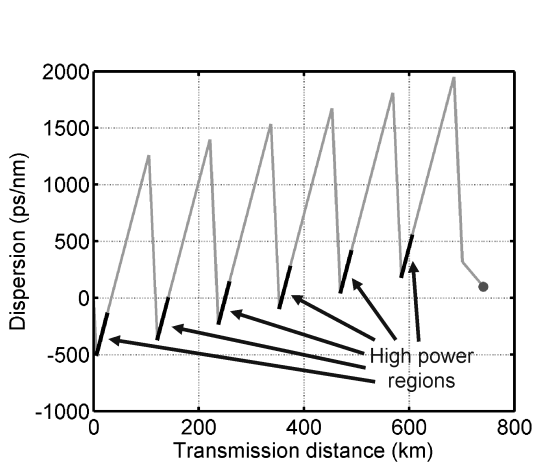


Figure 3.6: *Dispersion map of a transmission link with marked high power regions (with EDFAs for amplification).*

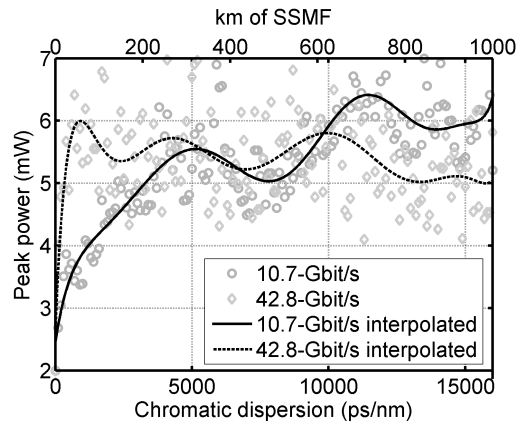


Figure 3.7: *Simulation: Peak power as a function of the dispersion for 10.7-Gbit/s and 42.8-Gbit/s NRZ-ASK (without attenuation).*

Figure 3.7 shows the signal peak power as a function of the chromatic dispersion for 10-Gbit/s NRZ-ASK and 40-Gbit/s NRZ-ASK (without fiber attenuation). The peak power of 10-Gbit/s NRZ-ASK is relatively low up to 300 km of SSMF, whereas the peak power of 40-Gbit/s NRZ-ASK reaches its maximum value already after 50-80 km of SSMF. It can then be concluded that for each data rate a different dispersion map is optimal.

Note that the illustration in Figure 3.7 is a simplified version, since the interplay of chirp through nonlinear impairments and chromatic dispersion is not considered. Therefore, the design of the transmission link is not straightforward, but requires numerous simulations. Many studies have been reported on the optimization of the dispersion map [41, 42, 43, 44].

3.4 Modulation formats

Many different formats have been introduced for digital transmission systems to encode an electrical binary data stream onto an optical carrier [45, 46]. The most straightforward technique to transmit data optically is by using the two-level binary amplitude-shift keying (ASK) format. For decades, the non-return-to-zero (NRZ) ASK modulation format has been used as the format of choice in optical transmission systems. However, when channel data rates increase to 40 Gbit/s and higher, the link parameters (dispersion map, fiber input power, etc.) must be controlled more precisely than at 10-Gbit/s transmission. Many simulations and experiments concerning transmission using advanced modulation formats have been reported striving for higher system tolerances at higher data rates. In this section the modulation formats will be discussed that are relevant for this thesis: ASK, duobinary, DPSK and DQPSK.

Many different criteria exist to assess the performance of a modulation format, such as the tolerance towards amplifier noise, chromatic dispersion, PMD, XPM, etc. A full

comparison of the modulation formats for all these criteria is out of the scope of this thesis. Each modulation format has its advantages and disadvantages and in general it can be said that there is not a single modulation format that is superior to all others. The discussion in this section will mainly focus on the tolerance towards amplifier noise and chromatic dispersion.

In the following subsections, four modulation formats will be discussed that are used in this thesis: NRZ-ASK, duobinary, RZ-DPSK and RZ-DQPSK. Before discussing the modulation formats in detail, simulation results of the modulation formats with the tolerance to amplifier noise and chromatic dispersion are presented.

The tolerance towards amplifier noise can be assessed by plotting the BER as a function of the OSNR. Figure 3.8a depicts such a plot for the modulation formats discussed in this section. Note that the performance of a certain modulation format is dependent on the full-width at half-maximum (FWHM) and order of the optical and electrical filters that are used at the receiver. In this simulation a first order Gaussian optical filter is used with a FWHM of 1.4 times the symbol rate. The electrical filter is a 5th order Bessel filter with a FWHM of 0.8 times the symbol rate. The sensitivity plots depicted in Figure 3.8a give a good indication of the performance of each modulation format. However, the sensitivity performance can be further improved by optimizing the optical and electrical bandwidth per modulation format individually. The sensitivity of a modulation format is defined as the OSNR that is required to obtain a certain BER value. In the simulated configuration, the required OSNRs for a BER of $1 \cdot 10^{-9}$ are 19.1 dB, 22.2 dB, 15.5 dB and 17.4 dB for the NRZ-ASK, duobinary, RZ-DPSK and RZ-DQPSK modulation formats, respectively.

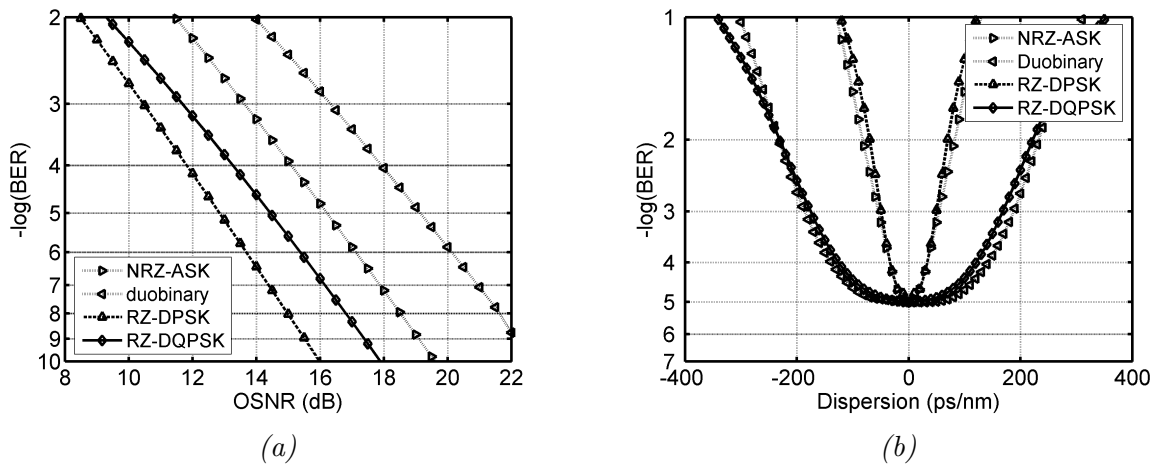


Figure 3.8: *Simulation: Comparison of 42.8-Gbit/s NRZ-ASK, duobinary, RZ-DPSK and RZ-DQPSK, a) BER as a function of the OSNR/0.1nm, b) Dispersion excursion.*

A simulated dispersion excursion is shown in Figure 3.8b. In this plot, the OSNR of the modulation formats is adjusted so that a BER of $1 \cdot 10^{-5}$ is obtained at 0 ps/nm chromatic dispersion. The required OSNR is 16.2 dB, 19.2 dB, 12.9 dB and 14.5 dB for the NRZ-ASK, duobinary, RZ-DPSK and RZ-DQPSK modulation formats, respectively. The

dispersion tolerance is defined as the amount of dispersion that can be tolerated before a certain BER penalty is obtained. For a worst BER of $1 \cdot 10^{-3}$ for instance, a dispersion tolerance of 108 ps/nm, 374 ps/nm, 100 ps/nm and 344 ps/nm is obtained for the NRZ-ASK, duobinary, RZ-DPSK and RZ-DQPSK modulation formats, respectively. It can be concluded that for the four modulation formats a considerable performance difference in both sensitivity as well as dispersion tolerance is observed. In the following sections, the modulation formats are discussed and the observed simulation results from Figures 3.8a and 3.8b will be explained.

3.4.1 Amplitude-shift keying

Figure 3.9a and 3.9b illustrate the modulation and detection of the two-level binary NRZ-ASK modulation format: light is sent in each bit-slot when a mark is transmitted and blocked for each space.

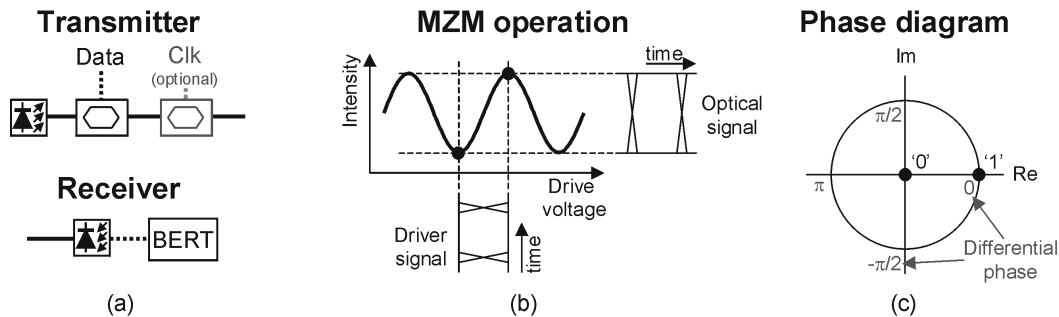


Figure 3.9: NRZ-ASK modulation format, a) modulation and detection, b) MZM operation, c) Phase constellation diagram.

NRZ-ASK can be realized by modulating the CW output of a laser with a MZM. The electrical *Data* signal is fed to the MZM with a peak-to-peak (pp) voltage of $V_{pp} = V_{\pi}$. The bias voltage of the electrical signal is set in the quadrature-point of the MZM modulator curve. The phase constellation diagram of the ASK signal is depicted in Figure 3.9c. In this diagram it can be seen that for the spaces, no light is present and that the phase for the marks is constant. As described in Section 3.1, a photodiode is used at the receiver to convert the NRZ-ASK signal to the electric domain. Note that in the receiver drawn in Figure 3.9a, the CRU and DFF are incorporated in the bit error ratio tester (BERT).

An RZ modulated signal can be generated by pulse carving the optical signal with an extra MZM modulator. RZ modulation results in a reduction of the DGD-induced ISI and thereby increases the PMD tolerance [47]. Furthermore, the peak power of RZ pulses is higher for equal mean optical power, which results in a sensitivity improvement of about 1-2 dB (depending on the pulse width). However, the signal spectrum of RZ pulses is broader than that of an NRZ signal. As a result, RZ-ASK modulation formats are in general less tolerant towards chromatic dispersion [47]. When a MZM is used for pulse carving, three different duty cycles can be generated by setting different bias voltages and drive currents,

namely 67%, 50% and 33%. Table 3.2 provides an overview of the bias voltage and drive currents required for each duty cycle.

RZ Modulation type	V_{bias}	V_{pp}	Drive Frequency
33%	crest	$2 \cdot V_{\pi}$	$f_{data}/2$
50%	quadrature	V_{π}	f_{data}
67%	trough	$2 \cdot V_{\pi}$	$f_{data}/2$

Table 3.2: *Driving parameters for pulse carving using a MZM*

The shorter the pulses are, the broader the optical bandwidth of the data signal becomes. Hence most RZ transmission experiments using WDM with a narrow channel spacing employ the 67% and 50% duty cycles for pulse carving [34, 48].

3.4.2 Duobinary

A promising advanced modulation format is the optical duobinary format. Duobinary coding was initially introduced for electrical signals [49, 50]. An electrical duobinary signal is a 3-level signal that is generated by splitting a data sequence and recombining them after delaying one arm with one bit period [50].

The duobinary modulation format has afterwards been adapted for fiber-optic transmission systems [51, 52, 53]. Instead of using a three level amplitude signal, additional phase engineering is added to an ASK signal. The optical envelope and phase of an optical duobinary signal are illustrated in Figure 3.10.

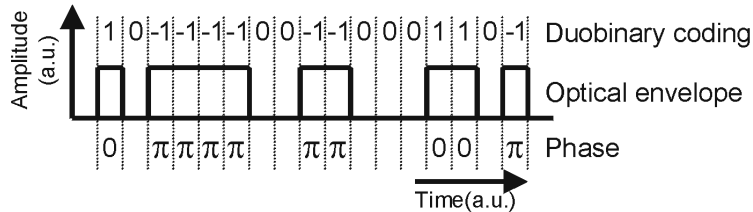


Figure 3.10: *Optical envelope and phase of a duobinary signal as a function of time.*

The '-1' in this plot represents a bit with a ' π '-shifted phase with respect to the '1' bit. Whenever an odd number of spaces is transmitted, the phase of the following marks is changed by π (e.g. from '1' to '-1' or vice versa) [54]. The additional phase engineering significantly reduces the ISI due to chromatic dispersion. When an isolated space is sent between sequences of marks (e.g. '101'), energy of the marks leaks through chromatic dispersion into the bitslot of the isolated space. For ASK modulation formats, the energy of the neighboring marks fills the isolated space, resulting in a bit-error at the comparator of the receiver. Since with the duobinary modulation format, a π -phase difference is present between the two marks, they will cancel each other. As a result, the isolated space is preserved. In practice the dispersion tolerance of a duobinary signal is approximately

three times that of the dispersion tolerance of NRZ-ASK [53]. The increased chromatic dispersion tolerance can be seen from the simulated eye diagrams that are shown in Figure 3.11.

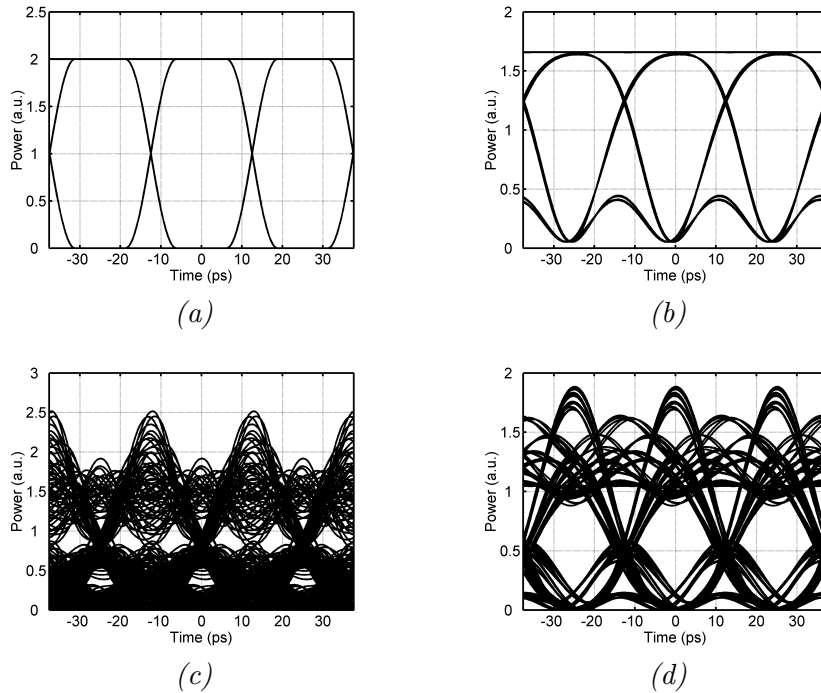


Figure 3.11: 40-Gbit/s simulated eye diagrams a) NRZ-ASK, back-to-back, b) duobinary, back-to-back, c) NRZ-ASK, after 10 km transmission through SSMF, d) duobinary, after 10 km transmission through SSMF.

The back-to-back eye diagrams of 40-Gbit/s NRZ-ASK and 40-Gbit/s duobinary are depicted in Figure 3.11a and 3.11b. In the back-to-back configuration, the NRZ-ASK eye diagram is cleaner and more open than the eye diagram of the duobinary signal. However, after transmission through 10 km of SSMF, the eye diagram of the NRZ-ASK signal is totally distorted (Figure 3.11c), whereas the eye diagram of the duobinary signal is still relatively open (Figure 3.11d). The large tolerance towards chromatic dispersion is evident from Figure 3.8b as well. Apart from the large dispersion tolerance, the duobinary modulation format is very robust to narrow-band optical filtering [55], making duobinary ideal for 40-Gbit/s WDM transmission at a narrow channel spacing (50 GHz) [56]. A drawback of the duobinary modulation format is that in general a higher OSNR is required to obtain the same BER. In the back-to-back OSNR to BER performance (Figure 3.8a) it can be seen that compared to the NRZ-ASK modulation format, 3.1 dB more OSNR is required to obtain the same BER value. However, through narrowband optical filtering the sensitivity of duobinary can significantly be improved [57].

Figure 3.12a and 3.12b show a commonly used implementation to create an optical duobinary signal [58]. Other implementations as well as an in-depth study of duobinary

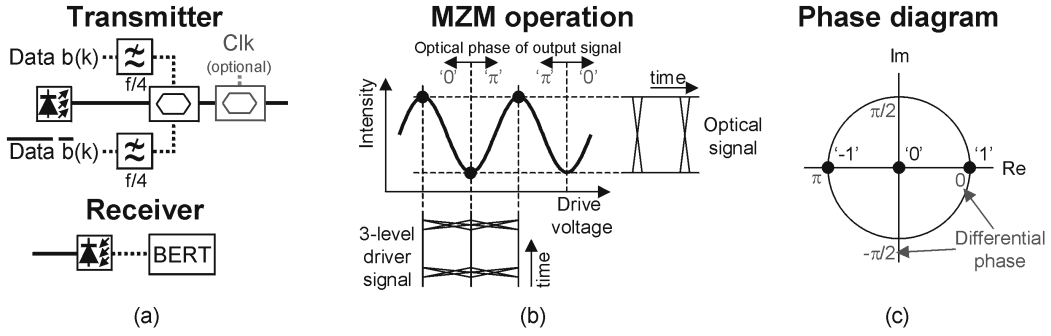


Figure 3.12: *Duobinary modulation format, a) modulation and detection, b) MZM operation, c) Phase constellation diagram.*

coding can be found in [59] and references therein. At the transmitter, both *data* and \overline{data} are low-pass filtered with a quarter of the data rate ($f/4$) and fed to a dual-drive MZM. As a result, the MZM is effectively modulated with a three-level electrical signal as depicted in 3.12b. By biasing the MZM in the trough and applying a peak-to-peak voltage of $V_{pp} = V_{\pi}$ for both *data* and \overline{data} a duobinary signal is generated. A π phase difference is present between the left and right side of the trough of the MZM curve. Hence the phase engineering is added implicitly to the signal with this modulation technique. The receiver structure is the same as that used for ASK modulation.

Figure 3.12c shows the phase constellation diagram of the duobinary signal. Similar to the NRZ-ASK modulation format, the space corresponds to the logical '0'. Two marks can be identified in the diagram, namely a '1' and a '-1', corresponding to bits with a relative phase difference of π .

Similar to the NRZ-ASK modulation format, it is possible to cascade a second MZM to create RZ-duobinary. Several RZ-duobinary modulation formats have been proposed in order to improve the tolerance towards PMD. However, the RZ pulse carving significantly reduces the chromatic dispersion tolerance. Since the chromatic dispersion tolerance is one of the main reasons to use duobinary modulation, duobinary is mostly used without RZ pulse carving.

At the receiver, the optical signal is converted to the electric domain by a photodiode. The phase information of the duobinary signal is in this conversion lost as the photodiode is only sensitive to the intensity of the signal, not the phase. As a result, pre-coding is required in order to receive the data signal correctly after transmission. When the input data sequence before modulation of bit k is represented by $d(k)$, the pre-coded data $b(k)$ can be described as

$$b(k) = d(k) \oplus b(k-1) \quad (3.19)$$

where \oplus is a logic exclusive OR (XOR) operation. The necessity of the pre-coding can be circumvented in laboratory experiments by using a pseudo random bit sequence (PRBS) code for transmission. A convenience of the PRBS code is that without pre-coding, the

PRBS property of the signal is maintained after detection.

3.4.3 Differential phase-shift keying

Recently strong interest has been shown in two phase-shift-keying (PSK) modulation formats for long-haul transmission: DPSK and DQPSK [60]. For these differential PSK modulation formats the information is coded in the phase-difference instead of the amplitude of the signal. Figure 3.13a and 3.13b illustrate the modulation and detection of the DPSK modulation format. Other implementations to generate and detect a DPSK signal are extensively discussed in [61]. The required components for the DPSK transmitter are

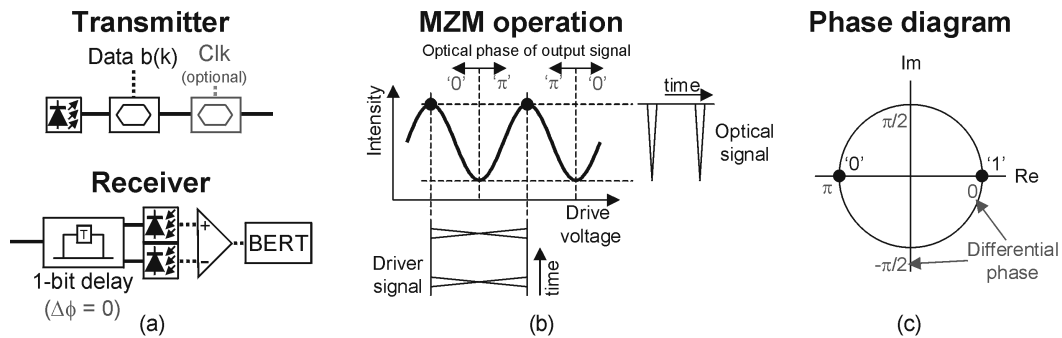


Figure 3.13: *DPSK modulation format, a) modulation and detection, b) MZM operation, c) Phase constellation diagram.*

the same as those used for the modulation of NRZ-ASK (Section 3.4.1). DPSK is created by biasing the electrical signal in the trough of the MZM curve. The peak-to-peak amplitude of the electrical signal is $V_{pp} = 2 \cdot V_{\pi}$, which is twice the amplitude that is required for the modulation of NRZ-ASK. In the phase constellation diagram of the DPSK signal (Figure 3.13c), it can be seen that '0' and '1' bits are encoded as marks with a π phase shift in between them. Comparing the phase constellation diagram of DPSK to that of ASK (Figure 3.9c), it can be seen that the distance between the points is twice that of DPSK. As a result, DPSK has in combination with balanced detection, a 2.8-dB higher sensitivity in the linear regime. In the back-to-back OSNR performance shown in Figure 3.8a, a sensitivity improvement of 3.6 dB is observed for RZ-DPSK with respect to NRZ-ASK. From this sensitivity improvement, 2.8 dB results from the balanced detection and 0.8 dB from the RZ-pulse carving. An additional advantage of DPSK is that it is relatively robust towards narrowband optical filtering [62]. Figure 3.8b shows that the dispersion tolerance of RZ-DPSK (100 ps/nm) is comparable to that of NRZ-ASK (108 ps/nm).

Figure 3.14a shows the measured eye diagram of 10.7 Gbit/s NRZ-DPSK. Compared to the NRZ-ASK modulation format (Figure 3.11), the DPSK signal has a more continuous power envelope because marks are present in each bit-slot. However, a bitpattern dependent intensity change is still present between the bit-slots. With an extra MZM an RZ-DPSK signal can be created. In comparison to NRZ-DPSK, RZ-DPSK cleans up the

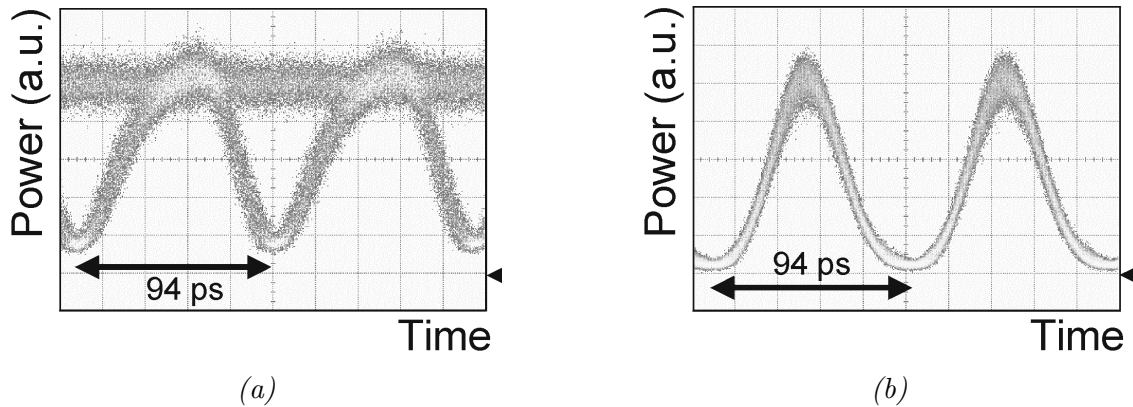


Figure 3.14: Measured eye diagrams of a 10.7-Gbit/s DPSK signal before the MZDI, a) NRZ, b) RZ with 50% pulse carving.

amplitude noise between the bit-slots and thus creates a more regular pulse shape. Figure 3.14b shows the measured eye diagrams of 10.7-Gbit/s RZ-DPSK. The pulse width of the depicted eye diagram is 50%. It has been shown that compared to ASK modulation formats, the continuous power envelope of NRZ [63] and RZ-DPSK [64, 65], significantly reduces impairments through SPM and XPM.

At the receiver, a photodiode is used to convert the data signal from the optical to the electrical domain. As the photodiode is only sensitive to the optical intensity and not to the optical phase, the information of the DPSK signal needs to be converted from the phase to the amplitude domain. Many different demodulation schemes have been proposed [66], but the most common implementation is based on a Mach-Zehnder delay interferometer (MZDI). The principle and layout of a MZDI are shown in Figure 3.15. The eye diagrams of a 42.7-Gbit/s RZ-DPSK signal before and after the MZDI are depicted as well.

The MZDI is an interferometric structure with a delay T of one bit-period in one of its arms. As a result, the signal inserted into the MZDI is split and when the pulses recombine, pulse k of the signal will interfere with pulse $k - 1$. The delay of the MZDI is fine tuned by $\Delta\Phi$ with an active temperature control so that no phase offset is present between the two recombining bits. Constructive interference between the bits occurs when no phase difference is present. Similarly, destructive interference takes place when a π phase difference is present. By subsequently combining the constructive and destructive signals through balanced detection, a 2.8-dB sensitivity improvement with respect to NRZ-ASK is obtained [62]. Two photodiodes convert the optical information to the electrical domain after which they are fed to a differential amplifier. At the output of the amplifier, a symmetric eye around 0 V is obtained. An advantage of the symmetric eye diagram obtained through balanced detection, is that the optimal threshold for the DFF is around 0 V. In contrary to the NRZ-ASK and duobinary modulation format, the optimal threshold is independent of the optical power incident on the photodiodes.

Due to the differential detection of the DPSK, pre-coding is required for DPSK transmission. The same coding scheme can be used as for duobinary transmission. Similar to

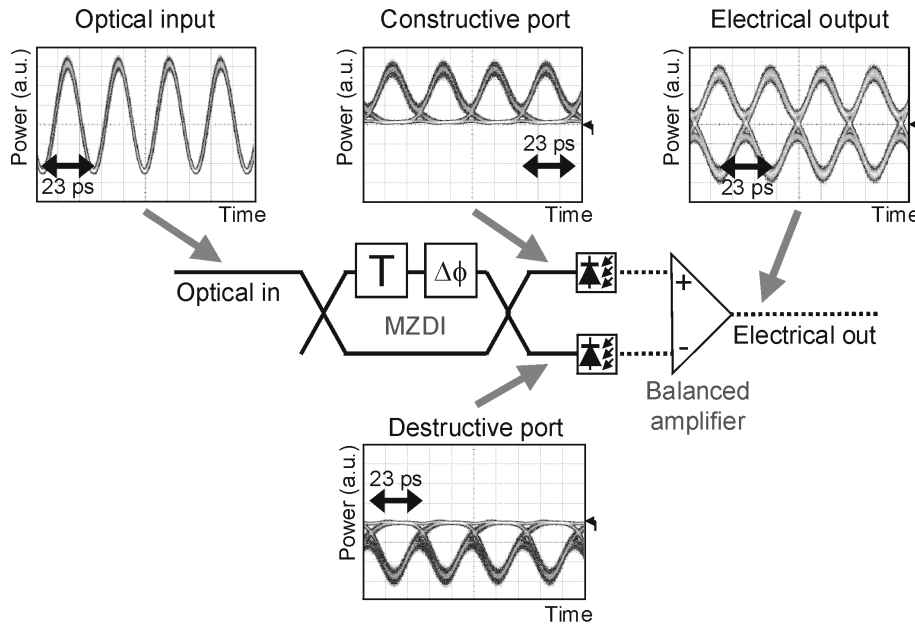


Figure 3.15: *Balanced detection of a 42.7-Gbit/s RZ-DPSK signal.*

duobinary laboratory experiments, pre-coding can be circumvented for DPSK modulation by using a PRBS sequence. The main disadvantage of the DPSK modulation format is its sensitivity towards nonlinear phase noise (NPN) impairments. NPN and the compensation of NPN through OPC is further discussed in Chapter 6. Another concern with DPSK arises when it is used together with WDM ASK modulated signals on the same transmission link. It has been shown that, especially at 10-Gbit/s, XPM caused by neighboring ASK-modulated channels can significantly impair the transmission performance of the DPSK modulated channel [63, 67].

3.4.4 Differential quadrature-phase-shift keying

DQPSK is widely researched nowadays as a promising modulation format for future optical transmission systems. Similar to DPSK, DQPSK encodes the information in the phase differences of the transmitted signal. In a DQPSK signal, each transmitted symbol contains two information bits, namely one 'in-phase' and one 'quadrature'. Therefore, the symbol rate is half the symbol rate of the other discussed modulation formats resulting in a favorable spectral width. As chromatic dispersion and PMD scale with the symbol rate, the DQPSK modulation format has high tolerances for chromatic dispersion and PMD at the same bit rate as binary modulation [68, 69, 70]. The high dispersion tolerance can clearly be seen in Figure 3.8b. At a BER of $1 \cdot 10^{-3}$ a dispersion tolerance of 344 ps/nm is obtained, which is comparable to that of duobinary (374 ps/nm). The sensitivity performance plotted in Figure 3.8a shows however, that compared to duobinary, RZ-DQPSK has a 4.8 dB better sensitivity at a BER of $1 \cdot 10^{-9}$. Even compared to NRZ-ASK, a sensitivity

improvement of 1.7 dB is obtained with RZ-DQPSK.

A DQPSK modulator can either be created by a parallel [71] or a serial [68] modulator structure. Figure 3.16a and 3.16b show the modulation and detection of a DQPSK signal

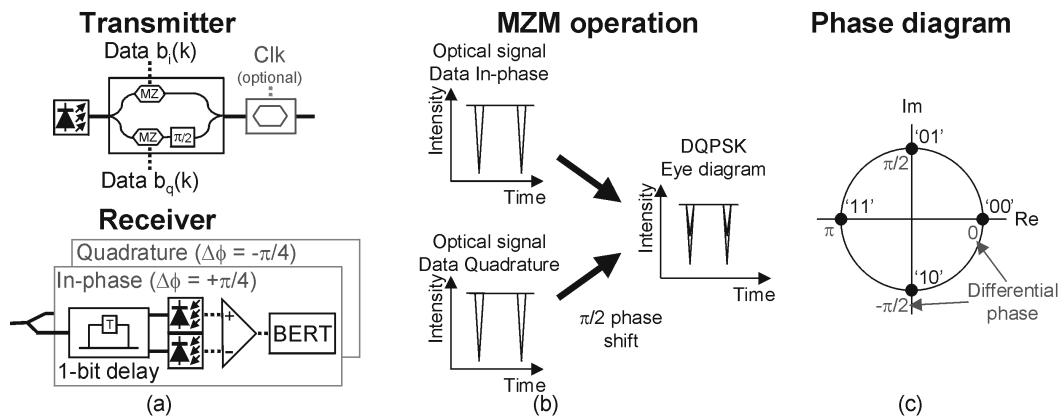


Figure 3.16: *DQPSK modulation format, a) modulation and detection, b) MZM operation, c) Phase constellation diagram.*

with the parallel modulator structure. The DQPSK modulator is an integrated super Mach-Zehnder structure incorporating two parallel MZMs. This integrated MZM structure is preferable over discrete components, since integration greatly increases the stability of the modulator. The output of a DFB laser is fed into the super MZM, where it is split in two arms, each containing a MZ modulator biased in the trough of the MZM curve and driven with a $2 \cdot V_\pi$ peak-to-peak amplitude. Hence, each MZM effectively creates a DPSK signal. Before recombining the two branches, the relative phase shift between the two parallel modulators is adjusted to $\pi/2$ by an integrated phase shifter. When both DPSK coded signals are then combined, the signals interfere resulting in a signal with four distinct phase levels. The phase constellation diagram of the DQPSK signal is depicted in Figure 3.16c. Taking the phase of the '00'-bit as reference, the information bits '01', '11' and '10' correspond to a phase difference with that reference of $\pi/2$, π and $-\pi/2$, respectively. At the receiver, MZDIs are used to convert the information from the phase to the amplitude domain. The in-phase and quadrature component of the DQPSK signal are detected by adjusting the phase difference in the arms of the MZDIs to $+\pi/4$ and $-\pi/4$, respectively.

A disadvantage using a super MZM for modulation is that for current devices, the required driving voltage of $2 \cdot V_\pi$ is high and typically in the order of 12 V. At high data rates (> 10 Gbit/s) this puts stringent requirements on the specifications of the driver amplifiers. Driving the modulator with a driving voltage lower than $2 \cdot V_\pi$ results in increased amplitude noise. The influence of a too low driving voltage can be suppressed by using the RZ pulse format. Figure 3.17a and 3.17b depict the eye diagram of a 42.8-Gbit/s RZ and a 42.8-Gbit/s NRZ DQPSK signal.

Although a relatively broad '1'-rail is still present in the RZ-DQPSK eye diagram, it can be seen that through RZ pulse carving most of the amplitude modulation noise is removed.

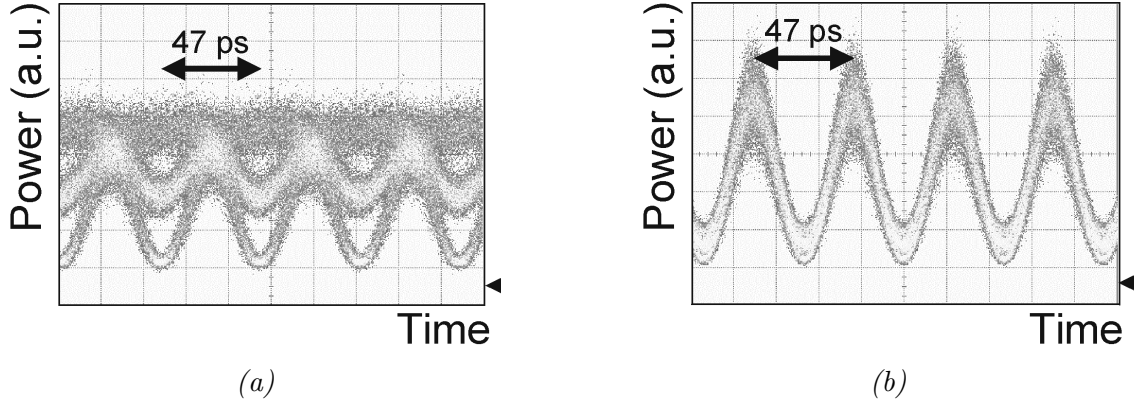


Figure 3.17: Measured eye diagrams of a 42.8-Gbit/s DQPSK signal before the MZDI, a) NRZ, b) RZ with 50% pulse carving.

As a result, the receiver sensitivity is significantly improved. The receiver sensitivity is the optical signal-to-noise ratio (OSNR) required to obtain a certain BER value. Typically a sensitivity improvement of about 2-3 dB in OSNR can be obtained through RZ pulse carving. In contrast, for a simulated optimal DQPSK signal the OSNR sensitivity difference between RZ and NRZ pulse shaping is limited to about 1-2 dB. Similar to DPSK, a concern with DQPSK is that it is sensitive to NPN as well as XPM impairments of neighboring NRZ-ASK channels.

Due to the signal mixing that occurs at the transmitter as well as the 1-bit delay MZDI, pre-coding is required for DQPSK transmission. With each symbol, two bits are transmitted. When k represents the current bits to be sent and $d_i(k)$ and $d_q(k)$ represent the in-phase and quadrature bit of the data signal, respectively, the encoded bits $b_i(k)$ and $b_q(k)$ for a parallel DQPSK modulator are given by [72]

$$b_i(k) = \left(\overline{b_q(k-1) \oplus b_i(k-1)} \right) \left(\overline{d_i(k) \oplus b_i(k-1)} \right) + \left(b_q(k-1) \oplus b_i(k-1) \right) \left(\overline{d_q(k) \oplus b_i(k-1)} \right) \quad (3.20)$$

and

$$b_q(k) = \left(\overline{b_q(k-1) \oplus b_i(k-1)} \right) \left(\overline{d_q(k) \oplus b_i(k-1)} \right) + \left(b_q(k-1) \oplus b_i(k-1) \right) \left(d_i(k) \oplus b_i(k-1) \right) \quad (3.21)$$

DQPSK pre-coding has been shown experimentally for a serial modulator structure in [73]. In laboratory testing environment, pre-coding is mostly circumvented by programming the BER tester with the expected bit sequence.

3.5 Summary

In this chapter, a conventional transmission link is discussed consisting of a transmitter, transmission line and receiver. At the transmitter, the electrical data stream is converted to the optical domain. The transmission capacity can be increased by the use of WDM, where multiple channels at different wavelengths are multiplexed and transmitted over the same fiber.

In a fiber-optic transmission line, optical amplifiers are used to compensate for the loss of the fiber. Each optical amplifier adds ASE noise to the signal and thereby degrades the OSNR. The amount of OSNR degradation is dependent on the signal power launched into the amplifier. In general it can be said that the higher the signal power is that an EDFA receives, the smaller the OSNR degradation is. However, a higher launch power into the fiber will result in an increased influence of nonlinear effects. Hence, a trade-off exists between the OSNR after transmission and the amount of nonlinear effects generated along the transmission line.

At data rates higher than 2.5 Gbit/s, the chromatic dispersion must be compensated for in long-haul transmission links. The accuracy with which the post compensation must be matched to the fiber-link dispersion is strongly dependent on the data rate: doubling the data rate reduces the dispersion tolerance by a factor of four. In a conventional transmission system, inline DCF modules are employed to periodically compensate for the chromatic dispersion of the fiber. Since the peak-power is dependent on the chromatic dispersion, the dispersion map can be optimized to reduce nonlinear impairments caused by the Kerr-effect.

Many different modulation formats have been proposed for fiber-optic transmission systems. The relevant modulation formats for this thesis are: ASK, duobinary, DPSK and DQPSK.

- ASK

ASK is a frequently used modulation format, since it is straightforward to generate with only few components required. An ASK signal can either be RZ or NRZ. Through RZ pulse carving the sensitivity of the signal and its tolerance towards PMD are slightly increased. A drawback, however, is that due to the pulse carving the optical spectrum broadens, which reduces the chromatic dispersion tolerance.

- Duobinary

The duobinary modulation format can be employed to substantially increase the tolerance towards chromatic dispersion. In practice the use of duobinary more than doubles the dispersion tolerance with respect to NRZ-ASK. Another key advantage of the duobinary modulation format is that it has an increased robustness to narrow-band optical filtering, allowing transmission with a narrow channel spacing. The main disadvantage of duobinary is that in general a higher OSNR is required at the receiver compared to NRZ-ASK. Duobinary is created by adding extra phase-engineering to the signal and thereby adds more complexity to the transmitter. However, a conventional ASK receiver can be used to detect the duobinary signal.

- DPSK

In a DPSK signal, the information is encoded in the phase difference of the bits. Through balanced detection a receiver sensitivity improvement of 3 dB can be obtained. Furthermore, DPSK is relatively tolerant to narrow-band optical filtering. Balanced detection at the receiver is realized by a MZDI. Disadvantages of DPSK are that both transmitter and receiver structure are more complex and that it is sensitive towards NPN.

- DQPSK

The DQPSK signal is similar to DPSK, however instead of two levels, four phase-levels are used to differentially encode the information. Therefore, each transmitted symbol contains two information bits, namely one 'in-phase' and one 'quadrature'. Advantages of DQPSK are its favorable spectral width and high tolerances for chromatic and polarization-mode dispersion at the same bit rate as binary modulation. Furthermore, the sensitivity of DQPSK is 1-2 dB better than that of NRZ-ASK. The main disadvantages of DQPSK are that it is impaired by NPN and that it is the most complex format to realize compared to the modulation formats discussed.

Throughout this thesis, the 'conventional' transmission system is referred to as the transmission link where DCF modules are used to periodically compensate for chromatic dispersion. In the next chapter an OPC-based transmission link is described. Instead of inline DCF modules, the chromatic dispersion is compensated for in this transmission link by conjugating all WDM channels mid-link.

Chapter 4

Optical phase conjugation

The concept of OPC is adopted from electric communication systems and radar applications [74, 75]. Yariv *et al.* introduced OPC for optical communication systems in 1979 for the compensation of chromatic dispersion [40]. In this work it was theoretically shown that the chromatic dispersion impairments in a fiber section before phase conjugation can be compensated for by the chromatic dispersion in the second fiber section.

Apart from chromatic dispersion, OPC can be employed to compensate for the Kerr-effect. The ability to compensate for SPM through OPC was numerically shown by Fisher *et al.* in 1983 [76]. In that case, phase distortions before conjugation that occur through SPM are undone by SPM-induced phase distortions after conjugation. The first experimental verifications of optical transmission with OPC were reported in 1993 [77, 78].

In this chapter the device aspects as well as the transmission aspects of OPC will be discussed¹. The first section discusses the processes that can be used to optical phase conjugate a signal. Section 4.2 then discusses the different media that can be employed for OPC. Different methods to create a polarization independent subsystem are discussed in Section 4.3. Finally in Section 4.4 the transmission aspects of OPC are discussed.

4.1 Processes

The earliest realizations of OPC were based on stimulated Brillouin scattering [79]. However, to date most of the more advance OPC-media are based on either FWM or DFG. Figure 4.1 illustrates the OPC concept from black-box perspective. The data signal at fre-

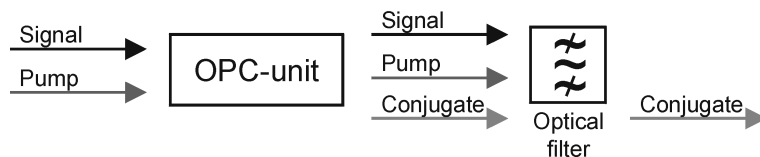


Figure 4.1: *Concept of the phase conjugation of a data signal.*

¹The results described in this chapter are published in P1, P4, P21

quency ω_{signal} is coupled together with a pump signal at frequency ω_{pump} and afterwards fed in an OPC-medium. At the output of the OPC-unit, a conjugate signal is present at a different wavelength ω_{conj} . The conjugate wavelength is subsequently separated from the pump and the original data signal by an optical filter, such as a BPF.

4.1.1 Four-wave mixing

FWM has been discussed in Section 2.4.3 as a degrading effect for optical transmission systems. However, it can be used as well to optically phase conjugate a signal. The phase conjugation is realized by a data signal ω_{signal} that interacts with a relatively strong pump signal ω_{pump} thus generating a phase conjugated FWM product ω_{conj} for which holds

$$\omega_{conj} = \omega_{pump} + \omega_{pump} - \omega_{signal} \quad (4.1)$$

This type of FWM, where only three wavelengths are involved, is often referred to as degenerate FWM. The generation of FWM requires a medium with a strong $\chi^{(3)}$ nonlinearity. Since other Kerr-effect nonlinear impairments, such as SPM and XPM, originate from the $\chi^{(3)}$ nonlinearity as well, they occur in the conversion process and thereby distort the signal.

4.1.2 Difference-frequency generation

Difference-frequency generation (DFG) is another method to realize OPC. The DFG process is based on the second-order nonlinear susceptibility ($\chi^{(2)}$), rather than on the third-order susceptibility ($\chi^{(3)}$) that is responsible for FWM. When two signals with frequencies ω_1 and ω_2 are inserted into a medium with a high $\chi^{(2)}$ susceptibility, two nonlinear interactions occur, namely sum-frequency generation (SFG) and DFG. The wavelengths of the SFG product ω_{SFG} and the DFG product ω_{DFG} are present at deterministic frequencies, given by

$$\omega_{SFG} = \omega_1 + \omega_2 \quad (4.2)$$

$$\omega_{DFG} = \omega_1 - \omega_2 \quad (4.3)$$

A schematic description of DFG and SFG is given in Figure 4.2. In quantum mechanical terms, what happens is that two photons are annihilated in SFG and produce a new photon that carries the energy of the two that disappeared. The frequency of the new photon equals the sum of the two annihilated photons, since the frequency of a photon is proportional to its energy. With DFG, the photon with the highest energy (=highest frequency) is annihilated and a photon of the other inserted frequency is produced. Because of the energy conservation law, an extra photon with the difference in energy between the annihilated and the produced photon is generated at a third frequency. As three photons are involved in both DFG and SFG, they are in general referred to as three-wave mixing processes.

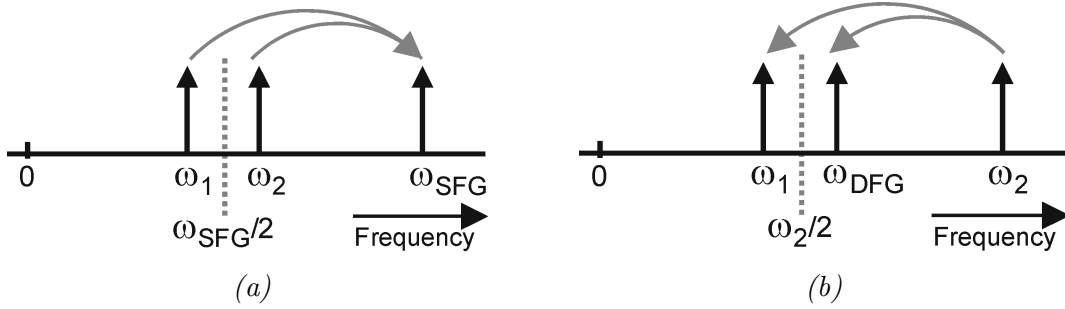


Figure 4.2: Principle of $\chi^{(2)}$ processes, a) sum-frequency generation (SFG), b) difference frequency generation (DFG)

An advantage of the DFG process is that it is instantaneous and phase sensitive in its response. Therefore, DFG allows transparent conversion with respect to data rate and modulation format [80, 81]. Furthermore, since DFG is a $\chi^{(2)}$ process, nonlinear impairments caused by the $\chi^{(3)}$ process are small and can be neglected [82, 83]. When DFG is used for OPC, the photon energy of the pump needs to be higher than that of the signal so that

$$\omega_{conj} = \omega_{pump} - \omega_{signal} \quad (4.4)$$

In order to conjugate an optical signal for instance from 194.6 THz (1540.6 nm) to 192 THz (1561.4 nm), a pump signal is required at 386.6 THz (775.5 nm). As the conventional EDFAs do not operate in this region, it is not straightforward to provide a strong enough pump signal. Furthermore, the coupling of the pump into the waveguide is difficult as most waveguides are multi-mode at this wavelength.

4.1.3 Cascaded second-harmonic generation and difference-frequency generation

The 700-800 nm pump laser required for the DFG based phase conjugation can be circumvented by using a cascaded process of second-harmonic generation (SHG) and DFG for phase conjugation. SHG is a special form of SFG, where the two photons of the same wavelength are annihilated to be replaced by a photon at double the frequency. The principle of the cascaded SHG and DFG process is shown in Figure 4.3. Through SHG, the pump signal at frequency ω_{pump} is up-converted to the frequency $2\omega_{pump}$. DFG occurs simultaneously where the second harmonic $2\omega_{pump}$ interacts with the input signal, at frequency ω_{signal} , to generate a phase conjugated signal at $\omega_{conj} = 2\omega_{pump} - \omega_{signal}$. Due to the fact that the optical spectrum of the phase conjugated signal is the inverse of the inserted data signal, phase conjugation is often referred to as spectral inversion (SI). The inversion of the optical spectrum is illustrated in Figure 4.3.

In general, cascaded SHG:DFG has a lower efficiency than DFG. However, the advantage of cascaded SHG:DFG is that the pump signal can be generated with conventional

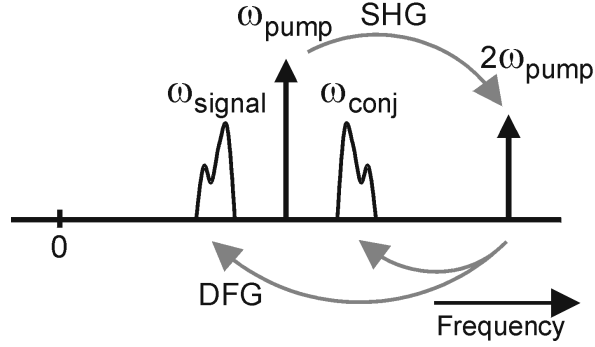


Figure 4.3: Principle of the cascaded SHG and DFG process.

long-haul equipment that operates in the C-band (DFB laser and EDFA). Therefore, in most cases the use of SHG:DFG is the preferred solution for telecommunication applications.

4.2 Media

Many different media can be employed to optically phase conjugate a signal through FWM, DFG or SHG:DFG. In this section four frequently used OPC-media are discussed. Two of these media are based on FWM, namely

- Silica as a fiber based solution
- Indium gallium arsenide phosphide as an SOA based solution

and two OPC-media employ either DFG or cascaded SHG:DFG

- Lithium niobate
- Aluminum gallium arsenide

The most important figures of merit to characterize the quality of an OPC-unit are the conversion efficiency and the wavelength acceptance bandwidth. The conversion efficiency can either be expressed as the internal or the external conversion efficiency. The external conversion efficiency η_{ext} is defined as the ratio between the optical power of the conjugated signal P_{conj} and the power of the data signal that is inserted into the OPC $P_{signal_{in}}$

$$\eta_{ext} = \frac{P_{conj}}{P_{signal_{in}}} \quad (4.5)$$

In this efficiency, the loss of the device itself is included. The internal conversion efficiency η_{int} is defined by

$$\eta_{int} = \frac{P_{conj}}{P_{signal_{out}}} \quad (4.6)$$

where both $P_{signalout}$ and P_{conj} are measured at the output of the OPC-unit, therefore excluding the loss of the device. All conversion efficiencies reported in this thesis are internal conversion efficiencies. The conversion efficiency is dependent on the wavelength difference $\Delta\omega$ between pump signal and data signal. The wavelength acceptance bandwidth $\Delta\omega$ of an OPC-unit is defined as the wavelength range for which the conversion efficiency is within 3-dB of the maximum conversion efficiency.

4.2.1 Silica

Silica fiber can be used to optically phase conjugate a signal through FWM. The conversion efficiency of a fiber-based OPC scales with the power of the pump signal as well as with the nonlinear coefficient γ of the fiber. The nonlinear coefficient varies per fiber and is a measure for the strength of the $\chi^{(3)}$ nonlinearity, and thereby the FWM generated. For a fixed pump power, a fiber with a higher nonlinear coefficient will provide a stronger FWM product and thus higher conversion efficiency.

For the FWM process it is essential that the phase of the data signal is matched with the phase of the pump signal. Phase matching in a fiber is obtained when the three interacting waves of the FWM process (data, pump and FWM conjugate) have the same phase-velocity. This is difficult to realize due to the chromatic dispersion of the fiber. In practice, the pump signal must be set to the zero-dispersion wavelength of the fiber for the best conversion efficiency. Therefore, DSF was initially used for OPC-based experiments, since these fibers have a zero-dispersion wavelength around 1550 nm [77, 78].

However a problem with DSF is that fluctuations in the zero dispersion wavelength reduce the phase matching and thereby limit the conversion bandwidth. Highly-nonlinear fiber (HNLF) can be used to significantly increase the conversion bandwidth and efficiency. The zero-dispersion wavelength of HNLF is similar to DSF around 1550 nm. However, its nonlinear coefficient ($\gamma \approx 15 \text{ W}^{-1} \text{ km}^{-1}$) is considerably greater than the nonlinear coefficient of DSF ($\gamma \approx 1\text{-}4 \text{ W}^{-1} \text{ km}^{-1}$). As a result, a short HNLF of ca. 750 m can obtain a similar conversion efficiency as a DSF of over 10 km [84]. When HNLFs are used for optical phase conjugation, a large acceptance bandwidth can be obtained and conversion of many WDM channels can be realized. In [85] a wavelength acceptance bandwidth of 72 nm is reported as well as WDM conversion of 32 channels at 100 GHz channel spacing. The internal conversion efficiency in this experiment is -11.2 dB.

An advantage of a fiber-based OPC is that it is a passive solution. However, disadvantages are that SBS introduces extra loss when a high power pump signal is used and that the wavelength of the pump signal must be set at the zero dispersion wavelength of the fiber. Furthermore, as more than 100 m fiber is required for a fiber-based FWM it can not be created with integrated optics.

4.2.2 Indium gallium arsenide phosphide

Indium gallium arsenide phosphide (InGaAsP) on an indium phosphide (InP) substrate is the most common technology to create a semiconductor optical amplifiers (SOA). Although

the SOA is a semiconductor device, designed to amplify an optical signal, it can as well be used to conjugate a signal through FWM. Similar to the EDFA, the amplification principle of the SOA is based on stimulated emission from stored carriers. The nonlinear coefficient of the semiconductor material is significantly higher than that of silica. Therefore, an FWM-conjugate can be generated in a significantly shorter interaction length. Typical lengths for an SOA are between 500 μm and 2000 μm . The SOA does not have a zero dispersion wavelength like silica-based OPC-units. As a result, the conversion efficiency is relatively independent of the exact location of the pump signal. Conversion efficiencies of up to -7 dB have been reported [86]. A key advantage of using an SOA for phase conjugation is that it is a very compact solution. Additionally, SOAs can be integrated together with other components such as optical couplers, AWGs, etc. Since the SOA is an optical amplifier, a significantly lower pump signal is required compared to the HNLF.

On the down side, the SOA is an active device and therefore consumes electrical power, produces heat and potentially breaks down. The acceptance bandwidth of 8 nm is relatively small [86] and the influence of XPM between different WDM channels is, due to the amplification of the SOA, significantly stronger than that occurring in fiber-based OPC-media. Therefore, the number of WDM channels that can be converted with an SOA is limited. The noise figure of an SOA is relatively high (typically $F = 6\text{-}8.5$ dB [87]), which has a great impact on the OSNR of the FWM conjugate. Figure 4.4 shows an experiment where the OSNR of the phase conjugate FWM product at the output of the SOA is plotted as a function of the OSNR of the data signal before entering the SOA.

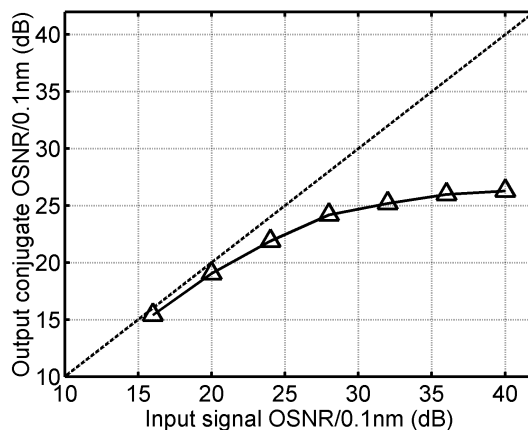


Figure 4.4: *Phase conjugate OSNR as a function of the input signal OSNR.*

The straight line in Figure 4.4 represents the ideal conversion where no ASE noise is introduced by the SOA: $OSNR_{signal_{in}} = OSNR_{conj}$. For low input OSNR, optical phase conjugation through FWM in an SOA introduces a small OSNR penalty of about 1 dB. For high OSNR values, this OSNR penalty increases to more than 13 dB. Hence, it can be concluded that the ASE from the SOA limits the maximum converted OSNR.

4.2.3 Lithium niobate

Lithium-niobate (LiNbO_3) is a colorless solid crystal that is widely used for the realization of integrated optical (sub)components such as for instance MZMs. The LiNbO_3 material is transparent to wavelengths ranging from about 400 nm to 5000 nm. An important property of the LiNbO_3 is that it lacks inversion symmetry and can therefore be exploited for DFG and SFG. However, similar to FWM, both SFG and DFG are only generated when the phases between the interacting wavelengths are matched. In a conventional LiNbO_3 waveguide, used to create MZMs for instance, practically no phase matching occurs due to the dispersion of the lithium niobate material. Full phase-matching between different WDM channels can thus not be obtained. However, by periodically poling the LiNbO_3 waveguide it is possible to create quasi-phase matching (QPM). This device is usually referred to as a periodically-poled lithium niobate (PPLN) waveguide. The principle of QPM through periodic poling is shown in Figure 4.5 for SHG.

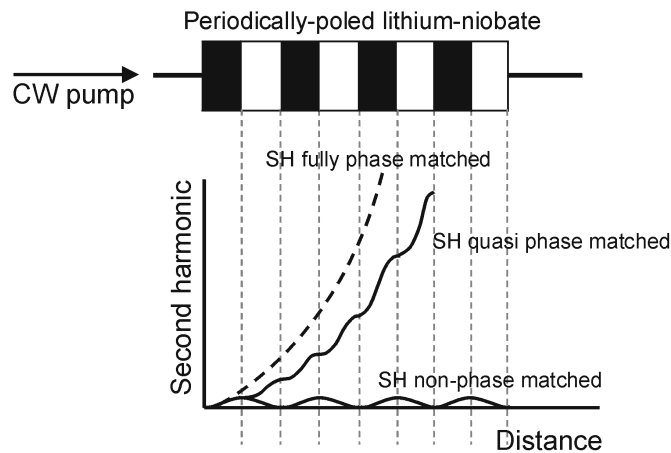


Figure 4.5: *Principle of quasi phase matching.*

Through SHG of a pump signal (or sometimes referred to as fundamental), a second harmonic is generated. Due to the dispersion of the waveguide a phase mismatch occurs between the pump signal and its second harmonic. Therefore, without phase matching, the SHG power grows until a π phase shift is reached between the pump signal and its second harmonic and decreases to zero again as the phase shift becomes $2 \cdot \pi$. The propagation length where the phase of the pump signal and its second harmonic are shifted by π is referred to as the phase matching period or coherence length. Efficient SHG generation can be obtained by first order QPM through periodic poling: the sign of the nonlinear susceptibility is reversed with every phase matching period so that the change of the sign of the nonlinear coefficient causes constructive interference in the next segment. The phase matching period of the periodic poling determines the wavelength of the pump signal. A typical value for the phase matching period is $\approx 16.5 \mu\text{m}$. An in-depth study of the relation between the periodic poling and the wavelength acceptance of the pump signal can be found in [88]

In lithium niobate material no ‘natural’ waveguide is present. By creating a waveguide in the LiNbO_3 , the propagation loss of the material is significantly reduced. A common technique to create a waveguide in lithium niobate is by the diffusion of titanium (Ti). With this diffusion process, the refractive index of the LiNbO_3 is slightly increased near the surface of the material where Ti is present. Through the difference in refractive index between the surface and the rest of the LiNbO_3 , a waveguide is created.

A disadvantage of OPC through a PPLN waveguide is that a high power optical signal will cause space-charge fields and electro-optic refractive index changes in the LiNbO_3 material. This is often referred to as the photorefractive effect. Note that the changes in refractive index that arises due to the photorefractive effect are not permanent, but can be eliminated by heating the device. At high temperatures, the photorefractive effect is significantly reduced. Therefore, typical operating temperatures for a PPLN waveguide range from 180° to 200° Celsius. Because of this high operating temperature, pigtail fibers cannot be glued to the waveguide with generally available techniques. Free-space optics has then to be used to couple the light into and out of the waveguide.

It has been shown that the photorefractive effect can be reduced if the lithium-niobate is slightly doped with magnesium-oxide (MgO) [89]. This significantly lowers the operating temperature. In several recent transmission experiments MgO-doped PPLN waveguides are employed operating at 50° to 90° Celsius [90, 80, 81]. The lower operating temperature allows gluing the fibers to the waveguide, which is essential for subsystem integration.

The operating temperature of the waveguide influences the phase matching condition for the pump signal. This property is therefore used to tune the phase matching condition to a specific wavelength. The dependence of the temperature on the pump wavelength is approximately 0.16 nm/Kelvin . Therefore, the tuning range of a PPLN-waveguide is limited: In order to cover the whole C-band ($\approx 35 \text{ nm}$) a change in operating temperature of $> 210^\circ$ Celsius is required. For a Ti:PPLN, with an operating temperature range of 180° to 200° Celsius, the tuning range of the pump signal is approximately 3.2 nm .

With the cascaded SHG:DFG process, conversion efficiencies of up to -7 dB have been reported [91, 92, 93]. During the conversion process negligible noise is added to the phase conjugated signal [83]. The PPLN waveguide has a broadband conversion bandwidth (typically $> 50 \text{ nm}$) and is capable of conjugating multiple WDM channels with one single unit. Simultaneous phase conjugation of up to $103 \times 10 \text{ Gbit/s}$ has been demonstrated by Yamawaku *et al.* [94]. The optical spectrum after the PPLN waveguide is depicted in Figure 4.6. In this 10-Gbit/s NRZ-ASK experiment 103 channels with a 25-GHz channel spacing in the C-band (1531 nm to 1551 nm), are optically phase conjugated with one PPLN waveguide to the L-band (1559 nm to 1579 nm). Thus with one PPLN-unit, a total capacity of over 1 Tbit/s is conjugated. The conversion efficiency in this experiment is approximately -15 dB . At the output of the PPLN waveguide, the phase conjugated channels are mirrored with respect to the pump signal. In this experiment, the pump signal is present at 1555 nm . It is clearly visible in Figure 4.6 that the conjugated channels are spectrally inverted with respect to the optical spectrum of the inserted data signals.

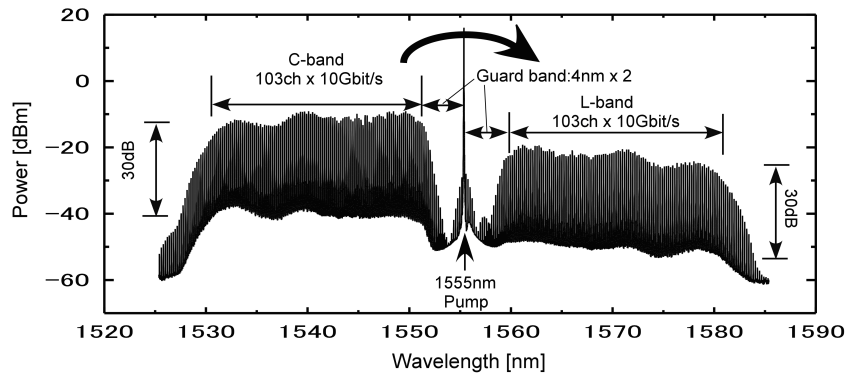


Figure 4.6: *Output spectrum of the PPLN waveguide. Conversion of 103x10Gbit/s NRZ-ASK from the C-band to the L-band (from Yamawaku et al. [94].*

4.2.4 Aluminum gallium arsenide

Instead of a LiNbO_3 crystal, OPC through DFG can be realized as well with aluminum gallium arsenide (AlGaAs) on a gallium arsenide (GaAs) substrate [86]. GaAs is a multifunctional material that is used to create many types of optical devices, such as optical switches, lasers, diodes, etc. In an AlGaAs-based OPC, the light is confined in a $1\ \mu\text{m}$ thick waveguide of AlGaAs, trapped by two AlGaAs cladding layers with a different composition [95]. It is possible as well to use other semiconductor materials such as InGaAsP for OPC through DFG. However, all DFG conversions reported so far were conducted with AlGaAs waveguides.

Similar to LiNbO_3 , the dispersion of the AlGaAs waveguide distorts the phase matching condition. Therefore, periodic-poling is required to compensate for the dispersion of the medium. The processes required to implement periodic-poling in an AlGaAs waveguide are described in [95].

A key advantage of AlGaAs waveguides is that these semiconductors can be designed to be polarization insensitive. Furthermore, the acceptance bandwidth of an AlGaAs waveguide is very large; In [96] an acceptance bandwidth of over 90 nm is reported. The $\chi^{(2)}$ nonlinearity of AlGaAs [97] is about three times higher than that of lithium niobate [98].

However, although this technique could potentially yield a high conversion OPC unit, the conversion efficiencies reported so far are relatively low because of high scattering loss caused by waveguide corrugations. By pumping the AlGaAs waveguide with a laser at 771 nm a conversion efficiency of ≈ -17 dB was reported in [96]. The low conversion efficiency originates from the fact that at the pump wavelength (771 nm) a loss of 45 dB/cm was observed in this experiment. No cascaded SHG:DFG experiments have been reported so far with an AlGaAs waveguide. The cascaded SHG:DFG process would probably further reduce the conversion efficiency, since two nonlinear interactions are required for conjugation.

4.3 Subsystems

Except for AlGaAs, a concern with all OPC-media is that they are polarization dependent. In a transmission system, signals have an arbitrary polarization that is different for each WDM channel and can change quickly over time. Hence polarization independent OPC is required for transmission. Polarization independence can be obtained through the use of a polarization diversity subsystem. In this section, two polarization diversity schemes will be discussed for the PPLN-waveguide: the parallel [99] and the counter-directional [100] polarization diversity structure.

4.3.1 Parallel polarization diversity

The parallel polarization diversity structure is depicted in Figure 4.7. The signal (at random polarization) is combined with a pump signal and fed into a polarization beam splitter (PBS). After the PBS, in both arms of the parallel structure, a PPLN waveguide is present. The pump wavelength is launched at 45° with respect to the principal axes of the first PBS such that both PPLN waveguides receive the same amount of optical pump power. The two waveguides must be nearly identical with the same conversion efficiency and periodic poling. This can for example be realized by using two waveguides on a single PPLN crystal. The output ports of the PBS are polarization maintaining fibers and aligned such that the PPLN waveguides receive the data and pump signal in the TM polarization. After phase conjugation, the signal is recombined by a second PBS. In one of the arms of the polarization diversity structure a delay line is present which is used to equalize the optical length of both arms. This delay line must be significantly more precise than the bit duration of the signal, since unequal lengths of the arms of the parallel structure would result in DGD. The parallel polarization diversity based OPC unit was initially introduced using FWM in two SOAs [101] and afterwards adapted for conversion using two PPLN waveguides [90].

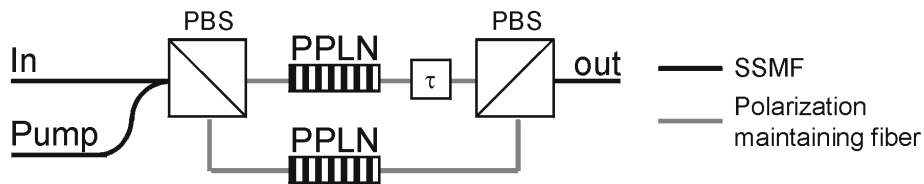


Figure 4.7: *Parallel polarization independent OPC unit.*

Several experiments described in this thesis (Chapter 5) are conducted using a parallel polarization diversity scheme for OPC. The measured polarization dependent loss (PDL) for this unit is less than 0.5 dB. The two PPLN waveguides used for OPC are doped with MgO, allowing the OPC-units to be operated at 90° Celsius. Quasi phase matching inside the PPLN waveguides is realized with a phase matching period of $17.1 \mu\text{m}$. As a result, the center or pump frequency is at 1546.12 nm. The optical power of the pump signal is set to

150 mW per PPLN waveguide. With this configuration, the conversion efficiency is about -16.5 dB. The noise output of the phase conjugator unit, with no input signals, is measured at less than -65 dBm per 0.1-nm bandwidth. The net loss of the phase conjugator plus filters is 23 dB.

4.3.2 Counter-directional polarization diversity

The counter-directional OPC structure is realized by using both directions of propagation in a single PPLN waveguide [100]. The layout of the counter-directional OPC structure is depicted in Figure 4.8. A polarization beam splitter (PBS) splits the incoming signal into TE and TM mode. The TM mode is phase conjugated in the PPLN waveguide and subsequently converted to TE mode by aligning the TE with the TM mode in a splice. The TE mode is first converted from the TE to the TM mode and afterwards phase conjugated. Both counter propagating modes are recombined at the PBS to effectively provide polarization independent phase conjugation. The pump signal is added before the data signal enters the polarization diversity structure. In order to pump both directions of the PPLN waveguide, the pump signal is launched at 45° with respect to the principal axes of the PBS such that the pump signal is split in a 50% – 50% ratio. The main advantages of the counter-directional OPC structure over the parallel structure is that only one PPLN waveguide is required and that both parts of the data (TE and TM mode) travel through the same path. As a result, both parts of the signal will arrive at the PBS at the same time. Hence the counter-directional OPC unit has inherently negligible DGD. A disadvantage however is that this scheme can be impaired by multiple path interference when the extinction ratio of the PBS is too low.

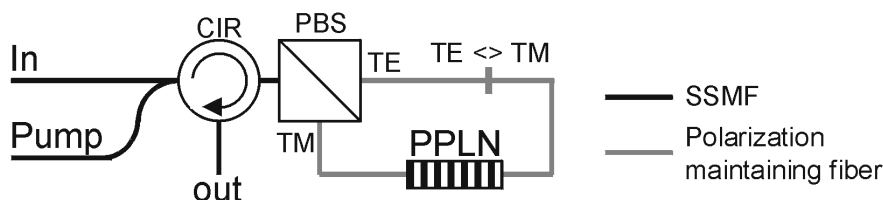
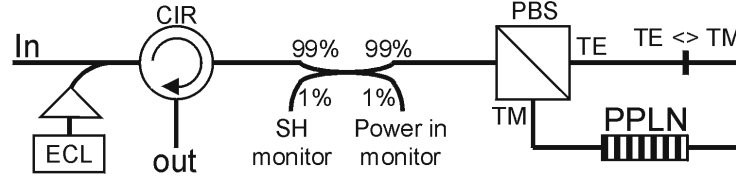


Figure 4.8: Counter-directional polarization independent OPC unit.

The experiments described in Chapter 7 are conducted using the counter-directional polarization independent OPC unit. The experimental setup of the PPLN subsystem used in these experiments is depicted in Figure 4.9. The measured PDL of the total PPLN subsystem is less than 0.4 dB. The PPLN waveguide used for OPC operates at 202.3° Celsius in order to reduce the photorefractive effect. Quasi phase matching inside the PPLN waveguide is realized by reversing the sign of the nonlinear susceptibility every 16.3 μm . The center or pump wavelength of the waveguide is located at 1543.4 nm.

In order to monitor the amount of second harmonic that is generated (present at ≈ 750 nm), a 99% to 1% coupler is inserted between the PBS and the circulator. Monitoring the


 Figure 4.9: *Experimental setup of the PPLN subsystem.*

SH is impossible after the circulator, since it blocks wavelengths lower than ca. 1000 nm. The 99% to 1% coupler is used as well to monitor the total optical power launched into the PPLN subsystem. The fiber-to-fiber coupling loss of the PPLN waveguide is approximately 6 dB. With the components used for polarization diversity, the loss is about 2 dB higher. A CW pump signal is generated at 1543.4 nm using an external cavity laser (ECL) and amplified to 388 mW. The incoming data signals are amplified so that the optical power is approximately 10 mW per channel at the polarization beam splitter. The conversion efficiency of the PPLN waveguide with these powers is -9.2 dB.

4.4 Transmission systems

In the previous sections, OPC was considered from a device and subsystem perspective. In this section the transmission aspects of OPC will be discussed. The principle of OPC is described in the first section. In the second section two types of transmission links will be discussed, namely inline OPC and mid-link OPC.

4.4.1 OPC concept

As mentioned in the introduction of this chapter, OPC can be employed to compensate for chromatic dispersion as well as the Kerr-effect. Let us consider a transmission line with an OPC in the middle. From Section 2.4 we recall the NLSE of a signal in a nonlinear, dispersive and lossy medium (equation 2.18)

$$\frac{\partial A}{\partial z} = -\frac{\alpha}{2}A - \frac{j}{2}\beta_2 \frac{\partial^2 A}{\partial T^2} + \frac{1}{6}\beta_3 \frac{\partial^3 A}{\partial T^3} + j\gamma |A|^2 A$$

Equation 2.18 describes the evolution of A in the first part of the transmission link, before the OPC. Through phase conjugation the signal is complex conjugated. When the OPC is located at position z_0 , the phase conjugation process can be described as [102, 103]

$$A(z_0 + \delta) = A^*(z_0 - \delta) \quad (4.7)$$

where δ represents an infinitesimal small transmission distance. By applying condition 4.7, the propagation through the rest of the transmission link equation can be used to described with 2.18 .

However, in order to see the effect of phase conjugation on dispersion and nonlinear impairments, one can describe the NLSE in the second part of the transmission link without applying the conversion as defined in equation 4.7. The NLSE in the second part of the transmission link is then described by considering A^* instead of A . This way, the discontinuity in A that is introduced by equation 4.7 can be circumvented. Equation 2.18 is then expressed after OPC by [104]

$$\frac{\partial A^*}{\partial z} = -\frac{\alpha}{2}A^* + \frac{j}{2}\beta_2\frac{\partial^2 A^*}{\partial T^2} + \frac{1}{6}\beta_3\frac{\partial^3 A^*}{\partial T^3} - j\gamma|A^*|^2 A^* \quad (4.8)$$

Note that in this equation the signal evolution over the fiber in the second part of the transmission link is still denoted by A . Table 4.1 summarizes each individual term of the NLSE before (equation 2.18) and after (equation 4.8) optical phase conjugation. From this table it can be concluded that the sign of the GVD and the Kerr-effect terms are inverted whereas the sign of the attenuation and the slope terms remain unchanged.

term	before conjugation	after conjugation
Attenuation	$-\frac{\alpha}{2}A$	$-\frac{\alpha}{2}A^*$
GVD	$-\frac{j}{2}\beta_2\frac{\partial^2 A}{\partial T^2}$	$\frac{j}{2}\beta_2\frac{\partial^2 A^*}{\partial T^2}$
Slope	$\frac{1}{6}\beta_3\frac{\partial^3 A}{\partial T^3}$	$\frac{1}{6}\beta_3\frac{\partial^3 A^*}{\partial T^3}$
Kerr-effect	$j\gamma A ^2 A$	$-j\gamma A^* ^2 A^*$

Table 4.1: *Terms of the NLSE before and after phase conjugation*

The fact that the sign of the attenuation term is the same before and after phase conjugation is to be expected since the fiber loss is not compensated for through phase conjugation. Compensation of the GVD and the Kerr-effect can be realized through OPC since the signs of these terms are inverted by the conjugation operation.

Watanabe and Shirasaki presented a general condition for compensation of the Kerr-effect [105]. In their considerations, the dispersion slope is neglected ($\beta_3 = 0$), which simplifies the NLSE to:

$$\frac{\partial A}{\partial z} = -\frac{\alpha}{2}A - \frac{j}{2}\beta_2\frac{\partial^2 A}{\partial T^2} + j\gamma|A|^2 A \quad (4.9)$$

Figure 4.10 visualizes the considered OPC based transmission line.

The OPC unit is present at $z = 0$, $-L_1$ is the transmission distance before the OPC unit and L_2 is the transmission distance after the OPC unit. The fiber parameters α , β_2 and γ are dependent on the transmission distance z . A normalized amplitude $u(z, T)$ is defined so that $|u|^2 = 1$. The complex amplitude of the signal is written as

$$A(z, T) = a(z)u(z, T) \quad (4.10)$$

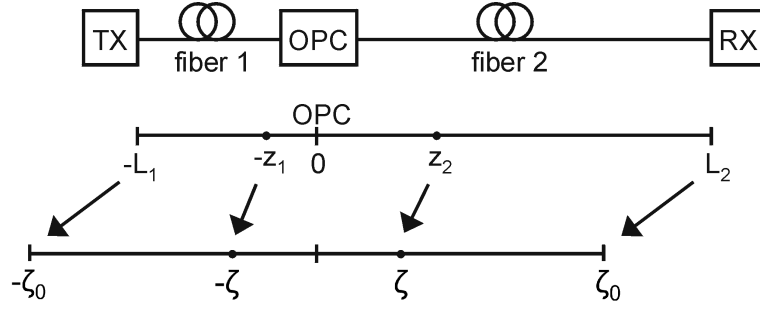


Figure 4.10: Normalization of the transmission distance with respect to the OPC.

where $a(z) \in \mathfrak{R}$ is dependent on $\alpha(z)$ as follows

$$a(z) = a(0) \exp \left[-\frac{1}{2} \int_0^z \alpha(z) dz \right] \quad (4.11)$$

Substituting equation 4.10 in 2.18, the NLSE can be expressed by

$$\frac{\partial u}{\partial z} = -\frac{\alpha(z)}{2} u - \frac{u}{a(z)} \frac{\partial a(z)}{\partial z} - \frac{j}{2} \beta_2(z) \frac{\partial^2 u}{\partial T^2} + j\gamma(z) a^2(z) |u|^2 u \quad (4.12)$$

and using equation 4.11, equation 4.12 becomes

$$\frac{\partial u}{\partial z} = -\frac{j}{2} \beta_2(z) \frac{\partial^2 u}{\partial T^2} + j\gamma(z) a^2(z) |u|^2 u \quad (4.13)$$

By normalizing the transmission distance with the following transformation

$$\zeta = \int_0^z \gamma(z) a^2(z) dz \quad (4.14)$$

the normalized NLSE can be expressed as

$$\frac{1}{\gamma(z) a^2(z)} \frac{\partial u}{\partial z} = -\frac{j\beta_2(z)}{2\gamma(z) a^2(z)} \frac{\partial^2 u}{\partial T^2} + j |u|^2 u \quad (4.15)$$

$$\frac{\partial u}{\partial \zeta} = -jB(\zeta) \frac{\partial^2 u}{\partial T^2} + j |u|^2 u \quad (4.16)$$

where

$$B(\zeta) = \frac{\beta_2(\zeta)}{2\gamma(\zeta) a^2(\zeta)} \quad (4.17)$$

The complex conjugate of 4.16 is

$$\frac{\partial u^*}{\partial \zeta} = jB(\zeta) \frac{\partial^2 u^*}{\partial T^2} - j |u^*|^2 u^* \quad (4.18)$$

Complete compensation of the phase-shift caused by dispersion and SPM can be realized when the distortions due to the phase-shift at the position $-\zeta$ in fiber 1 are exactly the same as the distortions at position $+\zeta$ in fiber 2. This is realized when

$$\frac{\beta_2(-\zeta)}{2\gamma(-\zeta)a^2(-\zeta)} = \frac{\beta_2(\zeta)}{2\gamma(\zeta)a^2(\zeta)} \quad (4.19)$$

In the first part of the transmission link, $u(-\zeta)$ obeys the evolution of 4.16. And given 4.19, $u^*(\zeta)$ obeys the evolution 4.18 after OPC. Condition 4.19 can be rewritten in z -coordinates through

$$\int_0^{-z_1} \gamma(z)a^2(z)dz = - \int_0^{z_2} \gamma(z)a^2(z)dz \quad (4.20)$$

and thereby obtaining

$$\frac{\beta_2(-z_1)}{\gamma(-z_1)a^2(-z_1)} = \frac{\beta_2(z_2)}{\gamma(z_2)a^2(z_2)} \quad (4.21)$$

$a^2(z)$ corresponds to the optical power $P(z)$ in Watt and hence 4.19 can be written as

$$\frac{\beta_2(-z_1)}{\gamma(-z_1)P(-z_1)} = \frac{\beta_2(z_2)}{\gamma(z_2)P(z_2)} \quad (4.22)$$

Basically the Kerr-effect can be totally compensated for when the ratio of nonlinear effects ($\gamma(z)P(z)$) to chromatic dispersion ($\beta_2(z)$) is equal at $-z_1$ and z_2 . In such a transmission line, OPC is capable of compensating both chromatic dispersion and nonlinear impairments [105].

In the considerations of Watanabe and Shirasaki (from equation 4.9 to 4.22), the dispersion slope of the fiber is neglected. From Table 4.1 it can be seen that the slope is not compensated for through OPC. The accumulating slope along the transmission line can impair the transmission performance. Two aspects of the accumulating slope should be taken into account, namely the impact of the uncompensated slope on the channel itself (“intra-channel slope effect”) and the impact on the inter-channel nonlinear impairments (“inter-channel slope effect”).

- Intra-channel slope effect

At data rates up to 40 Gbit/s, the uncompensated slope has almost no influence on the performance since the optical spectrum is relatively small (< 0.8 nm). However due to the slope, the effective chromatic dispersion before the post-compensation unit varies for different channels, which results in different optimal post-compensations. In most OPC-based transmission experiments reported so far, the effect of the accumulated slope is compensated for by optimizing the post-compensation after transmission on a per-channel basis [84, 106, 107, 108]. At data rates higher than 40 Gbit/s, dispersion slope can become a dominating impairment. In this case, compensation for the third order dispersion can be realized by a slope compensator [109].

- Inter-channel slope effect

Due to the dispersion slope, the neighboring channels will have a different dispersion before and after OPC. This complicates the compensation of inter-channel nonlinear impairments: XPM and FWM. Taking XPM as an example, the compensation through OPC would occur when the XPM experienced in the first part of the transmission link is exactly the same as the XPM experienced in the second part. However, due to the fiber slope (which is not compensated for through OPC) this is not the case. Figure 4.11 illustrates the influence of one co-propagating channel on a data channel before and after OPC.

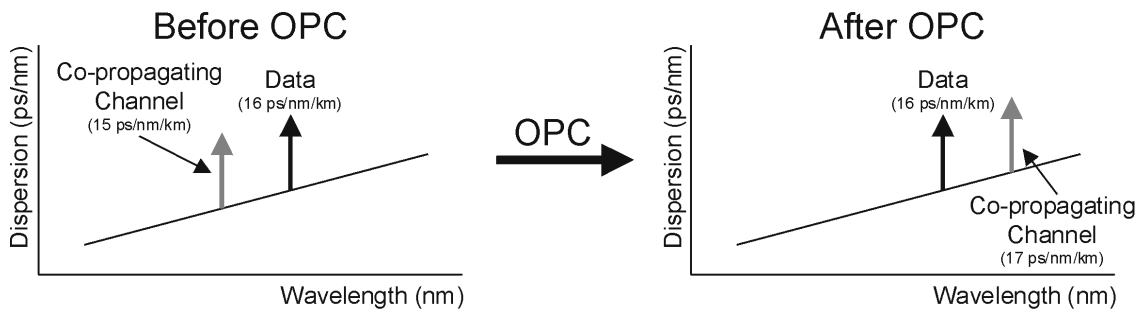


Figure 4.11: *Influence of XPM of one co-propagating channel before and after OPC.*

In this example, the GVDs before OPC of the data and co-propagating channel are 16 ps/nm/km and 15 ps/nm/km, respectively. For simplicity it is assumed that the OPC does not introduce a wavelength shift, but does mirror the optical spectrum with respect to its center frequency. After conjugation, the GVD of the data channel is still 16 ps/nm/km. The GVD of the co-propagating channel is however 17 ps/nm/km instead of 15 ps/nm/km. As a result, the influence of the co-propagating channel through XPM will be different in the second part of the transmission link (after conjugation) compared with the first part of the transmission link (before conjugation).

The compensation of XPM never has been shown experimentally through OPC. However, several experiments have reported that OPC can compensate for FWM [110, 111, 112]. The reason compensation of FWM was measured in these experiments is that the transmission distances were very short (10 to 20 km). As a result, the dispersion difference through the dispersion slope is very small. Similar to XPM, the compensation of FWM is questionable for long-haul, multi-span transmission. The compensation of XPM through OPC will be further discussed in simulation and experiment in Section 5.1

An important consideration of equation 4.22 is that total compensation of chromatic dispersion and the Kerr-effect can only be realized in a perfectly symmetric transmission link with respect to $\beta_2(z)$, $\gamma(z)$ and $P(z)$. However, due to the attenuation of the optical fiber, the power envelope along the transmission line is non-constant. This complicates

realizing a power symmetric transmission line with respect to the OPC unit. In Figure 4.12 the power envelope along the transmission line is depicted for an EDFA and a Raman amplified transmission line. In the EDFA amplified system, the power envelope with

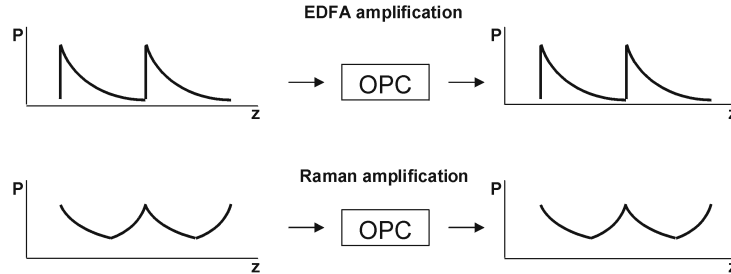


Figure 4.12: *Power envelope along the transmission line for an EDFA amplified and a Raman amplified transmission system.*

respect to the OPC unit is asymmetric, which reduces the amount of Kerr-effect that can be compensated for. It has been shown by Brener *et al.* that a more symmetric power envelope along the transmission line can be created by using Raman amplification and thereby obtain a significantly better compensation of nonlinear impairments [90]. In this proof-of-principle experiment, high input powers were used to show the impact of nonlinear impairments in a 160-km transmission link. The effective Raman gain as defined in equation 3.18 is a measure for the power symmetry of the transmission link. In the experiment of Brener, an almost fully symmetric power envelope was created with an on-off Raman gain of $G_{on-off} = 21.4 \text{ dB}$, which coincides in this experiment with an effective Raman gain of $G_{eff} = 2 - 3 \text{ dB}$. This high Raman gain can only be realized with extremely high Raman pump powers. The impact of a more power symmetric transmission link is clearly visible for this relatively short distance transmission experiment using high input powers.

For long-haul transmission, the impact of power symmetry reduces. Chowdhury *et al.* showed in [80] that for long-haul transmission, compensation of nonlinear impairments can be obtained as well using a hybrid EDFA/Raman amplification with an effective Raman gain of $G_{eff} = -10 \text{ dB}$. In Section 7.2.3 a transmission experiment will be discussed showing that even without Raman amplification, long-haul transmission can be realized with mid-link OPC. In this experiment only a 27% decrease in obtainable transmission distance is measured compared to the same system with a hybrid EDFA/Raman amplification scheme.

4.4.2 Inline optical phase conjugation

An inline OPC link is created by adding an OPC module to a conventional transmission link. In such a link, dispersion compensation is realized by DCF modules and the OPC unit is used solely for the compensation of nonlinear impairments.

The key advantage of inline OPC is that the dispersion map of the transmission link can be optimized for the compensation of nonlinear impairments in combination with OPC.

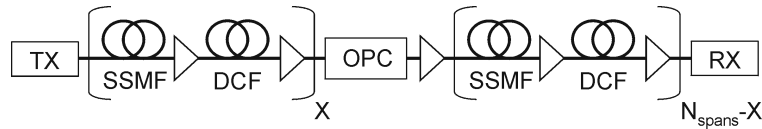


Figure 4.13: Configuration of an inline-OPC transmission link.

In [107], the compensation of intra-channel nonlinear impairments by OPC is reported for four 40-Gbit/s WDM carrier-suppressed RZ (CSRZ) channels at 100-GHz channel spacing. In this experiment a 50% increase in transmission reach is obtained through inline OPC. The compensation of intra-channel nonlinear impairments has been shown for a 40-Gbit/s DPSK single channel experiment as well [80]. The inline OPC configuration is very tolerant towards the exact placement of the OPC-unit. Investigations reported in [113] show that for the compensation of nonlinear impairments, the location of the OPC can vary from nearly $1/3^{rd}$ and $2/3^{rd}$ of the transmission line.

The main disadvantage of the inline OPC configuration is that both OPC and DCF modules are required. Therefore, the inline OPC configuration is not a cost effective solution.

4.4.3 Mid-link optical phase conjugation

In literature, mid-link OPC is occasionally referred to as mid-link spectral-inversion (MSLI). In earlier experiments where only one span was bridged mid-link OPC is referred to as mid-span spectral inversion (MSSI). The configuration and dispersion map of a multi-span mid-link OPC system are shown in Figure 4.14. In this example, a transmission link with

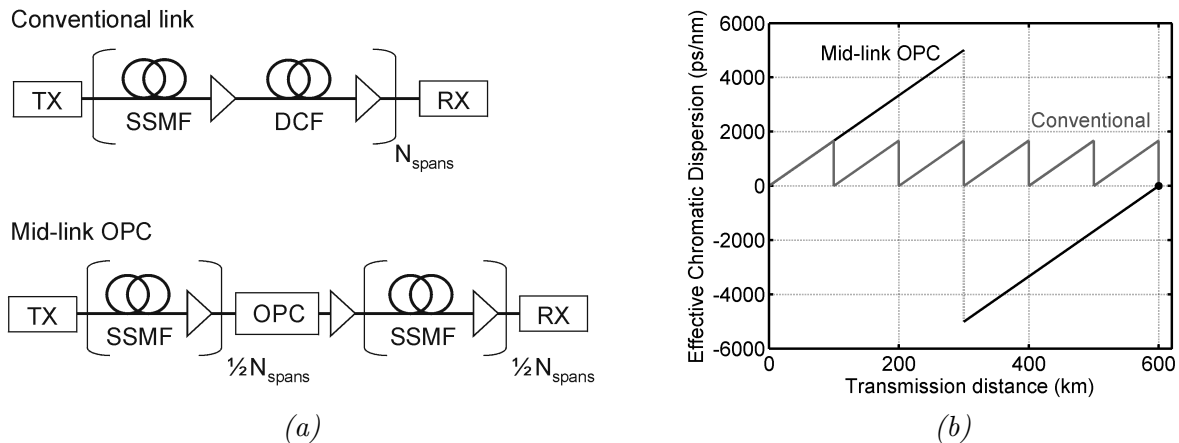


Figure 4.14: Mid-link OPC and conventional transmission link, a) Transmission link, b) Dispersion map for $N = 6$

six 100-km SSMF spans is illustrated. As a reference the dispersion map of a conventional transmission link is plotted as well. For simplicity, the pre- and post-compensation are set

to 0 ps/nm. Additionally, the chromatic dispersion is in the conventional transmission link fully compensated for after each span.

In the mid-link OPC configuration, the inline DCF modules are removed from the transmission link. As a result a single-stage amplifier can be used for inline amplification instead of the double-stage, required for the conventional transmission link. Whereas in a conventional transmission system the inline dispersion compensation is a design parameter of the transmission link (Section 3.3), the dispersion map of mid-link OPC is inherently the same for all transmission links. Through OPC, the sign of the effective chromatic dispersion is inverted (Table 4.1). Thereby a chromatic dispersion near 0 ps/nm is obtained after transmission.

However, the simplified dispersion map of mid-link OPC has some implications for the high power regions in the transmission link. The high power regions of the DCF- and the OPC-based transmission link are depicted for a 6 span transmission link in Figure 4.15a and 4.15b. In the DCF-based transmission scheme, the pre- and inline-compensation

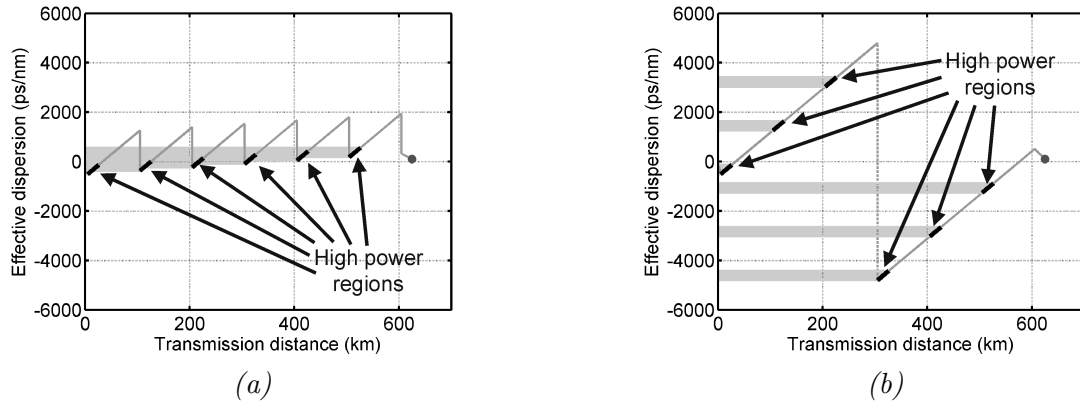


Figure 4.15: Dispersion map with the high power regions marked, a) DCF-based transmission link, b) OPC-based transmission link.

can be adjusted such that the high power regions are located in the optimal dispersion areas where the peak power of the signal is relatively low. However, in the OPC-based configuration, the dispersion accumulates along the transmission link. Already after three spans of SSMF, an accumulated chromatic dispersion of over 4000 ps/nm is obtained. Therefore, the high power regions are ‘spread’ over the dispersion map. As a result, the pre-compensation cannot be used to place all high power regions in a dispersion area where the signal peak power is relatively low.

Another drawback of mid-link OPC’s dispersion map is that extra OPC-units are required in links employing optical add-drop multiplexers (OADM). For decades, optical transmission links were mainly point-to-point links where all the wavelengths of a certain link traverse the same path. In order to increase the flexibility of the optical network, OADMs can be used. An example of a link with an OADM is shown in Figure 4.16 In this example an OADM is placed in the middle of an eight-span transmission link. At the OADM, several WDM channels are “dropped” (removed from the transmission line) and

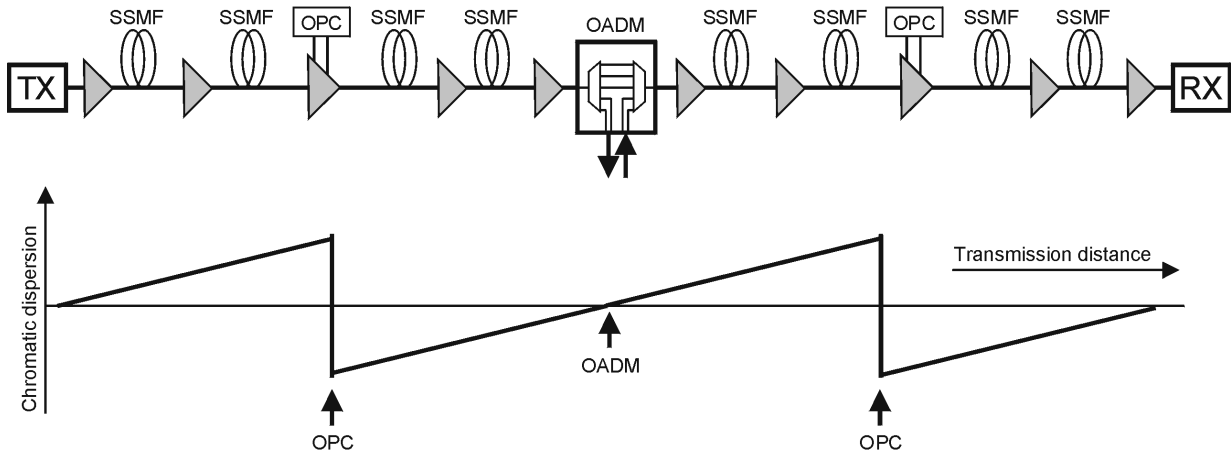


Figure 4.16: *Example of an OADM in a transmission link.*

other channels are added. The advantage of using OADMs is that the through traffic (the channels that are not affected by the OADM) does not have to go through OEO, which saves a lot of equipment and therefore money. At the OADM, an accumulated dispersion of ≈ 0 ps/nm is required so that the dropped channels can be detected. If the OADM is not present in the transmission link, the OPC can be placed in the middle of the link. However, with the OADM, two OPC-units are required, namely one before and one after the OADM. This significantly reduces the cost-effectiveness of OPC in transmission links with many OADM nodes.

A problem arises with mid-link OPC for asymmetric transmission links or links with an odd span-count. In such a transmission link, the OPC cannot be placed in the middle of the transmission link. In this case, the OPC-unit is placed “off-center” and an extra DCF module is employed to obtain full dispersion compensation. Mid-link OPC with off-center placement is further discussed in Section 5.3.

4.5 Summary

In this chapter, different aspects of OPC are discussed, from processes to OPC transmission links. Three OPC processes are commonly used to phase conjugate an optical signal, namely FWM, DFG and cascaded SHG:DFG. FWM is based on the $\chi^{(3)}$ nonlinearity that is used in either a HNLF or an SOA.

- Silica

The silica based FWM offers a large acceptance bandwidth (72 nm) and a relatively high conversion efficiency (≈ -10 dB). Other advantages of silica are that it is a passive solution and that multiple WDM channels can be conjugated with a single unit. Limitations of the silica based FWM are that the pump wavelength must be fixed at the zero dispersion wavelength and that optical integration is not possible.

- Indium gallium arsenide phosphide

Indium gallium arsenide phosphide can be used to create an SOA. The SOA is a compact FWM-based solution that offers relatively high conversion efficiency and no restrictions on the wavelength of the pump signal. The main drawbacks are that the acceptance bandwidth is small (8 nm) and that the noise figure of the SOA is relatively high. Furthermore, XPM between channels limits the amount of WDM channels that can be converted.

Both DFG and cascaded SHG:DFG processes are based on the $\chi^{(2)}$ nonlinearity. The main advantage of using a $\chi^{(2)}$ process for OPC instead of $\chi^{(3)}$ (e.g. FWM), is that disturbing nonlinear impairments caused by the $\chi^{(3)}$ process, such as SPM and XPM, are negligible. For $\chi^{(2)}$ a medium is required that lacks inversion symmetry. Two such materials are discussed: LiNbO₃ and AlGaAs. In both media phase matching is realized by periodic poling.

- LiNbO₃

The periodically-poled LiNbO₃ (PPLN) offers a large acceptance bandwidth (> 50 nm) and a relatively high conversion efficiency (≈ -7 dB). The main disadvantage is however that LiNbO₃ suffers from the presence of the photorefractive effect. The photorefractive effect can be mitigated by heating the device. The operating temperature ranges from 50° to 200° (dependent on the PPLN-type). Another disadvantage is that the pump wavelength must match the phase matching wavelength.

- AlGaAs

The main advantage of AlGaAs is that the waveguide can be designed so that polarization independent OPC can be realized. All other media are polarization dependent. Similar to the PPLN, the pump wavelength must be set to the phase matching wavelength. The acceptance bandwidth of AlGaAs is large (90 nm) and the $\chi^{(2)}$ nonlinearity of AlGaAs is about three times higher than that of LiNbO₃. However, due to the high scattering loss that is present in the devices reported so far, the conversion efficiency of AlGaAs is low (-17 dB using the DFG process).

The focus in this thesis is on transmission with a PPLN waveguide, since it is a compact device that offers transparent WDM conversion with high conversion efficiency. As the PPLN-waveguide is polarization dependent, a polarization diversity structure is required. Two commonly used polarization diversity structures are the parallel and the counter-directional structure.

OPC can be employed in a conventional link for the compensation of nonlinear impairments. This configuration is referred to as inline-OPC. In such a transmission link, DCF modules are used to compensate for the chromatic dispersion and an OPC is placed in the transmission line to conjugate the signal and thereby invert the distortions in the phase, caused by nonlinear impairments. As a result, phase distortions before conjugation that occur through the Kerr-effect are undone by phase distortions after conjugation.

CHAPTER 4. OPTICAL PHASE CONJUGATION

A more cost-effective solution is to use mid-link OPC. In this configuration OPC is used for both chromatic dispersion compensation and compensation of the Kerr-effect. Hence no inline DCF modules are used in this configuration. Instead the dispersion accumulates along the transmission line and is compensated for by placing an OPC mid-link. A disadvantage of this method is that inline OADMs require the use of more OPC-units. Furthermore, the placement of the OPC in an asymmetric transmission link is non-trivial.

Chapter 5

ASK based transmission

In this chapter the WDM transmission performance of both 10-Gbit/s and 40-Gbit/s NRZ-ASK is discussed using an OPC-based transmission link¹. The ability for OPC to compensate XPM in a long-haul DWDM 10-Gbit/s transmission system is assessed in Section 5.1. Section 5.2 discusses the transmission performance at 40 Gbit/s for an 800-km transmission link. The performance of the OPC-based transmission system is then compared with that of a DCF-based transmission system. Finally, in Section 5.4 OPC-based transmission is discussed using mixed data rates and mixed modulation formats. In this experiment, 42.7-Gbit/s and 10-Gbit/s NRZ-ASK WDM channels are combined with a 42.7-Gbit/s duobinary channel.

5.1 XPM-limited 10-Gbit/s ASK transmission

Increasing the transmission capacity is most easily achieved by enhancing the spectral efficiency. One way to increase the spectral efficiency in a WDM scheme, is by reducing the channel spacing. Using DCF for chromatic dispersion compensation, spectral efficiencies of up to 0.4 bit/s/Hz have been reported in 10-Gbit/s WDM transmission links with 25-GHz channel spacing [114, 115]. In ASK transmission systems with narrow channel spacing, the feasible transmission distance is mostly limited by inter-channel impairments such as XPM.

Using OPC for chromatic dispersion compensation, many WDM transmission experiments have been reported at a 10 Gbit/s data rate [85, 91, 116, 117]. However, a wide channel spacing is used (> 100 GHz) in all these experiments and therefore their performance is limited by deterministic single-channel distortions such as SPM and chromatic dispersion. In this section the performance of OPC is assessed for an XPM-limited transmission link with narrow channel spacings (< 100 GHz).

¹The results described in this chapter are published in P1, P6, P9-10, P22-P25

5.1.1 Simulation

The influence of XPM is assessed by simulating a transmission with and without neighboring channels. Simulations with and without mid-link OPC are conducted to evaluate the regenerative effect of phase conjugation. The dispersion map of a transmission line has a strong influence on the XPM. Therefore, two dispersion compensation schemes are investigated: the lumped and the periodic dispersion compensation scheme (Figure 5.1). The periodic dispersion map with OPC corresponds to the inline OPC configuration (4.4.2) and the lumped dispersion map to the mid-link OPC configuration (4.4.3). The simulations

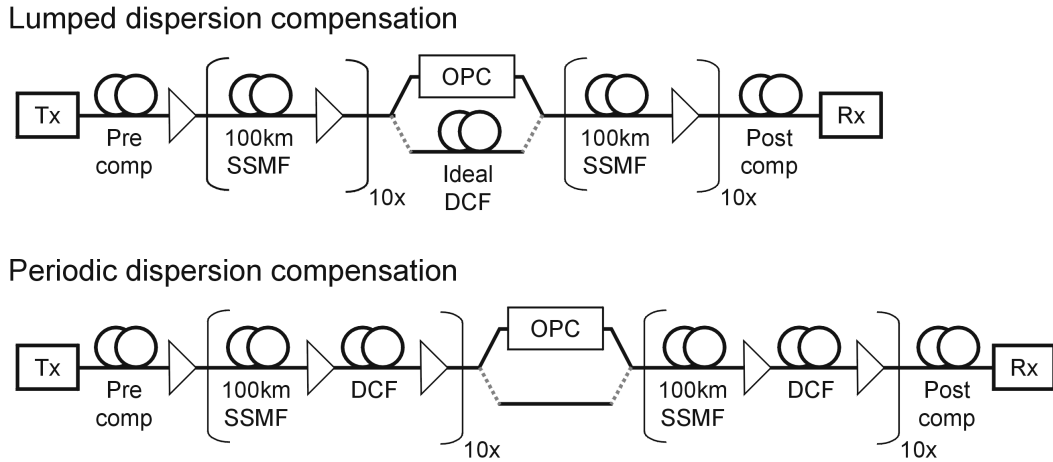


Figure 5.1: *Simulation setup of the lumped DCF and the OPC-based transmission line.*

are conducted using a split-step Fourier algorithm [20]. The performance of the signal is evaluated by the quality-factor (Q-factor) as defined in appendix B. A 10-Gbit/s PRBS data signal at 1550.9 nm (193.3 THz) is simulated with a length of 2^8 bits. The simulation rate is 16 samples per bit and the step size is chosen such that the maximum nonlinear phase shift is 0.294 degrees (0.005 rad). Noise is treated analytically in the simulations and the noise figure of the inline amplifiers is set to 4 dB. The following parameters are used for the SSMF fiber: $L = 100$ km, $\alpha = 0.2$ dB/km, $D = 17$ ps/nm/km (at 1550.9 nm), $S = 0.057$ ps/nm²/km and $\gamma = 1.2993$ W⁻¹ km⁻¹. The transmission distance is fixed to 2000 km for all simulations. In the simulations with OPC, an ideal phase conjugator is used as defined in equation 4.7. After transmission, the Q-factor is optimized by varying the post-compensation with a granularity of 100 ps/nm.

The DCF modules used in the periodic dispersion maps have the following parameters: $\alpha = 0.5$ dB/km, $D = -102$ ps/nm/km (at 1550.9 nm), $S = -0.34$ ps/nm²/km and $\gamma = 2.5$ W⁻¹ km⁻¹. In order to reduce the nonlinear impairments in the DCF modules, the launch power into the DCF is chosen 6 dB lower than the launch power used for the SSMF. The periodic dispersion map (pre-compensation and inline-compensation) is optimized for transmission with 50-GHz spaced WDM channels. For all simulations with the periodic dispersion map, the pre-compensation and inline-compensation used are -510 ps/nm and +40 ps/nm/span, respectively [42, 44].

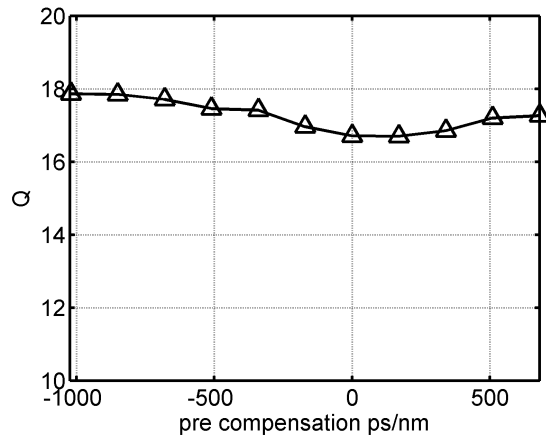


Figure 5.2: *Pre-compensation variation for the lumped dispersion map with mid-link OPC.*

In the simulations with the lumped dispersion map without OPC, an ideal lumped DCF is used mid-link to compensate for the chromatic dispersion, so that the effective dispersion map of the transmission link with and without OPC is the same. Figure 5.2 shows the Q-factor as a function of the pre-compensation for the lumped dispersion map with OPC after 2000 km transmission. In this single channel simulation, the input power into the SSMF is set to 3 dBm. From Figure 5.2 it can be seen that the dependence of the Q-factor on the pre-compensation is relatively small: when varying the pre-compensation from -1020 ps/nm to +680 ps/nm, the Q-factor changes by only 1.5. As discussed in section 4.4.3, the small influence of the pre-compensation on the transmission performance is to be expected, since in the mid-link OPC configuration the dispersion map cannot be used to reduce the peak power of the signal in the high power regions. For all lumped dispersion maps the same pre-compensation is chosen as used in the DCF-based configuration (-510 ps/nm).

Figure 5.3a and 5.3b depict the contour diagrams of the Q-factor as a function of the SSMF launch power and residual dispersion with and without OPC. In these plots, the performance is shown for single channel transmission with the lumped dispersion map. The input power is varied from -8 dBm to 8 dBm per channel and the dispersion from -1600 ps/nm to 1600 ps/nm. At low input powers (< -4 dBm), the performance is limited by ASE and therefore the Q-factors in both configurations are similar. At high input powers (> -4 dBm), where SPM is the dominating impairment, the performance with OPC is significantly better than the performance without OPC: the maximum Q-factor after transmission is 9.7 and 20.5 for the configuration without and with OPC, respectively. Without OPC, the ORD is ≈ 800 ps/nm providing the best Q-factor after transmission. This positive residual dispersion is optimal since it partly compensates impairments through SPM [118]. The ORD for the configuration with OPC is ≈ 0 ps/nm. It can therefore be concluded that most SPM is compensated for in the configuration with OPC, resulting in the Q-factor improvement of 10.8. Apart from the higher Q-factor, the OPC configuration has a larger dispersion tolerance as well. For a Q-factor > 6 the tolerance towards chromatic

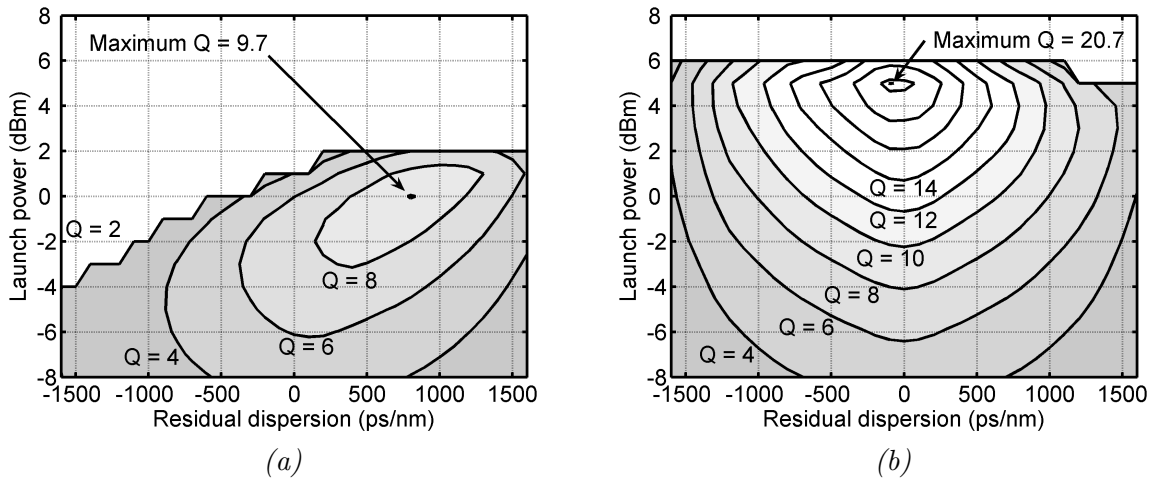


Figure 5.3: *Lumped dispersion map, single channel: Contour diagram of the Q-factor as a function of the input power per channel and residual dispersion, a) without OPC, b) with OPC*

dispersion is 1,960 ps/nm and 2,920 ps/nm for the configuration without and with OPC, respectively.

Figure 5.4a and 5.4b depict the Q-factor in contour diagrams for a periodic dispersion map without and with OPC. The maximum Q-factor without OPC (25.7) is slightly higher than the maximum Q-factor with OPC (23.8). The ORD is 600 ps/nm and -500 ps/nm for the configuration without and with OPC, respectively. Remarkable is that the ORD with OPC is obtained for -500 ps/nm. This negative residual dispersion indicates that the inline-compensation of the periodic dispersion map, which is optimized without OPC, is not optimal for OPC transmission. The dispersion tolerance (Q-factor > 6) is higher

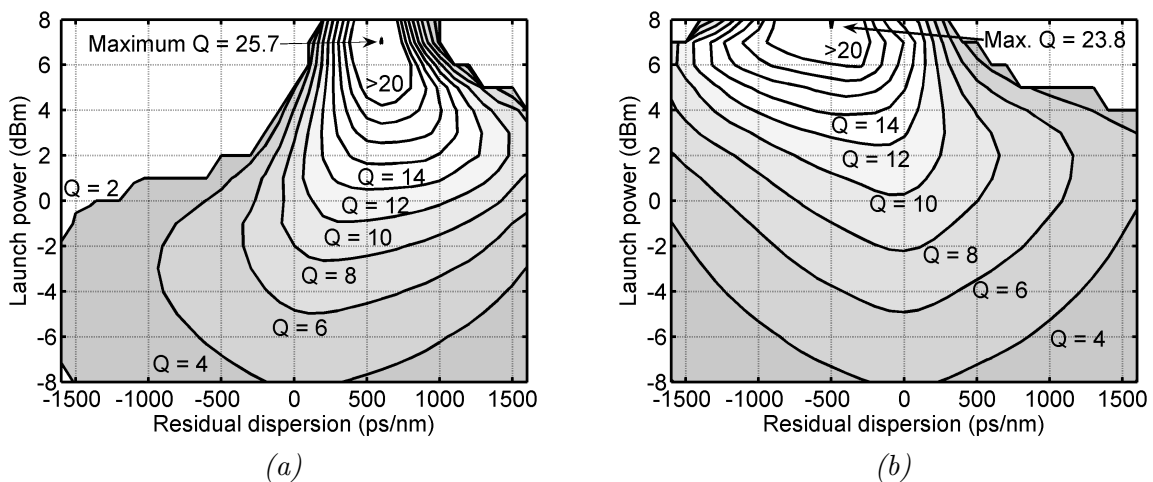


Figure 5.4: *Periodic dispersion map, single channel: Contour diagram of the Q-factor as a function of the input power per channel and residual dispersion, a) without OPC, b) with OPC*

5.1. XPM-LIMITED 10-GBIT/S ASK TRANSMISSION

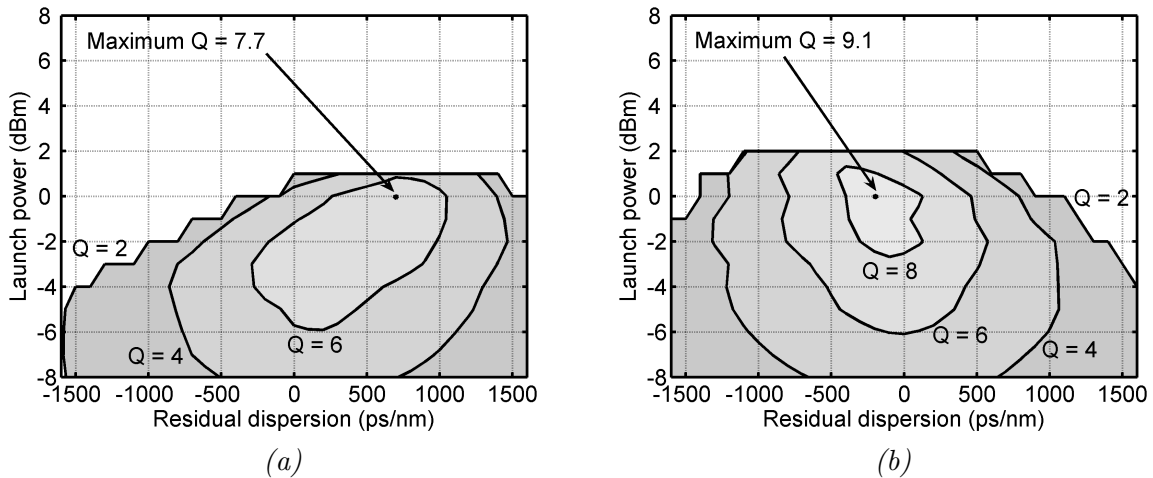


Figure 5.5: *Lumped dispersion map, 5 WDM channels with 50-GHz channel spacing: Contour diagram of the Q-factor as a function of the input power per channel and residual dispersion, a) without OPC, b) with OPC*

with OPC (2,900 ps/nm) than without OPC (2,050 ps/nm). Furthermore, at the launch power resulting in the best Q-factor after transmission, the dispersion tolerance in the configuration with OPC ($\approx 1,700$ ps/nm at 8 dBm) is significantly larger than that without OPC (≈ 800 ps/nm at 7 dBm).

The maximum Q-factor with OPC is similar for the lumped (20.7) and the periodic (23.8) dispersion maps. In the configuration without OPC, however, a significant performance difference is observed. The maximum Q-factor of the periodic dispersion map (25.7) is 16 higher than the maximum Q-factor obtained for the lumped dispersion map (9.7). This performance difference is caused by the fact that in the lumped configuration higher peak powers occur, resulting in an enhanced SPM. In Figure 3.7 (Section 3.3) it can be seen that when the dispersion is not compensated for, the peak power of a 10-Gbit/s NRZ-ASK signal linearly increases up to a dispersion of 5000 ps/nm. In the periodic dispersion map, the dispersion is compensated for after each span. As shown in the dispersion map depicted in Figure 4.15a, the high power regions can, with a proper design of the pre- and inline-compensation, all be located in the dispersion area (< 5000 ps/nm) where the signal peak power is relatively low. In the lumped dispersion map, the chromatic dispersion is compensated for mid-link and as illustrated in Figure 4.15b, the high power regions are spread over the whole dispersion map. In the 2000 km simulations discussed in this section, the high power regions are spread over a dispersion range of $\pm 16,000$ ps/nm. As a result, the peak powers in the high power regions are for a system with a lumped dispersion map significantly higher than those that occur in a system with periodic dispersion compensation. These higher peak powers in the lumped dispersion map are the cause of the increased SPM penalty.

By simulating five co-propagating WDM channels at a 50-GHz grid, the influence of XPM is assessed. Figure 5.5 shows for the lumped dispersion map (with and without OPC)

the contour diagrams of the Q-factor as a function of the input power per channel and residual dispersion. In these simulations, the Q-factor of the middle channel (experiencing most XPM) is assessed. The maximum Q-factors for the lumped DCF and the OPC-based configuration are 7.7 and 9.1, respectively. The dispersion tolerances in this configuration for a Q-factor > 6 are 1,340 ps/nm with OPC and 1,430 ps/nm with DCF. For low input powers (< -4 dBm), the influence of ASE is dominant over nonlinear effects such as XPM. ASE is independent of the neighboring channels and therefore the performance for low input powers is similar to the performance obtained in the single channel simulations. At higher input powers (> -4 dBm), a strong performance degradation due to XPM is observed in the configuration with OPC compared with the single channel simulation. As a result, the performance improvement obtained through OPC is significantly lower: instead of the Q-factor improvement of 10.8 in the single channel configuration, a Q-factor improvement of 1.4 is observed for the WDM simulation. In Figure 5.6a and 5.6b the Q-factor contour plots are depicted for the periodic dispersion map, with and without OPC. The maximum

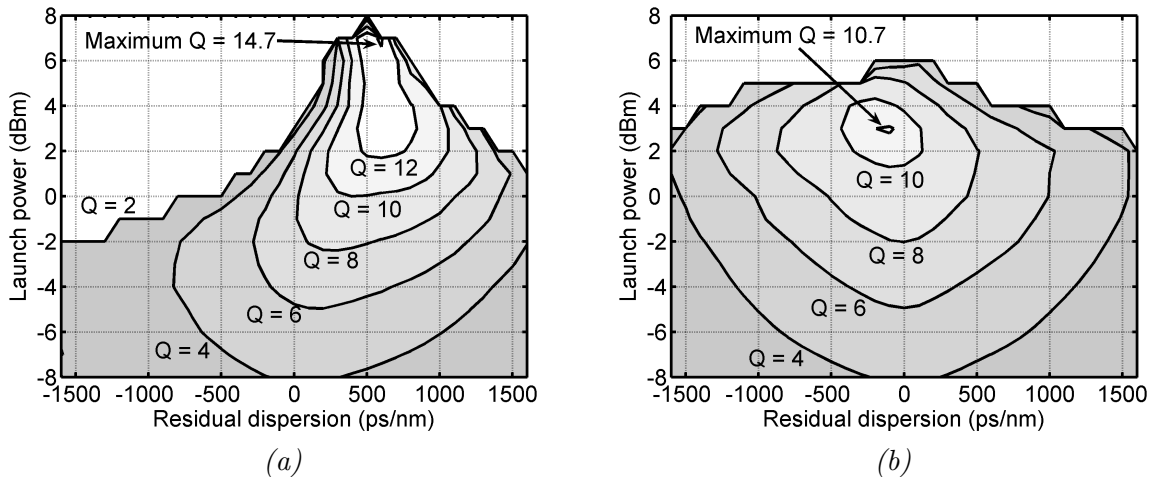


Figure 5.6: *Periodic dispersion map, 5 WDM channels with 50-GHz channel spacing: Contour diagram of the Q-factor as a function of the input power per channel and residual dispersion, a) without OPC, b) with OPC*

Q-factor without OPC (14.7) is higher than that obtained with OPC (10.7). Despite the difference in maximum Q-factor, a larger tolerance towards residual dispersion is obtained in the OPC-based configuration: for a Q-factor > 6 the dispersion tolerance is 1,760 ps/nm for the DCF and 2,320 ps/nm for OPC-based configuration. Similar to the single channel case, the difference in maximum Q-factor is small for the lumped (9.1) and periodic (10.7) dispersion map when OPC is employed, whereas without OPC a large performance difference is present: in the configuration without OPC, the maximum Q-factor of the periodic dispersion map (14.7) is 7 higher than the maximum Q-factor obtained for the lumped dispersion map (7.7).

To increase the influence of XPM, simulations are conducted where the channel spacing is reduced from 50 GHz to 25 GHz. Figure 5.7 shows the performance of the lumped

5.1. XPM-LIMITED 10-GBIT/S ASK TRANSMISSION

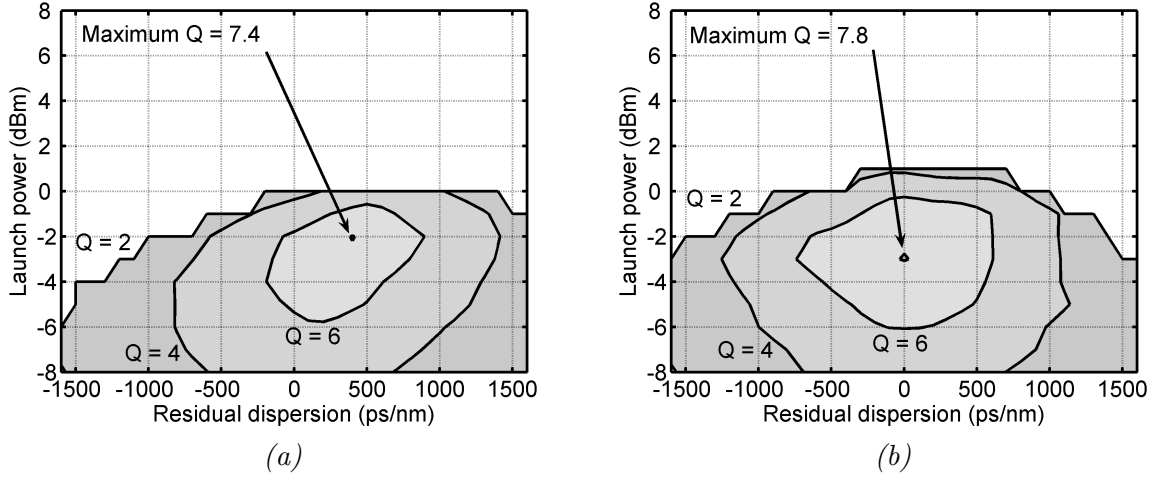


Figure 5.7: *Lumped dispersion map, 5 WDM channels with 25-GHz channel spacing: Contour diagram of the Q-factor as a function of the input power per channel and residual dispersion, a) without OPC, b) with OPC*

dispersion map for five WDM channels with 25-GHz channel spacing. The maximum Q-factor for the OPC and lumped DCF configuration are 7.8 and 7.4, respectively. Hence, by reducing the channel spacing from 50 GHz to 25 GHz, the improvement in Q-factor through OPC is only 0.4 instead of 1.4. The dispersion tolerance for Q-factor > 6 is 1,070 ps/nm and 1,350 ps/nm for the configuration without and with OPC, respectively.

In Figure 5.8a and 5.8b the Q-factor contour diagrams are plotted of the periodic dispersion map for five 25-GHz spaced WDM channels without and with OPC. The maximum Q-factor is 9.1 for the configuration with as well as the configuration without OPC. Furthermore, a similar dispersion tolerance is obtained for a Q-factor > 6 : 1,280 ps/nm for the configuration without OPC and 1,390 ps/nm for the configuration with OPC.

Table 5.1 summarizes the maximum Q-values and Table 5.2 the residual dispersion tolerances that are obtained in the different 10-Gbit/s simulations. It can be concluded that

Maximum Q-factor	lumped map DCF	lumped map OPC	periodic map DCF	periodic map OPC
single channel	9.7	20.7	25.7	23.8
WDM 50-GHz spacing	7.7	9.1	14.7	10.7
WDM 25-GHz spacing	7.4	7.8	9.1	9.1

Table 5.1: *Summary of the maximum Q-factors obtained in the 10-Gbit/s single channel and WDM simulations*

the lumped dispersion map of mid-link OPC introduces a relatively high SPM penalty compared with a periodic dispersion map for transmission at a 10-Gbit/s data rate. Through mid-link OPC, most of the SPM can be compensated for so that the performance is compa-

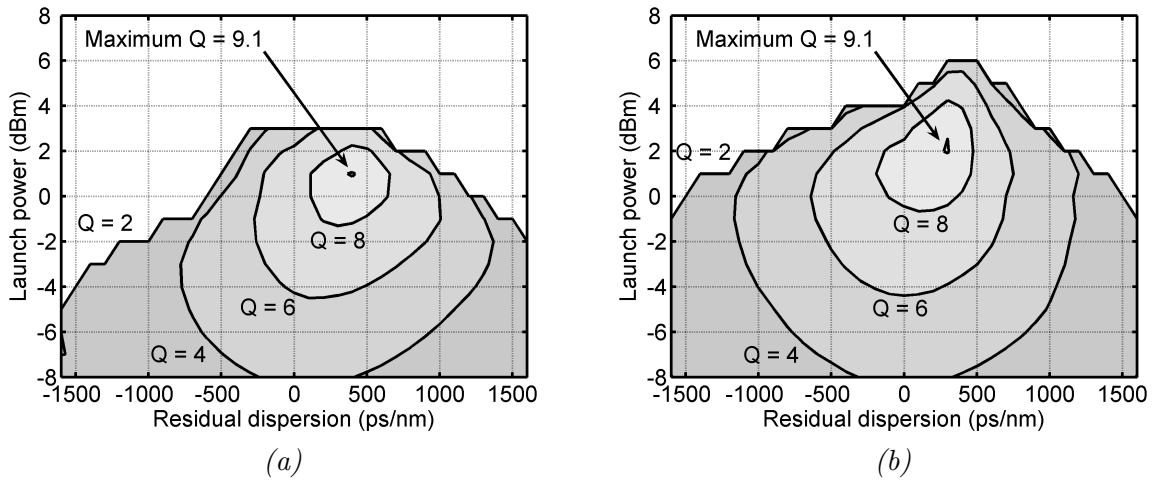


Figure 5.8: *Periodic dispersion map, 5 WDM channels with 25-GHz channel spacing: Contour diagram of the Q-factor as a function of the input power per channel and residual dispersion, a) without OPC, b) with OPC*

Dispersion tolerance Q-factor > 6 [ps/nm]	lumped map DCF	lumped map OPC	periodic map DCF	periodic map OPC
single channel	1,960	2,920	2,050	2,900
WDM 50-GHz spacing	1,340	1,430	1,760	2,320
WDM 25-GHz spacing	1,070	1,350	1,280	1,390

Table 5.2: *Summary of the maximum dispersion tolerances obtained in the 10-Gbit/s single channel and WDM simulations*

erable (without XPM) to that of an optimized periodic dispersion map. The improvements in Q-factor when OPC is introduced mid-link instead of DCF are 10.8, 1.4 and 0.4 for single channel, 50-GHz WDM and 25-GHz WDM transmission, respectively. Thus, for stronger influence of XPM induced nonlinear impairments, smaller Q-factor improvements are obtained through OPC. Therefore, the ability for OPC to compensate for XPM in a lumped dispersion map is questionable.

The periodic dispersion map is well suited for transmission at 10 Gbit/s. Nevertheless, it can be concluded that the added value of OPC in a periodic dispersion map is marginal: by introducing OPC, the dispersion tolerance is broadened, but the maximum Q-factor is reduced. However, the performance of the periodic dispersion map is in these simulations optimized without OPC. As proposed in [119], the performance of OPC in a periodic dispersion map can significantly be improved by optimizing the pre- and inline-compensation with OPC.

5.1.2 Experiment

In order to experimentally verify the performance of OPC in the XPM-limited regime, transmission experiments are conducted using an 800-km straight line. In this experiment seven WDM channels are transmitted and the influence of XPM is assessed by measuring the BER performance for two different channel spacings: 50 GHz and 25 GHz. Figure 5.9 shows the experimental setup. Seven CW signals (1550.92 nm the central wavelength) are

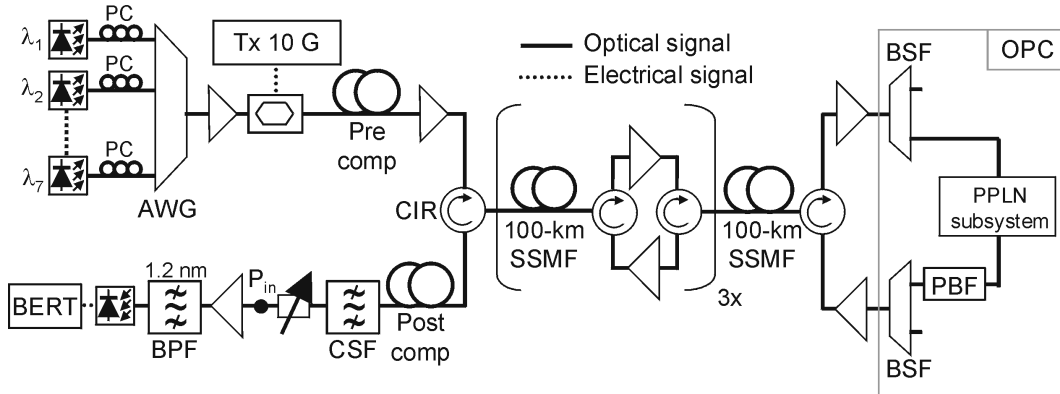


Figure 5.9: *Experimental setup of the 10-Gbit/s WDM transmission line with 25-GHz channel spacing.*

co-polarized by polarization controllers (PC) and NRZ modulated at 9.95-Gbit/s with a $2^{31} - 1$ pseudo random bit sequence (PRBS). The optical spectrum of the seven 25-GHz spaced channels is depicted in Figure 5.10a. A pre-compensation of -340 ps/nm is used before transmission to de-correlate the different wavelength channels. The transmission link consists of four spans of 100-km SSMF. In the transmission link no DCF is used. The input power into the SSMF is fixed to 1 dBm per channel. The total transmission distance is extended to 800 km by propagating forward and backward through the same link. Optical circulators (CIR) are used in the transmission link to separate the forward and backward propagating signals. In this configuration an ideally symmetrical setup in the transmission line is created with respect to the phase conjugator, which is placed after the first 400 km.

The phase conjugator spectrally mirrors the incoming data channels with respect to its pump wavelength (1546.12 nm). Figure 5.10b shows the optical spectrum at the output of the PPLN subsystem. Before the data signals are inserted into the PPLN subsystem, a band-selection filter (BSF) removes the out of band ASE. After the PPLN subsystem, the pump signal is removed by a pump-block filter (PBF) and the original data signals are suppressed by a BSF. Figure 5.10c shows the optical spectrum after the optical filtering. In the middle of the optical spectrum (at 1546.12nm) a residual of the suppressed pump can be seen. The PPLN subsystem used in this experiment is based on the parallel polarization diversity scheme as discussed in Section 4.3.1. After transmission the residual dispersion is optimized to obtain the best BER performance with a granularity of ≈ 50 ps/nm. The

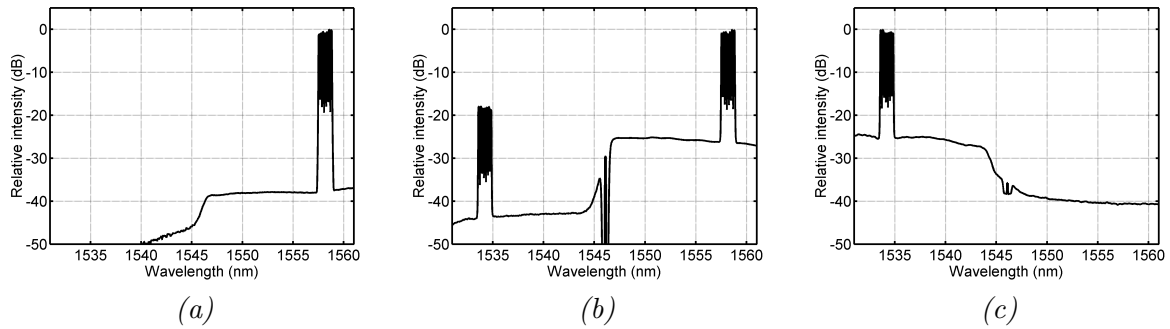


Figure 5.10: *Optical spectra a) back-to-back, b) after the PPLN subsystem, c) after the BSF, at the output of the OPC*

middle channel is selected using a 0.2 nm CSF and after amplification and filtering (1.2 nm BPF) the BER is assessed with a BER tester.

Figure 5.11 shows the back-to-back eye diagram as well as the eye diagram after 400-km and 800-km transmission (WDM, 25-GHz spacing). The open eye diagram obtained after the 800-km transmission demonstrates the reconstruction of a good quality signal through optical phase conjugation. Since no DCF is used in the transmission link the eye in the middle of the link (400 km) is severely distorted due to dispersion.

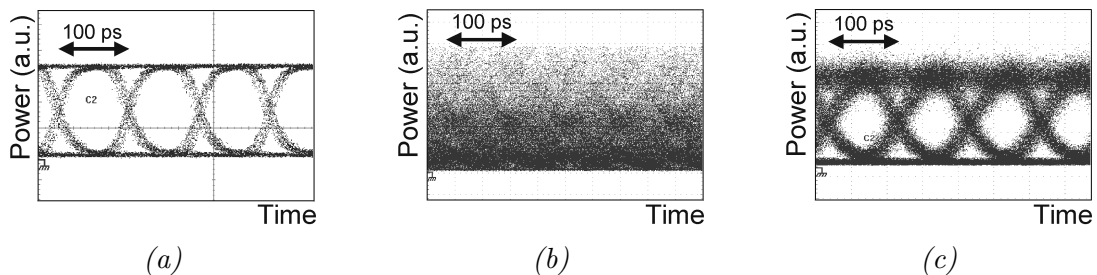


Figure 5.11: *Eye diagram a) back-to-back, b) after 400 km transmission, c) after 800 km transmission*

In Figure 5.12 the BER of the central wavelength channel (experiencing the most inter-channel nonlinear effects) is depicted as a function of the received optical power at the transmitter. A small BER penalty is measured when the OPC is introduced in the back-to-back configuration. This penalty results from the extra filtering and amplification required for the OPC-unit. The BER performance is depicted after transmission for two configurations: WDM at 50-GHz and WDM at 25-GHz channel spacing. Although error-free operation ($BER < 10^{-10}$) is achieved, an error floor is present at both 25-GHz and 50-GHz channel spacing. At low BER values ($BER \approx 10^{-9}$), the received power penalty compared with the back-to-back configuration is 8 dB and 5 dB for the 25-GHz and 50-GHz channel spacings, respectively. Since reducing the channel spacing from 50 GHz to 25 GHz results in a 3-dB received power penalty due to XPM it can be concluded that in this configuration, phase conjugation does effectively not compensate for inter-channel nonlinear effects

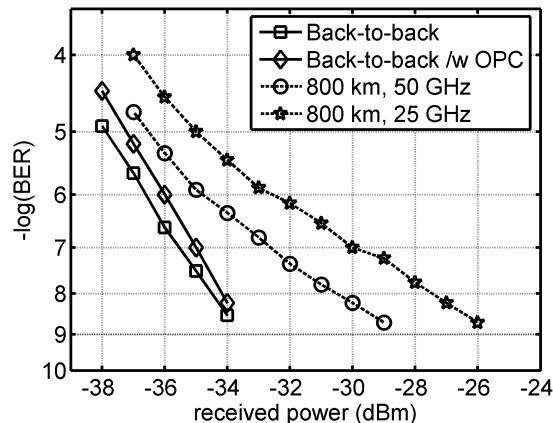


Figure 5.12: *BER performance as a function of the received power: back-to-back, back-to-back with OPC and after 800-km WDM transmission at a 25-GHz and a 50-GHz grid.*

such as XPM.

In both simulation and transmission experiment discussed in this section, compensation of XPM through OPC could not be measured. However, Simulations reported in [119] show that XPM compensation can be realized by optimizing the periodic dispersion map with OPC. In these simulations the dispersion map is optimized for the inline-OPC link, instead of adding an OPC to an optimized conventional link.

5.2 WDM 40-Gbit/s ASK transmission

An effective method to reduce power consumption as well as the number of active components in a transmission link is by increasing the data rate. In the SONET and SDH protocol, it is the convention to increase the data rate in steps of four. As a result many WDM transmission experiments have been conducted with various ASK modulation formats in conventional transmission links [120, 48, 34].

Using OPC for chromatic dispersion compensation, many transmission experiments have been reported at a 40-Gbit/s data rate. In [84], five 40-Gbit/s channels at 200-GHz channel spacing are transmitted over 105 km of SSMF using HNLF for OPC. All other OPC-based experiments reported so far using 40-Gbit/s ASK (or higher data rates), are single channel experiments [121, 101, 122, 123, 124, 125]. In this section the performance of 42.8-Gbit/s transmission is assessed with 16 WDM channels at 100 GHz channel spacing. The transmission performance of mid-link OPC is compared to that of a conventional transmission system using an 800-km straight-line of SSMF.

For both the DCF-based and the OPC-based setup, the same transmitter (Figure 5.13a) and receiver (Figure 5.13b) are used. The WDM transmitter consists of sixteen DFB lasers with wavelengths ranging from 1548.5 nm to 1560.6 nm (100-GHz spacing), which are multiplexed in an AWG and modulated at 42.6 Gbit/s ($2^{31}-1$ PRBS). After the modulator,

a DCF module is used to decorrelate and pre-compensate the different channels in the fiber. The optimal pre-compensation for the OPC-based and the DCF-based configuration is found to be -510 ps/nm and -340 ps/nm, respectively. The receiver is depicted in Figure 5.13b. The chromatic dispersion is optimized per channel using a variable dispersion compensator with a granularity of ≈ 10 ps/nm. Subsequently, the signal is amplified and filtered by a bandpass filter (BPF) with a full-width at half-maximum (FWHM) of ≈ 80 -GHz. After the BPF, the signal is converted to the electric domain by a photodiode and detected on a BER tester (BERT).

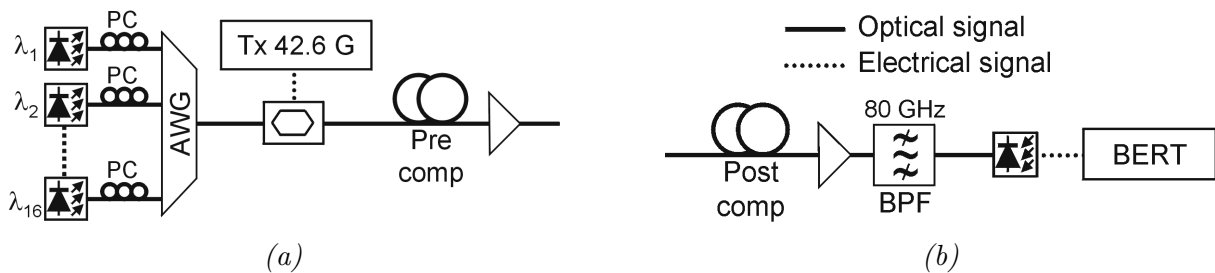


Figure 5.13: *Experimental setup of a) Transmitter, b) Receiver*

The OPC and DCF-based transmission line are depicted in Figure 5.15 and 5.14, respectively. Both transmission lines consists of eight 100-km spans of SSMF. In the DCF-based configuration each SSMF span is followed by a two-stage amplifier with a DCF between the two stages. The loss of the SSMF spans varies between 21 dB and 24 dB, the loss of the DCF modules varies between 10 dB and 13 dB. The optimal channel input power into the SSMF, defined as the input power resulting in the lowest BER after transmission, is found to be 2 dBm per channel. The input power into the DCF is set to -1 dBm per channel. In transmission systems with SSMF fiber and a data rate of 40 Gbit/s at 100-GHz channel spacing, nonlinear intra-channel impairments such as SPM dominate over nonlinear inter-channel impairments such as XPM and FWM [41, 42]. As well known for conventional DCF-based 40-Gbit/s NRZ transmission systems, a systematic inline-compensation of the chromatic dispersion at every span can be employed in order to reduce the effect of SPM and thereby improve the overall transmission quality of the link [44, 43]. In this experiment, the inline-compensation is set to -45 ps/nm/span.

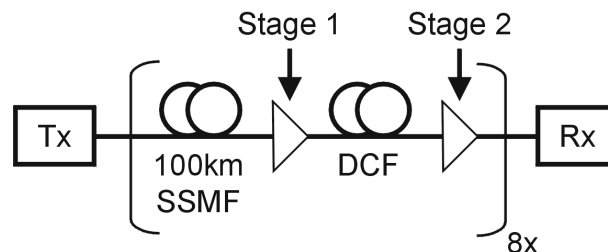


Figure 5.14: *Experimental setup DCF-based transmission line.*

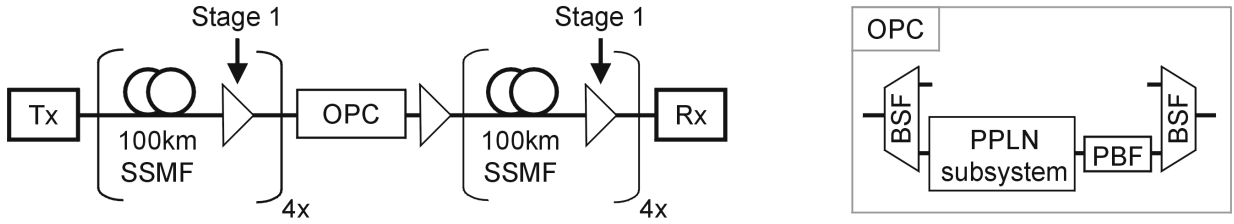


Figure 5.15: *Experimental setup OPC-based transmission line.*

In the OPC-based configuration each 100-km SSMF span is followed by a single stage amplifier to compensate for the fiber loss. The optimal input power into the SSMF is found to be 3 dBm per channel, 1 dB higher compared with the DCF-based configuration. In the middle of the transmission link, the OPC subsystem is located. The same parallel polarization diversity subsystem is used as described in Section 4.3.1. Due to the conjugation, the wavelengths 1548.5 nm ... 1560.6 nm are converted to 1543.7 nm ... 1531.9 nm. The optical spectrum after the PPLN-subsystem is depicted in Figure 5.16a. Since in this setup no in-line DCF is needed, single-stage amplifiers are used for in-line amplification. Hence instead of one preamplifier per span, for the PPLN only one extra amplifier is required for the whole link.

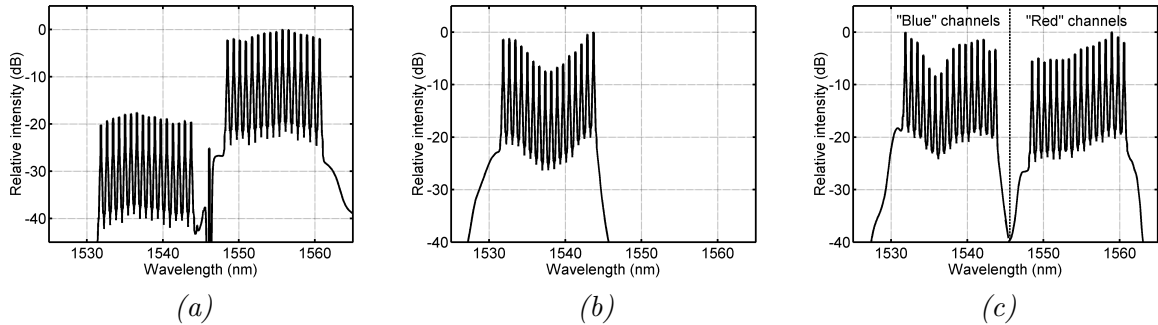


Figure 5.16: *Spectra a) after the PPLN-subsystem, b) after transmission for the OPC-based configuration, c) after transmission for the DCF-based configuration (spectral resolution of 0.1 nm).*

Figure 5.16b and 5.16c depict the spectrum of the WDM signals at the receiver for the OPC and DCF-based configuration. Note that for the DCF-based transmission, the two sets of channels (red and blue channels) correspond to two different experiments. In these optical spectra, a gain ripple is clearly visible. This ripple, created by unequal gain of the EDFAs in the system, introduces a non-uniform performance of the WDM channels. In the DCF-based configuration, the gain ripple of the blue channels is due to the EDFA gain tilt (present near 1530 nm) higher (8.2 dB) than that of the red channels (5.5 dB). After transmission, the OSNR of the red channels is ≈ 22.9 dB. The OSNR of the blue channels is ≈ 21 dB, 1.9 dB lower than that the red channel with the worst BER. The lower OSNR is caused by the higher noise factor of the amplifiers and the higher gain

ripple on the blue channels (as shown in Figure 5.16b). Due to the higher gain ripple, the channel power into the SSMF diverted more from channel to channel in the blue channel case, resulting in a larger difference in OSNR per channel after transmission. For the OPC-based configuration, the OSNR is ≈ 23.5 dB for all 16 channels and the gain ripple 7 dB. Even though the gain ripple is higher in the OPC setup compared with the red-channels of the DCF-based setup, the OSNR of the OPC setup is slightly higher than that of the red channels in the DCF-based setup. There are two reasons for the higher OSNR in the OPC-based configuration. First of all, the OPC-configuration uses single-stage inline amplifiers instead of the two-stage in the DCF-based configuration saving more than a decibel in noise factor per inline node. In order to cover the loss of the OPC-unit an extra single-stage amplifier is required, though the impact of this extra amplifier is small. Secondly, the optimal input power into the fiber is higher in the OPC-based configuration ($P_{in} = 3$ dBm) than in the DCF configuration ($P_{in} = 2$ dBm). The optimal channel power in the 40-Gbit/s OPC experiment is higher than the optimal channel power used for the 10-Gbit/s WDM experiment (1 dBm), discussed in the previous section (Section 5.1). Even though the spectral efficiency of both experiments is the same (0.4 bit/s/Hz), the 10-Gbit/s experiment is XPM limited due to the narrow channel spacing of 25 GHz. In the case of the 40-Gbit/s/channel transmission at 100-GHz spacing, intra-channel nonlinear impairments such as SPM are dominant over XPM.

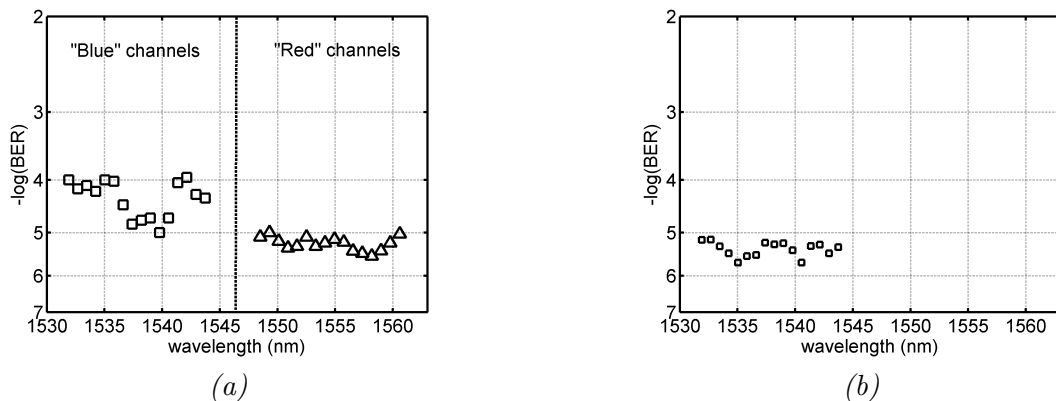


Figure 5.17: BER of all 16 WDM channels for a) the “Blue” and “Red” channels of the DCF-based configuration, b) the OPC-based configuration.

The BER of the WDM channels is depicted in Figure 5.17a and 5.17b for the DCF-based and the OPC-based configuration. The best and worst BER performance of the blue channels in the DCF-based configuration are $1 \cdot 10^{-5}$ and $1 \cdot 10^{-4}$. For the red channel the best and worst BER are $3 \cdot 10^{-6}$ and $1 \cdot 10^{-5}$. The BER performance of the red channels is better, mostly because the OSNR of the red channels is higher after transmission. The best and worst BER obtained in the OPC-based configuration is $2.1 \cdot 10^{-6}$ and $7.1 \cdot 10^{-6}$. The difference between the best and worst channel is less than one decade, which is comparable to the spread of the red channels in the DCF-based configuration. Note however that mid link, the OPC converts the data signals from the red side to the blue side of the C-band.

Even though transmission in the blue subband limits the performance of the DCF-based transmission system, after 400 km of transmission in the blue subband and 400 km in the red subband, the BER for the OPC setup is better than the BER of both DCF-based configurations. It can therefore be concluded that compared to the conventional transmission system, the lumped dispersion map of the mid-link OPC does not introduce an extra penalty. This can be explained by considering the peak-power as a function of the dispersion (Figure 3.7, Section 3.3). Unlike 10-Gbit/s NRZ-ASK, there is practically no difference in the peak-power between low and high dispersion values at 40-Gbit/s NRZ-ASK.

In the DCF-based configuration there is a significant performance difference in the BERs of the blue channels and the red channels. In the OPC-based system, all channels are equally transmitted in both the blue part and in the red part of the C-band. Therefore, the performance difference of the individual channels is smaller in the OPC setup compared with the DCF-based configuration. A dynamic gain equalizer (DGE) can be employed to reduce the gain ripple significantly and thereby improving the performance for both the DCF-based and the OPC-based configuration.

A drawback from using OPC for chromatic dispersion compensation is that the slope of the transmission fiber is not compensated for, which leads to a difference in optimal post-compensation. In the OPC experiments, the measured difference in optimal post-compensation between the first and the sixteenth channel is 560 ps/nm. A variable dispersion compensator is used in this experiment to maximize the BER performance per channel. At higher data rates (> 100 Gbit/s), the dispersion slope can as well impair the BER performance of a single channel [126]. In this case a slope compensator must be used to compensate for the fiber slope. Advantages of the slope compensator are that it can be used at any point of the transmission link and that all channels are slope matched with one single device, which is more cost effective.

5.3 Asymmetric OPC-placement

In the transmission experiments conducted so far, the transmission link used is symmetric (meaning that the same amount of transmission fiber is used before and after conjugation). Many commercial transmissions are however not ideally symmetric and/or have an odd span count. In order to apply OPC in these transmission links, the OPC-unit needs to be placed off-center. In an OPC-based transmission system, impairments that occurred in the first part of the link (before conjugation) are canceled by impairments that occur in the second part of the link (after conjugation). Hence impairments are not regenerated directly by the OPC, but implicitly by the transmission link after conjugation. An asymmetric transmission link, reduces the link-symmetry and thereby the degree in which impairments are compensated for. The performance of the OPC in an asymmetric configuration is tested by adding or removing one span from a 800-km straight line. As a result, the following four configurations are assessed: $(X,Y) = (3,4), (4,3), (4,5), (5,4)$. Where X represents the number of spans before and Y the number of spans after the OPC-unit.

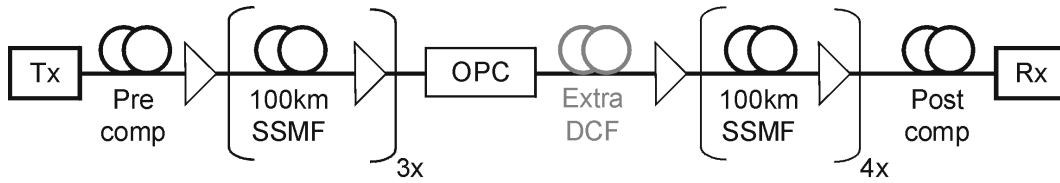


Figure 5.18: *Experimental setup of OPC-based transmission with an asymmetric transmission link: $(X, Y) = (3, 4)$.*

Figure 5.1 depicts the experimental setup of the OPC-based setup for the configuration with $(X, Y) = (3, 4)$. A single channel 40-Gbit/s NRZ signal is generated at 1550.9 nm. Before transmission, a pre-compensation of -340 ps/nm is used. In the off-center configuration, the chromatic dispersion is not totally compensated for by OPC. In order to compensate for the residual chromatic dispersion, additional compensation is required. In this experiment a DCF module is added for additional dispersion compensation. The dispersion maps are depicted in Figure 5.19 for two configuration: $(X, Y) = (3, 4)$ and $(X, Y) = (4, 3)$. Depending on the off-center configuration, an extra DCF module is added

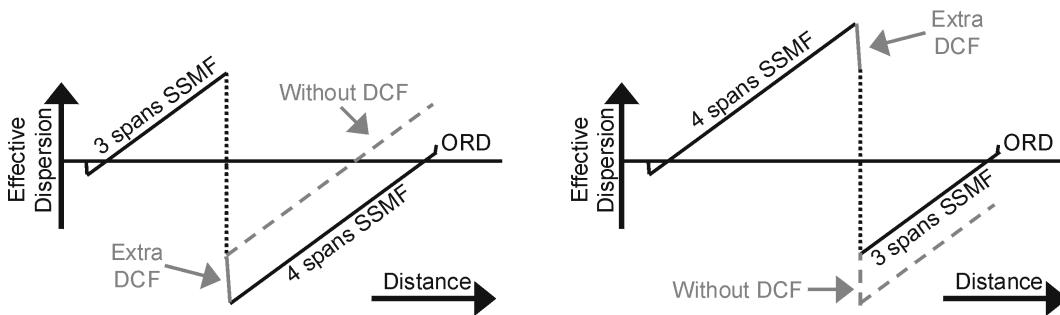


Figure 5.19: *Dispersion map of two off-center placed OPC links: $(X, Y) = (3, 4)$ and $(X, Y) = (4, 3)$.*

before or after the OPC configuration. The launch power in this experiment is fixed to 4 dBm/channel for the SSMF and -1 dBm for the extra DCF as well as the pre- and post-compensation. The OPC-unit used in these experiments is a parallel polarization diversity subsystem as described in Section 4.3.1.

Figure 5.20 depicts the BER performance as a function of the post-compensation for several off-center configurations. Additionally, the symmetric setup $(X, Y) = (4, 4)$ is also depicted. The BER for the best $(X, Y) = (3, 4)$ and the worst $(X, Y) = (5, 4)$ configuration at optimal post-compensation is $1.2 \cdot 10^{-7}$ and $3.4 \cdot 10^{-6}$, respectively. Comparing the off-center configurations to the symmetric setup, no extra power penalty resulting from the off-center placement can be seen. Instead, the two off-center configuration with 700-km total transmission length $(X, Y) = (3, 4)$ and $(4, 3)$ have a better performance than the symmetrical configuration with a total transmission length of 800 km. In the 700-km configurations less amplifiers are needed, hence the OSNR at the receiver is about half

5.4. MIXED DATA RATE, MIXED MODULATION FORMAT TRANSMISSION

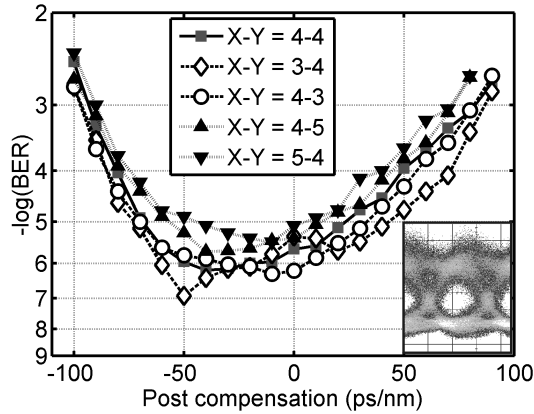


Figure 5.20: BER performance as a function of the post-compensation for several off-center placements

a dB higher. This performance improvement dominates any potential penalties from an asymmetric placement of the OPC-unit. Similarly, the performance in BER is slightly reduced due to a small OSNR decrease when the transmission link is extended to 900 km $(X,Y) = (4,5)$ and $(5,4)$. In all four off-center configurations, no strong BER impairment has been observed after transmission.

5.4 Mixed data rate, mixed modulation format transmission

It is foreseen that in future transmission systems different modulation formats and data rates are used simultaneously in the same transmission line. The experiment discussed in this section describes the WDM transmission of 42.7-Gbit/s NRZ, 42.7-Gbit/s duobinary

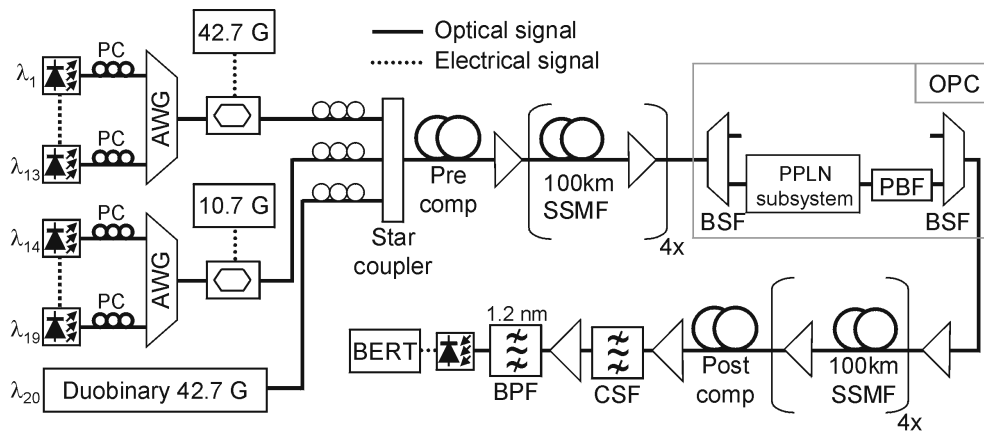


Figure 5.21: Experimental setup.

CHAPTER 5. ASK BASED TRANSMISSION

and 10-Gbit/s NRZ over the same transmission line [81]. Figure 5.21 depicts the experimental setup. At the transmitter all channels, 42.7-Gbit/s NRZ, 10-Gbit/s NRZ and 42.7-Gbit/s duobinary, are combined using a star coupler. All signals are co-polarized in order to create worst case inter-channel interactions. The PRBS length for all modulation formats is $2^{31} - 1$. After the transmitter a DCF module with a chromatic dispersion of $D_{pre} = -170$ ps/nm is used for pre-compensation.

The transmission link and OPC unit are similar to those described in Section 5.2. The SSMF input power is set to 0.8 dBm/channel for all 10-Gbit/s channels and to 2.8 dBm/channel for all 42.7-Gbit/s channels (NRZ and duobinary). At the end of the transmission link, a tunable dispersion compensator is used to optimize the residual chromatic dispersion at the receiver. Finally, the channels are filtered with a CSF. The FWHM of the channel selection filter used is 80 GHz, 42 GHz and 22 GHz for the 42.7-Gbit/s NRZ, 42.7-Gbit/s duobinary and 10.7-Gbit/s NRZ channels, respectively.

The 20 data channels at the transmitter are shown in Figure 5.22a. The 42.7-Gbit/s

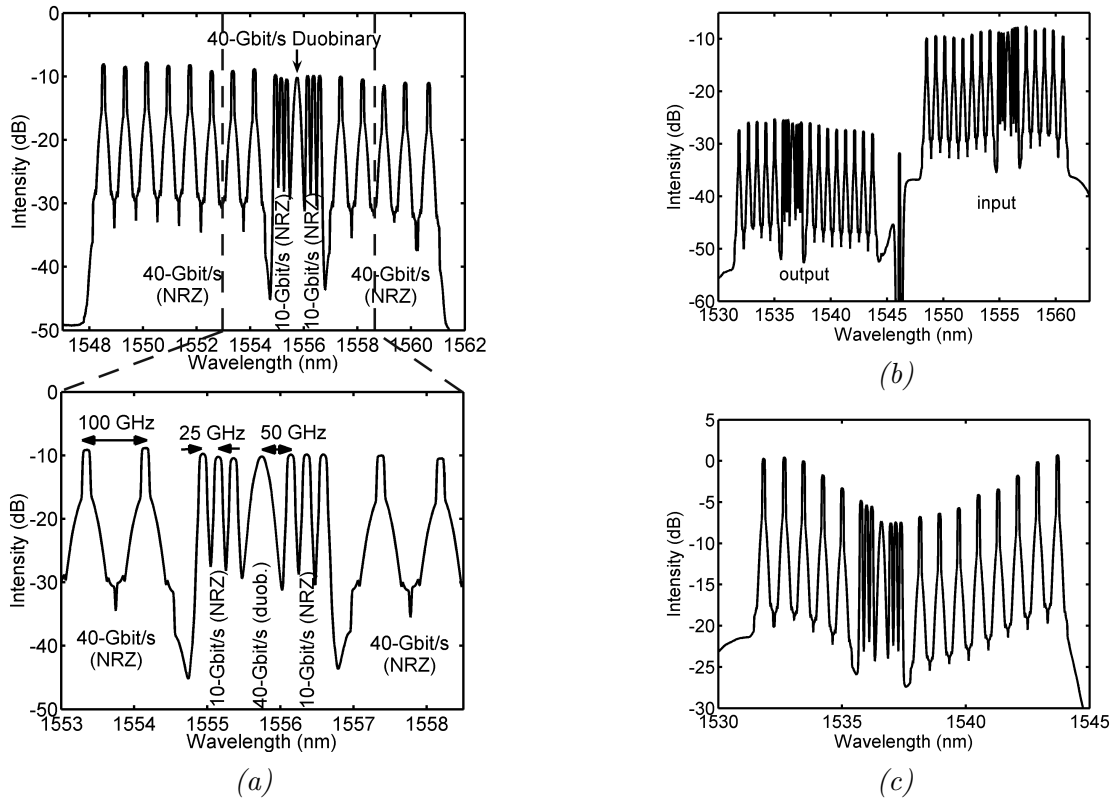


Figure 5.22: *Optical spectra ($RB = 0.1$ nm) a) output of the transmitter, b) after the PPLN-subsystem and the PBS, c) after 800km transmission.*

duobinary data channel is launched at 1555.8 nm (before the OPC unit). At 50-GHz spacing, on each side of the duobinary channel, three 25-GHz spaced 10-Gbit/s data channels are placed. The six 10-Gbit/s data channels are surrounded by thirteen 42.7-Gbit/s chan-

5.4. MIXED DATA RATE, MIXED MODULATION FORMAT TRANSMISSION

nels placed on a 100-GHz grid. All channels together cover the higher wavelength part (red part) of the C-band ranging from 1548.5 nm to 1560.6 nm.

Figure 5.22b depicts the optical spectrum after passing through the optical phase conjugator but before the filters used to suppress the input channels. All data channels are converted from the higher part of the C-band to the lower part. In the middle of the plot, at 1546.1 nm, the residual of the suppressed pump can be seen. The optical spectrum after transmission is depicted in Figure 5.22c. The OSNR after transmission is greater than 20.5 dB and 22.3 dB for all 10-Gbit/s NRZ and 42.7-Gbit/s NRZ channels, respectively. The 42.7-Gbit/s duobinary channel has an OSNR of 23.6 dB. Figure 5.23 depicts the BERs before FEC of all twenty channels.

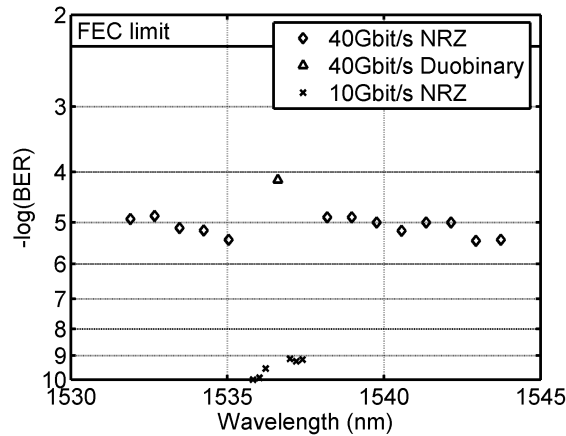


Figure 5.23: BER performance before FEC after transmission for all 20 channels.

For the 10-Gbit/s NRZ channels (plotted as crosses in Figure 5.23), a BER performance is measured varying between $1 \cdot 10^{-10}$ and $2 \cdot 10^{-9}$. Due to the narrow channel spacing of 25 GHz an OSNR penalty of about 1 dB is present from cross-phase modulation. For the 42.7-Gbit/s duobinary channel (plotted as a triangle in Figure 5.23), a BER performance is measured of $7.2 \cdot 10^{-5}$, which is worse than the BER performance of all the 42.7-Gbit/s NRZ channels, still the BER of the duobinary channel is more than a decade below the FEC threshold. As discussed in Section 3.4, the BER penalty of the duobinary modulation format is caused by the fact that this modulation format requires in general a higher OSNR after transmission in order to obtain the same BER. To ensure that this worst channel is error-free, the BER after FEC is measured for six hours. In this measurement interval, no uncorrected errors or lost frames were detected. The BER performance of the thirteen 42.7-Gbit/s NRZ data channels (plotted as diamonds in Figure 5.23) varies between $2 \cdot 10^{-5}$ and $4 \cdot 10^{-6}$. These BERs are slightly worse than the performance measured in the 16x42.7-Gbit/s transmission experiment discussed in Section 5.2, resulting from a slight OSNR degradation due to the more complicated transmitter structure and the slightly lower launch power into the SSMF (2.8 dBm instead of 3 dBm). From this experiment it can be concluded that the transmission of mixed data rates and modulation formats can be realized without introducing a significant BER penalty.

5.5 Summary

This chapter is mainly concerned with the transmission performance of NRZ-ASK in a mid-link OPC transmission system. The lumped dispersion map, that is inherent to the use of mid-link OPC introduces SPM penalties for the 10-Gbit/s NRZ-ASK modulation format. Through OPC, the SPM is mostly compensated for. As a result, a large dispersion tolerance after transmission is obtained. In 10-Gbit/s WDM transmission systems with narrow channel spacing, the performance is mainly limited by XPM. Due to the slope of the transmission fiber, which is not compensated for, the compensation of XPM with OPC is questionable. In both simulation and experiment no XPM compensation through OPC could be observed.

When the data rate is increased to 40 Gbit/s, the influence of XPM is low for the SSMF fiber type. The transmission in this regime is mostly limited by SPM and IXPM/IFWM. Successful WDM transmission of 16x42.7 Gbit/s at a 100-GHz spacing is realized over 800 km of SSMF. The lumped dispersion map does not introduce an extra SPM penalty at the 40-Gbit/s data rate. As a result, a better BER performance is obtained compared to a conventional transmission system.

In the mid-link OPC configuration, the OPC-unit must be placed in the middle of the transmission link. However, most commercial transmission links are not symmetric and will require the OPC to be placed off-center. In a single channel 42.7-Gbit/s NRZ-ASK transmission experiment, several off-center configurations were tested with a transmission distance ranging from 700 km to 900 km. A DCF unit at the phase conjugator was used to compensate for the residual chromatic dispersion. In all four off-center configurations, no strong BER impairment has been observed after transmission.

Finally, a transmission experiment is conducted where different modulation formats and different data rates are transmitted over the same transmission line. In this experiment a total of 20 WDM channels are transmitted, namely 13x42.7-Gbit/s NRZ, 6x10-Gbit/s NRZ and 1x42.7-Gbit/s duobinary. The BER of the duobinary channel, with the worst BER performance, was observed for several hours after FEC. In this interval no uncorrected errors or lost frames are detected. From this experiment it can be concluded that the transmission of mixed data rates and modulation formats can be realized without introducing a significant BER penalty.

Chapter 6

Nonlinear phase noise compensation

Recently strong interest has been shown in PSK formats in order to increase the robustness of the transmission links. However, unlike ASK modulation formats, PSK modulated signals can be impaired by nonlinear phase noise (NPN). NPN results from power fluctuations originating from ASE noise. Along the transmission line these power fluctuations are converted into phase fluctuations through the Kerr effect. NPN is often referred to as the Gordon-Mollenauer effect [127, 128]. In [129] it is observed that due to NPN, the 3-dB sensitivity advantage of DPSK is eliminated after long-haul transmission so that similar performance for RZ-ASK and RZ-DPSK is measured.

In order to extend transmission distance in these long haul transmission systems, NPN compensation schemes can be employed. The nonlinear phase shift due to NPN is dependent on the intensity of the signal. Therefore, the intensity of the signal can be used at the receiver to compensate for the NPN induced phase shift [130, 131]. This method is referred to as post nonlinearity compensation (PNC). Several implementations have been proposed, for example by using a nonlinear optical component [131], a phase modulator [130] or electronic circuits [132, 133]. A disadvantage of this method is that since this is a single channel solution, a PNC-unit is required for each WDM channel. Even though the principle of PNC has been shown experimentally in different configurations [134, 135], no successful transmission experiments have been reported so far.

In this chapter the compensation of nonlinear phase noise by using OPC is discussed¹. After a description of NPN in Section 6.1 and a theoretical analysis in Section 6.2, a proof-of-principle experiment is described in 6.3.

6.1 Nonlinear phase noise in long-haul transmission systems

As discussed in Section 3.4, a PSK modulated signal has a continuous power envelope since marks are present in each bitslot. Due to this continuous power envelope, the SPM induced

¹The results described in this chapter are published in P1, P3, P19, P21, P38

phase shift is equal for all pulses and thus impairments through SPM are in general smaller for DPSK modulated signals compared to OOK modulated signals. However, along the transmission line, ASE from EDFA amplifiers causes a variation in the amplitude of the signal. Subsequently, the amplitude noise is converted into phase noise through the Kerr-effect. This impairment is referred to as NPN. Figure 6.1 shows the phase constellation diagrams for a DPSK modulated signal without and with nonlinear phase noise. In this figure the normalized amplitude of the DPSK signal is plotted as defined in equation 4.10

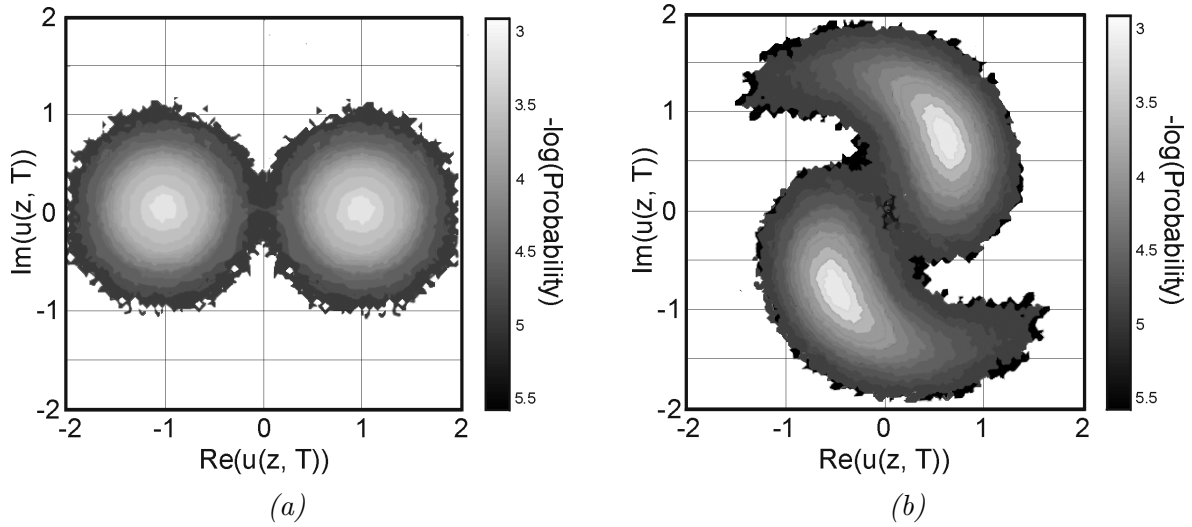


Figure 6.1: *DPSK constellation diagram after transmission, a) without nonlinear phase noise (no Kerr effect), b) with nonlinear phase noise*

In this simulation a transmission link of 40 spans was simulated. The span length was 90 km and the dispersion of the fiber was neglected. The input power into the transmission fiber was 0 dBm and the noise factor of the amplifiers was set to 8.5 dB. In the phase constellation diagram depicted in Figure 6.1a, the nonlinear coefficient of the fiber was set to $\gamma = 0 \text{ W}^{-1} \text{ km}^{-1}$ so that the Kerr-effect is not considered. It can be seen in this plot that without nonlinear phase noise, the two logical phase states of the DPSK signal (at -1 and 1) broaden symmetrically due to ASE. In Figure 6.1b, the nonlinear coefficient of the fiber is set to $\gamma = 1.2993 \text{ W}^{-1} \text{ km}^{-1}$. With nonlinear phase noise, the constellation diagram gets tails after transmission that are proportional to the signal power due to the interaction between ASE and the Kerr effect.

6.2 Theory of nonlinear phase noise

Initially, OPC was proposed for the reduction of Gordon-Haus Jitter in soliton transmission systems [136]. Gordon-Haus Jitter limits the system performance in soliton-based transmission systems, where frequency fluctuations resulting from EDFAs noise induce timing jitter on the signal. Lorattanasane and Kikuchi proposed to use OPC for the compensa-

6.2. THEORY OF NONLINEAR PHASE NOISE

tion of phase-noise in a long-haul ASK coherent transmission line [104]. This principle is applicable to phase shift keyed transmission as well. In a coherent transmission system phase sensitive detection occurs at the receiver using a local oscillator. Fluctuations in the phase of the received signal on the bit-level impair the system performance because the local oscillator cannot correct for the fast phase changes. The impact of NPN is then similar to that for PSK based transmission for coherent transmission systems.

The mechanism for phase noise compensation by mid-link OPC is depicted in Figure 6.2. In this example a system with six spans is discussed with and without OPC. At

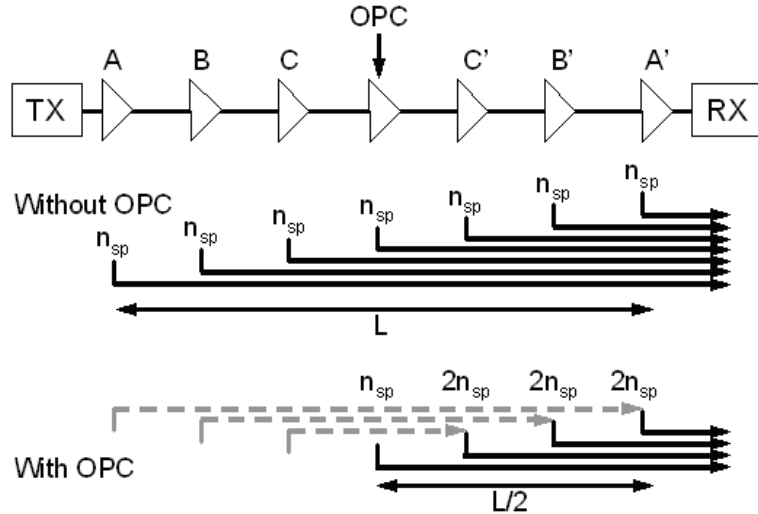


Figure 6.2: Mechanism for phase noise compensation as introduced by Lorattanasane and Kikuchi (after [104]).

the receiver, the accumulated phase noise is proportional to $n_{sp}L^3$ where L denotes the total system length and n_{sp} the spontaneous emission factor of the EDFA. The factor n_{sp} provides a measure for the generated amount of ASE. When mid-link OPC is employed, the nonlinear phase noise generated by the Kerr effect can be partly compensated for. In the six span example, depicted in Figure 6.2, it can be seen that the phase noise introduced by amplifier B is compensated for when the signal reaches amplifier B'. The ASE induced power fluctuations originating from amplifier B generate phase fluctuations (phase noise) through the Kerr effect while propagating in the first half of the system. This phase noise is compensated for by OPC in the second half of the system. When the signal reaches amplifier B' the amount of phase noise caused by the ASE from amplifier B is compensated for. It can be found that the accumulated phase noise variance in this case is proportional to $2n_{sp}(L/2)^3 = n_{sp}L^3/4$, resulting in about 6 dB phase noise suppression [104].

The 6 dB phase noise reduction also holds for a long haul PSK link with a system length much longer than the dispersion length [137]. In such a system, the soliton condition is maintained adiabatically and the growth of the soliton power and phase perturbations can be approximated using the correlation equations as studied in [138]. Assuming a lossless, dispersion-less transmission system, the variance of the amplitude noise $\langle p^2 \rangle$ can be

CHAPTER 6. NONLINEAR PHASE NOISE COMPENSATION

expressed by [137]

$$\frac{d\langle p^2 \rangle}{dz} = \sigma_p \quad (6.1)$$

where $\langle \rangle$ denotes an ensemble average, z represents the transmission distance with the initial position at $z = 0$ and σ_p the amount of amplitude noise that is effectively added per kilometer through ASE. Note that in this consideration, the noise of the amplifiers increases continuously along the transmission line. In an EDFA based transmission system noise is added at the amplifiers only, and thus in a discrete way. However, for long-haul transmission systems with many amplifiers the difference between continuous and discrete noise addition will be relatively small.

The solution to equation 6.1 is given by

$$\langle p^2 \rangle = \langle p^2 \rangle_0 + \sigma_p z \quad (6.2)$$

where $\langle p^2 \rangle_0$ is the amplitude noise variance before transmission. The correlation between the variance of the amplitude and the phase noise $\langle p\phi \rangle$, can be expressed by

$$\frac{d\langle p\phi \rangle}{dz} = \bar{\gamma} \langle p^2 \rangle \quad (6.3)$$

where $\bar{\gamma}$ is the effective nonlinear coefficient. Integrating equation 6.3 gives

$$\langle p\phi \rangle = \langle p\phi \rangle_0 + \langle p^2 \rangle_0 \bar{\gamma} z + \sigma_p \bar{\gamma} z^2 / 2 \quad (6.4)$$

where $\langle p\phi \rangle_0$ represents the combined amplitude and phase noise before transmission. The variance of the phase noise $\langle \phi^2 \rangle$ can then be expressed by the following correlation equation

$$\frac{d\langle \phi^2 \rangle}{dz} = \sigma_\phi + 2\bar{\gamma} \langle p\phi \rangle \quad (6.5)$$

where σ_ϕ corresponds to the amount of (linear) phase noise that is added through ASE. σ_ϕ is related to σ_p as $\sigma_p \approx \sigma_\phi / 4$ [137]. The integration of 6.5 gives

$$\langle \phi^2 \rangle = \langle \phi^2 \rangle_0 + 2\langle p\phi \rangle_0 \bar{\gamma} z + \langle p^2 \rangle_0 \bar{\gamma}^2 z^2 + \sigma_\phi z + \sigma_p \bar{\gamma}^2 z^3 / 3 \quad (6.6)$$

When an ideal modulator is assumed, no amplitude variations will be present at the transmitter. This results in the following set of conditions

$$\langle p^2 \rangle_0 = 0 \quad (6.7)$$

$$\langle p\phi \rangle_0 = 0 \quad (6.8)$$

$$\langle \phi^2 \rangle_0 = 0 \quad (6.9)$$

Figure 6.3a shows the phase noise variance $\langle \phi^2 \rangle$ as a function of the transmission distance. In this plot, both transmission distance and phase variance are normalized so

6.2. THEORY OF NONLINEAR PHASE NOISE

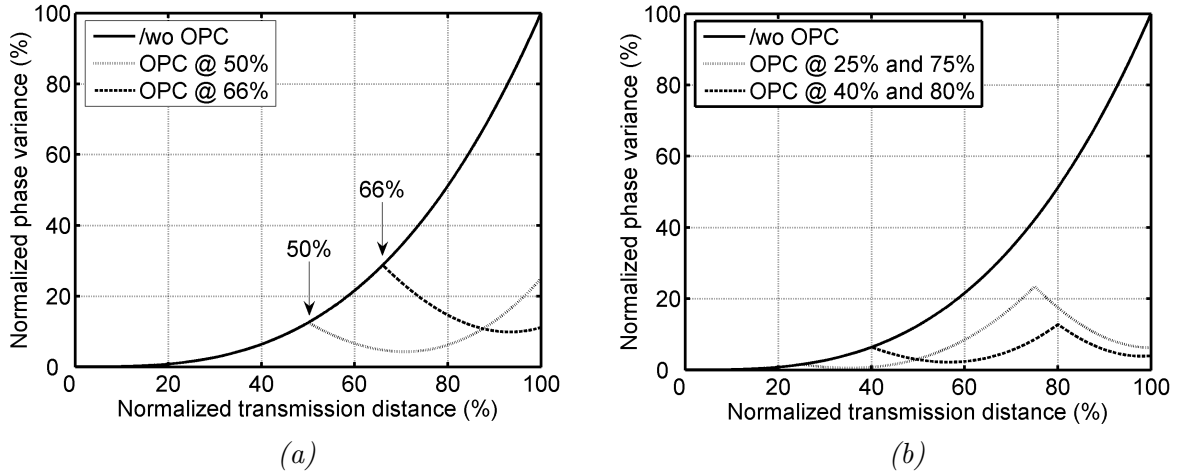


Figure 6.3: Normalized phase noise as a function of the normalized transmission distance with (/w) and without (/wo) OPC. After McKinstrie et al. [137]. a) using 1 OPC, b) using 2 OPCs

that without OPC 100% of phase variance is obtained after 100% transmission. The phase variance is $\langle \phi^2 \rangle = 0$ for $z = 0$ and increases due to NPN with $z^3/3$. When an OPC is inserted into the transmission link, the sign of $\langle p\phi \rangle$ (equation 6.4) is inverted at the OPC while the signs of the quadratic terms ($\langle p^2 \rangle$ (equation 6.2) and $\langle \phi^2 \rangle$) (equation 6.6) are unaffected. From Figure 6.3a it can be seen that by placing the OPC in the middle (at 50%) of the transmission line, the phase variance is reduced to 25% (6 dB) after transmission. The compensation of NPN can be improved by optimizing the location of the OPC along the transmission link. The amplitude noise added by optical amplifiers that are located behind the OPC-unit produce NPN that is not compensated for through OPC. The optimum location of the OPC to compensate NPN is therefore at 66% instead of 50% [137]. With the OPC placed at this location, the phase variance after transmission is reduced to 11.1% (9.5 dB) after transmission. However, in this case, OPC cannot compensate for the chromatic dispersion of the total transmission link.

Alternatively, two OPC units can be employed to obtain a further reduction of nonlinear phase noise. Figure 6.3b shows the NPN represented by the normalized phase variance ($\langle \phi^2 \rangle$) as a function of the normalized transmission distance for 2 OPCs. In order to obtain full compensation of the chromatic dispersion, the OPC units must be placed at X% and (X+50)% in the transmission line, with X a fraction of the transmission line between 0% and 50%. The optimal phase noise suppression in combination with full chromatic dispersion compensation is obtained when the OPC units are placed at 25% and 75% of the transmission line. The accumulated phase noise variance is then proportional to $2(2n_{sp})(L/4)^3 = n_{sp}L^3/16$, resulting in about 12dB phase noise suppression [104, 137]. The phase noise suppression can be increased to 14 dB by placing the OPC units at 40% and 80% of the transmission line, which however does not result in full dispersion compensation [137]. An overview of the predicted phase noise reduction and amount of dispersion compensation feasible for different configuration is given in table 6.1.

CHAPTER 6. NONLINEAR PHASE NOISE COMPENSATION

	1 OPC 50%	1 OPC 66%	2 OPCs 25/75%	2 OPCs 40/80%
Phase noise reduction (dB)	6	9.5	12	14
Dispersion Comp. (%)	100	66	100	80

Table 6.1: *Predicted phase noise reduction and dispersion compensation for different OPC configurations*

So far, an ideally modulated signal is assumed that does not introduce any amplitude noise ($\langle p^2 \rangle_0 = 0$). However, the bandwidth of the Mach-Zehnder modulator limits in practice the quality of the signal e.g. extinction ratio, rise/fall time, etc. This becomes a problem when advanced modulation formats such as RZ-DQPSK are employed. A conventional way to generate DQPSK is by using an integrated DQPSK modulator with two parallel MZMs within a super Mach-Zehnder structure as shown in Figure 3.16 (Section 3.4.4). For the generation of DQPSK, the required amplitude of the driver voltages is $2 \cdot V_\pi$. At data rates of 20 Gbit/s and more, the broadband amplification of a driver signal is not trivial and results in modulation instabilities. As a result the '1' rail of the RZ-DQPSK signal broadens due to amplitude fluctuations. In the eye diagrams of the 42.7 Gbit/s NRZ and RZ-DQPSK signal the broad '1'-rail can clearly be seen (Figure 3.17 in Section 3.4.4). Amplitude fluctuations caused by the super Mach-Zehnder structure can be treated equivalent to an amplifier at the transmitter with a high noise factor and will cause NPN through the Kerr effect.

The influence of modulation instabilities can be assessed by introducing an average noise amplitude power at the transmitter, which is represented in equations 6.2, 6.4 and 6.6 by $\langle p^2 \rangle_0$. In order to exclusively study the influence of modulation instabilities, ideal noise-less amplifiers are considered along the transmission line by setting the strength of the power-induced and the noise-induced phase kicks to zero ($\sigma_p = \sigma_\phi = 0$). Figure 6.4 depicts the phase variance due to modulator instabilities as a function of the transmission distance. Similar to Figure 6.3, both transmission distance and phase variance are normalized such that without OPC 100% of phase variance is obtained after 100% transmission. The phase variance is $\langle \phi^2 \rangle = 0$ for $z = 0$ and increases with z^2 without OPC. The optimal OPC location for modulation instabilities is mid-link (50%). At this location, the phase variance due to modulator instabilities is completely compensated for. For ASE induced NPN (Figure 6.3a), the optimal location for OPC is at 66% of the transmission line. Considering modulator instabilities, the OPC placed at 66% of the transmission line results in a residual phase noise of 10%. An explanation for the difference in the optimal OPC location is that the source of the amplitude fluctuations due to modulator instabilities originates solely from the transmitter, whereas with "conventional" NPN the amplitude fluctuations due to ASE-noise are added along the transmission line.

In a real transmission system NPN induced by both modulator instabilities and ASE is present. Therefore, the optimum OPC location depends on which NPN source is dominant. In equations 6.2 - 6.6 the modulator instabilities are represented by the average noise

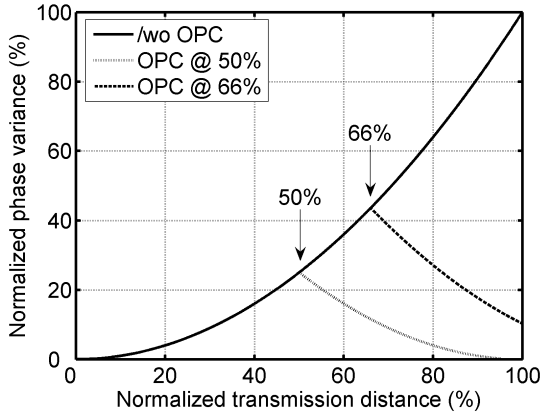


Figure 6.4: Normalized phase variance due to MI-NPN as a function of the transmission distance.

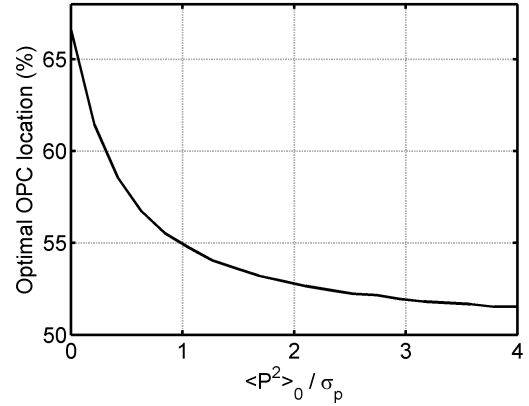


Figure 6.5: Optimal OPC location as a function of the ratio modulation instability to ASE ($\langle p^2 \rangle_0 / p\phi$).

amplitude power at the transmitter ($\langle p^2 \rangle_0$). The ASE is represented by the strength of the noise-induced power (σ_p) and phase (σ_ϕ) kicks. Both sources of NPN can be considered by introducing a ratio of modulator instabilities to ASE ($\langle p^2 \rangle_0 / \sigma_p$). Note that the relation $\sigma_\phi \approx \sigma_p / 4$ relates the noise-induced phase kicks to the noise-induced power kicks. When $\langle p^2 \rangle_0 / \sigma_p = 0$, no modulator instabilities are present in the system and ASE induced NPN is the dominating impairment. Increasing the ratio $\langle p^2 \rangle_0 / \sigma_p$ will increase the influence of the NPN through modulator imperfections on the transmission system. Figure 6.5 shows the optimal OPC location as a function of the modulator imperfections to ASE ratio $\langle p^2 \rangle_0 / \sigma_p$. As expected, the optimum location of the OPC is 66% when only ASE induced NPN is considered ($\langle p^2 \rangle_0 / \sigma_p = 0$). It shifts towards the middle of the transmission line with increasing modulator imperfections.

Due to the periodic power amplification in a long-haul transmission link modulation instability (MI) sidebands can occur and compensation of nonlinear phase noise by means of OPC can be less effective [139]. MI can be mitigated by managing the local dispersion with a periodic dispersion map [140]. Hence, for transmission systems using DCF for periodic chromatic dispersion compensation MI is not significant. MI might impair the performance of transmission systems using OPC for dispersion compensation, but results reported so far have not shown MI induced degradation [141, 142]. Since for high values of chromatic dispersion (e.g. SSMF) the impact of MI is decreased [104], we assume that for the SSMF the contribution of MI is relatively small.

6.3 Experiment

In this section a proof-of-principle experiment is described showing that OPC can effectively compensate for impairments due to nonlinear phase noise. The influence of NPN on the

performance of the system can be measured by changing the OSNR at the transmitter while keeping the OSNR at the receiver constant. At low OSNR, the signal is very noisy and therefore strong noise induced power fluctuations are present. Hence when a signal with a low OSNR is transmitted a strong influence of NPN will be present. At high transmitted OSNR, the noise induced power fluctuations are small along the transmission line and only little NPN will be present.

6.3.1 Nonlinear phase noise impairment on DPSK transmission

The experimental setup of the proof-of-principle experiment is depicted in Figure 6.6. A single channel NRZ-DPSK signal is generated at 1558.2 nm by a DFB laser and a MZM. For reference measurements, the same modulator structure can as well be used to generate an NRZ-ASK signal. The bit-rate is 10.7-Gbit/s and the length of the pseudo random bit sequence used is $2^{31} - 1$. Before transmission, a noise generation scheme consisting of a variable optical attenuator (VOA), an optical amplifier and a BPF, is inserted, enabling setting the OSNR of the data signal at system input. The signal is also pre-compensated by using a DCF with -510 ps/nm. The transmission line consists of eight spans of 100-km SSMF. The average inline-compensation per span is 55 ps/nm.

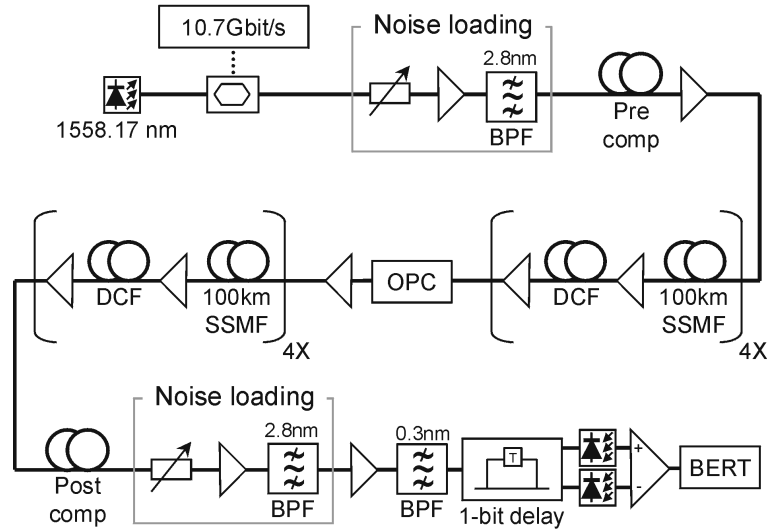


Figure 6.6: *Experimental setup showing the influence of nonlinear phase noise on NRZ-DPSK transmission.*

Nonlinear phase noise is an interaction between ASE and SPM. In the 800-km long transmission line the effect of nonlinear phase noise will not be clearly present for optimized transmission parameters. Hence apart from artificially reducing the OSNR at the transmitter to increase the ASE, high launch powers are used into the SSMF to enhance Kerr-effect. The input powers into the SSMF and DCF are 11.5 dBm and 1.5 dBm, respectively. The loss of the SSMF spans varied between 21 dB and 24 dB and the loss of the DCF modules varied between 10 dB and 13 dB. After transmission, the post-compensation

is optimized to achieve the minimum BER. At the receiver, the OSNR is kept constant at 12 dB using an attenuator, an EDFA and a 2.8-nm BPF. Subsequently, a 0.3-nm BPF removes the out-of-band ASE. The DPSK detector consists of a MZDI with a 1-bit delay (93.5 ps), a balanced receiver and a 10.7-Gbit/s BER tester.

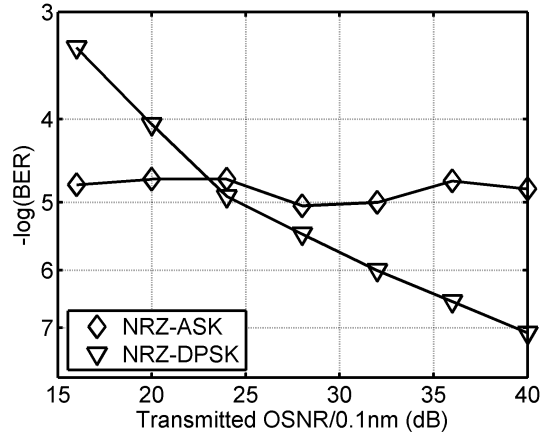


Figure 6.7: Measured BER as a function of the transmitted OSNR for NRZ-DPSK and NRZ-ASK without OPC. The received OSNR is fixed to 12 dB/0.1nm.

Figure 6.7 shows the BER after 800-km transmission as a function of the transmitted OSNR for NRZ-DPSK and NRZ-ASK. At high transmitted OSNR (40 dB), the NRZ-DPSK modulation format outperforms the NRZ-ASK modulation format by over two decades of BER. Similar to the results reported in [128], the BER performance of the NRZ-DPSK modulation format is severely affected by nonlinear phase noise when the OSNR of the transmitter is reduced, whereas for the NRZ-ASK modulation format, the performance is unaffected. As a result, when the transmitted OSNR is reduced to 16 dB, the BER performance of the NRZ-DPSK modulation format is more than a decade worse than the performance of the NRZ-ASK modulation format.

6.3.2 OPC for nonlinear phase noise compensation

In order to study the effect of OPC on the impairments due to nonlinear phase noise, a phase conjugator is added in the middle of the 800-km transmission line. OPC of the data signal is realized by FWM in a SOA. Figure 6.8 shows the experimental setup of the SOA-based OPC subsystem. The data is combined with the amplified output of a distributed feedback pump laser and fed into a 2-mm long SOA. The polarization of the pump and the data signal are co-polarized before entering the SOA. Inside the SOA, the pump signal at 1555.7 nm and the data signal at 1558.2 nm generate an FWM conjugate at 1553.3 nm. Figure 6.9 depicts the optical spectrum after the SOA. In this plot, three signals can be identified, namely the incoming data signal, CW pump and FWM conjugate. The injection current of the SOA is set to 730 mA and the optical powers launched into the SOA are 11

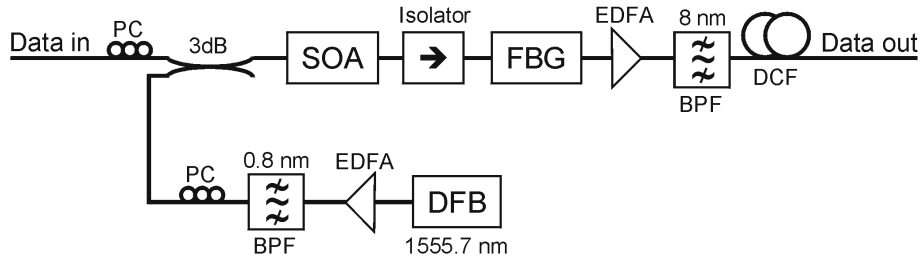


Figure 6.8: Layout of the SOA-based OPC subsystem.

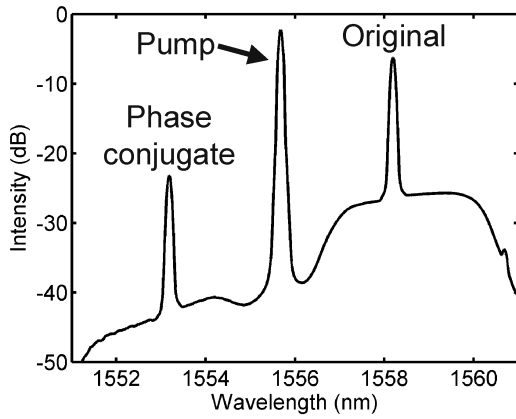


Figure 6.9: Optical spectrum of the pump, data and FWM conjugate at the output of the SOA, before the FBG (res. bw. = 0.1 nm).

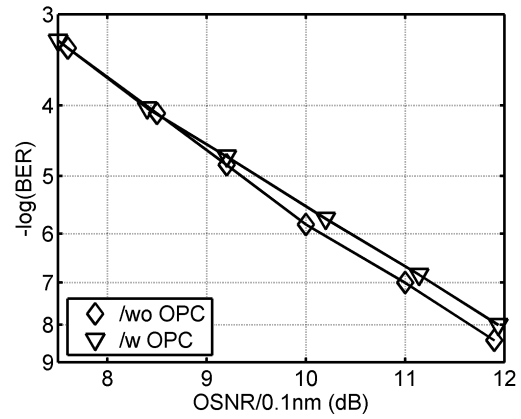


Figure 6.10: Back-to-back BER performance /w and /wo OPC for 10.7-Gbit/s NRZ-DPSK as a function of the OSNR/0.1 nm.

dBm and 1 dBm for the control and the data signals, respectively. The saturation power of the SOA is 8 dBm. After conversion the pump is removed by an FBG. An isolator prevents light reflected by the FBG from propagating back into the SOA. Finally the original data signal is removed using an 8-nm BPF.

The measured conversion efficiency is -16.4 dB. Figure 6.10 depicts the back-to-back BER performance as a function of the OSNR with and without OPC. The measured OSNR penalty due to the OPC is ≈ 0.2 dB on average. This is a good indication that the FWM conversion process does not introduce significant nonlinear impairments.

The phase conjugated signal has the inverted signal spectrum from the incoming data signal. Through this process, the sign of the effective cumulative chromatic dispersion is inverted as well. Similar to [143], the same cumulative dispersion as in the non-OPC configuration is obtained by using a DCF module after the OPC to shift the effective accumulated chromatic dispersion to the value it has before OPC. The chromatic dispersion as a function of the transmission distance for the link with OPC is depicted in Figure 6.11.

The BER performance as a function of the transmitted OSNR for the transmission system with and without OPC is plotted in Figure 6.12. At low transmitted OSNR (16

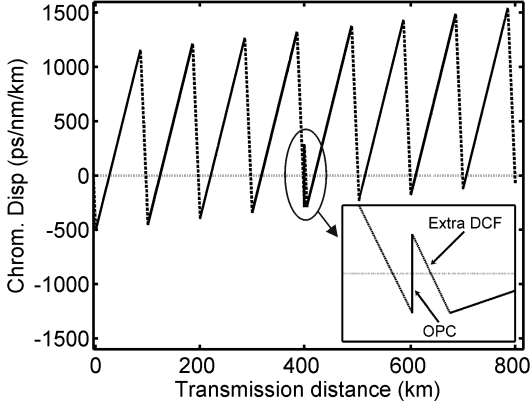


Figure 6.11: The chromatic dispersion as a function of the transmission distance for the link with OPC.

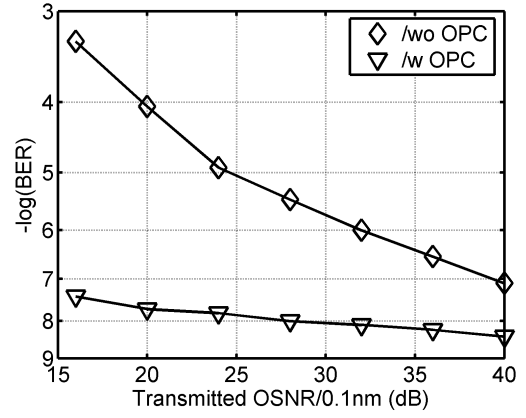


Figure 6.12: BER performance /w and /wo OPC for 10.7-Gbit/s NRZ-DPSK as a function of the transmitted OSNR at 12-dB received OSNR/0.1nm.

dB), the performance of the system without OPC is impaired by over four decades of BER due to nonlinear phase noise, whereas the BER performance of the OPC based system is degraded by less than one decade. It can hence be concluded that in this configuration, most of the nonlinear phase noise is compensated for.

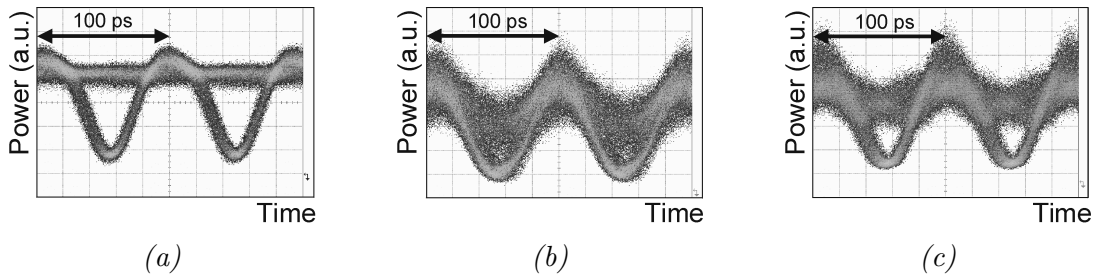


Figure 6.13: 10-Gbit/s NRZ-DPSK eye diagram before the MZDI a) back-to-back, b) after transmission at high transmitted OSNR (40 dB) without OPC, c) with OPC

At high transmitted OSNR (40 dB), where the effect of the nonlinear phase noise is low, the OPC based configuration shows about one decade of improvement in BER compared with the DCF based configuration. The simulations discussed in the next section (6.3.3) will show that the BER improvement at high transmitted OSNR results from a compensation of SPM through OPC. The influence of SPM can be seen in the experimental eye diagrams before the MZDI. Figure 6.13a shows the back-to-back eye diagram of the NRZ-DPSK signal. Figure 6.13b and 6.13c show the eye diagrams after transmission at high transmitted OSNR without and with OPC. It can be seen especially at the transitions between the bits that the eye diagram is less distorted when OPC is employed.

6.3.3 Verification through simulations

The experimental results presented in the previous subsection are verified by simulations [144]. In these simulations, the propagation of the signal is simulated using a linear convolution (asymmetric) split-step Fourier algorithm. A 10.7-Gbit/s NRZ-DPSK signal at 1550 nm is used. The phase-noise of the laser is neglected and an ideal model is assumed for the MZM. The noise figure of the inline amplifiers is 4 dB. ASE noise is added at the transmitter and at every amplifier along the line and the interaction of ASE and the signal due to SPM is taken into account. Monte Carlo simulations are used to estimate the BER. Fragments of a PRBS with the length of $2^{32} - 1$ are used in the simulation. The maximum length of the bits simulated per point is 2 million. In order to reduce the simulation time the bit sequence is divided into smaller blocks that can be processed by Fast Fourier transformation (FFT) methods. The number of points for the FFT is 8192 and the dependencies between the blocks are taken into account by the overlap-add method [145]. Additionally, to further reduce simulation time, the simulation for a certain point is stopped when 100 errors occurred. The simulation rate is 16 samples per bit and the step size was chosen so that the maximum nonlinear phase shift is 0.1 degrees (0.0017 rad). It was verified that smaller step size does not change the results.

The reliability of the results of the Monte Carlo simulations depends on the number of transmitted bits 'N' and the number of errors 'n' and can be estimated by means of confidence intervals [145]. E.g., for $N = 10^6$ and $n = 10^2$, the probability that $8 \cdot 10^{-5} < \text{BER} < 1.2 \cdot 10^{-4}$ is 99%. The dispersion map, the input powers and span count are equal to those of the experimental setup. The decision threshold for the NRZ-DPSK signal is fixed to zero. For simulation ideal phase conjugation is assumed, since in the experimental setup a power penalty of only less than 0.2 dB is measured for the OPC. The optical filter used before the photodiode is a Gaussian filter of the 2nd order with 42-GHz 3dB-bandwidth. The photo-diode is modeled as an ideal squarer and is followed by an electrical low-pass filter of 10-th order with 7.5 GHz 3dB-bandwidth. The amount of post-compensation is optimized for operation with and without OPC individually at high-transmitted OSNR. Figure 6.14 depicts BER performance as a function of the residual chromatic dispersion at high transmitted OSNR. With OPC, most SPM is compensated for through phase conjugation, hence the accumulated dispersion is optimal around 0 ps/nm. Without OPC, positive residual dispersion is optimal after transmission since the dispersion partly compensates for the SPM. The residual dispersions used in the simulations are -202 ps/nm and 798 ps/nm for the system with and without OPC, respectively.

Figure 6.15 depicts the BER performance with and without OPC with optimized post-compensation. The receiver OSNR is kept constant at 9 dB. The receiver OSNR in the simulations is set lower than in the experiments, since the used Monte Carlo approach restricts the BER that can be simulated with reasonable computation effort. We also carried out simulations with and without OPC where the effect of nonlinear phase noise is switched off. In these simulations, the noise is computed analytically and added at the receiver. In these simulations, the transmitted OSNR does not influence the BER performance after transmission. Therefore, the BER performances for the simulations

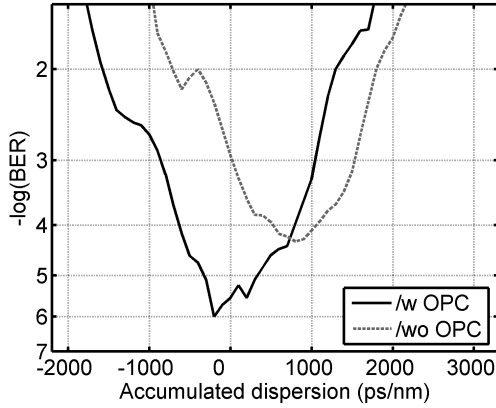


Figure 6.14: *Simulation: BER performance as a function of the residual dispersion at 9-dB received OSNR/0.1nm, /wo OPC and /w OPC.*

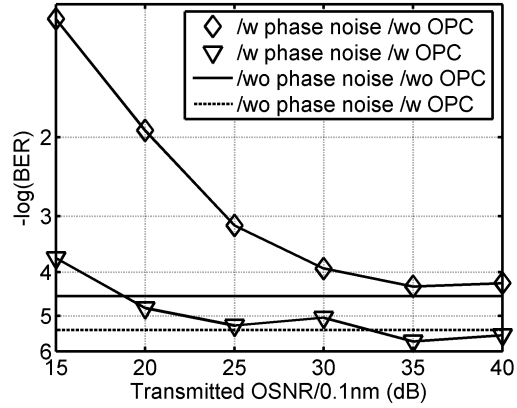


Figure 6.15: *Simulation: BER performance as a function of the transmitted OSNR at 9-dB received OSNR/0.1nm, /wo OPC and /w OPC.*

without nonlinear phase noise are represented as horizontal lines in Figure 6.15.

Comparing the simulation (Figure 6.15) and experimental (Figure 6.12) results, a good agreement can be seen: at low transmitted OSNR, a significant improvement in BER performance is present when an OPC is introduced into the transmission link to compensate for nonlinear phase noise. At high transmitted OSNR a one decade BER improvement through OPC is obtained in both simulation and experiment. When in the simulation, the effect of nonlinear phase noise is neglected and the noise is computed analytically, this decade of BER improvement is still present. It can hence be concluded that the improvement at high transmitted OSNR is due to SPM compensation in the OPC configuration.

6.3.4 OPC placement

The capability of the OPC to compensate for NPN is dependent on the location of the OPC-unit (as described in Section 6.2). In order to know what the tolerances are for the OPC placement it is interesting to test the dependence of the BER performance on the location of the OPC within the link. In this experiment, the OPC location is varied over all inline nodes and the BER is measured. The BER performance after the 800-km transmission link for the highest (40 dB) and the lowest (16 dB) transmitted OSNRs is plotted in Figure 6.16. The two lines at a BER of $5 \cdot 10^{-4}$ dB and a BER of $8 \cdot 10^{-8}$ dB represent the performance of the system without OPC at 16-dB and 40-dB transmitted OSNR, respectively. As with all experiments described in this section, the OSNR at the receiver is kept constant at 12 dB.

The best OPC performance is obtained, when the device is placed in the middle of the link. The performance of mid-link OPC decreases by less than one decade when the location of the OPC-unit is varied from (X=3, Y=5) to (X=5, Y=3), this corresponds

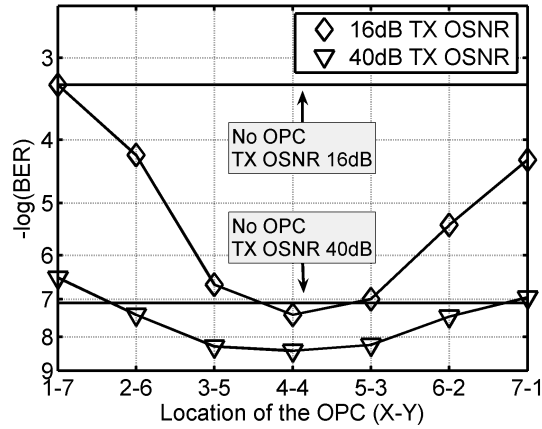


Figure 6.16: BER performance for 10.7-Gbit/s NRZ-DPSK as a function of the location of the OPC ($X - Y$), where X =number of spans before OPC, Y =number of spans after OPC.

to nearly 1/3 to 2/3 of the transmission line. The least effective location of the OPC is after the first ($X=1, Y=7$) or before the last ($X=7, Y=1$) span. The performance at these places is comparable to the performance of the transmission link without OPC. A signal is regenerated indirectly because of OPC. Hence the phase of the signal is conjugated and the signal distortions are reverted along the rest of the transmission line. When the OPC is placed too early in the link, no distortions occurred yet, hence the cancellation effect is small. When the OPC is placed near the end of the transmission link, the signal distortions cannot totally be reverted in the rest of the transmission line. This reduces the cancellation effect as well. Additionally, due to the noise of the SOA, the OSNR is reduced in the OPC, which causes impairments due to nonlinear phase noise in the transmission path after the OPC. In order to show the effect of nonlinear phase noise in the 800-km proof of principle experiment, noise is added at the transmitter (amplifier A in Figure 6.2). This corresponds to the situation where NPN through modulator instabilities is dominant. In a transmission link where ASE induced NPN is dominant, the optimum placement of the OPC is at 66% in a real-world transmission line (see Section 6.2), as opposed to 50% as found for the proof of principle experiment. However, as we have shown in Figure 6.16 and Figure 6.3 the compensation of nonlinear phase noise through OPC is highly tolerant to the placement of the OPC.

6.4 Summary

In this chapter, the influence of NPN is assessed for 10.7-Gbit/s NRZ-DPSK and the compensation of NPN through OPC is studied. Differential phase encoded signals can be impaired by nonlinear phase noise. Nonlinear phase noise results from ASE induced power fluctuations that are converted along the transmission line into phase fluctuations through the Kerr effect. NPN is a nonlinear impairment that cubically grows along the

transmission link.

OPC can be employed to reduce the impairments of NPN. A maximum NPN suppression of 9.5 dB is obtained when the OPC is placed at 66% of the transmission link. Apart from ASE noise induced NPN, a second source of NPN is the imperfection of the modulator, which causes amplitude fluctuations. These amplitude fluctuations will cause NPN through the Kerr effect and can be treated equivalent to an amplifier at the transmitter with a high noise factor. NPN caused by modulator imperfections can completely be compensated for when the OPC is placed at 50% of the transmission link. Both modulator imperfections and ASE are present in a transmission link. The optimal OPC-location is therefore dependent on which type of NPN is dominant.

In a proof-of-principle experiment, the compensation of NPN is shown. NPN is introduced into the transmission link by artificially reducing the OSNR at the transmitter, while keeping the OSNR at the receiver constant. In this experiment a BER improvement of over four decades of BER is observed through a compensation of NPN with OPC. Furthermore, the location of the OPC-unit was varied from the first to the last span of the transmission link. The dependence of the location of the OPC within the transmission link is assessed as well. It is shown that the placement of the OPC-unit is not critical for the compensation of NPN; allowing a relative penalty of 1 decade in BER from the optimum, the OPC-unit can be varied from nearly 1/3 to 2/3 of the transmission link.

In the next chapter, long-haul transmission without noise loading at the transmitter is studied with the DQPSK modulation format. In this experiment mid-link OPC (50% placement) is used to compensate for the detrimental impact of SPM-induced nonlinear impairments, including nonlinear phase noise. This makes it possible to combine both nonlinear phase noise compensation and chromatic dispersion compensation, thereby utilizing both interesting aspects of OPC.

Chapter 7

DQPSK based transmission

DQPSK is an attractive modulation format to increase the spectral efficiency. Especially at a 40-Gbit/s line rate, DQPSK received a lot of attention recently [69, 70, 93]. In this chapter the combination of DQPSK with OPC is studied¹. In the first section the performance of 21.4-Gbit/s DQPSK is assessed. The second section discusses the transmission performance at 42.8-Gbit/s. In both sections, the OPC-based transmission performance is compared with the performance of an optimized conventional transmission link. The transmission link in these experiments is realized with hybrid EDFA/Raman amplification. The performance of OPC in a link using EDFAs only is studied in Section 7.2.3

7.1 21.4-Gbit/s DQPSK transmission

Figure 7.1 depicts the BER as a function of the received OSNR in a back-to-back configuration. Plotted are the sensitivity measurements for 21.4-Gbit/s RZ-DPSK and 21.4-Gbit/s RZ-DQPSK.

The theoretical difference in performance between 21.4-Gbit/s RZ-DPSK and 21.4-Gbit/s RZ-DQPSK is ≈ 1.8 dB at low BER values ($1 \cdot 10^{-8}$) and ≈ 1 dB for high BER values ($1 \cdot 10^{-3}$) [61]. In this experiment a performance difference between RZ-DPSK and RZ-DQPSK of 0.8 and 0.4 is measured for a BER of $1 \cdot 10^{-8}$ and $1 \cdot 10^{-3}$, respectively. The difference between the theory and experiment can be explained by considering that the symbol rate of 21.4-Gbit/s RZ-DPSK (21.4-GSymbol/s) is twice that of 21.4-Gbit/s RZ-DQPSK (10.7-GSymbol/s). For detection of the RZ-DPSK signal, the 21.4-Gbit/s must be demultiplexed to 10.7-Gbit/s, whereas the RZ-DQPSK signal can be detected directly by the 10.7-Gbit/s BER tester. As a result, a small sensitivity penalty is introduced by the extra multiplexer in the 21.4-Gbit/s RZ-DPSK configuration. Additionally, the optical filter used at the receiver has a full-width at half-maximum (FWHM) of 0.2 nm, which introduces a penalty for RZ-DPSK at the 21.4-Gbit/s symbol rate due to narrowband filtering.

¹The results described in this chapter are published in P1-P4, P16-P18, P20, P30

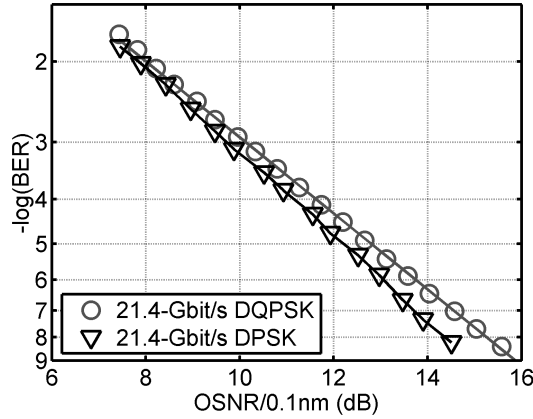


Figure 7.1: *Back-to-back receiver sensitivity.*

7.1.1 DCF-based DQPSK transmission

The experimental setup of the DCF-based re-circulating loop is depicted in Figure 7.2.

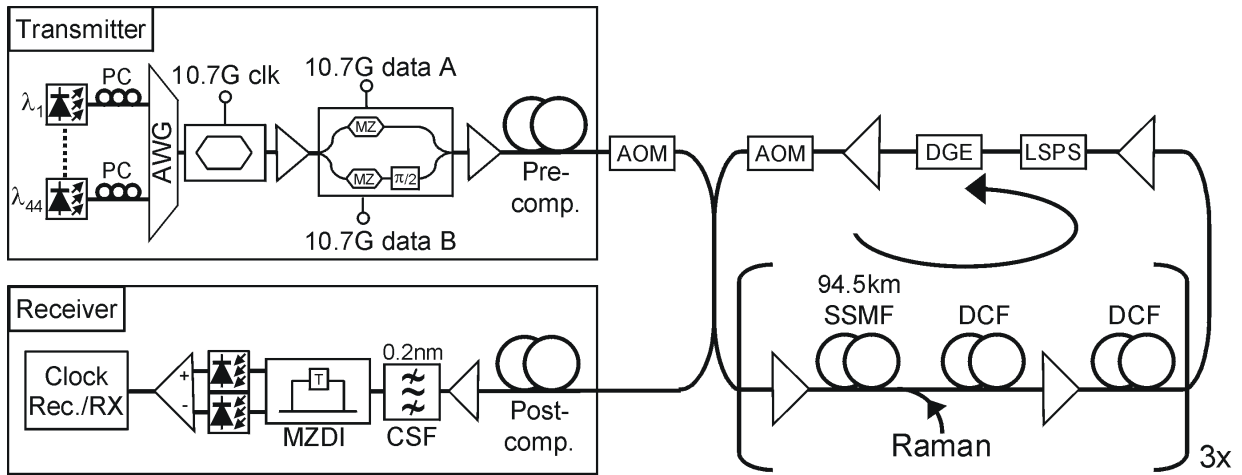


Figure 7.2: *Experimental setup of the DCF-based transmission link.*

At the transmitter, 44 continuous wave signals on a 50-GHz grid are generated in the C-band by DFB lasers and multiplexed by using an AWG. Subsequently a modulator cascade consisting of two external LiNbO₃ MZMs is used to generate RZ-DQPSK. The first modulator is driven with a 10.7-GHz clock signal, carving a pulse with a 50% duty cycle. The second modulator is an integrated DQPSK modulator with two parallel MZMs within a super Mach-Zehnder structure as described in Section 3.4.4. Two 10.7-Gbit/s data streams (one inverted: data A, one non-inverted: data B) with a relative delay of 5 bits for de-correlation of the bit sequences are used for modulation of the 21.4-Gbit/s DQPSK signal. The length of the PRBS used is $2^{15} - 1$. No longer PRBS lengths can be

7.1. 21.4-GBIT/S DQPSK TRANSMISSION

used without pre-coding in this experiment since the DQPSK modulation format requires the BER test set to be programmed. Alternatively, pre-coding of both data sequences can be used, which does not restrict the length of the PRBS [146].

The transmission line consists of three 94.5-km spans of SSMF with a chromatic dispersion of ≈ 16 ps/nm/km and an average span loss of 21.5 dB (including 1.5 dB loss of couplers required for Raman amplification). The loss of the SSMF spans is compensated for by using a hybrid Raman/EDFA structure for signal amplification. The average on/off Raman gain of the backward pumped Raman pumps is ≈ 11 dB. After each span a DCF module is used to compensate for the chromatic dispersion. 20% of the DCF is placed between the Raman pump and the first stage of the inline amplifier to balance the DCF insertion loss. A loop-synchronous polarization scrambler (LSPS) is used to reduce the statistical correlation of loop-induced polarization effects. Power equalization of the WDM channels is provided by a channel based DGE with a bandwidth of 0.3 nm, hence spectral filtering of the signals occurs with every re-circulation. After transmission, the dispersion is optimized on a per-channel basis with a 10 ps/nm granularity. Subsequently a narrow-band 0.2-nm CSF is used to select the desired channel. After a one-bit (94 ps) MZDI and a balanced detector, the clock is recovered and the performance of the signal is evaluated using a BERT, programmed for the expected sequence.

In order to optimize the performance of the DCF-based transmission system, the optical input power into the SSMF, the inline dispersion map and the pre-compensation is optimized at 4,500-km transmission distance. For this optimization the BER performance of three typical channels is measured, namely 1533.9 nm, 1549.7 nm and 1553.7 nm. The BER as a function of the input power per channel is depicted in Figure 7.3. The inline under-compensation in the input power variation experiment is set to ≈ 80 ps/nm/span and the pre-compensation is fixed at -850 ps/nm.

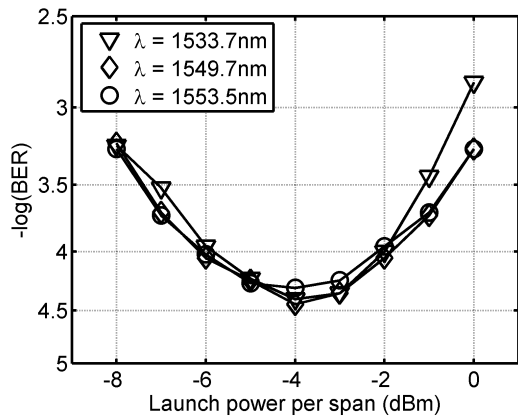


Figure 7.3: BER as a function of the input power per channel.

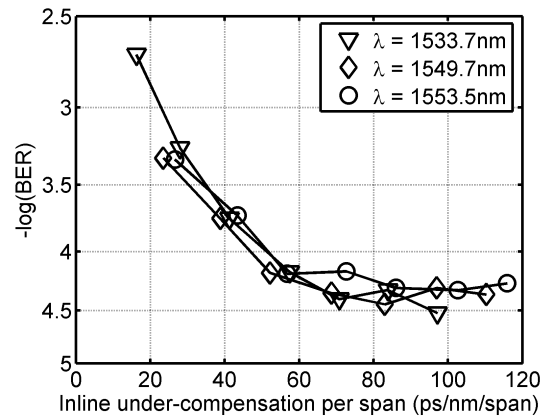


Figure 7.4: BER as a function of the inline under-compensation per span.

At low (-8 dBm) and high (0 dBm) input powers the BER is limited by ASE and nonlinear impairments, respectively. An optimum trade-off between the nonlinear impairments

and ASE is found for an input power of -4 dBm/channel, which is used in the transmission experiment. Figure 7.4 shows the BER as a function of the inline under-compensation per span. The input power is set to -4 dBm/channel and a pre-compensation of -850 ps/nm is used. At low inline under-compensation values, the influence of XPM and XPM induced nonlinear phase noise becomes more severe due to insufficient walk-off between the channels [147]. Up to an inline under-compensation of 110 ps/nm/span no decrease in BER is detected, which indicates a high tolerance for 21.4-Gbit/s RZ-DQPSK towards suboptimal dispersion maps. A high inline under-compensation is impractical for ultra long-haul transmission, since huge amounts of post-compensation are then required at the receiver. Considering this trade-off an inline under-compensation of around 80 ps/nm/span is chosen.

In Figure 7.5 the BER performance as a function of the pre-compensation is plotted. The input power is set to -4 dBm/channel in this experiment and the inline under-

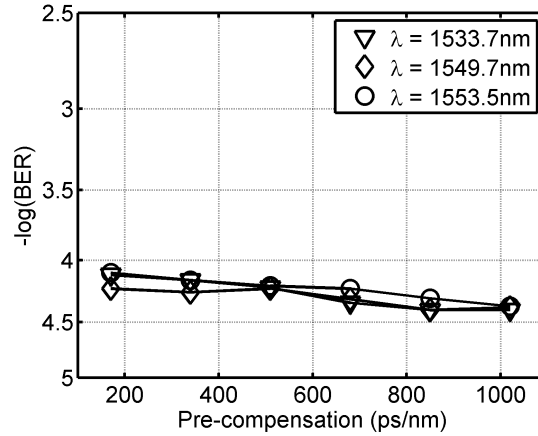


Figure 7.5: BER as a function of the pre-compensation.

compensation is fixed to 80 ps/nm/span. From this plot we can conclude that the amount of pre-compensation does not have a strong influence on the performance of DQPSK transmission. The pre-compensation used in the transmission experiment is -850 ps/nm. Using these optimized parameters, the BER of a typical channel (in-phase, 1550.7 nm) is assessed as a function of the transmission distance as plotted in Figure 7.6 on double logarithmic axes. At shorter distances, the degradation of the BER represents a straight line on a double the logarithmic scale. After 5,000-km transmission, the BER degradation accelerates with respect to the straight line. For the RZ-DQPSK modulation format, it has been shown that single channel impairments are dominant over multi channel impairments [148]. Hence we conjecture that the accelerated degradation in BER of the conventional transmission results from SPM induced impairments such as nonlinear phase noise as previously observed in [129]. The BER performance of all 44 wavelengths after 7,100 km (25 circulations through the re-circulating loop) are shown in Figure 7.7. Both the in-phase and quadrature channels are depicted. All BER values are well below the FEC threshold as defined in 3.1.

7.1. 21.4-GBIT/S DQPSK TRANSMISSION

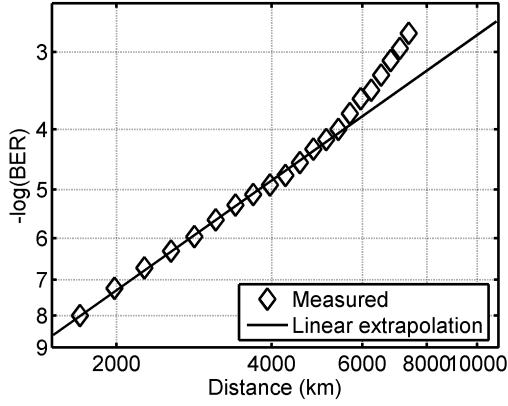


Figure 7.6: BER of a typical channel (in-phase, 1550.7 nm) as a function of transmission distance.

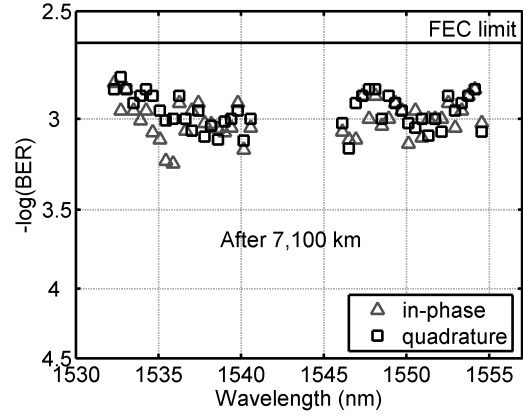


Figure 7.7: In-phase and quadrature BER values for the DCF-based configuration after 7,100-km transmission.

7.1.2 OPC-based DQPSK transmission

The experimental setup of the OPC-based configuration is depicted in Figure 7.8. In the OPC-based configuration, the inline DCF modules for chromatic dispersion compensation are removed and an OPC is inserted in the middle of the transmission link for compensation of dispersion and nonlinear impairments. The rest of the transmission system (transmitter, receiver, SSMF, amplifiers, etc.) is the same as in the DCF-based configuration discussed in the previous section. The average effective Raman gain in this experiment is -10.3 dB. This is significantly below the gain required for power symmetry. The input power per channel into the SSMF is -2.9 dBm (13.5 dBm total input power).

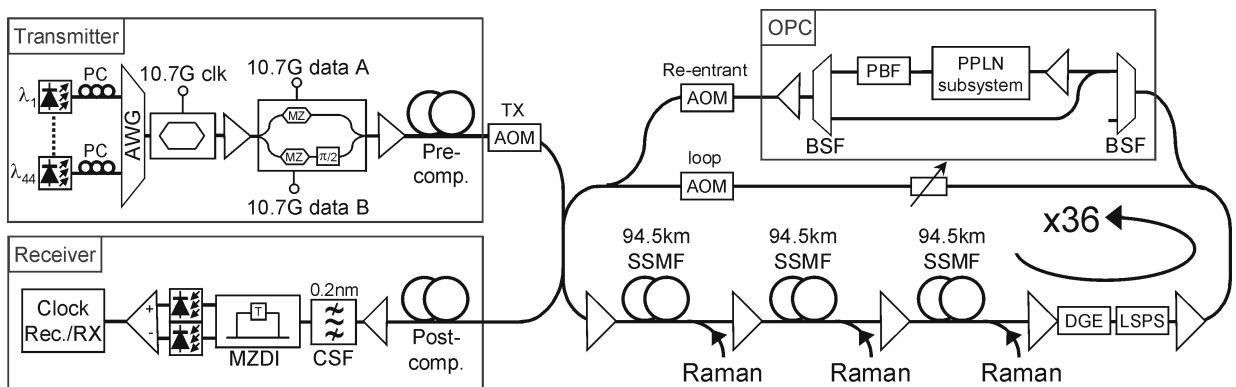


Figure 7.8: Experimental setup of the OPC-based transmission link.

The signals are optically phase conjugated in the middle of the transmission link. In the re-entrant re-circulating loop structure this is realized after half the re-circulations (18x) by opening the loop acousto-optic modulator (AOM) and closing the re-entrant AOM for one

re-circulation. Hereby the signals are fed through the OPC subsystem. In this subsystem, the 22 channels from 1532.3 nm to 1540.6 nm, used to balance the signal in the amplifiers, are removed using a BSF. Subsequently, the remaining 22 channels from 1546.1 nm to 1554.5 nm are phase conjugated in the PPLN subsystem. At the output of the PPLN, the phase conjugated signals are present mirrored with respect to the pump and range from 1532.3 nm to 1540.6 nm. Note that the re-entrant AOM is placed at the end of the re-entrant branch, not at the beginning. If the re-entrant AOM were placed at the beginning, high power transients would occur in the EDFAs of the re-entrant branch because of the switching of the AOM. The optical spectrum directly after the PPLN subsystem is depicted in Figure 7.9.

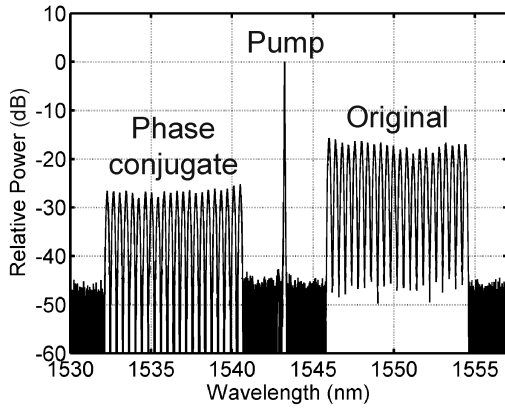


Figure 7.9: *Optical spectrum at the output of the PPLN-waveguide after 18 circulations in the loop (res. bw. = 0.01 nm).*

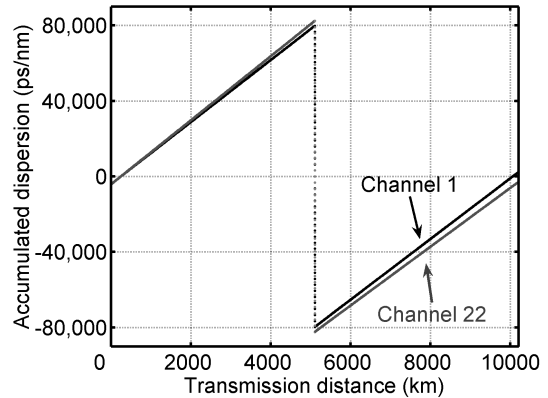


Figure 7.10: *Accumulated dispersion as a function of the transmission distance for channel 1 and channel 22.*

Similar to the DCF-based transmission experiment a loop-synchronous polarization scrambler is used to reduce the statistical correlation of loop-induced polarization effects. Hence at the input of the PPLN subsystem, the channel polarizations are randomized by the transmission fiber and thus polarization independence for the OPC is required. The diversity scheme used in this experiment to create polarization independent OPC is based on the counter propagating polarization diversity scheme as discussed in Section 4.3.

After the polarization diversity structure, the pump signal is suppressed through a PBF and the original data signal is removed using a band selection filter. Finally, the phase conjugated channels are recombined with the 22 channels (ranging from 1546.1 nm to 1554.5 nm) to balance the signal propagating through another 18 circulations in the re-circulating loop.

In Figure 7.10 the dispersion map of the 10,200-km transmission line for the 22 evaluated channels is depicted. In the first 5,100 km, before the OPC, the accumulated dispersion of the signals increases to 79,600 ps/nm and 82,400 ps/nm for channels 1 (1546.1 nm) and 22 (1554.5 nm), respectively. At the optical phase conjugator, all signals are mirrored with respect to the pump and the sign of the accumulated dispersion is inverted. Due to

7.1. 21.4-GBIT/S DQPSK TRANSMISSION

the SSF slope of $0.063 \text{ ps/nm}^2/\text{km}$ the channels experience a different dispersion in the second half than in the first half of the link. As a result, after 10,206 km, the difference in accumulated dispersion between channel 1 and channel 22 is 5,206 ps/nm. The amount of pre-compensation ($-4,082 \text{ ps/nm}$) is chosen such that the required post compensation is centered around 0 ps/nm for the WDM channels. In this experiment, the OPC unit compensates for an accumulated chromatic dispersion of over 160,000 ps/nm.

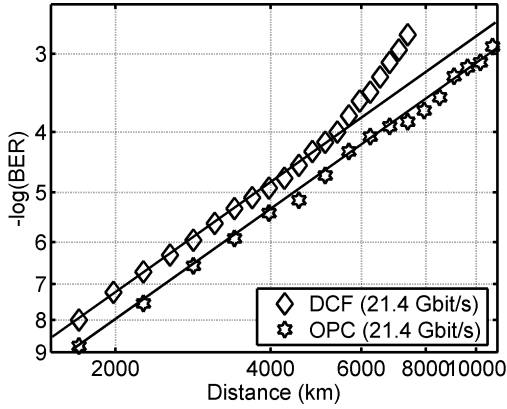


Figure 7.11: BER performance as a function of transmission distance for the DCF and the OPC-based transmission system.

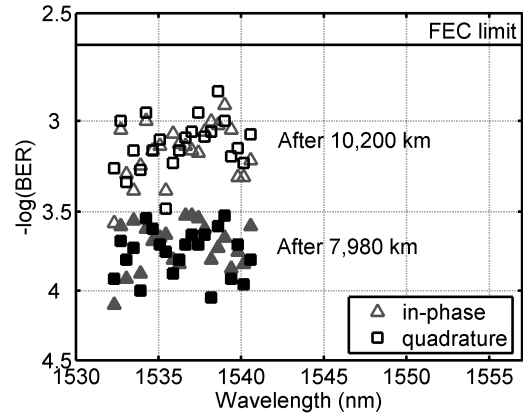


Figure 7.12: In-phase and quadrature BER values for the mid-link OPC-based configuration.

Figure 7.11 shows the measured BER performance of a typical channel (in-phase, 1535.1 nm) as a function of the transmission distance. As a reference, the typical channel (in-phase, 1550.7 nm) of the DCF-based transmission experiment is depicted as well (same curve as in Figure 7.6). Up to 5,000 km, the BER for both configurations show a straight line on a double logarithmic scale. For transmission over more than 5,000 km, the DCF-based transmission is strongly impaired by nonlinear effects and deviates from the straight line, whereas the performance for the OPC-based transmission is virtually unaffected. Figure 7.12 shows the BER values for the OPC-based transmission after 7,980 km (28 circulations through the re-circulating loop) and after 10,200 km (36 circulations through the re-circulating loop). Both the in-phase and quadrature channels are depicted. Note that the BER performance is evaluated for the 22 phase conjugated channels. A second OPC would be required to conjugate and enable measuring the other 22 channels. The worst BER values are $3.0 \cdot 10^{-4}$ and $1.4 \cdot 10^{-3}$ after 7,940-km and 10,200-km transmission, respectively. Both in-phase and quadrature components show similar performance. For the 7,940-km transmission experiment the average BER measured ($2.0 \cdot 10^{-4}$) is more than a decade below the FEC threshold. When the transmission distance is increased to 10,200 km the measured BER values of all channels are still well below the FEC threshold. In the DCF-based configuration (Figure 7.7), similar BER values are obtained after 7,100 km, hence OPC enabled a distance increase of 44%.

The variance in BER performance for the OPC-based transmission after 10,200-km

transmission (Figure 7.12) is larger than in the DCF-based transmission after 7,100-km transmission (Figure 7.7). This results partly from the fact that the BER values of the OPC-based transmission are measured after 36 circulations through the loop instead of 25 in the DCF case. As well, in the OPC configuration, the 22 measured channels propagated the first half of the link in the upper part of the C-band (1546.1 nm to 1554.5 nm) and after OPC, the second half of the link in the lower part of the C-band (1532.3 nm to 1540.6 nm), which complicates spectral flattening with a DGE in the OPC-based configuration.

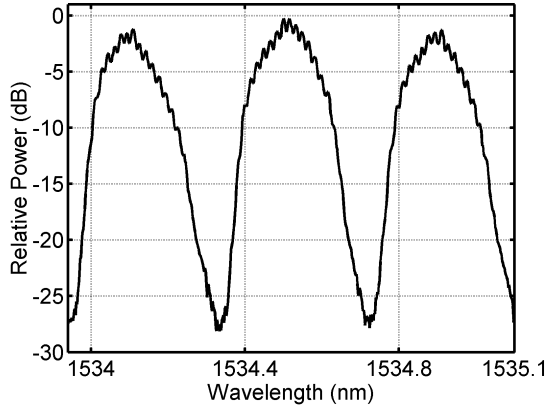


Figure 7.13: *Optical spectrum of the RZ-DQPSK signals after transmission (res. bw. = 0.01 nm).*

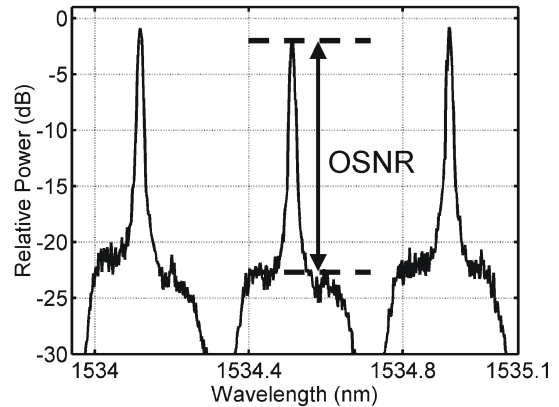


Figure 7.14: *Optical spectrum of CW signals after transmission (res. bw. = 0.01 nm).*

The OSNR after transmission is a good measure to assess how much the system is impaired by nonlinear effects. In the experiments described so far, the extrapolation method was employed to determine the OSNR of a WDM channel. In this long haul experiment, however, the extrapolation method can not be employed with modulated channels due to the channel based DGE. With the DGE, the attenuation of each individual WDM channel is set to obtain a flat WDM spectrum. As a result, the noise intensity differs per WDM channel and cannot be extrapolated. Figure 7.13 shows the optical spectrum of an RZ-DQPSK signal after transmission. From this figure it is not possible to determine the noise intensity and hence the OSNR per channel. Figure 7.14 depicts the same optical spectrum as in Figure 7.13 where the modulated RZ-DQPSK signals are replaced by CW tones. In this figure, the intensity of the noise can be measured and hence the OSNR per channel can be determined. With this method, the OSNR of a signal after transmission through the re-circulating loop can be estimated with a ca. 1 dB accuracy. Using CW tones it was found that through mid-link OPC an OSNR improvement of about 1 dB is obtained. An average OSNR of 11.4 ± 0.5 dB was measured after 10,200-km transmission in the mid-link OPC configuration. The OSNR for the DCF-based configuration after 7,100-km transmission is 12.1 ± 0.5 dB. Given the average BER after transmission ($7.8 \cdot 10^{-4}$ and $1.1 \cdot 10^{-3}$ dB for the OPC and the DCF-based setup, respectively) this coincides with an OSNR penalty compared with back-to-back of 1.1 ± 0.5 dB for the OPC-based and 2 ± 0.5 dB for the

DCF-based configuration. A smaller OSNR penalty is obtained in the OPC-based configuration even though the transmission distance is longer and the launch power higher than in the conventional link. This indicates that through OPC, the nonlinear impairments are reduced.

7.2 42.8-Gbit/s DQPSK transmission

Enhancing the spectral efficiency is a suitable method to increase transmission capacity. DQPSK can be employed to realize transmission with 0.8-bit/s/Hz spectral efficiency by transmitting 42.8-Gbit/s RZ-DQPSK at 50-GHz channel spacing [69]. In this section, the transmission performance of 42.8-Gbit/s RZ-DQPSK with 50-GHz channel spacing is assessed with and without OPC. The 40 Gbit/s line rate is furthermore interesting as it is part of the SDH/SONET hierarchy.

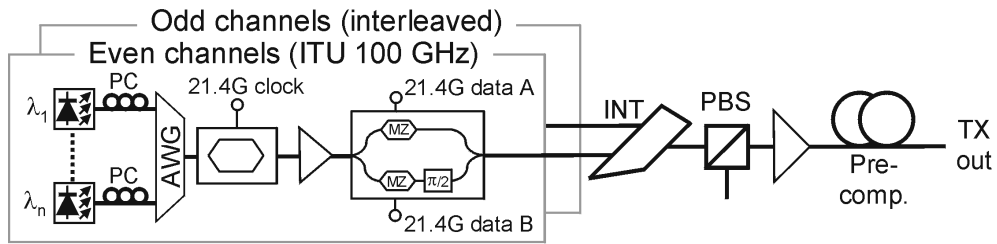


Figure 7.15: 42.8-Gbit/s DQPSK transmitter (TX).

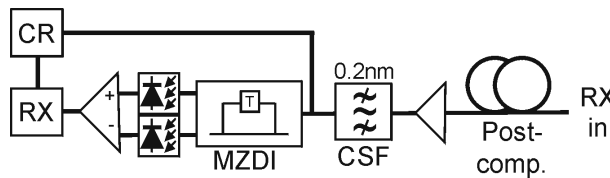


Figure 7.16: 42.8-Gbit/s DQPSK receiver (RX).

Figure 7.15 and 7.16 depict the experimental setup of the transmitter and receiver, respectively. The OPC and DCF-based transmission lines are the same as described in the 21.4-Gbit/s RZ-DQPSK transmission experiment (Section 7.1). However, as the optical spectrum of 42.8-Gbit/s RZ-DQPSK is twice as broad as that of 21.4-Gbit/s RZ-DQPSK, a different transmitter structure is required. In the 21.4-Gbit/s RZ-DQPSK experiments all channels are modulated with one set of modulators. The optical spectrum of 21.4-Gbit/s RZ-DQPSK is small enough so that no linear cross talk occurs after modulation at 50-GHz channel spacing. In the 42.8-Gbit/s RZ-DQPSK experiments the even and odd channels need to be modulated separately with two parallel modulator chains, otherwise significant impairments would occur due to linear cross-talk between the WDM channels [149]. Each modulator chain consists of a pulse carver and a parallel DQPSK modulator. The pulse

CHAPTER 7. DQPSK BASED TRANSMISSION

carver MZM is fed with 21.4 GHz so that a pulse with a 50% duty cycle is created. The second modulator is an integrated DQPSK modulator with two parallel MZMs within a super Mach-Zehnder structure. A 21.4-Gbit/s data stream is created by electrically multiplexing two 10.7-Gbit/s PRBS signals with a length of $2^{15} - 1$ and a relative delay of 16 bits. This 21.4-Gbit/s data stream is split and fed to both inputs of the 42.8-Gbit/s DQPSK modulator with a relative delay of 10 bits of the bit sequences for de-correlation. After modulation, the even and odd channels are combined with a 50-GHz interleaver. A PBS ensures that all channels are co-polarized for worst-case interaction.

The receiver structure used in this experiment is as well a bit different from that used in the 21.4-Gbit/s RZ-DQPSK transmission experiment (Section 7.1). It was found that the CDR operated more stable when it was fed with the signal before the MZDI. Therefore, after the post-compensation and the CSF, the signal is split and one part is used for clock recovery. The other part is fed to the two-bit (94 ps) MZDI followed by a balanced detector. After the balanced detector, the signal is de-multiplexed from 21.4 Gbit/s to 10.7 Gbit/s and evaluated using a BER-tester programmed for the expected bit sequence. The de-multiplexer is automatically reset every loop re-circulation, hence the measured BER corresponds to the average BER of both 10.7-Gbit/s tributaries.

The back-to-back performance of the 21.4-Gbit/s RZ-DQPSK and the 42.8-Gbit/s RZ-DQPSK is depicted in Figure 7.17. At high BER values ($1 \cdot 10^{-3}$) a 3-dB difference

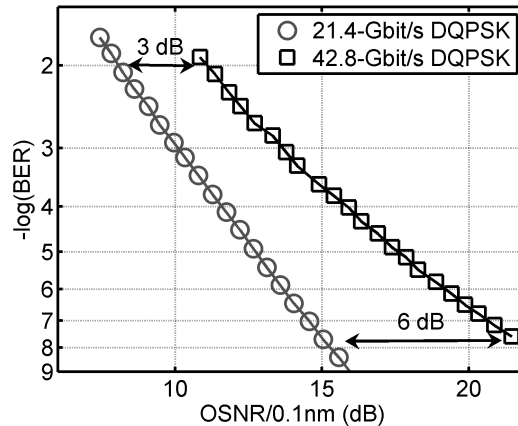


Figure 7.17: Back-to-back BER as a function of the OSNR/0.1nm, for 21.4-Gbit/s and 42.8-Gbit/s RZ-DQPSK.

in OSNR is present between the 21.4-Gbit/s and 42.8-Gbit/s RZ-DQPSK curves, which is to be expected due to the difference in data rate. For low BER values ($1 \cdot 10^{-9}$), the OSNR difference between the modulation-formats increases to 6 dB. The increase in OSNR difference at low BER values is a result of modulator imperfections that are more severe for 42.8-Gbit/s RZ-DQPSK and the narrowband optical filtering of the 0.2-nm CSF that is used to select the desired channel. It has been shown that for 42.8-Gbit/s RZ-DQPSK a CSF of 0.3-nm is optimal [70]. The impact on 42.8-Gbit/s RZ-DQPSK of the 0.2-nm CSF

can be seen in the back-to-back eye diagrams without (7.18a and b) and with (Figure 7.18c and d) narrowband filtering. However, in this transmission experiment the performance is assessed near the FEC threshold, where the penalty of doubling the data rate is only slightly in excess of 3-dB in the regime of interest ($\text{BER} \approx 1 \cdot 10^{-3}$). Hence, doubling the data rate in this experimental setup gives a minor decrease in receiver sensitivity.

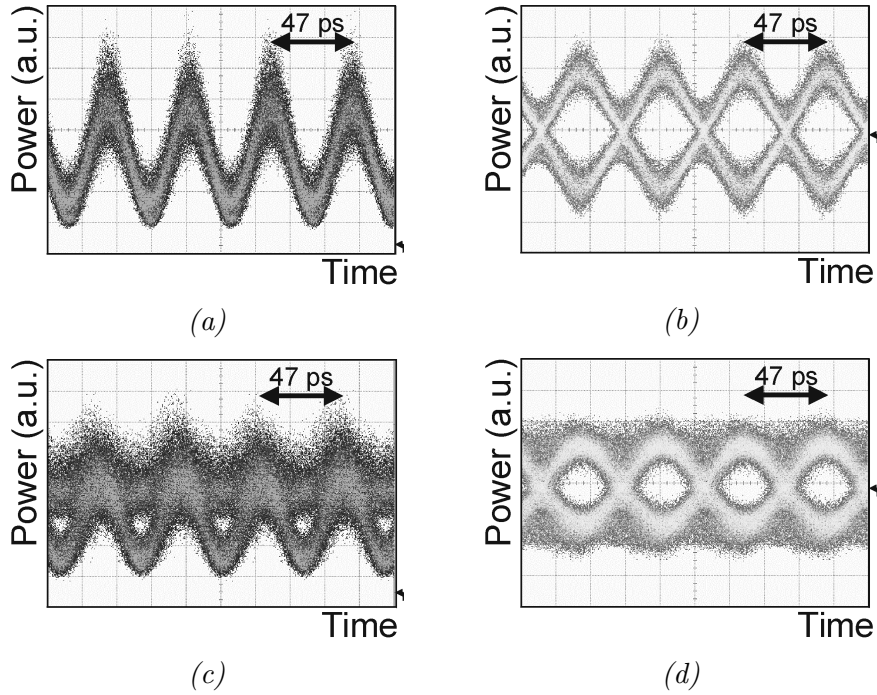


Figure 7.18: 42.8-Gbit/s back-to-back DQPSK eye diagrams a) eye diagram single channel before the MZDI, b) eye diagram single channel after the MZDI, c) eye diagram /w narrowband filtering before the MZDI, d) eye diagram /w narrowband filtering after the MZDI.

7.2.1 DCF-based DQPSK transmission

Similar to the 21.4-Gbit/s DQPSK experiment, the performance of the DCF-based transmission system is optimized by varying the optical input power into the SSMF, inline dispersion map and pre-compensation. In this experiment 18 channels are transmitted on a 50-GHz ITU grid (Figure 7.20), 9 channels in the lower part of the C-band (from 1534.25 nm to 1537.40 nm) and 9 channels in the higher part of the C-band (from 1549.32 nm to 1552.52 nm). The BER performance is measured for both center channels in the lower and higher part of the C-band (1535.9 nm and 1551.0 nm) after 2,260-km of transmission, which corresponds to eight circulations through the re-circulating loop. Figure 7.19a shows the BER as a function of the input power per channel. The inline under-compensation in the input power variation experiment is set to ≈ 33 ps/nm/span and the pre-compensation is fixed to -1020 ps/nm. An optimum input power of -3.5 dBm/channel is chosen. At high input powers, the performance of the two measured channels is slightly different. This

CHAPTER 7. DQPSK BASED TRANSMISSION

effect is observed as well in the 16x40-Gbit/s transmission experiment (Section 5.2, Figure 5.17). In order to have a constant gain over the whole C-band, the setting of the amplifiers are such that the noise figure across the C-band is non-constant. At short wavelengths of the C-band (near 1530 nm) the noise figure is slightly higher than the noise figure at longer wavelengths (near 1565 nm).

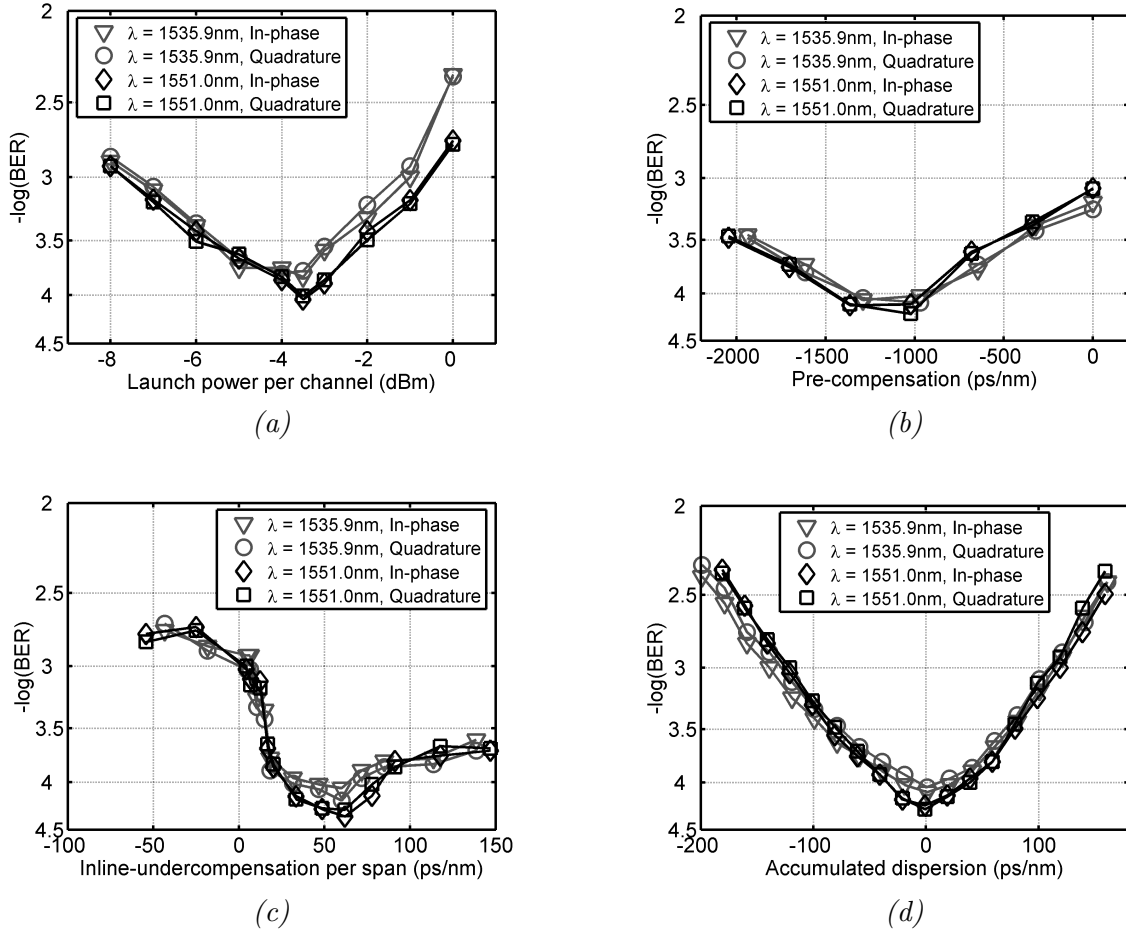


Figure 7.19: Dispersion and power map optimization for 42.8 Gbit/s after 2260 km, a) BER as a function of the input power, b) BER as a function of the pre-compensation, c) BER as a function of the inline under-compensation per span, d) BER as a function of the accumulated dispersion.

The BER performance as a function of the inline under-compensation per span is plotted in Figure 7.19b. The input power is set to -3.5 dBm/channel and a pre-compensation of -1020 ps/nm is used. The measured results show that analogue to the 21.4-Gbit/s DQPSK experiment, the influence of XPM and XPM induced nonlinear phase noise becomes more severe at low inline under-compensation [147]. At high inline under-compensation per span only a slight decrease in performance is measured. For further experiments, the inline under-compensation of ≈ 60 ps/nm/span is used. Figure 7.19c depicts the BER as a

function of the pre-compensation. In this experiment, the input power and inline under-compensation are fixed to -3.5 dBm/channel and ≈ 60 ps/nm/span, respectively. Similar to the 21.4-Gbit/s DQPSK experiment the amount of pre-compensation does not have a strong influence on the performance of DQPSK transmission. Only close to 0-ps/nm pre compensation insufficient pulse spreading occurs, which slightly decreases the measured performance. The pre-compensation used in the transmission experiment is -1020 ps/nm.

For all these measurements, the post-compensation was optimized after transmission. Using the optimized parameters, the BER as a function of the accumulated dispersion after 2,260-km transmission is shown in Figure 7.19d. The best BER performance is $8.5 \cdot 10^{-5}$, giving over a decade of margin with respect to the FEC threshold.

Figure 7.21 depicts the average BER performance of the two center channels (1549.32 nm and 1552.52 nm) as a function of the transmission distance. Similar to the 21.4-Gbit/s RZ-DQPSK transmission experiment, the BER decrease represents a straight line on a double the logarithmic scale. However, after 2,500 km transmission it deviates from this line due to increased penalties resulting from a combination of SPM and NPN. The maximum attainable transmission distance for a BER of $\approx 1 \cdot 10^{-3}$ is about 3,000 km. Compared to the experiment at 21.4-Gbit/s RZ-DQPSK, the maximum attainable transmission distance is reduced by a factor of 2.4.

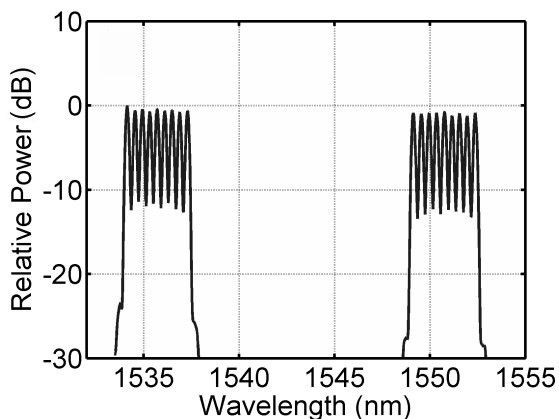


Figure 7.20: *Optical spectrum of the 18 WDM channels used for the optimization of the DCF-based configuration (res. bw. = 0.1 nm).*

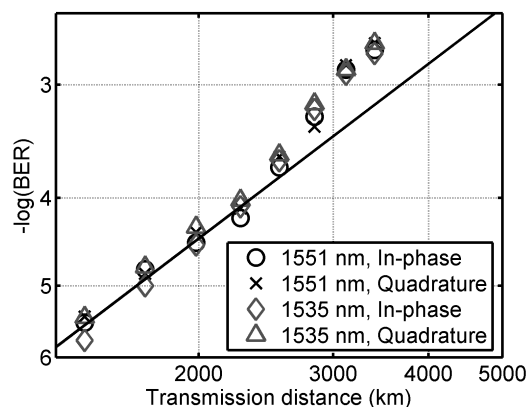


Figure 7.21: *BER performance of the two center channels (1549.32 nm and 1552.52 nm) as a function of the transmission distance.*

7.2.2 OPC-based DQPSK transmission

In the OPC-based transmission experiment, 26 WDM channels are transmitted at 42.8-Gbit/s (> 1 Tbit/s aggregate capacity). At the transmitter, 52 channels are modulated in total, since 26 extra WDM channels are used in the re-circulating loop to balance the gain spectrum of the amplifiers. As with the OPC-based experiment at 21.4-Gbit/s DQPSK,

the input power into the SSMF is -2.9 dBm/channel and the amount of pre-compensation (-2040 ps/nm) is chosen such that the required post compensation is centered around 0 ps/nm for the WDM channels. The polarization diversity subsystem, used for OPC is based on the counter-directional structure as described in Section 4.3.2. However, slightly different parameters are used for OPC: the pump laser is amplified to 500 mW and the power per channel is set to approximately 10 mW before the polarization beam splitter. The optical spectrum after conjugation is depicted in Figure 7.22a, showing a conversion efficiency of -7.2 dB. The optical spectrum at the receiver is depicted in Figure 7.22b.

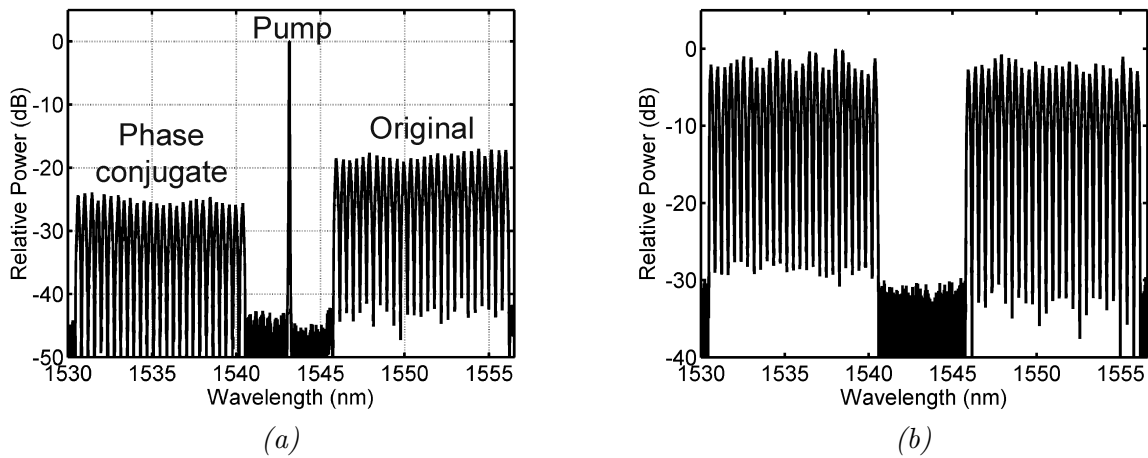


Figure 7.22: *Optical spectra (res. bw. = 0.01 nm), a) at the output of the OPC subsystem after eight circulations in the loop, b) after 4,500 km of transmission.*

The performance of 42.8-Gbit/s RZ-DQPSK transmission is evaluated after 4500-km transmission for the 26 phase conjugated channels. In Figure 7.23, the BER of both the in-phase and quadrature channels are depicted. Both in-phase and quadrature components show similar performance, with a slightly better performance for the in-phase tributary due to modulator imperfections. The worst BER measured is $1.3 \cdot 10^{-3}$; hence all measured channels are well below the FEC limit. The received OSNR of all channels after 4,500-km transmission is approximately 15.5 dB on average, which corresponds to a 2-dB OSNR penalty compared with the back-to-back performance. This indicates only minor influence of nonlinear phase noise distortions.

Figure 7.24 depicts the eye diagrams before and after the MZDI of the 42.8 Gbit/s RZ-DQPSK signal after 4,500 km transmission with OPC. The BER performance as a function of the transmission distance was assessed as well. For this experiment, the same 18 WDM channels are used as in the DCF-based configuration (Figure 7.20): nine channels that are phase conjugated (from 1549.32 nm to 1552.52 nm) and an additional nine channels (from 1534.25 nm to 1537.40 nm) to balance the amplifiers. The reduction of the total WDM channels from 52 to 18 allowed the EDFAs to be operated in a slightly different configuration, resulting in a performance improvement of about half a decade in BER after transmission. The BER of the center channel (1535.8 nm after conjugation) as a function

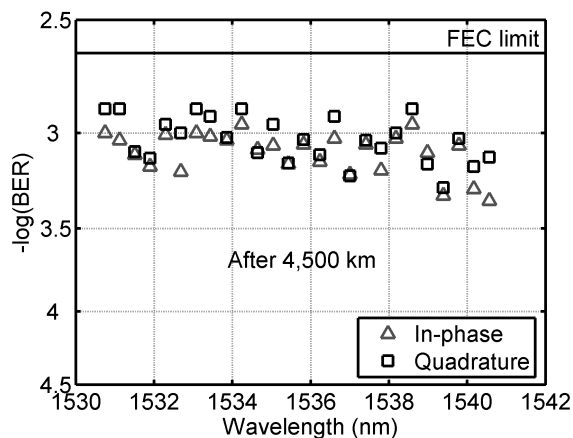


Figure 7.23: *In-phase and quadrature BER values for the mid-link OPC-based configuration after 4,500-km transmission.*

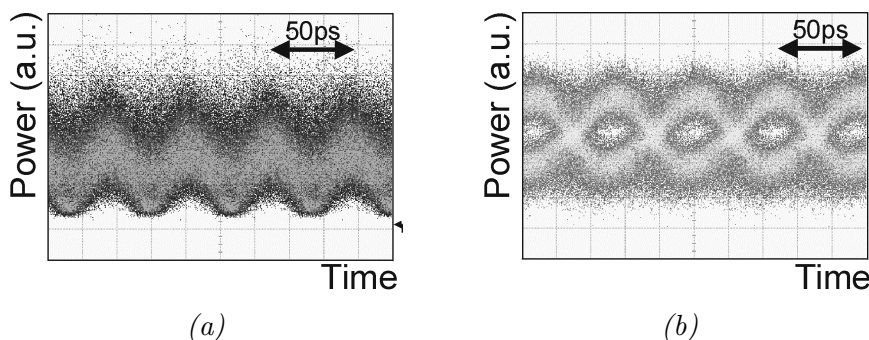


Figure 7.24: *42.8-Gbit/s DQPSK eye diagrams with narrowband filtering after 4,500-km transmission, a) before the MZDI, b) after the MZDI.*

of the transmission distance is depicted in Figure 7.25. As a reference, the performance of the DCF-based configuration is also depicted (same curve as in Figure 7.21). By adjusting the number of loop re-circulations, the transmission performance of the center channel (1535.8 nm after conjugation) is measured from 1,700 km up to 5,700 km. Similar to the experiments at 21.4 Gbit/s the BER performance of the DCF-based configuration shows an accelerated decrease after 2,500-km transmission, whereas the OPC-based performance is virtually unaffected by nonlinear impairments. The feasible transmission distance for a BER of $\approx 1 \cdot 10^{-3}$ is limited to approximately 5,000 km and 3,000 km for the OPC and the DCF-based configuration, respectively. The increase in transmission distance through OPC in this case is 60%. Hence, OPC effectively reduces the influence of nonlinear distortions and extends the reach of 42.8-Gbit/s RZ-DQPSK transmission.

In the mid-link OPC configuration an OSNR improvement is obtained since single stage amplifiers are used instead of the double stage amplifiers that are required for the DCF based configuration. In the experiments described in this section the OSNR im-

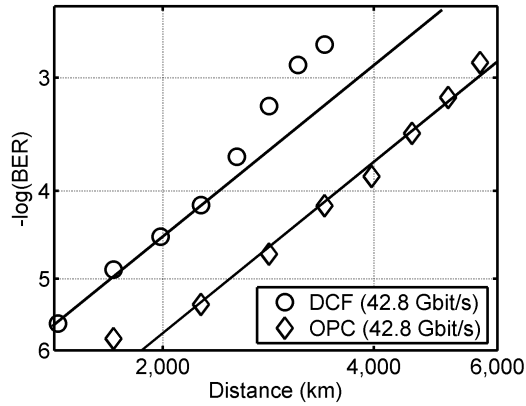


Figure 7.25: BER of the center channel (1535.8 nm after conjugation) as a function of the transmission distance for the DCF and the OPC-based configuration.

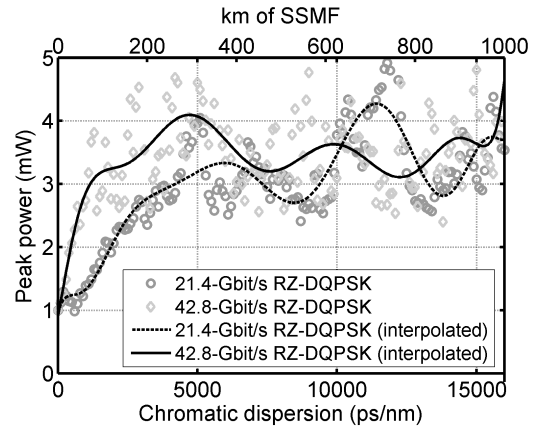


Figure 7.26: Simulation: Peak power as a function of dispersion with a constant optical power for 21.4-Gbit/s and 42.8-Gbit/s RZ-DQPSK.

provement obtained by using mid-link OPC is about 1 dB. However, when comparing the BER performance as a function of the transmission distance, it can be seen that for short transmission distances, the performance improvement of 21.4-Gbit/s RZ-DQPSK (7.11) is smaller than the performance improvement of 42.8-Gbit/s RZ-DQPSK (7.25). A possible explanation for the larger performance difference observed for 42.8-Gbit/s RZ-DQPSK is that the penalty of the mid-link OPC dispersion map is smaller than at 21.4-Gbit/s RZ-DQPSK. Figure 7.26 shows the simulated peak power of 21.4-Gbit/s and 42.8-Gbit/s as a function of the dispersion for a constant mean signal power. The peak power of 21.4-Gbit/s RZ-DQPSK (with a symbol rate of 10.7-Gbit/s) is relatively small for low dispersion values; a peak power of 3 mW is obtained for a dispersion of 4,200 ps/nm, whereas at 42.8-Gbit/s RZ-DQPSK 3 mW peak power is already obtained with 1,150 ps/nm dispersion. As a result, the dispersion map of mid-link OPC introduces a penalty at 21.4-Gbit/s RZ-DQPSK compared to the dispersion map of a conventional transmission system. At 42.8-Gbit/s, little difference is present between the peak power at low or at high dispersion values. Therefore, a significantly larger performance improvement is obtained through mid-link OPC compared to the performance at 21.4-Gbit/s.

In the back-to-back configuration doubling the data rate from 21.4 Gbit/s to 42.8 Gbit/s resulted in an OSNR penalty of about 3-dB. This same performance difference is measured in the mid-link OPC configuration; doubling the data rate from 21.4-Gbit/s RZ-DQPSK to 42.8-Gbit/s RZ-DQPSK results in a decrease of roughly half the attainable transmission distance. For the DCF-based configuration doubling the data rate reduced the attainable transmission distance by a factor of 2.4. The decrease in performance is caused by increased penalties resulting from both SPM and NPN.

7.2.3 OPC-based transmission without Raman amplification

In the ultra long-haul DQPSK transmission experiments discussed so far, Raman amplification has been employed to increase the transmission performance. As discussed in Section 4.4.1, Raman amplification increases the power symmetry of the transmission link with respect to the OPC and thereby its regeneration capabilities. In this section the transmission performance of WDM 42.8-Gbit/s DQPSK is assessed in an OPC-based transmission system without Raman amplification. The experimental setup is depicted in Figure 7.27. The

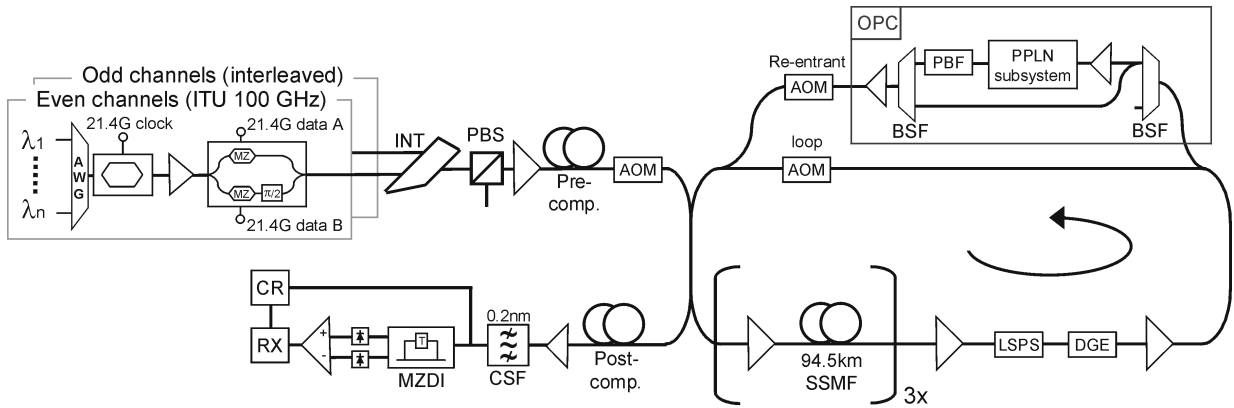


Figure 7.27: *Experimental setup of the 42.8-Gbit/s DQPSK experiment without Raman amplification.*

18 WDM channels are used in this experiment as depicted in Figure 7.20. Nine channels are phase conjugated in the middle of the transmission link (from 1549.32 nm to 1552.52 nm) and an additional nine channels (from 1534.25 nm to 1537.40 nm) to balance the amplifiers before and after conjugation. The average span loss of the three 94.5-km SSMF spans is 20 dB. The same amount of pre-compensation is used as in the Raman experiment (-2040 ps/nm). The optimal launch power into the SSMF is determined by varying the launch power per channel from -6 dBm to +4 dBm after 1,700-km transmission (6 circulations through the re-circulating loop). The BER performance as a function of the launch power is depicted in Figure 7.28 for the center channel (1535.8 nm after conjugation). The optimal launch power is found to be 0 dBm, which is significantly higher than the input power used in the Raman amplified system. As illustrated in Figure 3.2 (Section 3.2), the lowest power in a transmission link is increased by using Raman amplification. Since the lowest power in a transmission system limits the OSNR after transmission, a higher input power is optimal in the EDFA only configuration. The BER performance of the center channel (1535.8 nm after conjugation) as a function of the transmission distance is depicted in Figure 7.29 on a double logarithmic scale. As a reference, the BER performance of the DCF and OPC configuration with Raman amplification is depicted as well. The power envelope in the EDFA only scheme is significantly less symmetric than the Raman aided configuration. Furthermore, more nonlinear effects occur in the EDFA only system as the launch power is ca. 3 dB higher than the launch power used in the transmission link

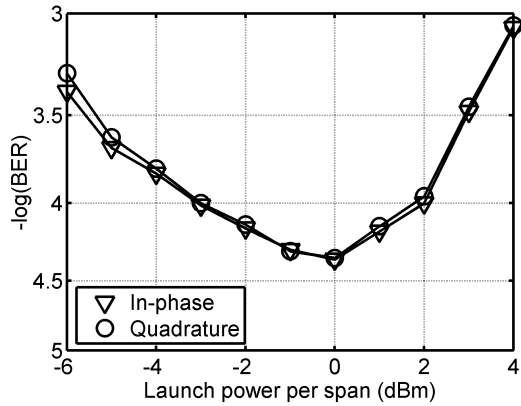


Figure 7.28: BER performance of the center channel as a function of the input power into the SSF after 1,700-km transmission.

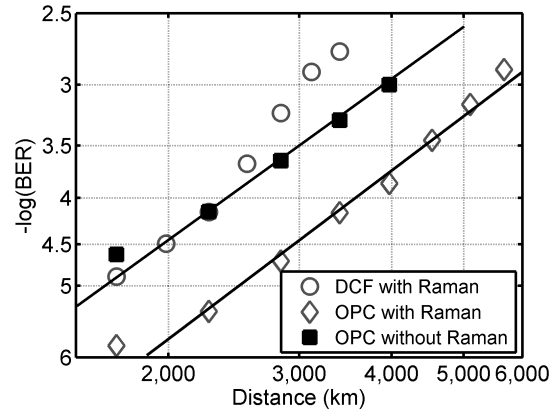


Figure 7.29: BER performance of the center channel (1535.8 nm after conjugation) as a function of the transmission distance.

with Raman amplification. However, no significant influence of nonlinear impairments is seen in the BER performance. Similar to the OPC transmission experiment with Raman amplification, a straight BER line is observed on a double logarithmic scale. After 3,970 km transmission, a BER of $\approx 1 \cdot 10^{-3}$ is obtained in the EDFA only configuration. With Raman amplification a BER of $\approx 1 \cdot 10^{-3}$ is obtained after approximately 5,500-km of transmission. Hence by removing the Raman amplification from the transmission link, the feasible transmission distance is reduced by only 27%. It can thus be concluded that even in the asymmetric power configuration of the EDFA only transmission system, long-haul transmission can be realized through mid-link OPC with a limited penalty.

7.3 Summary

DQPSK is a promising modulation format to realize transmission with a high spectral efficiency. In this chapter the transmission performance of an OPC-based transmission link is compared to that of a conventional transmission system for 21.4-Gbit/s and 42.8-Gbit/s RZ-DQPSK. The transmission system consisted of a re-entrant, re-circulating loop of three 94.5-km spans of SSF using a hybrid EDFA/Raman scheme for amplification.

For 21.4-Gbit/s RZ-DQPSK the transmission performance of the conventional transmission scheme was optimized with respect to the input power, pre-compensation and inline under-compensation. In this experiment 44 WDM channels were transmitted at 50-GHz channel spacing. Using the optimized dispersion map, error-free transmission after FEC was realized over 7,200 km. With mid-link OPC configuration, the attainable transmission distance is increased to 10,200 km, which corresponds to an increase of 44%. The increase in feasible transmission distance through mid-link OPC is twofold. Firstly, in the OPC-based configuration, the OSNR is increased by about 1 dB because of the simplified inline amplifiers that can be used compared to the DCF-based transmission link. Secondly,

for transmission distances of over 5,000 km, intra-channel nonlinear impairments strongly degrade the BER performance in the DCF-based transmission link, whereas for the OPC based transmission link virtually no impact of nonlinear impairments is observed.

In a second transmission experiment, the data rate is increased to 42.8-Gbit/s. As a result, a 0.8-bit/s/Hz spectral efficiency is obtained by transmitting 42.8-Gbit/s RZ-DQPSK at 50-GHz channel spacing. In the mid-link OPC configuration a transmission distance of 4,500 km could be bridged, realizing error-free transmission after FEC for all 26 WDM channels. At a BER $1 \cdot 10^{-3}$ before FEC, the feasible transmission distance of the OPC-based and the DCF-based configuration is 5,000 and 3,000 km, respectively. Hence, it can be concluded for the OPC-based configuration that increasing the data rate from 21.4-Gbit/s to 42.8-Gbit/s RZ-DQPSK reduces the feasible transmission distance by about 50%. This factor of two reduction in feasible transmission distance corresponds to the 3-dB OSNR difference that is measured between 21.4-Gbit/s and 42.8-Gbit/s RZ-DQPSK in the back-to-back configuration. For the conventional transmission system, a greater reduction in the feasible transmission distance (factor of 2.4) is measured resulting from increased intra-channel nonlinear impairments.

The performance of 42.8-Gbit/s RZ-DQPSK is evaluated as well in a transmission link with only EDFAs for amplification, hence creating a strongly asymmetric power profile. The optimal input power was found to be 0 dBm, which is 3 dB higher than the input power used in the configuration with Raman amplification. The maximum feasible transmission distance for a BER of $\approx 1 \cdot 10^{-3}$ in this configuration was 3,970 km. When Raman amplification is employed to increase the power symmetry of the transmission link, the maximum feasible transmission distance is 5,500 km. From this relatively small difference in obtainable transmission distance, it can be concluded that the asymmetric power configuration of the configuration with EDFA only amplification causes only a limited penalty for long-haul transmission systems.

Chapter 8

Conclusions

In this thesis, the regenerative capabilities of OPC have been investigated for relevant nonlinear impairments that limit the performance of modern transmission systems. Apart from the ASK modulation format, the combination of OPC with several promising advanced modulation formats has been assessed.

The dispersion map of mid-link OPC introduces higher peak powers and thereby an SPM penalty for 10-Gbit/s transmission with respect to a conventional transmission system. The higher peak powers in the OPC-based transmission system are caused by the fact that the accumulated dispersion along the link of an OPC-based transmission system is significantly higher than that of a conventional transmission system. Through phase conjugation most of the SPM impairments are compensated for. In a system with multiple wavelength division multiplexed (WDM) channels at narrow channel spacing, cross-phase modulation (XPM) is the dominant transmission impairment. XPM is caused by the Kerr effect and can in theory be compensated for through OPC. However, in both simulation and experiment no XPM compensation through OPC could be observed. This can be explained by the fact that XPM is an inter-channel nonlinear impairment and therefore dependent on the bit sequence of the neighboring channels. As the slope of the transmission link is not compensated for, the XPM distortions that arise in the first part of the transmission link are different from the XPM distortions in the second part. It can be concluded that although XPM is in principle a deterministic effect it must be treated as a statistic, noise-like impairment which OPC cannot compensate for.

When the data rate is increased to 40-Gbit/s, inter-channel nonlinear impairments such as XPM are negligibly small. Instead, the transmission performance is limited by intra-channel nonlinear impairments. At a data rate of 42.7-Gbit/s, the performance was assessed of mid-link OPC in comparison to a conventional transmission system. In this transmission experiment 16 WDM channels at 100-GHz channel spacing are used for transmission. After 800 km transmission, a better bit error ratio (BER) performance is observed for the mid-link OPC system compared to the BER performance of the conventional transmission link. Thus, the dispersion map of mid-link OPC does not introduce a significant penalty for 40-Gbit/s transmission compared to the optimized dispersion map of the conventional transmission link. Furthermore, it is verified in a single channel 42.7-Gbit/s non-return-

CHAPTER 8. CONCLUSIONS

to-zero amplitude-shift-keying (NRZ-ASK) experiment, that mid-link OPC can be used in off-center configurations without strong impairments in the BER performance.

In future optical networks it is likely that mixed transmission lines exist where different modulation formats and different data rates are employed over the same transmission link. It is experimentally shown that mid-link OPC can be used to realize such a transmission link, transparent to modulation format and data rate: 40-Gbit/s NRZ-ASK, 40-Gbit/s duobinary and 10-Gbit/s NRZ-ASK are simultaneously transmitted over an 800 km transmission link. Transparent transmission lines are particularly appealing for network operators since existing networks can be upgraded without having to make changes in the transmission line.

The differential phase-shift-keying (DPSK) modulation format can be used in order to obtain a 3-dB improvement in sensitivity as well as an increased robustness to narrowband optical filtering. However, these phase encoded signals can be impaired by nonlinear phase noise (NPN). Using an 800-km straight line, the impact of NPN on a 10.7-Gbit/s NRZ-differential phase-shift-keying (NRZ-DPSK) signal is assessed. In this experiment, over four decades of BER improvement is observed through OPC showing that OPC is a very effective method to compensate for impairments caused by NPN. The dependence of the location of the OPC within the transmission link is assessed as well. Allowing a penalty of one decade in BER from the optimum, the OPC-unit can be varied over a wide range, from nearly 1/3 to 2/3 of the transmission link. It can thus be concluded that OPC is an effective method to compensate for impairments caused by NPN.

The DQPSK modulation format can be employed to realize transmission with a high spectral efficiency. The transmission performance of 21.4-Gbit/s RZ-DQPSK in combination with mid-link OPC is studied using a re-entrant re-circulating loop. Error-free transmission after forward error correction (FEC) of 22 WDM channels at 50 GHz channel spacing is demonstrated over 10,200 km with mid-link OPC for the compensation of chromatic dispersion and nonlinear impairments. In this experiment, the accumulated dispersion reaches to more than 80,000 ps/nm in the middle of the link, causing an extreme overlap of pulses. However, despite the high dispersion, the feasible transmission distance of the OPC based transmission system is 44% larger than that obtained in the conventional transmission link with a periodic dispersion map. This performance improvement results from an increase of the optical signal-to-noise ratio (OSNR) and a reduction of nonlinear impairments in the mid-link OPC configuration. It was observed that after 5,000-km transmission, the BER performance in the DCF-based transmission link is severely degraded by nonlinear impairments, whereas for the OPC based transmission link virtually no impact of nonlinear impairments is observed.

A 0.8-bit/s/Hz spectral efficient transmission system was realized by transmitting 42.8-Gbit/s RZ-DQPSK at 50-GHz channel spacing. At a BER $1 \cdot 10^{-3}$ before FEC, the feasible transmission distance of the OPC-based and the DCF-based configuration is 5,000 km and 3,000 km, respectively. Thus, doubling the data rate from 21.4-Gbit/s to 42.8-Gbit/s reduces the feasible transmission distance for mid-link OPC by about a factor of two. This difference in feasible transmission distance corresponds to the 3-dB OSNR penalty that is present between 21.4-Gbit/s and 42.8-Gbit/s RZ-DQPSK in the back-to-back config-

uration. For the DCF-based configuration a larger decrease in transmission distance is measured (factor of 2.4) due to increased penalties resulting from intra-channel nonlinear impairments. The improvement in feasible transmission distance through the use of OPC is 60% in this experiment.

The performance of 42.8-Gbit/s RZ-DQPSK is evaluated as well in an OPC-based transmission link with only Erbium-doped fiber amplifiers (EDFAs) for amplification. The optimal input power was found to be 0 dBm, which is 3 dB higher than the input power used in the configuration with Raman amplification. The maximum feasible transmission distance in this configuration was 4,000 km. Therefore, by removing the Raman amplifiers from the link, the maximum attainable transmission distance is reduced by only 27%. It can thus be concluded that even without Raman amplification, long-haul transmission can be realized with mid-link OPC.

CHAPTER 8. CONCLUSIONS

Chapter 9

Outlook

The polarization diverse PPLN structure used for OPC discussed in chapter 7 offers high conversion efficiency ($\approx -7dB$) and is capable of converting many WDM channels without a noticeable conversion penalty. However, in this configuration at least two extra amplifiers are required, namely one amplifier to boost the pump signal and one at the input of the OPC-subsystem to amplify the data channels. The additional amplifiers make OPC in this form a less cost-effective solution. This might offset the performance and cost reduction gains provided through OPC. One could potentially omit the pump booster by reducing the pump power, but this significantly reduces the conversion efficiency. Alternatively the amplifier for the data channels can be saved by reducing coupling losses, improving the conversion efficiency and increasing parametric amplification of the PPLN waveguide [150].

Due to the wavelength conversion in the OPC subsystem a second PPLN waveguide is required to phase conjugate all channels of the full C-band. Alternatively, as demonstrated by Kurz *et al.* [151], mode multiplexing in a PPLN waveguide can be employed for bidirectional phase conjugation. In such an OPC subsystem, higher order waveguide modes are used to separate the input signal from the phase conjugated signal, using asymmetric Y junctions. Mode multiplexing would simplify the design of the OPC subsystem, omitting filters to remove the input channels and minimizing the wavelength shift inherent to OPC.

Apart from the PPLN waveguide, other media such as AlGaAs are interesting candidates for creating OPC. The main advantage of AlGaAs is that it can be designed to be polarization insensitive and therefore does not require a polarization diversity structure. Furthermore AlGaAs does not suffer from restrictions due to the photorefractive effect and has a higher nonlinear coefficient than lithium-niobate [86]. Although the conversion efficiency shown so far is relatively low, this technique could potentially yield a high conversion OPC unit.

Ideally these developments will yield an OPC subsystem that is transparent with respect to insertion loss, which would greatly ease the application of OPC in real-world applications. Considering the advantages for transmission applications, mid-link OPC has significant potential when combined with high data rate transmission. The dispersion map of mid-link OPC is less suited for 10-Gbit/s transmission systems than the dispersion map of a conventional transmission system. Furthermore, 10-Gbit/s WDM transmission

CHAPTER 9. OUTLOOK

systems are mostly limited by XPM, which practically cannot be compensated for using mid-link OPC.

DQPSK has a favorable spectral width making it robust against narrow band filtering. Therefore, DQPSK is the ideal modulation format to realize transmission with a high spectral efficiency at a bitrate of 40-Gbit/s or higher. However, a concern with DQPSK is impairments induced by intra-channel nonlinear impairments, such as nonlinear phase noise. The results obtained for 42.8-Gbit/s RZ-DQPSK show that the transmission performance of 42.8-Gbit/s RZ-DQPSK combined with OPC provides an excellent robustness against intra-channel nonlinear impairments and hence offers a robust solution for future long-haul transport systems.

Appendix A

List of symbols and abbreviations

A.1 List of symbols

$A(z, t)$	Amplitude as a function of time and distance
A_{eff}	Effective mode area of a fiber
α	Attenuation constant of an optical fiber in Neper
α_{dB}	Attenuation constant of an optical fiber in decibel
B_0	Reference bandwidth
B_m	Modal birefringence
β	propagation constant
c	Speed of light in vacuum ($c = 2.998 \cdot 10^8$ m/s)
$\chi^{(n)}$	Susceptibility of the n-th order
D	Dispersion parameter
D_{inline}	Inline-compensation
D_{post}	Post-compensation
D_{pre}	Pre-compensation
d_{12}	Walk-off parameter (XPM)
$\Delta\tau$	Differential group delay
$\overline{\Delta\tau}$	PMD-Value
$E\{\cdot\}$	Expectation value
EOP	Eye Opening Penalty
ϵ_0	Permittivity of vacuum
f	Frequency
f_0	Carrier frequency
F	Noise figure (optical amplifier)
G	Gain (optical amplifier)
γ	Nonlinear coefficient of the fiber
h	Planck's constant ($h = 6.6256 \cdot 10^{-34}$ Js)
I	Intensity of an optical signal
L	Fiber length

APPENDIX A. LIST OF SYMBOLS AND ABBREVIATIONS

L_D	Dispersive length
L_{eff}	Effective length
L_{NL}	Nonlinear length
L_W	Walk-off length
λ	Wavelength
n	Refractive index
n_{sp}	Spontaneous emission factor
ω	Radial frequency
P	Optical power
ϕ	Phase
ϕ_{SPM}	SPM-induced phase shift
S	Dispersion slope parameter
T_0	Pulse width
T_B	Bit period
t	Time
V_{pp}	Peak-to-peak voltage

A.2 List of Abbreviations

AlGaAs	Aluminum gallium arsenide
AOM	Acousto-optic modulator
ASE	Amplified spontaneous emission
ASK	Amplitude-shift-keying
AWG	Arrayed waveguide grating
BER	Bit error ratio
BERT	Bit error ratio tester
BPF	Band-pass filter
BSF	Band-selection filter
CDR	Clock and data recovery
CRU	Clock recovery unit
CS	Carrier suppressed
CSF	Channel-selection filter
CW	Continuous wave
DCF	Dispersion compensating fiber
DFB	Distributed feedback
DFF	D-flip-flop
DFG	Difference frequency generation
DGD	Differential Group Delay
DGE	Dynamic gain equalizer
DML	Directly modulated laser
DPSK	Differential phase-shift-keying
DQPSK	Differential quadrature phase-shift-keying
DSF	Dispersion-shifted fiber
ECL	External cavity laser
EDFA	Erbium-doped fiber amplifier
EO	Eye opening
EOP	Eye opening penalty
FBG	Fiber-Bragg grating
FEC	Forward error correction
FFT	Fast Fourier transformation
FWHM	Full-width at half-maximum
FWM	Four-wave mixing
GaAs	Gallium arsenide
GVD	Group velocity dispersion
HNLF	Highly-nonlinear fiber
IFWM	Intra-channel four-wave mixing
InGaAsP	Indium gallium arsenide phosphide
InP	Indium phosphide
INT	Interleaver

APPENDIX A. LIST OF SYMBOLS AND ABBREVIATIONS

ISI	Inter symbol interference
ITU	International Telecommunication Union
IXPM	Intra-channel cross-phase modulation
LiNbO ₃	Lithium-niobate
LSPS	Loop-synchronous polarization scrambler
MgO	Magnesium-oxide
MI	Modulation instability
MLSI	Mid-link spectral inversion
MSSI	Mid-span spectral-inversion
MZM	Mach-Zehnder modulator
MZDI	Mach-Zehnder delay interferometer
NPN	Nonlinear phase noise
NRZ	Non-return-to-zero
NZDSF	Non-zero dispersion shifted fiber
OADM	Optical add-drop multiplexer
OC	Optical carrier
OEO	Optical-electric-optical
OOK	On-off keying
OPC	Optical phase conjugation
ORD	Optimal residual dispersion
OSNR	Optical signal-to-noise ratio
PBF	Pump-block filter
PBS	Polarization beam splitter
PC	Polarization controller
PDL	Polarization dependent loss
PP	Peak-to-peak
PM	Phase modulator
PMD	Polarization mode dispersion
PNC	Post nonlinearity compensation
PPLN	Periodically-poled lithium-niobate
PRBS	Pseudo random bit sequence
PSBT	Phase shaped binary transmission
PSK	Phase-shift-keying
PSP	Principle state of polarization
QPM	Quasi-phase matching
RX	Receiver
RZ	Return-to-zero
Q-factor	Quality-factor
SE	Spectral efficiency
SH	Second harmonic
SHG	Second harmonic generation
SI	Spectral inversion
SOA	Semiconductor optical amplifier

A.2. LIST OF ABBREVIATIONS

SOP	State of polarization
SPM	Self phase modulation
SRS	Stimulated Raman scattering
SBS	Stimulated Brillouin scattering
SFG	Sum-frequency generation
SSMF	Standard single-mode fiber
STM	Synchronous transport module
TDC	Tunable dispersion compensator
Ti	Titan
TX	Transmitter
VOA	Variable optical attenuator
WDM	Wavelength division multiplexing
XPM	Cross phase modulation

APPENDIX A. LIST OF SYMBOLS AND ABBREVIATIONS

Appendix B

Performance evaluation of a transmission link

In order to assess the quality of a transmission link, it is common to measure the bit error ratio (BER). For N detected bits in which n errors occur, the BER ratio is defined as

$$BER = \frac{n}{N} \quad (\text{B.1})$$

Suppose a signal is detected with a BER of $1 \cdot 10^{-9}$. The BER tester in this case registers one error every 10^9 bits on average. At a data rate of 10 Gbit/s, this means that statistically, ten errors are measured per second. In order to increase the reliability of the measurement it is common to at least measure 100 errored bits per BER ratio sample. Measuring BER values smaller than $1 \cdot 10^{-12}$ is therefore impractical, since at 10 Gbit/s this will take over two hours. For a BER smaller than $1 \cdot 10^{-12}$ it is common in literature to refer to the signal as “error-free”.

B.1 Eye opening penalty

Whereas through counting bit-errors, a BER of $1 \cdot 10^{-9}$ takes only a couple of seconds to be measured, it is not as easily simulated. The 10^9 bits, required to statistically measure a single bit-error, are very time consuming to simulate. A method to assess the quality of a signal in simulations is by using the eye opening penalty (EOP). Various different definitions of the eye opening penalty are used throughout literature. A common definition of the EOP is

$$EOP = \frac{2 \cdot mean}{EO} \quad (\text{B.2})$$

where *mean* is the mean value of the eye diagram and *EO* the eye opening. The eye opening of an eye diagram is the difference between the minimum ‘1’ and the maximum ‘0’-level ($EO = \min('1') - \max('0')$). In order to take timing jitter of the receiver into account, the EO is a square with 20% of the bit duration T_B . Figure B.1 shows the EO

APPENDIX B. PERFORMANCE EVALUATION OF A TRANSMISSION LINK

and mean value of a back to back signal. Usually, the EOP is referred to logarithmically

$$EOP[dB] = -10 \cdot \log(EOP) \quad (\text{B.3})$$

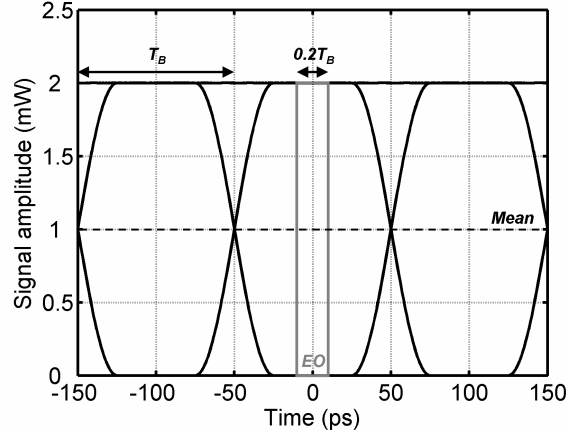


Figure B.1: *Eye diagrams of a back to back 10-Gbit/s NRZ-ASK signal showing the EO and mean value.*

B.2 Q-factor

The disadvantage of the EOP is that it is difficult to relate an EOP to a BER value. Therefore, in many simulations, the quality-factor, or Q-factor is used. Figure B.2 depicts the probability density of the '0' and the '1' bits of a noisy signal. In this figure, I_0 and I_1 represent the mean values of the 'zeros' and 'ones', respectively.

The BER is dependent on the decision threshold of the DFF (as illustrated in Figure 3.1, chapter 3) The optimal decision threshold for the receiver DFF is represented by I_D and can be expressed by

$$I_D = \frac{\sigma_0 I_1 + \sigma_1 I_0}{\sigma_0 + \sigma_1} \quad (\text{B.4})$$

where σ_0 and σ_1 represent the variance of the 'zeros' and 'ones', respectively. The Q-factor is defined by

$$Q \equiv (I_1 - I_D)/\sigma_1 = (I_D - I_0)/\sigma_0 \quad (\text{B.5})$$

and combining equation B.4 with B.5, the Q-factor can be expressed by

$$Q = \frac{I_1 - I_0}{\sigma_1 + \sigma_0} \quad (\text{B.6})$$

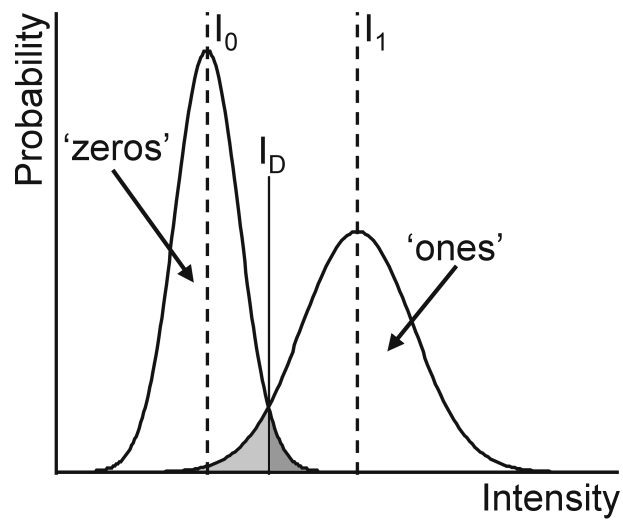


Figure B.2: *Probability density of a noisy signal as a function of the current of the photodiode.*

The Q-factor can be related to a BER according to

$$BER = \frac{1}{2} \operatorname{erfc} \left(\frac{Q}{\sqrt{2}} \right) \quad (\text{B.7})$$

APPENDIX B. PERFORMANCE EVALUATION OF A TRANSMISSION LINK

Appendix C

Periodically-poled lithium-niobate component

Figure C.1 shows the Ti:PPLN waveguide, developed by the Technical University of Paderborn (Technische Universität Paderborn) [92, 152, 150, 100]. This Ti:PPLN is used as phase conjugator in all experiments described in chapter 7 of the thesis.

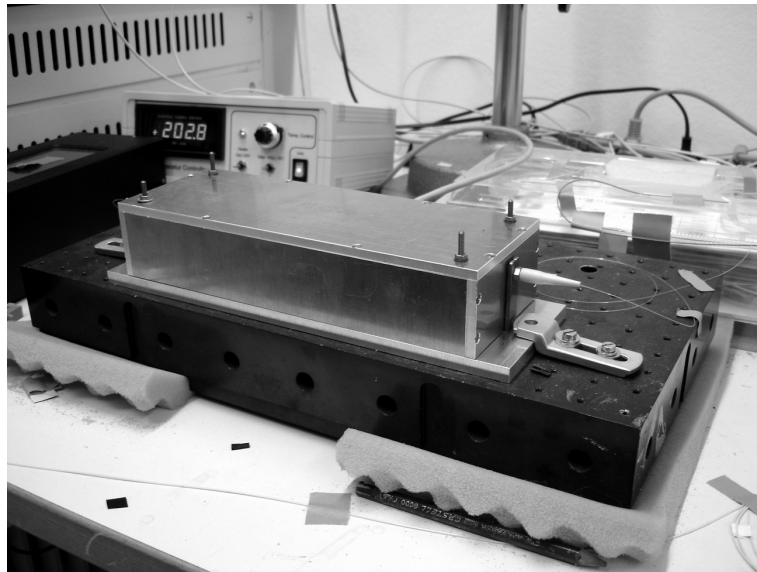


Figure C.1: *Ti:PPLN waveguide with the temperature controller in the background.*

The operating temperature for the PPLN-waveguide is ≈ 200 degrees Celsius. Free-space optics is used to couple the light in and out of the waveguide. For the alignment of the actuators at each side of the PPLN, visible light at ca. 700 nm is used. Figure C.2 shows the PPLN waveguide and the actuators. In this figure, the 700 nm CW propagates through the waveguide from right to left.

APPENDIX C. PERIODICALLY-POLED LITHIUM-NIOBATE COMPONENT

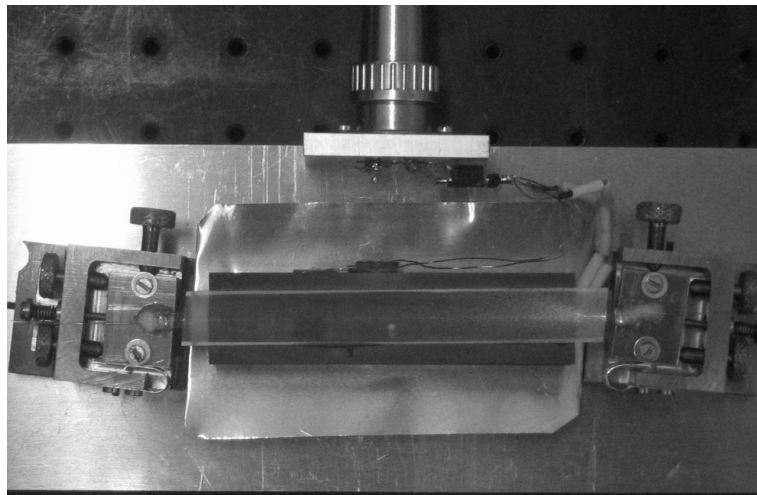


Figure C.2: *Close-up of the Ti:PPLN waveguide with actuators.*

Bibliography

- [1] J. Abbate, *Inventing the Internet (Inside Technology)*, third edition ed. the MIT press, 1999.
- [2] E. Voges and K. Petermann, *Optische Kommunikationstechnik*. Springer Verlag, 2002.
- [3] M. Nakamura, H. Ueda, S. Makino, T. Yokotani, and K. Oshima, “Proposal of networking by PON technologies for full and Ethernet services in FTTx,” *Journal of Lightwave Technology*, vol. 22, no. 11, pp. 2631 – 2640, November 2004.
- [4] P. E. Green, “Fiber to the home: The next big broadband thing,” *IEEE Communications Magazine*, vol. 42, no. 9, pp. 100 – 106, 2004.
- [5] K. C. Kao and G. A. Hockham, “Dielectric-fibre surface waveguides for optical frequencies,” *in proc. I.E.E.*, vol. 113, no. 7, pp. 1151 – 1158, 1966.
- [6] G. Keiser, *Optical Fiber Communications*, third edition ed. McGraw-Hill, 2000.
- [7] G. Mahlke and P. Gössing, *Fiber optic cables*, fourth edition ed. Publicis MCD, 2001.
- [8] G. P. Agrawal, *Fiber-optic communication systems*, second edition ed. John Wiley and Sons, 1997.
- [9] E.-G. Neumann, *Single-Mode Fibers*. Springer Verlag, 1988.
- [10] K. Nagayama, M. Kakui, M. Matsui, T. Saitoh, and Y. Chigusa, “Ultra-low-loss (0.1 484 dB/km) pure silica core fibre and extension of transmission distance,” *Electronics Letters*, vol. 38, no. 20, pp. 1168 – 1169, 2002.
- [11] S. Sudo, M. Kawachi, T. Edahiro, T. Izawa, T. Shioda, and H. Gotoh, “Low-OH-content optical fiber fabricated by vapour-phase axial-deposition method,” *Electronics Letters*, vol. 14, pp. 534 – 535, 1978.
- [12] S. R. Nagel, “Review of the depressed cladding single-mode fiber design and performance for the SL undersea system application,” *Journal of Lightwave Technology*, vol. 2, no. 6, pp. 792 – 801, 1984.

BIBLIOGRAPHY

- [13] “Optical system design and engineering considerations,” *International Telecommunication Union (ITU)*, vol. G. Sup. 39, October 2003.
- [14] M. Abrams, P. Becker, Y. Fujimoto, Oapos, V. Byrne, and D. Piehler, “FTTP deployments in the United States and Japan—equipment choices and service providers imperatives,” *Journal of Lightwave Technology*, vol. 23, no. 1, pp. 236 – 246, January 2005.
- [15] H. Thiele, P. Winzer, J. Sinsky, L. Stulz, L. Nelson, and F. Fidler, “160-Gb/s CWDM capacity upgrade using 2.5-Gb/s rated uncooled directly modulated lasers,” *Photonics Technology Letters*, vol. 16, no. 10, pp. 2389 – 2391, October 2004.
- [16] M. Duelk, “Next-Generation 100G Ethernet,” *in proc. ECOC*, vol. 2, p. Tu 3.1.2, 2005.
- [17] H.-G. Unger, *Optische Nachrichtentechnik*. Hüthig Verlag, 1990.
- [18] L. Grüner-Nielsen, M. Wandel, P. Kristensen, C. Jørgensen, L. Vilbrad Jørgensen, B. Edvold, B. Pálsdóttir, and D. Jakobsen, “Dispersion-compensating fibers,” *Journal of Lightwave Technology*, vol. 23, no. 11, pp. 3566 – 3579, 2005.
- [19] I. P. Kaminow and T. L. Koch, *Optical Fiber Telecommunication, volume IIIa*. Academic press, 1997.
- [20] G. P. Agrawal, *Nonlinear Fiber Optics*, third edition ed. Academic press, 2001.
- [21] M. Bohn, *Adaptive Entzerrung des Glasfaser-Übertragungskanal mit optischen Filterstrukturen in hochbitratigen Übertragungssystemen*. Shaker Verlag, 2006.
- [22] L. F. Mollenauer, M. J. Neubelt, S. G. Evangelides, J. P. Gordon, J. R. Simpson, and L. G. Cohen, “Experimental study of soliton transmission over more than 10,000 km in dispersion-shifted fiber,” *Optics Letters*, vol. 15, no. 21, pp. 1203 – 1205, 1990.
- [23] I. Morita, K. Tanaka, N. Edagawa, and M. Suzuki, “40 Gb/s single-channel soliton transmission over transoceanic distances by reducing Gordon-Haus timing jitter and soliton-soliton interaction,” *Journal of Lightwave Technology*, vol. 17, no. 12, pp. 2506 – 2511, 1999.
- [24] C. Xu, C. Xie, and L. Mollenauer, “Analysis of soliton collisions in a wavelength-division multiplexed dispersion-managed soliton transmission system,” *Optics Letters*, vol. 27, no. 15, pp. 1303 – 1305, 2002.
- [25] V. Mamyshev and N. A. Mamysheva, “Pulse-overlapped dispersion-managed data transmission and intrachannel four-wave mixing,” *Optics Letters*, vol. 24, no. 21, pp. 1454 – 1456, 1999.

- [26] I. Shake, K. Takara, K. Mori, S. Kawanishi, and Y. Yamabayashi, "Influence of inter-bit four-wave mixing in optical TDM transmission," *Electronics Letters*, vol. 34, no. 16, pp. 1600 – 1601, 1998.
- [27] I. P. Kaminow and T. Li, *Optical Fiber Telecommunication, volume IVB*. Academic press, 2002.
- [28] M. N. Islam, *Raman amplifiers for telecommunications 1*. Springer Verlag, 2004.
- [29] K.-P. Ho, "Statistical properties of stimulated Raman crosstalk in WDM Systems," *Journal of Lightwave Technology*, vol. 18, no. 7, pp. 915 – 921, 2000.
- [30] A. Chraplyvy, "Limitations on lightwave communications imposed by optical-fiber nonlinearities," *Journal of Lightwave Technology*, vol. 8, no. 10, pp. 1548 – 1557, 1990.
- [31] M. N. Islam, *Raman amplifiers for telecommunications 2*. Springer Verlag, 2004.
- [32] B. Huiszoon, R. J. W. Jonker, P. K. v. Bennekom, G. D. Khoe, and H. d. Waardt, "Cost-effective up to 40 Gb/s transmission performance of 1310 nm directly modulated lasers for short- to medium-range distances," *Journal of Lightwave Technology*, vol. 23, no. 3, pp. 1116 – 1125, 2005.
- [33] J. L. Vossen and W. Kern, *Thin film processes*. Academic press, 1978.
- [34] C. Rasmussen, S. Dey, F. Liu, J. Bennike, B. Mikkelsen, P. Mamyshev, M. Kimmitt, K. Springer, D. Gapontsev, and V. Ivshin, "Transmission of 40x42.7 Gbit/s over 5200 km UltraWave fiber with terrestrial 100 km spans using turn-key ETDM transmitter and receiver," *in proc. ECOC*, p. PD4.4, 2002.
- [35] E. Desurvire, *Erbium-Doped Fiber Amplifiers*. John Wiley and sons, 1994.
- [36] P. C. Becker, N. A. Olsson, and J. R. Simpson, *Erbium-Doped Fiber Amplifiers*. Academic press, 1999.
- [37] A. M. Vengsarkar and W. A. Reed, "Dispersion-compensating single-mode fibers: Efficient designs for first- and second-order compensation," *Optics Letters*, vol. 18, no. 11, pp. 924 – 926, 1993.
- [38] F. Quелlette, "Dispersion cancellation using linearly chirped bragg grating filters in optical waveguides," *Optics Letters*, vol. 12, no. 10, pp. 847 – 849, 1987.
- [39] T. Koch and R. Alferness, "Dispersion compensation by active predistorted signal synthesis," *Journal of Lightwave Technology*, vol. 3, no. 4, pp. 800 – 805, 1985.
- [40] A. Yariv, D. Fekete, and D. Pepper, "Compensation for channel dispersion by non-linear optical phase conjugation," *Optics Letters*, vol. 4, no. 2, pp. 52 – 54, 1979.

BIBLIOGRAPHY

- [41] A. Sano, Y. Miyamoto, S. Kuwahara, and H. Toba, "A 40-Gb/s/ch WDM transmission with SPM/XPM suppression through prechirping and dispersion management," *Journal of Lightwave Technology*, vol. 18, no. 11, pp. 1519 – 1527, 2000.
- [42] J.-P. Elbers and C. Glingener, "Efficient design of high-capacity dense wavelength-division multiplex systems," *International Journal of Electronics and Communications (AEU)*, vol. 55, no. 5, pp. 295 – 304, 2001.
- [43] G. Mohs, L. Didier Coelho, E. Gottwald, C. Scheerer, C. Fürst, A. Färbert, and C. Glingener, "Optimized inline dispersion compensation for self-phase modulation limited transmission," *in proc. OECC/IOOC*, pp. 262 – 263, 2001.
- [44] G. Lehmann and E. Meissner, "Dispersion management for the transmission of mixed data rates of 40 Gb/s and 10 Gb/s in the same fiber," *in proc. APOC*, vol. 4906, 2002.
- [45] S. Bigo, G. Charlet, and E. Corbel, "What has hybrid phase/intensity encoding brought to 40 Gbit/s ultralong-haul systems ?" *in proc. ECOC*, p. Th2.5.1, 2002.
- [46] A. H. Gnauck, X. Liu, X. Wei, D. M. Gill, and E. C. Burrows, "Comparison of modulation formats for 42.7-Gb/s single-channel transmission through 1980 km of SSMF," *Photonics Technology Letters*, vol. 16, no. 3, pp. 909 – 911, 2004.
- [47] A. Klekamp, R. Dischler, and W. Idler, "Impairments of bit-to-bit alternate-polarization on non-linear threshold, CD and DGD tolerance of 43 Gb/s ASK and DPSK formats," *in proc. OFC*, p. OFN3, 2005.
- [48] J.-X. Cai, M. Nissov, A. N. Pilipetskii, C. R. Davidson, R.-M. Mu, M. A. Mills, L. Xu, D. Foursa, R. Menges, P. C. Corbett, D. Sutton, and N. S. Bergano, "1.28 Tb/s (32 x 40 Gb/s) transmission over 4,500 km," *in proc. ECOC*, vol. 6, p. PD.M.1.2, 2001.
- [49] A. Lender, "The duobinary technique for high-speed data transmission," *IEEE Transactions on Communications and Electronics*, vol. 82, p. 214 – 218, 1963.
- [50] A. Lender, "Correlative digital communication techniques," *IEEE Transactions on Communications*, vol. 12, no. 4, pp. 128 – 135, 1963.
- [51] A. J. Price and N. Le Mercier, "Reduced bandwidth optical digital intensity modulation with improved chromatic dispersion tolerance," *Electronics Letters*, vol. 31, no. 1, pp. 58 – 59, 1995.
- [52] D. Penninckx, M. Chbat, L. Pierre, and J.-P. Thiery, "The phase-shaped binary transmission (PSBT): A new technique to transmit far beyond the chromatic dispersion limit," *Photonics Technology Letters*, vol. 9, no. 2, p. 259 – 261, 1997.

- [53] T. Ono, Y. Yano, K. Fukuchi, T. Ito, H. Yamazaki, M. Yamaguchi, and K. Emura, "Characteristics of optical duobinary signals in terabit/s capacity, high-spectral efficiency WDM systems," *Journal of Lightwave Technology*, vol. 16, no. 5, pp. 788 – 797, 1998.
- [54] A. Lender, "Correlative level coding for binary data transmission," *IEEE Spectrum*, vol. 3, no. 4, pp. 104 – 115, 1966.
- [55] M. Shtaif and A. Gnauck, "The relation between optical duobinary modulation and spectral efficiency in wdm systems," *Photonics Technology Letters*, vol. 11, no. 6, pp. 712 – 714, 1999.
- [56] G. Charlet, J.-C. Antona, S. Lanne, P. Tran, W. Idler, M. Gorlier, S. Borne, A. Klekamp, C. Simonneau, L. Pierre, Y. Frignac, M. Molina, F. Beaumont, J.-P. Hamaide, and S. Bigo, "6.4 Tb/s (159 x 42.7 Gb/s) capacity over 21x100 km using bandwidth-limited phase-shaped binary transmission," in *proc. ECOC*, p. PD4.1, 2002.
- [57] H. Kim and C. X. Yu, "Optical duobinary transmission system featuring improved receiver sensitivity and reduced optical bandwidth," *Photonics Technology Letters*, vol. 14, no. 8, pp. 1205 – 1207, 2002.
- [58] K. Yonenaga and S. Kuwano, "Dispersion-tolerant optical transmission system using duobinary transmitter and binary receiver," *Journal of Lightwave Technology*, vol. 15, no. 8, pp. 1530 – 1537, 1997.
- [59] W. Kaiser, *Impact of advanced modulation formats on the system performance of high-speed optical transmission systems*. Shaker Verlag, 2003.
- [60] M. Daikoku, N. Yoshikane, and I. Morita, "Performance comparison of modulation formats for 40 Gbit/s DWDM transmission systems," in *proc. OFC*, p. OFN2, 2005.
- [61] C. Wree, *Differential Phase-Shift Keying for Long-Haul Fiber Optic Transmission Based on Direct Detection*. Shaker Verlag, 2004.
- [62] A. H. Gnauck and P. Winzer, "Optical phase-shift-keyed transmission," *Journal of Lightwave Technology*, vol. 23, no. 1, pp. 115 – 130, 2005.
- [63] M. Rohde, C. Casper, N. Heimes, M. Konitzer, E.-J. Bachus, and N. Hanik, "Robustness of DPSK direction transmission format in standard fibre WDM systems," *Electronics Letters*, vol. 36, no. 17, pp. 1483 – 1484, 2000.
- [64] T. Miyano, K. Fukutoku, K. Hattori, and H. Ono, "Suppression of degradation induced by SPM/XPM+GVD in WDM transmission using bit-synchronous intensity modulated DPSK," in *proc. OECC*, pp. 14D3-3, 2000.

BIBLIOGRAPHY

- [65] J.-K. Rhee, D. Chowdhury, K. S. Cheng, and U. Gliese, "DPSK 32x10 Gb/s Transmission Modeling on 5x90 km Terrestrial System," *Photonics Technology Letters*, vol. 12, no. 12, p. 1627–1629, 2000.
- [66] J. Kahn and K.-P. Ho, "Spectral efficiency limits and modulation/detection techniques for DWDM systems," *Journal of Selected Topics in Quantum Electronics*, vol. 12, no. 2, pp. 259–272, 2004.
- [67] B. Spinnler, N. Hecker-Denschlag, S. Calabro, M. Here, C.-J. Weiske, E.-D. Schmidt, D. v. d. Borne, G.-D. Khoe, H. de Waardt, R. Griffin, and S. Wadsworth, "Nonlinear tolerance of differential phase shift keying modulated signals reduced by XPM," in *proc. OFC*, p. TuF3, 2004.
- [68] C. Wree, J. Leibrich, and W. Rosenkranz, "RZ-DQPSK format with high spectral efficiency and high robustness towards fiber nonlinearities," in *proc. ECOC*, p. 9.6.6, 2002.
- [69] A. H. Gnauck, P. J. Winzer, S. Chandrasekhar, and C. Dorrer, "Spectrally efficient (0.8 b/s/Hz) 1-Tb/s (25x42.7 Gb/s) RZ-DQPSK transmission over 28 100-km SSMF spans with 7 optical add/drops," in *proc. ECOC*, p. PD Th4.4.1, 2004.
- [70] G. Charlet, P. Tran, H. Mardoyan, T. Lefrancois, T. Fauconnier, F. Jorge, and S. Bigo, "151x43Gb/s transmission over 4,080km based on Return-to-Zero Differential Quadrature Phase-Shift-Keying," in *proc. ECOC*, p. PD Th4.1.3, 2005.
- [71] R. A. Griffin, R. G. Walker, J. Hall, S. D. Wadsworth, K. Berry, A. C. Carter, M. J. Wale, J. Hughes, P. A. Jerram, and N. J. Parsons, "10 Gb/s optical differential quadrature phase shift key (DQPSK) transmission using GaAs/AlGaAs integration," in *proc. OFC*, p. PD FD6, 2002.
- [72] R. A. Griffin and A. C. Carter, "Optical differential quadrature phase-shift key (oDQPSK) for high capacity optical transmission," in *proc. OFC*, pp. 367–368, 2002.
- [73] M. Serbay, C. Wree, and W. Rosenkranz, "Implementation of differential precoder for high-speed optical DQPSK transmission," *Electronics Letters*, vol. 40, no. 20, pp. 1288–1289, 2004.
- [74] H. W. Bode, *Network Analysis and Feedback Amplifier Design*. D. van Nostrand company, 1945.
- [75] R. Stremler, *Introduction to Communication Systems*. Springer Verlag, 1977.
- [76] R. A. Fisher, B. R. Suydam, and D. Yevick, "Optical phase conjugation for time-domain undoing of dispersive self-phase-modulation effects," *Optics Letters*, vol. 12, no. 8, pp. 611–613, 1983.

- [77] S. Watanabe, T. Naito, and T. Chikama, "Compensation of chromatic dispersion in a single-mode fiber by optical phase conjugation," *Optics Letters*, vol. 5, no. 1, pp. 92 – 95, 1993.
- [78] A. Gnauck, R. Jopson, and R. Derosier, "10-Gb/s 360-km transmission over dispersive fiber using midsystem spectral inversion," *Photonics Technology Letters*, vol. 5, no. 6, pp. 663 – 666, 1993.
- [79] B. Y. Zeldovich, V. I. Popovichev, V. V. Ragulskii, and F. S. Faisullov, "Connection between the wavefronts of the reflected and exciting light in stimulated Mandel'shtam-Brillouin scattering," *Sov. Phys. JETP*, vol. 15, pp. 109 – 110, 1972.
- [80] A. Chowdhury, G. Raybon, R.-J. Essiambre, J. Sinsky, A. Adamiecki, J. Leuthold, C. Doerr, and S. Chandrasekhar, "Compensation of intra-channel nonlinearities in 40 Gb/s pseudo linear systems using optical phase conjugation," *in proc. OFC*, p. PDP32, 2004.
- [81] S. L. Jansen, G. D. Khoe, H. d. Waardt, S. Spälter, C.-J. Weiske, A. Schöpflin, S. J. Field, H. E. Escobar, and M. H. Sher, "Mixed data rate and format transmission (40-Gbit/s NRZ, 40-Gbit/s duobinary, and 10-Gbit/s NRZ) by mid-link spectral inversion," *Optics Letters*, vol. 29, no. 20, pp. 2348 – 2350, 2004.
- [82] M. Chou, J. Hauden, M. Arbore, and M. Fejer, "1.5- μ m-band wavelength conversion based on difference-frequency generation in LiNbO₃ waveguides with integrated coupling structures," *Optics Letters*, vol. 23, no. 13, pp. 1004 – 1006, 1998.
- [83] H. Escobar and L. Marshall, "All-optical wavelength band conversion enables new scalable and efficient optical network architectures," *in proc. OFC*, vol. WH2, pp. 225 – 227, 2002.
- [84] S. Watanabe, S. Takeda, G. Ishikawa, H. Ooi, J. G. Nielsen, and C. Sonne, "Simultaneous wavelength conversion and optical phase conjugation of 200 Gb/s (5x40 Gb/s) WDM signal using a highly nonlinear fiber four-wave mixer," *in proc. ECOC*, pp. PD1–4, 1997.
- [85] S. Watanabe, S. Takeda, and T. Chikama, "Interband wavelength conversion of 320Gb/s (32x10 Gb/s) WDM signal using a polarization-insensitive fiber four-wave mixer," *in proc. ECOC*, no. PD, pp. 85–87, 1998.
- [86] S. J. B. Yoo, "Wavelength conversion technologies for WDM network applications," *Journal of Lightwave Technology*, vol. 14, no. 6, pp. 955 – 966, 1996.
- [87] Y. N. Singh, H. M. Gupta, and V. K. Jain, "Semiconductor optical amplifiers in wdm tree-net," *Journal of Lightwave Technology*, vol. 15, no. 2, pp. 252 – 260, 1997.
- [88] M.-H. Chou, *Optical frequency mixers using three-wave mixing for optical fiber communications*. Stanford University, 1999.

BIBLIOGRAPHY

- [89] Y. Furukawa, K. Kitamura, S. Takekawa, K. Niwa, and H. Hatano, "Stoichiometric MgLiNbO₃ as an effective material for nonlinear optics," *Optics Letters*, vol. 23, no. 24, pp. 1892 – 1894, 1998.
- [90] I. Brener, B. Mikkelsen, K. Rottwitt, W. Burkett, G. Raybon, J. B. Stark, K. R. Paramesawaran, M. H. Chou, M. M. Fejer, E. E. Chaban, R. Harel, , D. L. Philen, and S. Kosinski, "Cancellation of all Kerr nonlinearities in long fiber spans using a LiNbO₃ phase conjugator and Raman amplification," *in proc. OFC*, p. PD33, 2000.
- [91] I. Brener, M. H. Chou, G. Lenz, R. Scotti, E. E. Chaban, J. Shmulovich, D. L. Philen, S. Kosinski, K. R. Paramesawaran, and M. M. Fejer, "High efficiency (-7 dB), wideband (70 nm) and tunable LiNbO₃ waveguide mid-span spectral inverter and its use for dispersion compensation in 4x10Gbit/s," *in proc. ECOC*, vol. II, pp. 16 – 17, 1999.
- [92] G. Schreiber, H. Suche, Y. Lee, W. Grundkttter, V. Quiring, R. Ricken, and W. Sohler, "Efficient cascaded difference frequency conversion in periodically poled Ti:LiNbO₃ waveguides using pulsed and CW pumping," *Applied Physics B, Special Issue on Integrated Optics*, vol. 73, no. 5-6, pp. 501 – 504, 2001.
- [93] S. L. Jansen, D. v. d. Borne, A. Schöpflin, E. Gottwald, P. M. Krummrich, G. D. Khoe, and H. d. Waardt, "26x42.8-Gbit/s DQPSK Transmission with 0.8-bit/s/Hz Spectral Efficiency over 4,500-km SSMF using Optical Phase Conjugation," *in proc. ECOC*, p. PD Th4.1.5, 2005.
- [94] J. Yamawaku, H. Takara, T. Ohara, K. Sato, A. Takada, T. Morioka, O. Tadanaga, H. Miyazawa, and M. Asobe, "Simultaneous 25 GHz-spaced DWDM wavelength conversion of 1.03 Tbit/s in PPLN waveguide," *Electronics Letters*, vol. 39, no. 15, pp. 1144 – 1145, 2003.
- [95] S. J. B. Yoo, R. Bhat, C. Caneau, and M. A. Koza, "Quasi-phase-matched second-harmonic generation in AlGaAs waveguides with periodic domain inversion achieved by wafer-bonding," *Applied Physics Letters*, vol. 68, no. 19, pp. 3410 – 3412, 1996.
- [96] S. J. B. Yoo, C. Caneau, R. Bhat, M. A. Koza, A. Rajhel, and N. Antoniadis, "Wavelength conversion by difference frequency generation in AlGaAs waveguides with periodic domain inversion achieved by wafer bonding," *Applied Physics Letters*, vol. 68, no. 19, pp. 2609 – 2611, 1996.
- [97] L. B. F. and C. G. Bethea, "Nonlinear susceptibility of gap; relative measurement and use of measured values to determine a better absolute value," *Applied Physics Letters*, vol. 20, no. 8, pp. 272 – 275, 1966.
- [98] M. J. Weber, *CRC Handbook of Laser Science and Technology Supplement 2: Optical Materials*. Science and Behavior Books, 1994.

- [99] I. Brener, M. Chou, E. Chaban, K. Parameswaran, M. Fejer, and S. Kosinski, "Polarization-insensitive parametric wavelength converter based on cascaded nonlinearities in LiNbO₃ waveguides," *in proc. OFC*, pp. TuF1-1, 2000.
- [100] D. Caccioli, A. Paoletti, A. Schiffrini, A. Galtarossa, P. Griggio, G. Lorenzetto, P. Minzioni, S. Cascelli, M. Guglielmucci, L. Lattanzi, F. Matera, G. Tosi Beleffi, V. Quiring, W. Sohler, H. Suche, S. Vehovc, and M. Vidmar, "Field demonstration of in-line all-optical wavelength conversion in a WDM dispersion managed 40-Gbit/s link," *Journal of Selected Topics in Quantum Electronics*, vol. 10, no. 2, pp. 356 – 362, 2004.
- [101] U. Feiste, R. Ludwig, E. Dietrich, S. Diez, H. J. Ehrke, D. Razic, and H. Weber, "40 Gbit/s transmission over 434 km standard-fiber using polarisation independent mid-span spectral inversion," *Electronics Letters*, vol. 34, no. 21, pp. 2044 – 2045, 1998.
- [102] T. Merker, P. Meissner, and U. Feiste, "High bit-rate OTDM transmission over standard fiber using mid-span spectral inversion and its limitations," *Journal of Selected Topics in Quantum Electronics*, vol. 6, no. 2, pp. 258 – 262, 2000.
- [103] S. Watanabe, S. Kaneko, and T. Chikama, "Long-haul fiber transmission using optical phase conjugation," *Optical fiber technology*, vol. 2, pp. 169 – 178, 1996.
- [104] C. Lorattanasane and K. Kikuchi, "Design theory of long-distance optical transmission systems using midway optical phase conjugation," *Journal of Lightwave Technology*, vol. 15, no. 6, pp. 948 – 955, 1997.
- [105] S. Watanabe and M. Shirasaki, "Exact Compensation for both Chromatic Dispersion and Kerr Effect in a Transmission Fiber Using Optical Phase Conjugation," *Journal of Lightwave Technology*, vol. 14, no. 3, pp. 243 – 248, 1996.
- [106] S. L. Jansen, S. Spälter, G. D. Khoe, H. d. Waardt, H. E. Escobar, L. Marshall, and M. H. Sher, "16x40Gbit/s over 800km of SSMF using mid-link spectral inversion," *Photonics Technology Letters*, vol. 16, no. 7, pp. 1763 – 1765, 2004.
- [107] A. Chowdhury, G. Raybon, R.-J. Essiambre, and C. Doerr, "Optical phase conjugation in a WDM CSRZ pseudo-linear 40 Gb/s system for 4,800 km transmission," *in proc. ECOC*, p. PD Th4.5.6, 2004.
- [108] S. L. Jansen, D. v. d. Borne, C. Climent, M. Serbay, C.-J. Weiske, H. Suche, P. Krummrich, S. Spälter, S. Calabrò, N. Hecker-Denschlag, P. Leisching, W. Rosenkranz, W. Sohler, G. Khoe, T. Koonen, and H. d. Waardt, "10,200km 22x2x10Gbit/s RZ-DQPSK Dense WDM Transmission without Inline Dispersion Compensation through Optical Phase Conjugation," *in proc. OFC*, p. PDP28, 2005.

BIBLIOGRAPHY

- [109] X. Shu, K. Chisholm, and K. Sugden, "Design and realization of dispersion slope compensators using distributed Gires-Tournois etalons," *Photonics Technology Letters*, vol. 16, no. 4, pp. 1092 – 1094, 2004.
- [110] S. Watanabe, "Cancellation of four-wave mixing in a single-mode fiber by midway optical phase conjugation," *Optics Letters*, vol. 19, no. 17, pp. 1308 – 1310, 1994.
- [111] S. Watanabe and M. Shirasaki, "Cancellation of four-wave mixing in multichannel fibre transmission by midway optical phase conjugation," *Electronics Letters*, vol. 30, no. 14, pp. 1156 – 1157, 1994.
- [112] K. Kikuchi, "Elimination of four-wave mixing in dispersion-shifted optical fibers by using midway optical phase conjugation in a semiconductor optical amplifier," *in proc. CLEO*, no. CMG5, pp. 42 – 43, 1996.
- [113] G. Raybon, A. Chowdhury, R.-J. Essiambre, and C. Doerr, "Location optimization of a single optical phase conjugator in a 3,200-km, 40-Gb/s pseudo-linear transmission system," *in proc. ECOC*, p. Th2.5.5, 2004.
- [114] Y. Yamada, S.-I. Nakagawa, K. Takashina, T. Tawazawa, H. Taga, and K. Goto, "25 GHz spacing ultra-dense WDM transmission experiment of 1 Tbit/s (100 WDMx10 Gbit/s) over 7300 km using non pre-chirped RZ format," *Electronics Letters*, vol. 35, no. 25, p. 2212 – 2213, 1999.
- [115] C. Hullin, C. Gueritch, E. Grand, D. Lesterlin, S. Ruggeri, M. Adlerfliger, J. P. Blondel, V. Boudier, C. Trecasser, L. Curincks, E. Brandon, O. Courtois, and D. Filet, "Ultra long haul 2500 km terrestrial transmission of 320 channels at 10 Gbit/s over C+L bands with 25 GHz wavelength spacing," *in proc. ECOC*, p. 1.1.3., 2002.
- [116] S. Radic, R. M. Jopson, C. J. McKinstrie, A. H. Gnauck, S. Chandrasekhar, and J. C. Centanni, "Wavelength division multiplexed transmission over standard single mode fiber using polarization insensitive signal conjugation in highly nonlinear optical fiber," *in proc. OFC*, p. PD12, 2003.
- [117] R. Huang, D. Woll, I. White, H. Escobar, L. Marshall, G. Kra, and M. Sher, "Broadband dispersion compensation using mid-link spectral inversion enables performance improvement and cost reduction in optical networks," *in proc. NFOEC*, p. D9, 2003.
- [118] G. Bellotti, A. Bertaina, and S. Bigo, "Dependence of self-phase modulation impairments on residual dispersion in 10-Gb/s-based terrestrial transmissions using standard fiber," *Photonics Technology Letters*, vol. 11, no. 7, pp. 824 – 826, 1999.
- [119] G. L. Woods, P. Papaparaskeva, M. Shtaif, I. Brener, and D. A. Pitt, "Reduction of cross-phase modulation-induced impairments in long-haul WDM telecommunication systems via spectral inversion," *Photonics Technology Letters*, vol. 16, no. 2, pp. 677 – 679, 2004.

- [120] J.-P. Elbers, C. Scheerer, A. Färbert, C. Glingener, A. Schöpflin, E. Gottwald, and G. Fischer, “3.2 Tbit/s (80x40 Gbit/s) bidirectional DWDM/ETDM transmission,” *in proc. ECOC*, vol. PD2-5, pp. 32 – 33, 1999.
- [121] D. D. Marcenac, D. Nesses, A. E. Kelly, M. Brierley, A. D. Ellis, D. G. Moodie, and C. W. Ford, “40 Gbit/s transmission over 406 km of NDSF using mid-span spectral inversion by four-wave-mixing in a 2 mm long semiconductor optical amplifier,” *Electronics Letters*, vol. 33, no. 1, pp. 879 – 880, 1997.
- [122] M. F. C. Stephens, D. Nesses, K. A. Williams, R. V. Penty, I. H. White, and M. J. Fice, “Dispersion compensation at 40Gbit/s over 100km of standard fibre via mid-span spectral inversion in semiconductor optical amplifier with integrated pump laser,” *Electronics Letters*, vol. 35, no. 16, pp. 1359 – 1361, 1999.
- [123] S. Set, R. Girardi, B. Riccardi, B. Olsson, M. Puleo, M. Ibsen, R. Laming, P. Andrekson, F. Cisternino, and H. Geiger, “40Gbit/s field transmission over standard fibre using midspan spectral inversion for dispersion compensation,” *Electronics Letters*, vol. 35, no. 7, pp. 581 – 582, 1999.
- [124] U. Feiste, R. Ludwig, C. Schmidt, E. Dietrich, S. Diez, H. J. Ehrke, E. Patzak, H. Weber, and T. Merker, “80-Gb/s transmission over 160-km standard-fiber using optical phase conjugation in a sagnac-interferometer,” *Photonics Technology Letters*, vol. 11, no. 8, pp. 1063 – 1065, 1999.
- [125] J. Inoue, H. Sotobayashi, W. Chujo, and H. Kawaguchi, “80 Gbit/s OTDM signal transmission over 208 km standard fibre using midspan optical phase conjugation based on four-wave mixing in semiconductor optical amplifiers,” *Electronics Letters*, vol. 38, no. 15, pp. 819 – 821, 2002.
- [126] P. Kaewplung, T. Angkaew, and K. Kikuchi, “Feasibility of 100-Gb/s 10 000-km single-channel optical transmission by midway optical phase conjugation incorporated with third-order dispersion compensation,” *Photonics Technology Letters*, vol. 13, no. 4, pp. 293 – 295, 2001.
- [127] J. P. Gordon and L. F. Mollenauer, “Phase noise in photonic communications systems using linear amplifiers,” *Optics Letters*, vol. 15, no. 23, pp. 1351 – 1353, 1990.
- [128] H. Kim and A. H. Gnauck, “Experimental investigation of the performance limitation of DPSK systems due to nonlinear phase noise,” *Photonics Technology Letters*, vol. 15, no. 2, pp. 320 – 322, 2003.
- [129] T. Mizuochi, K. Ishida, T. Kobayashi, J. Abe, K. Kinjo, K. Motoshima, and K. Kasahara, “A comparative study of DPSK and OOK WDM transmission over transoceanic distances and their performance degradations due to nonlinear phase noise,” *Journal of Lightwave Technology*, vol. 21, no. 9, pp. 1933 – 1943, 2003.

BIBLIOGRAPHY

- [130] X. Liu, X. Wei, R. E. Slusher, and C. J. McKinstrie, “Improving transmission performance in differential phase-shift-keyed systems by use of lumped nonlinear phase-shift compensation,” *Optics Letters*, vol. 27, no. 18, p. 1616–1618, 2002.
- [131] C. Xu and X. Liu, “Postnonlinearity compensation with data-driven phase modulators in phase-shift keying transmission,” *Optics Letters*, vol. 27, no. 18, p. 1619–1621, 2002.
- [132] K.-P. Ho and J. M. Kahn, “Electronic compensation technique to mitigate nonlinear phase noise,” *Journal of Lightwave Technology*, vol. 22, no. 3, pp. 779–783, 2004.
- [133] S. Calabrò, D. v. d. Borne, S. L. Jansen, G. D. Khoe, and H. d. Waardt, “Improved detection of differential phase shift keyed transmission through multi-symbol phase estimation,” in *proc. ECOC*, p. We4.P.118, 2005.
- [134] J. Hansryd, J. Howe, and C. Xu, “Experimental demonstration of nonlinear phase jitter compensation in DPSK modulated fiber links,” *Photonics Technology Letters*, vol. 17, no. 1, pp. 232–235, 2005.
- [135] P. S. Devgan, M. Shin, V. S. Grigoryan, J. Lasri, and P. Kumar, “SOA-based regenerative amplification of phase noise degraded DPSK signals,” in *proc. OFC*, p. PDP34, 2005.
- [136] W. Forsyiaik and N. J. Doran, “Reduction of Gordon-Haus Jitter in Soliton Transmission Systems by Optical Phase Conjugation,” *Journal of Lightwave Technology*, vol. 13, no. 5, pp. 850–855, 1995.
- [137] C. J. McKinstrie, S. Radic, and C. Xie, “Reduction of soliton phase jitter by in-line phase conjugation,” *Optics Letters*, vol. 28, no. 17, pp. 1519–1521, 2003.
- [138] C. J. McKinstrie and C. Xie, “Phase jitter in single-channel soliton systems with constant dispersion,” *Journal of Selected Topics in Quantum Electronics*, vol. 8, no. 3, pp. 616–625, 2002.
- [139] X. Tang and Z. Wu, “Nonlinear noise amplification in optical transmission systems with optical phase conjugation,” *Journal of Lightwave Technology*, vol. 23, no. 5, pp. 1866–1873, 2005.
- [140] X. Tang and Z. Wu, “Suppressing modulation instability in midway optical phase conjugation systems by using dispersion compensation,” *Photonics Technology Letters*, vol. 17, no. 4, pp. 926–928, 2005.
- [141] S. L. Jansen, S. Spälter, G. D. Khoe, H. d. Waardt, M. H. Sher, D. Zhou, and S. J. Field, “Experimental comparison of mid-link spectral inversion and ‘conventional’ DCF based transmission in a DWDM system at 40 Gbit/s,” in *proc. APOC*, pp. 5625–39, 2004.

- [142] S. L. Jansen, D. v. d. Borne, P. M. Krummrich, G. D. Khoe, and H. d. Waardt, "Experimental Comparison of Optical Phase Conjugation and DCF Aided DWDM 2x10.7-Gbit/s DQPSK Transmission," *in proc. ECOC*, p. Th2.2.3, 2005.
- [143] A. Chowdhury and R.-J. Essiambre, "Optical phase conjugation and pseudolinear transmission," *Optics Letters*, vol. 29, no. 10, pp. 1105 – 1107, 2004.
- [144] S. L. Jansen, S. Calabrò, B. Spinnler, D. v. d. Borne, P. M. Krummrich, G. D. Khoe, and H. d. Waardt, "Nonlinear phase noise reduction in DPSK transmission by optical phase conjugation," *in proc. OECC*, pp. 6B1–3, 2005.
- [145] M. C. Jeruchim, P. Balaban, and K. S. Shanmugan, *Simulation of Communication Systems*. Plenum press, 1992.
- [146] M. Serbay, C. Wree, A. Schöpflin, C.-J. Weiske, D. v. d. Borne, S. L. Jansen, G. D. Khoe, P. M. Krummrich, P. Leisching, and W. Rosenkranz, "Coding Gain of FEC encoded 21.42Gb/s RZ-D(Q)PSK Using an Electrical Differential Quaternary Precoder," *in proc. ECOC*, p. We4.P.10, 2005.
- [147] H. Griesser and J. P. Elbers, "Influence of cross-phase modulation induced nonlinear phase noise on DQPSK signals from neighbouring OOK Channels," *in proc. ECOC*, p. Tu1.2.2, 2005.
- [148] D. v. d. Borne, S. L. Jansen, G. D. Khoe, H. d. Waardt, and E. Gottwald, "A comparison between multi-level modulation formats: 21.4-Gbit/s RZ-DQPSK and POLMUX-RZ-DPSK," *in proc. OFC*, p. OThR2, 2006.
- [149] P. J. Winzer, M. Pfennigbauer, and R.-J. Essiambre, "Coherent crosstalk in ultra-dense WDM systems," *in proc. ECOC*, p. Mo4.5.6, 2004.
- [150] W. Sohler, W. Grundkötter, J. H. Lee, Y. H. Min, V. Quiring, H. Suche, R. Schiek, T. Pertsch, F. Lederer, R. Iwanow, and G. I. Stegeman, "All-optical signal processing in periodically poled LiNbO₃ waveguide structures," *in proc. ECOC*, p. Tu 3.4.1, 2004.
- [151] J. Kurz, J. Huang, X. Xie, T. Saida, and M. Fejer, "Mode multiplexing in optical frequency mixers," *Optics Letters*, vol. 29, no. 6, pp. 551–553, 2004.
- [152] H. Suche, G. Schreiber, Y. L. Lee, V. Quiring, R. Ricken, W. Sohler, A. Paoletti, F. Carbone, D. Caccioli, and A. Schiffrini, "Efficient Ti:PPLN multi-wavelength converter for high bitrate WDM-transmission systems," *in proc. ECOC*, pp. 42 – 43, 2001.

BIBLIOGRAPHY

List of publications

Invited papers

- P1. S. L. Jansen, D. van den Borne, P. M. Krummrich, S. Spälter, G. D. Khoe, H. de Waardt, “Long-Haul DWDM Transmission Systems Employing Optical Phase Conjugation”, *Journal of Selected Topics in Quantum Electronics*, invited, to be published, 2006.
- P2. S. L. Jansen, D. van den Borne, P. M. Krummrich, S. Spälter, H. Suche, W. Sohler, G. D. Khoe, H. de Waardt, “Phase conjugation for increased system robustness”, in *proc. OFC*, invited, OTuK3, 2006.
- P3. S. L. Jansen, D. van den Borne, B. Spinnler, S. Calabrò, H. Suche, P. M. Krummrich, W. Sohler, G. D. Khoe and H. de Waardt, “Optical Phase Conjugation for ultra long-haul Phase Shift Keyed Transmission”, *Journal of Lightwave Technology*, invited, pp. 54 - 64, 2006
- P4. W. Sohler, W. Grundkötter, H. Herrmann, J. H. Lee, Y. H. Min, V. Quiring, H. Suche, R. Schiek, T. Pertsch, F. Lederer, R. Iwanow, G. I. Stegeman, S. L. Jansen, “All-optical wavelength conversion, parametric amplification, multiplexing, and switching in integrated PPLN-devices”, in *proc. ICTON*, invited, to be published, 2006.
- P5. S. Spälter, M. Heid, S. L. Jansen, G. Lehmann, E. Meissner and B. Lankl, “Ultra fast switching in OTDM networks”, in *proc. ECOC*, invited 11.4.1, Copenhagen, Denmark, 2002.

Journal papers

- P6. S. L. Jansen, G. D. Khoe, H. de Waardt, S. Spälter, C.-J. Weiske, M. Sher, D. Woll and H. E. Escobar, “Comparison between NRZ and duobinary modulation at 43Gbit/s for MLSI based and DCF based transmission systems”, *Journal of Lightwave Technology*, vol. 24, no. 2, pp. 734 - 739, 2006.

LIST OF PUBLICATIONS

- P7. S. L. Jansen, H. Chayet, E. Granot, S. Ben Ezra, D. van den Borne, P. M. Krummrich, D. Chen, G. D. Khoe and H. de Waardt, "Wavelength conversion of a 40Gbit/s NRZ signal across the entire C-band by an asymmetric Sagnac loop", *Photonics Technology Letters*, vol. 17, pp. 2137 - 2139, 2005.
- P8. S. L. Jansen, D. van den Borne, C. Climent, S. Spälter, P. M. Krummrich, G. D. Khoe and H. de Waardt, "Reduction of Gordon-Mollenauer phase noise by mid-link spectral inversion", *Photonics Technology Letters*, vol. 17, pp. 923 - 925, 2005.
- P9. S. L. Jansen, G. D. Khoe, H. de Waardt, S. Spälter, C.-J. Weiske, A. Schopflin, S. J. Field, H. E. Escobar and M. H. Sher, "Mixed Data Rate and Format Transmission (40Gbit/s NRZ, 40Gbit/s duobinary, 10Gbit/s NRZ) using Mid-Link Spectral Inversion", *Optics Letters*, Vol. 29, pp. 2348 - 2350, 2004.
- P10. S. L. Jansen, S. Spälter, G. D. Khoe, H. de Waardt and H. E. Escobar, L. Marshall, M. Sher, "16x40Gbit/s over 800km of SSMF using midlink spectral inversion", *Photonics Technology Letters*, vol. 17, pp. 1763 - 1765, 2004.
- P11. S. L. Jansen, M. Heid, S. Spälter, E. Meissner, C.-J. Weiske, A. Schopflin, G. D. Khoe and H. de Waardt, "Demultiplexing a 160 Gbit/s OTDM signal to 40 Gbit/s by FWM in SOA", *Electronics Letters*, vol. 38, pp. 978 - 980, 2002.
- P12. D. van den Borne, S. L. Jansen, N. E. Hecker-Denschlag, G. D. Khoe, and H. de Waardt, "Reduction of Nonlinear Penalties Through Polarization Interleaving in 2x10 Gb/s Polarization-Multiplexed Transmission", *Photonics Technology Letters*, vol. 17, 2005.
- P13. D. van den Borne, S. L. Jansen, G. D. Khoe, H. de Waardt, S. Calabrò, P. M. Krummrich, W. Schairer and C.-J. Weiske, "Inter-channel nonlinear transmission penalties in polarization-multiplexed 2x10Gbit/s DPSK transmission", *Optics Letters*, vol. 30, 2005.
- P14. T. Duthel, S. L. Jansen, M. Otto, P. M. Krummrich and C. G. Schffer, "Tunable all-fibre delay line filter for residual dispersion compensation in 40 Gb/s systems", *Electronics Letters*, vol. 40, pp.1291 - 1292, 2004.
- P15. A. Hodzic, N. Hecker-Denschlag, M. Winter, S. L. Jansen, K. Saucke and K. Petermann, "10 Gbit/s based NRZ DWDM systems using polarisation switching in single wavelength channel", *Electronics Letters*, vol. 39, pp. 1329 - 1330, 2003.

International conference papers

- P16. S. L. Jansen, D. van den Borne, A. Schpflin, E. Gottwald, P. M. Krummrich, G. D. Khoe and H. de Waardt, "26x42.8-Gbit/s DQPSK Transmission with 0.8-bit/s/Hz

LIST OF PUBLICATIONS

- Spectral Efficiency over 4,500-km SSMF using Optical Phase Conjugation”, in proc. ECOC, Post-Deadline, Th4.1.5, Glasgow, United Kingdom, 2005.
- P17. S. L. Jansen, D. van den Borne, P. M. Krummrich, G. D. Khoe and H. de Waardt, “Experimental Comparison of Optical Phase Conjugation and DCF Aided DWDM 2x10.7Gbit/s DQPSK Transmission”, in proc. ECOC, Th2.2.3, Glasgow, United Kingdom, 2005.
- P18. S. L. Jansen, D. van den Borne, P. M. Krummrich, G. D. Khoe and H. de Waardt, “Nonlinear phase noise degradation in ultra-long haul 2x10Gbit/s DQPSK transmission”, in proc. OECC, Post-Deadline, PDP 04, Seoul, South Korea, 2005.
- P19. S. L. Jansen, S. Calabrò, B. Spinnler, D. van den Borne, P. M. Krummrich, G. D. Khoe and H. de Waardt, “Nonlinear Phase Noise Reduction in DPSK Transmission by Optical Phase Conjugation”, in proc. OECC, 6B1-3, Seoul, South Korea, 2005.
- P20. S. L. Jansen, D. van den Borne, C. Climent, M. Serbay, C.-J. Weiske, H. Suche, P. M. Krummrich, S. Spälter, S. Calabrò, N. Hecker-Denschlag, P. Leisching, W. Rosenkranz, W. Sohler, G. D. Khoe, T. Koonen and H. de Waardt, “10,200km 22x2x10Gbit/s RZ-DQPSK Dense WDM Transmission without Inline Dispersion Compensation through Optical Phase Conjugation”, in proc. OFC, Post-Deadline, PDP 28, Anaheim, USA, 2005.
- P21. S. L. Jansen, D. van den Borne, C. Climent, S. Spälter, P. M. Krummrich, G. D. Khoe and H. de Waardt, “Reduction of nonlinear phase noise by mid-link spectral inversion in a DPSK based transmission system”, in proc. OFC, OThO5, Anaheim, USA, 2005.
- P22. S. L. Jansen, S. Spälter, G. D. Khoe, H. de Waardt, M. Sher, D. Zhou and S.J. Field, “Experimental Comparison of Mid-Link Spectral Inversion and ‘Conventional’ DCF based Transmission in a DWDM System at 40Gbit/s”, in proc. APOC, 5625-39, Beijing, China, 2004.
- P23. S. L. Jansen, S. Spälter, G. D. Khoe, H. de Waardt, D. Zhou, Q. Shu and L. Marshall, “The impact of asymmetric placement of a spectral inverter in a 40Gbit/s system”, in proc. ECOC, Th2.5.6, Stockholm, Sweden, 2004.
- P24. S. L. Jansen, G. D. Khoe, H. de Waardt, S. Spälter, D. Zhou, Q. Shu and D. Woll, “Dispersion tolerant, 40Gbit/s duobinary transmission over 800km without in-line dispersion management”, in proc. CLEO, CWA6, San Francisco, USA, 2004.
- P25. S. L. Jansen, G. D. Khoe, H. de Waardt, S. Spälter, H. E. Escobar, M. Sher, D. Woll and D. Zhou, “10 Gbit/s, 25GHz spaced transmission over 800km without using dispersion compensation modules”, in proc. OFC, ThT1, Los Angeles, USA, 2004.

LIST OF PUBLICATIONS

- P26. S. L. Jansen, G. D. Khoe, H. de Waardt, M. Heid, S. Spälter, E. Meissner, C.-J. Weiske and A. Schopflin, "Optimizing the wavelength configuration for FWM-based demultiplexing in a SOA", in proc. OFC, pp. 539-541, Atlanta, USA, 2003.
- P27. D. van den Borne, S. L. Jansen, E. Gottwald, G. D. Khoe and H. de Waardt, "Optical filtering tolerances of 42.8-Gbit/s RZ-DQPSK modulation", in proc. OECC, to be published, 2006.
- P28. D. van den Borne, S. L. Jansen, E. Gottwald, P. M. Krummrich, G. D. Khoe and H. de Waardt, "1.6-b/s/Hz Spectrally Efficient 40 x 85.6-Gb/s Transmission Over 1,700 km of SSMF Using POLMUX-RZ-DQPSK", in proc. OFC, post-deadline, PDP 34, Anaheim, USA, 2006.
- P29. D. van den Borne, S. L. Jansen, E. Gottwald, G. D. Khoe and H. de Waardt, "A Comparison between Multi-level Modulation Formats: 21-4Gbit/s RZ-DQPSK and POLMUX-RZ-DPSK", in proc. OFC, OThR2, Anaheim, USA, 2006.
- P30. D. van den Borne, S. L. Jansen, E. Gottwald, G. D. Khoe and H. de Waardt, "Line Optimization in Long-Haul Transmission Systems with 42.8-Gbit/s RZ-DQPSK modulation", in proc. OFC, OFD, Anaheim, USA, 2006.
- P31. D. van den Borne, S. Calabrò, S. L. Jansen, E. Gottwald, G. D. Khoe and H. de Waardt, "Differential Quadrature Phase Shift Keying with close to Homodyne Performance based on Multi-Symbol Phase Estimation", in proc. IEE seminar on electrical signal processing in optical communications, London, United Kingdom, December 2005.
- P32. M. Serbay, C. Wree, A. Schopflin, C.-J. Weiske, D. van den Borne, S. L. Jansen, G. D. Khoe, P. M. Krummrich, P. Leisching and W. Rosenkranz, "Coding Gain of FEC encoded 21.42Gb/s RZ-D(Q)PSK Using an Electrical Differential Quaternary Precoder", in proc. ECOC, We4.P.10, Glasgow, United Kingdom, 2005.
- P33. S. Calabrò, D. van den Borne, S. L. Jansen, G. D. Khoe and H. de Waardt, "Improved detection of differential phase shift keyed transmission through multi-symbol phase estimation" In proc. ECOC, We4.P.118, Glasgow, United Kingdom, 2005.
- P34. T. Duthel, S. L. Jansen, P. M. Krummrich, M. Otto and C. G. Schffer, "Residual dispersion compensation in a 40 Gb/s WDM system utilizing an all-fiber delay line filter", in proc. OFC, JWA20, Anaheim, USA, 2005.
- P35. D. van den Borne, S. L. Jansen, G. D. Khoe, H. de Waardt, S. Calabrò and N. E. Hecker-Denschlag, "Polarization interleaving to reduce inter-channel nonlinear penalties in polarization multiplexed transmission", in proc. OFC, JWA41, Anaheim, USA, 2005.

- P36. A. Hodzic, N. E. Hecker-Denschlag, M. Winter, S. L. Jansen, K. Saucke and K. Petermann, "Performance improvement of 10 Gb/s NRZ DWDM transmission using orthogonal polarizations of adjacent bits in a single wavelength channel", in proc. 16th Annual Meeting IEEE LEOS, pp. 845-846, Tucson, USA, 2003.
- P37. M. Heid, S. L. Jansen, S. Spälter, E. Meissner, W. Vogt and H. Melchior, "160-Gbit/s demultiplexing to base rates of 10 and 40 Gbit/s with a monolithically integrated SOA-Mach-Zehnder interferometer", in proc. ECOC, 8.4.3, Copenhagen, Denmark, 2002.

National conference papers

- P38. S. L. Jansen, D. van den Borne, P. M. Krummrich, G. D. Khoe and H. de Waardt, "Compensation of nonlinear phase noise impairments through optical phase conjugation in long-haul transmission systems", in proc. IEEE LEOS/BENELUX Annual Symposium, Mons, December 2005.
- P39. D. van den Borne, S. L. Jansen, E. Gottwald, P. M. Krummrich, P. Leisching, G. D. Khoe, H. de Waardt "A robust modulation format for 42.8-Gbit/s long-haul transmission: RZ-DPSK or RZ-DQPSK?", in proc. ITG, Leipzig, Germany, 2006.
- P40. D. van den Borne, S. L. Jansen, E. Gottwald, G. D. Khoe and H. de Waardt "Inter-channel Depolarization Impairments in 21.4-Gbit/s POLMUX OOK and DPSK Transmission", in Proc. IEEE LEOS/BENELUX Annual Symposium, pp. 133-136, Mons, Belgium, December 2005
- P41. T. Duthel, S. L. Jansen, P. M. Krummrich, M. Otto and C. G. Schffer, "Faseroptische Delay-Line-Filter zur Gruppenlaufzeitentzerrung in schnellen optischen bertragungssystemen", in proc. ITG, Leipzig, Germany, 2005.

LIST OF PUBLICATIONS

Samenvatting

Door de wereldomvattende belangstelling voor communicatiesystemen zoals het internet is de wens ontstaan de overdrachtsnelheid van deze systemen te vergroten. Dat vraagt nieuwe ontwerpen voor (optische) transmissiesystemen die er voor te zorgen dat bij hogere transmissiesnelheid over grotere afstanden de kwaliteit van de transmissie niet verslechtert. Optische fasen conjugatie (optical phase conjugation, OPC) is een methode om de kwaliteit van de transmissie link te verbeteren en de structuur van de link te vereenvoudigen. OPC kan gebruikt worden om deterministische, fase gerelateerde verstoringen in transmissie systemen te compenseren.

Dit proefschrift beschrijft de regeneratieve mogelijkheden van OPC voor de reductie van vervormingen die kunnen optreden in moderne transmissie systemen. Hoofdzakelijk zijn transmissie systemen onderzocht waarin OPC gebruikt wordt om naast niet-lineaire vervormingen ook chromatische dispersie te compenseren. In dergelijke systemen is de dispersiemap (het verloop van de dispersie als functie van de transmissie afstand) aantoonbaar anders dan dat in een conventioneel transmissie systeem. In een OPC transmissie systeem is de geaccumuleerde dispersie op de transmissie lijn namelijk significant hoger dan die in een conventioneel transmissie systeem.

Gebruik makend van het non return-to-zero amplitude-shift-keying (NRZ-ASK) modulatie formaat, hebben we de invloed onderzocht van de dispersiemap van OPC op niet lineaire verstoringen. Uit dit onderzoek is gebleken dat bij een overdrachtssnelheid van 10 Gbit/s, de peak powers die voorkomen in het OPC systeem, veel groter zijn dan in het conventionele transmissie systeem, waardoor een veel grotere invloed van zelf-fase modulatie (self-phase modulation, SPM) wordt veroorzaakt. Door fasen conjugatie wordt deze niet lineaire verstoring grotendeels gecompenseerd. Als echter niet één kanaal, maar meerdere WDM kanalen gebruikt worden, dan wordt bij kleine kanaalafstand kruis-fase modulatie (cross-phase modulation, XPM) de dominante verstoring op de transmissielijn. In principe is XPM een deterministische verstoring. Maar door de dispersie van de transmissielijn kan XPM in transmissie systemen niet als een deterministische verstoring beschouwd worden. Met simulaties en experimenten hebben we laten zien dat daardoor de regeneratieve capaciteit van OPC marginaal is voor de reductie van XPM.

In systemen met een overdrachtssnelheid van 40 Gbit/s per kanaal, zijn de peak powers die voorkomen in het OPC systeem ongeveer gelijk aan de peak powers die in het conventionele transmissie systeem voorkomen. Bovendien is in 40-Gbit/s/kanaal WDM systemen de invloed van XPM relatief laag. Over het algemeen zijn deze systemen gelimiteerd door

SAMENVATTING

1-kanaal verstoringen zoals SPM, intra-kanaal XPM en intra-kanaal FWM. We hebben experimenteel laten zien dat vergeleken met het conventionele systeem het OPC systeem beter presteert door de compensatie van 1-kanaal verstoringen.

Als OPC gebruikt wordt om dispersie te compenseren, dan moet de OPC-converter in het midden van de transmissie lijn opgesteld worden. In sommige transmissie systemen is het echter niet mogelijk de OPC exact in het midden te plaatsen. Vandaar dat configuraties getest zijn waarbij de OPC excentrisch opgesteld is. In verschillende configuraties met een lengte van 700 km tot 900 km is de OPC 100 km uit het midden opgesteld. In deze experimenten is vastgesteld dat er praktisch geen verslechtering optreedt vergeleken met de configuratie waarbij de OPC exact in het midden geplaatst is.

Het differential phase-shift keying (DPSK) modulatie formaat biedt veel voordelen ten opzichte van het conventionele ASK modulatie formaat: een 3 dB verbetering in de gevoeligheid (sensitivity), een grotere tolerantie voor smalbandige optisch filtering, etc. Een groot nadeel van DPSK modulatie formaten is echter dat deze gevoelig zijn voor niet lineaire fase ruis (nonlinear phase noise, NPN). In een 800-km transmissie link hebben we voor 10.7-Gbit/s DPSK de invloed van NPN bestudeerd. In dit experiment is een significante verbetering geobserveerd van het systeem met OPC ten opzichte van het systeem zonder OPC. De afhankelijkheid van de locatie van de OPC is ook bestudeerd. Als we een bit-fout ratio (bit-error rate, BER) penalty toelaten van 1 decade van het optimum, dan blijkt dat er voor de plek waar de OPC geplaatst wordt een extreme tolerantie bestaat: De plaats van de OPC kon gevarieerd worden van bijna $1/3e$ tot $2/3e$ van de transmissielijn.

De combinatie van OPC met 21.4-Gbit/s return-to-zero differential quadrature phase-shift keying (RZ-DQPSK) is bestudeerd in een experiment met lange afstand transmissie. De transmissie bleek na 10,200 km fout-vrij te zijn voor alle 22 golflengte divisie gemul-tieplexe (wavelength division multiplexed, WDM) kanalen. De geaccumuleerde dispersie komt in dit experiment tot meer dan 80,000 ps/nm. Dit is significant meer dan de dispersie in een conventioneel transmissie systeem (ca. 3,000 ps/nm). Door de hoge geaccumuleerde dispersie is er een extreem grote overlap van pulsen tijdens de transmissie. Met dit experiment hebben we echter laten zien dat ondanks de hoge dispersie, de haalbare transmissie afstand van het OPC experiment 44% groter is dan de afstand die gemeten is in het conventionele transmissie systeem.

Door de overdrachtssnelheid te verdubbelen naar 42.8-Gbit/s en de afstand van de WDM kanalen gelijk te houden, is transmissie gerealiseerd met een spectrale efficiency van 0.8-bit/s/Hz. De haalbare afstand met OPC zonder overdrachtsfouten was 5,000 km. Vergeleken met de haalbare afstand in het 21.4-Gbit/s RZ-DQPSK experiment is de haalbare transmissie afstand dus ongeveer een factor 2 kleiner. Deze factor komt exact overeen met het 3-dB OSNR verschil dat aanwezig is tussen 21.4-Gbit/s en 42.8-Gbit/s RZ-DQPSK in de back-to-back configuratie. Met het conventionele transmissie systeem resulteert het verdubbelen van de overdrachtssnelheid in een grotere reductie van de haalbare transmissie afstand (factor 2.4) door SPM en niet lineaire fase ruis. Ook in dit experiment is een significante verbetering gemeten door OPC te gebruiken: de haalbare transmissie afstand is 60% groter dan de afstand die gemeten is in het conventionele systeem.

Acknowledgments

During my Ph.D. research project, I had the chance to work with many different, creative people. The Ph.D. project is a collaboration between the Eindhoven, University of Technology and Siemens in Munich. The research described in this thesis was carried out in the Com FN T D HW-1 department at Siemens.

First, I would like to thank all my colleagues from the Electro-Optical Communications (ECO) group in Eindhoven and my colleagues from Siemens for the terrific time I had while conducting my research. In particular, I would like to thank Dr. Stefan Spälter for giving me the opportunity to do my Ph.D. research at Siemens in a time where positions in the industry were practically not available. He was a patient mentor who put great effort into teaching me how to conduct independent research. Additionally, I would like to thank Dr. Peter M. Krummrich for guiding me in the last two years of the project. His original ideas and constructive feedback helped me to improve the quality of my research and scientific publications.

I would like to thank Prof. Djan Khoe for allowing me to do my Ph.D. with the ECO group and for his flexibility in collaborating with Siemens. I would also like to thank him for his encouragement and enthusiasm throughout the course of the project. I am greatly indebted to Dr. Huug de Waardt for being a supportive advisor. I am especially thankful for his efforts in making the ‘distance’ between Munich and Eindhoven seem minimal.

During the research projects, it was a great pleasure to work together with Dirk van den Borne. His broad and in-depth knowledge on transmission impairments and advanced modulation formats was very useful in the many discussions we had. He continuously surprised me with out-of-the-box ideas and clever analytical observations.

I would like to thank Carlos Climent from the Technical University in Munich for the design, realization and testing of the re-entrant re-circulating loop. Without this tool it would never have been possible to realize the obtained results. Furthermore, I would like to thank Christian Palm from the University of Kiel for the many simulations he conducted on optical phase conjugation. His simulations, discussed in section 5.1, show a clear comparison between the different dispersion maps.

The two experts on DPSK simulations at Siemens, Stefano Calabrò and Bernhard Spinnler, were always available to answer difficult questions. They significantly contributed to the simulations showing that optical phase conjugation can be used to compensate for nonlinear phase noise.

I would like to thank Prof. N. Hanik, Prof. Ton Koonen, Prof. W. Rosenkranz and

ACKNOWLEDGMENTS

Dr. Jos van der Tol for the time they invested in improving the quality of the manuscript. Additionally, I would like to thank Bas Huiszoon and Dylan Masells for their valuable input to this thesis.

I would like to thank Dr. Marc Bohn for his support and interest in my work. I will cherish the many constructive discussions we had. I am very grateful for the two electrical magicians that we have at Siemens. If it were not for Claus-Jörg Weiske and Andreas Schöpflin many experiments would not have worked. Additionally, I would like to thank Dr. Cornelius Cremer, Dr. Ulrich Gaubatz, Dr. Erich Gottwald, Dr. Nancy Hecker-Denschlag, Dr. Gottfried Lehmann, Dr. Patrick Leisching, Erik de Man, Dr. Sebastian Randel, Dr. Joerg Reichert, Dr. Lutz Rap, Wolfgang Schairer and Dr. Ernst-Dieter Schmidt from Siemens. From the Eindhoven University of Technology I am equally thankful to Luc Augustin, Jeffrey Lee, Susan de Leeuw, Dr. Yong Liu, Dr. Eduward Tangdiongga, Jarek Turkiewicz and Erwin Verdurmen.

I am in debt to Murat Serbay from the University of Kiel for his help with computing the DQPSK coding during the first long-haul 21.4-Gbit/s RZ-DQPSK measurements and for his feedback on the draft of the thesis. I would also like to thank Stefan Schöllmann from the University of Kiel for his interest in my work.

I would like to thank everyone from the Lightbit corporation. In particular, I would like to express my gratitude to Dr. Hector Escobar, Dr. Mark Sher, Dr. Gabriel Kra, Dr. Simon Fields and Dr. Dirk Woll. Lightbit manufactured the parallel polarization diverse PPLN subsystem with which the experiments in Chapter 5 were conducted.

Furthermore, I would like to express my gratitude to Dr. H. Suche and Prof. W. Sohler from the Technical University in Paderborn. The experiments reported in Chapter 7 were conducted using a PPLN waveguide designed and manufactured by the University of Paderborn. I would like to thank Dr. H. Suche for his clear explanations and instructions of adjusting the PPLN-waveguide and his help with creating a counter-directional polarization diverse PPLN subsystem.

Apart from optical phase conjugation, I have conducted several measurements to assess the performance of a Sagnac loop for the regeneration of 40-Gbit/s NRZ-ASK. I would like to express my gratitude to the two companies I collaborated with on this project, namely the KaiLight photonics corporation and Dr. Sartorius' group at the Heinrich Hertz Institute.

I am very grateful to my parents Ben and Els for believing in me. I would like to thank Els for correcting the summary in Dutch and I would like to take this opportunity to thank Ben, for his unlimited interest in my Ph.D. thesis and for his constructive feedback to the manuscript. As well, I would like to thank my fantastic sister Malou and her boyfriend Bas van Veen for supporting me throughout the years.

Finally, I would like to thank my girlfriend Annette for her support, encouragement, patience and strength during my long shifts in the lab (and the weekends I worked at home). She was always there for me and this achievement truly is her's as well.

Curriculum Vitae

Sander Lars Jansen was born in Maartensdijk, The Netherlands, in 1978. He received his M.S. degree in electrical engineering in 2002 from the Eindhoven University of Technology, the Netherlands. In summer 2000 he was an intern at NEC in Tokyo, Japan where he developed an automated tracking program for a network of observation cameras. From November 2001 to July 2002 he conducted his master thesis at Siemens in Germany under the scope of the European funded IST project FASHION. For this project he realized an optical four-wave mixing based de-multiplexer capable of de-multiplexing 160-Gbit/s OTDM to 40-Gbit/s.

In November 2002 he started working toward a Ph.D. degree in electrical engineering at the University of Technology in Eindhoven, the Netherlands in collaboration with the Siemens AG in Munich, Germany. Main research topics are optical regeneration, optical phase conjugation and advanced modulation formats. In 2005, he was awarded the IEEE Lasers & Electro-Optics Society (LEOS) Graduate Student Fellowship.